Spatial particle correlations in ^{6}He and ^{8}He

P. Mei

GANIL T 2011 02

UNIVERSITÉ DE CAEN BASSE NORMANDIE

U.F.R. de Sciences

ÉCOLE DOCTORALE SIMEM

T H È S E

Présentée par

Mlle. Pu MEI

soutenue le

19 Septembre 2011

en vue de l'obtention du

DOCTORAT de l'UNIVERSITÉ de CAEN

Spécialité : Constituants élémentaires et physique théorique

Arrêté du 07 août 2006

Titre :

Spatial particle correlations in ^{6}He and ^{8}He

MEMBRES du JURY :

M. Jerzy DUDEK	Professeur	Université de Strasbourg (***Rapporteur***)
M. Kris HEYDE	Professeur	Université de Gand (***Rapporteur***)
M. Alahari NAVIN	Directeur de recherche	CNRS(GANIL)
M. Olivier JUILLET	Professeur	Université de Caen
M. Pieter VAN ISACKER	Chercheur	CEA(GANIL) (***Directeur de thèse***)

UNIVERSITÉ DE CAEN BASSE NORMANDIE

U.F.R. de Sciences

ÉCOLE DOCTORALE SIMEM

T H È S E

Présentée par

Mlle. Pu MEI

soutenue le

19 Septembre 2011

en vue de l'obtention du

DOCTORAT de l'UNIVERSITÉ de CAEN

Spécialité : Constituants élémentaires et physique théorique

Arrêté du 07 août 2006

Titre :

Spatial particle correlations in ^{6}He and ^{8}He

MEMBRES du JURY :

M. Jerzy DUDEK	Professeur	Université de Strasbourg (***Rapporteur***)
M. Kris HEYDE	Professeur	Université de Gand (***Rapporteur***)
M. Alahari NAVIN	Directeur de recherche	CNRS(GANIL)
M. Olivier JUILLET	Professeur	Université de Caen
M. Pieter VAN ISACKER	Chercheur	CEA(GANIL) (***Directeur de thèse***)

Contents

Acknowledgements

Fall is starting anew. Three years' time has slipped away in a blink of an eye, and yet when I look back, so many pieces of memories come to life.

And so comes the end of my Ph.D experience that wouldn't have come to pass, or wouldn't have been so colorful, if it weren't for the many people to whom I owe a debt of gratitude. To begin with, I'd like to thank the director of GANIL, Sydney Gales, for giving me the opportunity to do my Ph.D research in theoretical nuclear physics at GANIL. To my advisor, Dr. Pieter Van Isacker, I owe a special debt for his guidance and faith in me ; for giving me the independence I needed in my research while, with his breath and depth of knowledge, always setting me on the right track when I got lost.

I am also grateful to my committee members, Professor emeritus Kris Heyde, Directeur de recherche at CNRS Dr. Alahari Navin, Professor Olivier Juillet and Professor Jerzy Dudek. Thanks to the amiable Professor Heyde, who invited me to Gent for discussion, and whose erudition and meticulousness never cease to impress me. And thanks to Professor Olivier Juillet, President of my committee, whose reputation as an excellent professor and physicist precedes him, for his insightful comments and appreciation for this work.

Knowing Dr. Alahari Navin is a sheer pleasure. His enthusiasm for science and life, his frankness and concern for the people around people, especially young researchers are equalled by few. Every conversation with him is an enlightening

and inspirational treat, be it about physics or otherwise. Sir, in addition to my heartfelt thanks for spurring me on, you have my sincere respect.

I'm also blessed with so many colleagues turned friends.

The fun time at la Maison du Bonheur that I shared with its former members : Aurore (who despite being seven years my junior, always takes care of me), Guilain, Ketel (who often goes out of her way to pamper us with her cuisine), Marc-Olivier, Guillaume (Marassio) (Football nights without you aren't the same !) and Jo, will always be dear to me.

It is hard to enumerate all the people who were generous with their friendship and help : Denis (Keep up the parties !), Aradhana (who is like a big sister to me), Olivier (Sorlin), David, François, Yannen, Olivier (Delaune), Alex (Pichard), Alex (Lepailleur), Héloise, Pedja, Guillaume, Fanny, Jean-Pierre, Emanuel, Christelle, Bayen, as well as Sophie, Emilie, Véronique, Michel Lion...

To my former office mates Matt and Kouhei : I miss the long afternoon coffee break. And to my current office mates Marc and Kevin : My best wishes. I hope you will have as much fun as I did.

Finally, my deepest affection and earnest gratitude go to : my parents and my sister, for their unconditional love and support ; Françoise and Patrick, Annick and Joel, my sweetest "adoptive" French families, for treating me like their own daughter ; Dorothy, Thierry, Emily, Laurent, Mélany and Ludo for welcoming me with open arms into their loving family. Thanks to Jo for entertaining me with the magic of turning everything into happiness.

October 2011

1

Introduction

The subject of this thesis is triggered by our curiosity about the geometry of nuclei, especially ^{6}He and ^{8}He for the reasons that will be outlined below.

1.1 Two-particle systems

Two-particle systems refer to the nuclei with two identical valence nucleons. They are well exemplified by ^{6}He, which is typically depicted as a particularly stable ^{4}He (α particle) core having the proton and neutron $0s_{1/2}$ shells filled up, accompanied by two valence neutrons. Simple as it may seem, ^{6}He has been at the heart of a long-lasting debate as to whether the valence neutrons spend more time staying close to each other looking like a di-neutron (Fig. 1.1), or keeping their distance from each other to form a so-called cigar-like configuration (Fig. 1.2) (see Sec. 1.1.3). The nucleus of ^{6}He features elements of a rewarding investigation, among which are pairing, nuclear halo phenomenon, Borromean nuclei, etc.

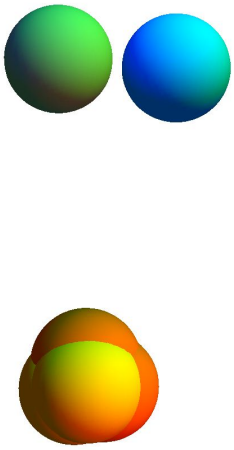

Figure 1.1: The di-neutron configuration of ^{6}He

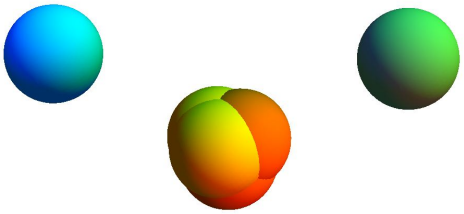

Figure 1.2: The cigar-like configuration of ^{6}He

1.1.1 Pairing

Identical nucleons tend to pair up. Pairing explains why all known even-even nuclei have $J^\pi = 0^+$ ground states, and most odd-mass nuclei have the total angular momentum of the last unpaired nucleon[†]. Another direct evidence is the odd-even mass difference, pointing to the fact that for the same type of nucleons, protons or neutrons, the gain in binding energy is larger when a doubly-even nucleus is formed than when its neighboring odd-mass isotones or isotopes are formed. This is illustrated in Fig. 1.3 by the staggering one-neutron separation energy $S(n)$ (Fig. 1.3(a)) of some ruthenium isotopes near $^{100}_{44}$Ru, and one-proton separation energy $S(p)$ (Fig. 1.3(b)) of some isotones of $^{100}_{44}$Ru. The staggering feature is shared by all isotopic and isotonic sequences of nuclei.

In the present context, the fact that ^{6}He has a ground state of 0^+, whereas ^{5}He, the isotope of ^{6}He with one less neutron, is unbound and has the total nuclear spin $3/2^-$, hints at the undisputed presence of pairing.

Two typical level schemes of singly magic nuclei with two valence nucleons that can be described within the pure shell model picture are presented in Fig.

[†]Strictly speaking, nuclei with more than one valence nucleon may have a total angular momentum other than that of the last unpaired nucleon in the ground state due to residual interactions. For instance, although both $^{45}_{22}$Ti and $^{47}_{22}$Ti have the last unpaired neutron in the shell $0f_{7/2}$, the former has a $7/2^-$ ground state while the latter, a $5/2^-$ ground state because of the quadrupole correlation.

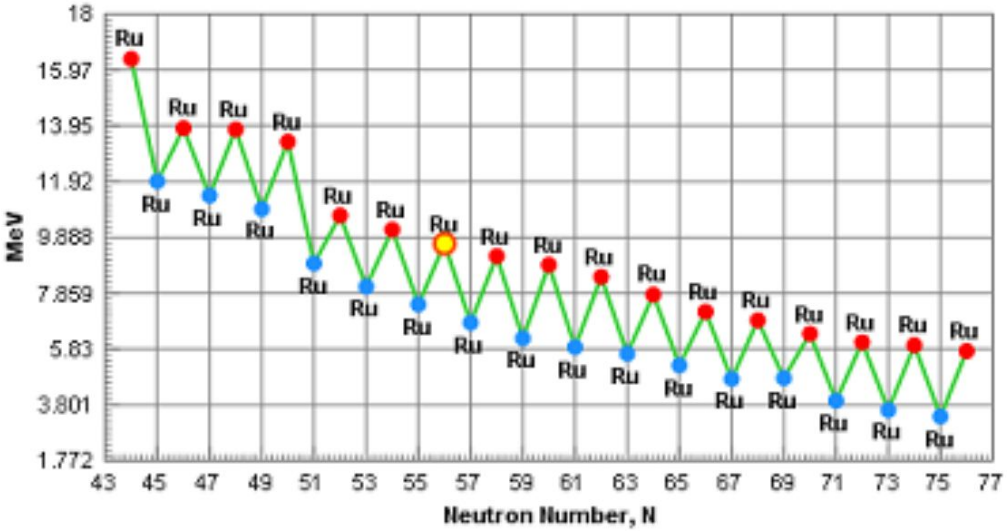

(a) Neutron separation energy of isotopes of ^{100}Ru

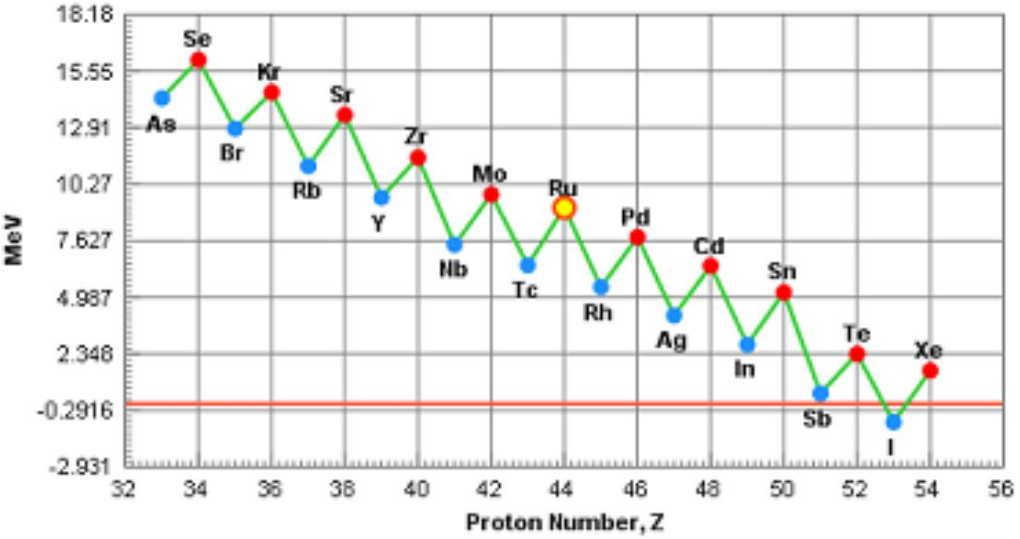

(b) Proton separation energy of isotones of ^{100}Ru

Figure 1.3: Neutron and proton separation energies of nuclei near ^{100}Ru (taken from http://www.obacs.com).

1.4. Both of them have a very low-lying 0^+ ground state and a succession of states with higher even angular momenta.

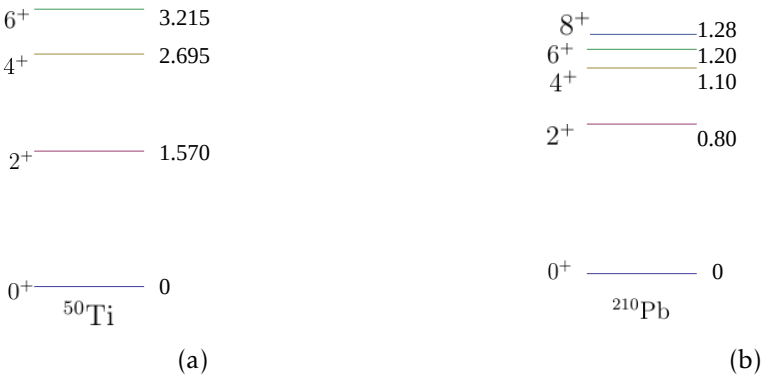

Figure 1.4: The level schemes of ^{50}Ti and ^{210}Pb (data taken from NNDC). The energies are in units of MeV.

The physical mechanism of the pairing effect on the level schemes can be better understood with multipole expansion. The multipole expansion is widely used to decompose two-body interactions into spherical tensor components as follows

$$\begin{aligned} V(|\vec{r}_1 - \vec{r}_2|) &= \sum_{k=0}^{\infty} v_k(r_1, r_2) P_k(\cos\theta_{12}) \\ &= \sum_{m=-k}^{k} \sum_{k=0}^{\infty} v_k(r_1, r_2) \frac{4\pi}{2k+1} \mathcal{Y}^*_{km}(\theta_1, \phi_1) \mathcal{Y}_{km}(\theta_2, \phi_2), \end{aligned}$$

where $v_k(r_1 r_2)$ is given by [1]

$$v_k(r_1, r_2) = \frac{2k+1}{2} \int V(|\vec{r}_1 - \vec{r}_2|) P_k(\cos\theta_{12}) d\cos\theta_{12}.$$

The pairing effect described by the level schemes above in Fig. 1.4 can be mocked up by a zero-range δ interaction that will be among the subjects discussed in Chapter 3. The multipole expansion of the δ interaction reads

$$\delta(\vec{r}_1 - \vec{r}_2) = \sum_{m=-k}^{k} \sum_{k=0}^{\infty} \frac{\delta(r_1 - r_2)}{r_1 r_2} \mathcal{Y}^*_{km}(\theta_1, \phi_1) \mathcal{Y}_{km}(\theta_2, \phi_2).$$

As far as two nucleons in the same shell j are concerned, the energy splitting originated by a δ interaction for a J-coupled state in jj-coupling scheme is given by the matrix element $\langle j^2; JM|\delta(\vec{r}_1 - \vec{r}_2)|j^2; JM\rangle$. Contributions from different multipole components then can be compared by including successively higher orders in the expansion of the interaction and plotting the level schemes. Such a plot is shown for $0h_{11/2}$ [2, 3] in Fig. 1.5. It is inferred from Fig. 1.5 that it is the

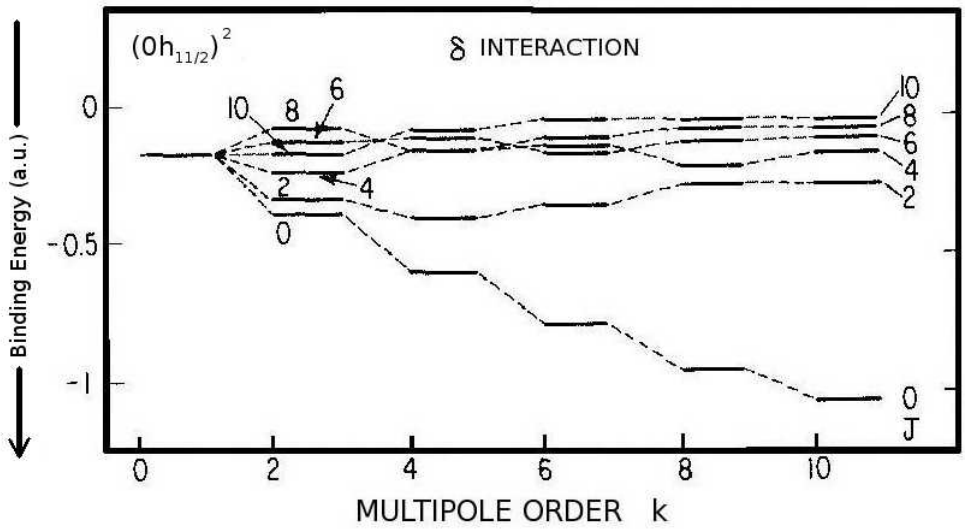

Figure 1.5: The level schemes of a $(0h_{11/2})^2$ configuration calculated by including successively higher multipole order components (taken from [3]).

high-order multipole components that account for the large energy gain for the 0^+ states. Consequently, pairing is often associated with attractive short-range interactions that high multipole order components dominate, which can be misleading because interactions originally defined in second quantization, such as the pairing interaction that correlates nucleons in zero-coupled pairs (see Chapter 4), cannot be analyzed in coordinate space in terms of their "range".

1.1.2 Nuclear halo and Borromean nuclei

The notion of halo pervades various scientific disciplines when an unusually diluted and extended component surrounding a more solid and massive core is

encountered. In nuclear physics, the 1/3 power law

$$R = r_0 A^{1/3}, \tag{1.1.1}$$

where $r_0 = 1.25$ fm and A is the mass number, followed at least roughly by the radii of stable nuclei, is defied by nuclei on the neutron and proton drip lines. ^{6}He, ^{11}Li, ^{11}Be, ^{19}C and ^{17}Ne, to name a few, all exhibit exceptionally large extensions of nuclear matter. The ^{11}Li nucleus, for one, is observed to have the nuclear radius of the much heavier ^{208}Pb nucleus [4]. Furthermore, in all those nuclei, the extended matter distribution is generated by a few valence nucleons, while loosely bound to a more stable core, extending far out into regions classically forbidden by the potential. The name halo nucleus was thus coined [4, 5]. Weakly bound, halo nuclei have a relatively short lifetime of the order of a few milliseconds to a few seconds, before undergoing decay.

The experimental evidence of halo includes

1. Unusually large interaction cross sections indicating large sizes [4];

2. Very narrow momentum distributions of constituents in high-energy fragmentation which, by virtue of the uncertainty principle, should be accompanied by large spatial extensions [6];

3. Electromagnetic dissociation cross sections orders of magnitude larger than for stable nuclei which is explained by very separated charge and mass centers [7].

At present, the accepted definition [8, 9] of a halo nucleus contains two criteria:

1. The total many-body wave function must have a cluster structure (> 50% probability of having a cluster component).

2. A large part (> 50%) of the wave function for the halo particles must be in the non-classical region of the cluster potentials.

The cluster structure in question is the one composed of constituents that it is easiest for the nucleus to break up into. For instance, ^{6}He and ^{11}Li can be seen as three-body structures, that is, two neutrons plus a core, and ^{11}Be a two-body structure with one neutron plus a core. These constituents are the building blocks of halo nuclei, and as such are the essential degrees of freedom. For halo nucleons to have a good chance of penetrating into forbidden regions, their angular momenta must be low; otherwise the centrifugal barrier would hamper the formation of halo. It has been shown that halo nucleons only exist as s and p waves [8, 9].

One intriguing class of halo nuclei is Borromean nuclei named after the Borromean rings (Fig. 1.6) appearing on the coat of arms of the Italian family of Borromeo since the 15th century. The three rings are interlocked in such a way

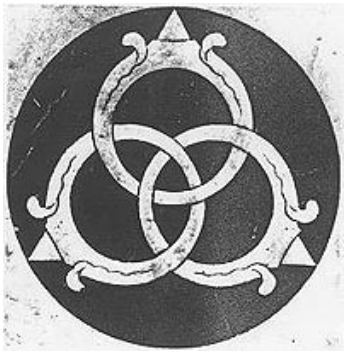

Figure 1.6: Borromean rings

that no two rings are linked; if any one of them is broken, the other two fall apart. Analogously, Borromean nuclei are the three-body halo nuclei in which none of the two-body subsystems are bound, and yet all together as a whole, the three constituents lead to a bound state. If we remove one valence neutron from ^{6}He (or ^{11}Li), the resulting isotope ^{5}He (or ^{10}Li) is unbound. Furthermore, the di-neutron subsystem is also unbound; thus ^{6}He and ^{11}Li are both Borromean nuclei.

1.1.3 Experimental and theoretical debates

Neither experimentalists nor theorists have reached a consensus on whether di-neutron or cigar is more probable in ^{6}He. Experimentally, a variety of methods have been used to look into neutron correlations in ^{6}He. Although people seem to agree on the co-existence of the two possible configurations, opinions are split concerning which one is predominant. For example, two neutron transfer [10], the elastic transfer in the ^{4}He(^{6}He, ^{6}He)^{4}He reaction [11] and neutron breakup [12] show a prevalence of the di-neutron configuration. On the other hand, the radiative capture of a proton on ^{6}He [13] indicates the contrary.

The theoretical side of the story is that, most people consent to the co-existence of the two configurations established by Zhukov *et al.* with the three-body calculation in Ref. [14]. Nevertheless, there is a dissenting voice coming from Suzuki who claims in Ref. [15] rather a pure di-neutron configuration.

Our intention is first to show that, the two configurations show up as a pure geometrical consequence of an identical nucleon pair in the $0p$ shell zero-coupled in the LS coupling scheme ($L = 0$, $S = 0$), and to provide theoretical predictions for the geometry of such correlated[†] identical nucleon pairs in any shell (Chapter 2), as well as for states with the total angular momentum L other than zero. Then, ^{6}He, a perfect laboratory for studying two-particle correlations, endowed with halo and Borromean particularities, will be considered (Chapter 3 and 4).

1.2 Four-particle systems

To pursue the study of the geometry of zero-coupled particles further, ^{8}He, a typical correlated four-particle system will be investigated as a prototype. ^{8}He boasts the largest neutron-to-proton ratio of any known particle-stable nucleus.

[†]If no ambiguity arises, we will use "correlated" to mean zero-coupled in the LS coupling scheme throughout.

The nature of the four valence neutrons in ^{8}He is still not quite clear. Some believe that like its isotope ^{6}He, ^{8}He is also a halo nucleus with four halo neutrons and an α particle core because of its large neutron density distribution. Others point out that the large neutron distribution in ^{8}He is better understood as a thick neutron skin [16]. In the ground state of ^{8}He, the four neutrons are usually considered to form a full $0p_{3/2}$ subshell [17], whereas recent studies [18, 19, 20, 21] suggest a non-negligible presence of the paired-up double di-neutron structure $(0p_{3/2})^2(0p_{1/2})^2$.

As for the geometric configurations of ^{8}He, we intend to extend the results obtained for two-particle systems to a general 0^+ state of four correlated identical particles in p shells, and find the connection with the two particle case, i.e. ^{6}He.(Chapter 5).

2

Two-particle correlations

2.1 Description of the approach

2.1.1 Choice of the LS-coupling scheme

Most of the calculations concerning two-particle correlations in this chapter will be done in the LS-coupling scheme. Although nuclear physicists, after the introduction of the nucleonic spin-orbital interaction by Mayer [22] and by Jensen *et al.* [23], have been converted to adopting the jj coupling scheme, the alternative LS coupling still has arguments in favor of it. One argument is that it allows a clear separation between spin and spatial degrees of freedom. One of the basic properties of nucleon-nucleon interactions is its short-range, attractive character which favors spatial symmetry and its consequences are most easily understood in LS coupling. To see why, let us consider a special case, an extreme limit of short-range interactions, the δ interaction that we will discuss later in detail. The δ interaction $\delta(\vec{r}_1 - \vec{r}_2)$ has non-vanishing two-body interaction matrix elements only between the space symmetric states with $S = 0, T = 1$, or $S = 1, T = 0$. Another argument is that realistic two-body shell-model interactions, such as

the USD interaction for the *sd* shell [24] and the GX1A interaction for the *pf* shell [25], have matrix elements more diagonal in *LS*-coupling than they are in *jj*-coupling. Last but not least, light nuclei (in the $0p$ shell and the beginning of $1s0d$ shell), to a good approximation can be classified in *LS* coupling [26].

2.1.2 Two-particle correlation functions

Since our intention is to learn about the spatial structure of two valence nucleons outside a much stabler core, as in the case of ^{6}He, one choice of physical observables to probe is the relative distance between the two nucleons and the distance between the core and the center of mass (henceforth denoted by CM) of the two nucleons[†]. Consequently, the expectation values of δ functions will be called two-particle correlation functions. A typical two-particle correlation function corresponds to the expectation value of $\delta(\vec{r}-\vec{r}_{12})$, where $\vec{r}_{12} \equiv \vec{r}_1 - \vec{r}_2$ is the difference between the position vectors of the two particles, $\vec{r}_1$ and $\vec{r}_2$, and $\vec{r}$ an arbitrary vector. The expectation value of this operator, multiplied with the appropriate volume element, measures the probability of finding the pair of particles separated by $\vec{r}$. Here one is only interested in this probability as a function of the distance $r_{12} \equiv |\vec{r}_1 - \vec{r}_2|$ between the two particles which then involves the operator $\delta(r - r_{12})$. Also, it is often useful to probe in addition the distance of the pair of particles from the core and this can be achieved by calculating the expectation value of $\delta(r - r_{12})\delta(R - R_{12})$ where $R_{12} \equiv |\vec{r}_1 + \vec{r}_2|/2$ is the radial coordinate of the CM of the two particles.

These notions can be defined for any quantum-mechanical many-body state in which case we define the correlation functions

$$
\begin{aligned}
C_{\alpha\alpha'}(\vec{r}) &\equiv \langle\alpha| \sum_{i>j=1}^{n} \delta(\vec{r}-\vec{r}_{ij})|\alpha'\rangle, \\
C_{\alpha\alpha'}(r) &\equiv \langle\alpha| \sum_{i>j=1}^{n} \delta(r-r_{ij})|\alpha'\rangle,
\end{aligned}
$$

[†]The CM issue will be discussed later.

$$C_{\alpha\alpha'}(r,R) \equiv \langle\alpha| \sum_{i>j=1}^{n} \delta(r-r_{ij})\delta(R-R_{ij})|\alpha'\rangle, \tag{2.1.1}$$

where the sum is over all particles in the many-body states $|\alpha\rangle$ and $|\alpha'\rangle$ with n particles, characterized by a set of quantum numbers, collectively denoted as α or α', and typically comprising the total orbital angular momentum L, the total spin S, the total angular momentum J and its projection M. It will often be convenient to refer to all correlation functions (2.1.1) simultaneously, in which case the notation $C_{\alpha\alpha'}$ will be used. The interpretation of $C_{\alpha\alpha'}$ as a probability distribution is valid in the diagonal case, $\alpha = \alpha'$, but expressions of the non-diagonal matrix elements are needed as well in the following. As the operators $\delta(r-r_{12})$ and $\delta(r-r_{12})\delta(R-R_{12})$ are scalar under rotation, their matrix elements are diagonal in J as well as in M. This is not the case for the operator $\delta(\vec{r}-\vec{r}_{12})$, which therefore leads to more complicated expressions for its matrix elements. Correlation functions satisfy the normalization conditions

$$\begin{aligned}
&\int_{\mathfrak{Re}^3} C_\alpha(\vec{r})d\vec{r} = \frac{n(n-1)}{2},\\
&4\pi\int_0^{+\infty} C_\alpha(r)r^2dr = \frac{n(n-1)}{2},\\
&16\pi^2\int_0^{+\infty} r^2dr\int_0^{+\infty} C_\alpha(r,R)R^2dR = \frac{n(n-1)}{2},\\
&\int_{\mathfrak{Re}^3} C_{\alpha\alpha'}(\vec{r})d\vec{r} = 0,\\
&\int_0^{+\infty} C_{\alpha\alpha'}(r)r^2dr = 0,\\
&\int_0^{+\infty} r^2dr\int_0^{+\infty} C_{\alpha\alpha'}(r,R)R^2dR = 0,
\end{aligned} \tag{2.1.2}$$

where the notation $C_\alpha \equiv C_{\alpha\alpha}$ is used. Note that these are generic conditions, valid for any of the correlation functions that will be derived below.

2.2 Two identical particles in LS-coupling

We begin with some elementary definitions, mainly to fix our notation. A single-particle state is determined by its spatial part $\phi_{n\ell m_\ell}(\vec{r}) \equiv \phi_{n\ell m_\ell}(r,\theta,\varphi) = \mathcal{R}_{n\ell}(r)\mathcal{Y}_{\ell m_\ell}(\theta,\varphi)$, characterized by the radial quantum number n, the orbital angular momentum ℓ, and its projection m_ℓ, multiplied with the spinor $\chi_{1/2,m_s}$ with $m_s = \pm\frac{1}{2}$ in units of $\hbar$. For two nucleons of the same type, as is the case of the halo neutrons of ^{6}He, the single-particle isospin projection on z is ± 1, and the total isopin is $T = 1$. In such a case, a two-nucleon state in LS coupling is denoted by $|n_1\ell_1\tfrac{1}{2}, n_2\ell_2\tfrac{1}{2}; LSJM_J\rangle \equiv |n_1\ell_1 n_2\ell_2; LSJM_J\rangle$. As the particles always have $s = \frac{1}{2}$, their spins are not shown explicitly but their coupled value is indicated as S.

When the two identical particles ($T = 1$) are in the same $n\ell$ orbital, the values of the total orbital angular momentum L and the total spin S are restricted by the overall antisymmetry of the wave function, that is, even L for $S = 0$ (spatially symmetric) and odd L for $S = 1$ (spatially antisymmetric). Since the operators $\delta(r - r_{12})$ and $\delta(r - r_{12})\delta(R - R_{12})$ are diagonal in the spin quantum numbers, the correlation functions only depend on the orbital angular momenta ℓ and L. Note, however, that allowed values of L are determined by S, so there exists an *indirect* dependence on the total spin of the two particles. For completeness the total angular momentum J, obtained from the coupling of L and S, and its projection M_J can also be given.

2.2.1 Talmi-Moshinsky transformation

The evaluation of the correlation functions $C_{\alpha\alpha'}$ is significantly simplified if the particles are placed in a harmonic-oscillator potential. The simplification arises because for the harmonic oscillator the transformation from the individual particle coordinates $\vec{r}_1$ and $\vec{r}_2$ to the relative and CM coordinates, $\vec{r}_{12} = (r_{12},\theta_{12},\varphi_{12}) \equiv \vec{r}_1 - \vec{r}_2$ and $\vec{R}_{12} = (R_{12},\Theta_{12},\Phi_{12}) \equiv (\vec{r}_1 + \vec{r}_2)/2$, can be carried

out by means of Talmi-Moshinsky brackets [27, 28, 29] that can be calculated with an efficient algorithm [30].

We recall that a Talmi-Moshinsky bracket, denoted here by $a^{n_1\ell_1 n_2\ell_2}_{n\ell\mathcal{N}\mathcal{L},L}$, is characterized by the radial and orbital quantum numbers of the two particles ($n_1\ell_1$ and $n_2\ell_2$), the similar quantum numbers pertaining to the relative and CM coordinates ($n\ell$ and $\mathcal{N}\mathcal{L}$), and the coupled angular momentum L,

$$\begin{aligned}
&\langle\vec{r}_1,\vec{r}_2|n_1\ell_1 n_2\ell_2;LM_L\rangle \\
&= \sum_{n\ell\mathcal{N}\mathcal{L}} a^{n_1\ell_1 n_2\ell_2}_{n\ell\mathcal{N}\mathcal{L},L}\langle\vec{r}_{12}/\sqrt{2},\sqrt{2}\vec{R}_{12}|n\ell\mathcal{N}\mathcal{L};LM_L\rangle \\
&= \sum_{n\ell\mathcal{N}\mathcal{L}} a^{n_1\ell_1 n_2\ell_2}_{n\ell\mathcal{N}\mathcal{L},L}[\phi_{n\ell}(\vec{r}_{12}/\sqrt{2})\otimes\phi_{\mathcal{N}\mathcal{L}}(\sqrt{2}\vec{R}_{12})]^{(L)}_{M_L} \\
&= \sum_{n\ell\mathcal{N}\mathcal{L}} a^{n_1\ell_1 n_2\ell_2}_{n\ell\mathcal{N}\mathcal{L},L}\mathcal{R}_{n\ell}(r_{12}/\sqrt{2})\mathcal{R}_{\mathcal{N}\mathcal{L}}(\sqrt{2}R_{12})[\mathcal{Y}_\ell(\theta_{12},\varphi_{12})\otimes\mathcal{Y}_\mathcal{L}(\Theta_{12},\Phi_{12})]^{(L)}_{M_L}.
\end{aligned} \tag{2.2.1}$$

The number of oscillator quanta is the same before and after the transformation which translates into the condition $2n_1+\ell_1+2n_2+\ell_2 = 2n+\ell+2\mathcal{N}+\mathcal{L}$. In these expressions $\mathcal{R}_{n\ell}(r)$ is the radial wave function of the harmonic oscillator [1] with r expressed in units of the oscillator length $b=\sqrt{\hbar/m\omega}$ where m is the nucleon mass and ω the oscillator frequency. Note that we follow the conventions of Barber and Cooper [30] for the definition of Talmi-Moshinsky brackets, which is different from those used by Brody and Moshinsky [31]. The latter does not have the scale factors $\sqrt{2}$ and $1/\sqrt{2}$ for r and R respectively.

2.2.2 Expressions of the correlation function matrix elements

When dealing with composite wave functions and spherical tensor operators, one can resort to the Wigner-Eckart theorem in order to separate out the dependence of matrix elements on the projection m, and the reduction rules for spherical tensor operators to reduce the matrix elements to basic one-body matrix elements [1]. The Wigner-Eckart theorem and the reduction rules facilitate

the evaluation of the matrix elements of correlation functions.

a. Calculation of $C_{\alpha\alpha'}(\vec{r})$

By use of the multipole expansion

$$\delta(\vec{r}-\vec{r}_{12}) = \frac{\delta(r-r_{12})}{r r_{12}} \sum_{\lambda\mu} \mathcal{Y}^*_{\lambda\mu}(\theta,\varphi)\mathcal{Y}_{\lambda\mu}(\theta_{12},\varphi_{12}), \tag{2.2.2}$$

the first of the correlation functions (2.1.1) can be expressed as

$$\begin{aligned}
&\langle n_1\ell_1 n_2\ell_2; LM_L SM_S|\delta(\vec{r}-\vec{r}_{12})|n_1'\ell_1' n_2'\ell_2'; L'M_L' S'M_S'\rangle \\
&= \delta_{SS'}\delta_{M_S M_S'}(-)^{L+L'-M_L}\left[\frac{(2L+1)(2L'+1)}{32\pi}\right]^{1/2}\sum_{\lambda\mu}(-)^{\lambda}\sqrt{2\lambda+1}\begin{pmatrix} L & \lambda & L' \\ -M_L & \mu & M_L' \end{pmatrix} \\
&\quad\times\mathcal{Y}^*_{\lambda\mu}(\theta,\varphi)\sum_{n\ell n'\ell'\mathcal{N}\mathcal{L}}(-)^{\mathcal{L}}\sqrt{(2\ell+1)(2\ell'+1)}\, a^{n_1\ell_1 n_2\ell_2}_{n\ell\mathcal{N}\mathcal{L},L}\, a^{n_1'\ell_1' n_2'\ell_2'}_{n'\ell'\mathcal{N}\mathcal{L},L'} \\
&\qquad\times\begin{pmatrix} \ell & \lambda & \ell' \\ 0 & 0 & 0 \end{pmatrix}\begin{Bmatrix} \ell & L & \mathcal{L} \\ L' & \ell' & \lambda \end{Bmatrix}\mathcal{R}_{n\ell}(r/\sqrt{2})\mathcal{R}_{n'\ell'}(r/\sqrt{2}),
\end{aligned} \tag{2.2.3}$$

where the symbols in round and curly brackets are Wigner $3j$ symbols and Racah coefficients, respectively [1].

b. Calculation of $C_{\alpha\alpha'}(r)$

The correlation function $C_{\alpha\alpha'}(r)$ is independent of the polar and azimuthal angles, allowing a simpler expression of matrix element:

$$\begin{aligned}
&\langle n_1\ell_1 n_2\ell_2; LM_L SM_S|\delta(r-r_{12})|n_1'\ell_1' n_2'\ell_2'; L'M_L' S'M_S'\rangle \\
&= \delta_{SS'}\delta_{M_S M_S'}\delta_{LL'}\delta_{M_L M_L'}\int_{\mathfrak{Re}^3} d\vec{R}_{12}\int_{\mathfrak{Re}^3} d\vec{r}_{12}\sum_{n\ell\mathcal{N}\mathcal{L}} a^{n_1\ell_1 n_2\ell_2}_{n\ell\mathcal{N}\mathcal{L},L}\langle n\ell\mathcal{N}\mathcal{L}; LM_L|\vec{r}_{12}/\sqrt{2}, \sqrt{2}\vec{R}_{12}\rangle \\
&\times\delta(r-r_{12})\sum_{n'\ell'\mathcal{N}'\mathcal{L}'} a^{n_1'\ell_1' n_2'\ell_2'}_{n'\ell'\mathcal{N}'\mathcal{L}',L}\langle\vec{r}_{12}/\sqrt{2}, \sqrt{2}\vec{R}_{12}|n'\ell'\mathcal{N}'\mathcal{L}'; LM_L\rangle.
\end{aligned} \tag{2.2.4}$$

When expressed in spherical coordinates, Eq.(2.2.4) takes the following form:

$$
\begin{aligned}
&\langle n_1\ell_1 n_2\ell_2; LM_L SM_S|\delta(r-r_{12})|n_1'\ell_1' n_2'\ell_2'; L'M_L' S'M_S'\rangle \\
&= \delta_{SS'}\delta_{M_S M_S'}\delta_{LL'}\delta_{M_L M_L'} \\
&\times \int_0^{+\infty} R_{12}^2 dR_{12} \int_0^{\pi} \sin\Theta_{12} d\Theta_{12} \int_0^{2\pi} d\Phi_{12} \int_0^{+\infty} r_{12}^2 dr_{12} \int_0^{\pi} \sin\theta_{12} d\theta_{12} \int_0^{2\pi} d\phi_{12} \\
&\times \sum_{n\ell\mathcal{N}\mathcal{L}} a_{n\ell\mathcal{N}\mathcal{L},L}^{n_1\ell_1 n_2\ell_2} \langle n\ell\mathcal{N}\mathcal{L}; LM_L|r_{12}/\sqrt{2}, \theta_{12}, \phi_{12}, \sqrt{2}R_{12}, \Theta_{12}, \Phi_{12}\rangle \delta(r-r_{12}) \\
&\times \sum_{n'\ell'\mathcal{N}'\mathcal{L}'} a_{n'\ell'\mathcal{N}'\mathcal{L}',L}^{n_1'\ell_1' n_2'\ell_2'} \langle r_{12}/\sqrt{2}, \theta_{12}, \phi_{12}, \sqrt{2}R_{12}, \Theta_{12}, \Phi_{12}|n'\ell'\mathcal{N}'\mathcal{L}'; LM_L\rangle. \qquad (2.2.5)
\end{aligned}
$$

The radial and angular parts can then be evaluated separately. It follows from the closure relation that:

$$
\int_0^{+\infty} R_{12}^2 |\sqrt{2}R_{12}\rangle\langle\sqrt{2}R_{12}| dR_{12} = \frac{1}{2\sqrt{2}}\hat{1}.
$$

One also has

$$
\int_0^{+\infty} r_{12}^2 |r_{12}/\sqrt{2}\rangle \delta(r-r_{12}) \langle r_{12}/\sqrt{2}| dr_{12} = |r/\sqrt{2}\rangle r^2 \langle r/\sqrt{2}|.
$$

Eq.(2.2.5), then, can be expressed in the bra-ket notation:

$$
\begin{aligned}
&\langle n_1\ell_1 n_2\ell_2; LM_L SM_S|\delta(r-r_{12})|n_1'\ell_1' n_2'\ell_2'; L'M_L' S'M_S'\rangle \\
&= \frac{1}{2\sqrt{2}} \delta_{SS'}\delta_{M_S M_S'}\delta_{LL'}\delta_{M_L M_L'} r^2 \sum_{n\ell\mathcal{N}\mathcal{L}} \sum_{n'\ell'\mathcal{N}'\mathcal{L}'} a_{n\ell\mathcal{N}\mathcal{L},L}^{n_1\ell_1 n_2\ell_2} a_{n'\ell'\mathcal{N}'\mathcal{L}',L}^{n_1'\ell_1' n_2'\ell_2'} \\
&\times \langle n\ell\mathcal{N}\mathcal{L}; LM_L|r/\sqrt{2}\rangle\langle r/\sqrt{2}|n'\ell'\mathcal{N}'\mathcal{L}'; LM_L\rangle, \qquad (2.2.6)
\end{aligned}
$$

which leads to:

$$
\begin{aligned}
&\langle n_1\ell_1 n_2\ell_2; LM_L SM_S|\delta(r-r_{12})|n_1'\ell_1' n_2'\ell_2'; L'M_L' S'M_S'\rangle \\
&= \frac{1}{2\sqrt{2}} \delta_{SS'}\delta_{M_S M_S'}\delta_{LL'}\delta_{M_L M_L'} r^2 \sum_{n\ell\mathcal{N}\mathcal{L}} \sum_{n'\ell'\mathcal{N}'\mathcal{L}'} a_{n\ell\mathcal{N}\mathcal{L},L}^{n_1\ell_1 n_2\ell_2} a_{n'\ell'\mathcal{N}'\mathcal{L}',L}^{n_1'\ell_1' n_2'\ell_2'}
\end{aligned}
$$

$$
\begin{aligned}
&\times \sum_{\substack{m_1 m_2 \\ m_1' m_2'}} \langle \ell m_1 \mathcal{L} m_2 | L M_L \rangle \langle \ell' m_1' \mathcal{L}' m_2' | L M_L \rangle \langle n \ell m_1 \mathcal{N} \mathcal{L} m_2 | r/\sqrt{2} \rangle \langle r/\sqrt{2} | n' \ell' m_1' \mathcal{N}' \mathcal{L}' m_2' \rangle \\
&= \frac{1}{2\sqrt{2}} \delta_{SS'} \delta_{M_S M_S'} \delta_{LL'} \delta_{M_L M_L'} r^2 \sum_{n \ell \mathcal{N} \mathcal{L}} \sum_{n' \ell' \mathcal{N}' \mathcal{L}'} a^{n_1 \ell_1 n_2 \ell_2}_{n \ell \mathcal{N} \mathcal{L}, L} a^{n_1' \ell_1' n_2' \ell_2'}_{n' \ell' \mathcal{N}' \mathcal{L}', L} \\
&\times \sum_{\substack{m_1 m_2 \\ m_1' m_2'}} \langle \ell m_1 \mathcal{L} m_2 | L M_L \rangle \langle \ell' m_1' \mathcal{L}' m_2' | L M_L \rangle \langle n \ell m_1 | r/\sqrt{2} \rangle \langle r/\sqrt{2} | n' \ell' m_1' \rangle \langle \mathcal{N} \mathcal{L} m_2 | \mathcal{N}' \mathcal{L}' m_2' \rangle \\
&= \frac{1}{2\sqrt{2}} \delta_{SS'} \delta_{M_S M_S'} \delta_{LL'} \delta_{M_L M_L'} \delta_{\ell \ell'} r^2 \sum_{n \ell \mathcal{N} \mathcal{L}} \sum_{n' \ell' \mathcal{N}' \mathcal{L}'} \delta_{\mathcal{N} \mathcal{N}'} \delta_{\mathcal{L} \mathcal{L}'} a^{n_1 \ell_1 n_2 \ell_2}_{n \ell \mathcal{N} \mathcal{L}, L} a^{n_1' \ell_1' n_2' \ell_2'}_{n' \ell \mathcal{N} \mathcal{L}, L} \\
&\times \sum_{\substack{m_1 m_2 \\ m_1' m_2'}} \delta_{m_1 m_1'} \delta_{m_2 m_2'} \langle \ell m_1 \mathcal{L} m_2 | L M_L \rangle^2 \langle n \ell m_1 | r/\sqrt{2} \rangle \langle r/\sqrt{2} | n' \ell m_1 \rangle \\
&= \frac{1}{2\sqrt{2}} \delta_{SS'} \delta_{M_S M_S'} \delta_{LL'} \delta_{M_L M_L'} r^2 \sum_{n n' \ell \mathcal{N} \mathcal{L}} a^{n_1 \ell_1 n_2 \ell_2}_{n \ell \mathcal{N} \mathcal{L}, L} a^{n_1' \ell_1' n_2' \ell_2'}_{n' \ell \mathcal{N} \mathcal{L}, L} \mathcal{R}_{n \ell}(r/\sqrt{2}) \mathcal{R}_{n' \ell}(r/\sqrt{2}).
\end{aligned}
\tag{2.2.7}
$$

The total number of oscillator quanta is conserved, entailing the following relations:

$$
\begin{aligned}
2n_1 + \ell_1 + 2n_2 + \ell_2 &= 2n + \ell + 2\mathcal{N} + \mathcal{L}, \\
2n_1' + \ell_1' + 2n_2' + \ell_2' &= 2n' + \ell + 2\mathcal{N} + \mathcal{L},
\end{aligned}
\tag{2.2.8}
$$

from which it follows that $\ell_1 + \ell_2$, $\ell_1' + \ell_2'$ and $\ell + \mathcal{L}$ have the same parity.

c. Calculation of $C_{\alpha\alpha'}(r, R)$

In the same fashion, we obtain for $C_{\alpha\alpha'}(r, R)$ the matrix element

$$
\begin{aligned}
&\langle n_1 \ell_1 n_2 \ell_2; L M_L S M_S | \delta(r - r_{12}) \delta(R - R_{12}) | n_1' \ell_1' n_2' \ell_2'; L' M_L' S' M_S' \rangle \\
&\quad = \delta_{SS'} \delta_{M_S M_S'} \delta_{LL'} \delta_{M_L M_L'} r^2 R^2 \sum_{\substack{n n' \ell \\ \mathcal{N} \mathcal{N}' \mathcal{L}}} a^{n_1 \ell_1 n_2 \ell_2}_{n \ell \mathcal{N} \mathcal{L}, L} a^{n_1' \ell_1' n_2' \ell_2'}_{n' \ell \mathcal{N}' \mathcal{L}, L} \\
&\qquad \times \mathcal{R}_{n \ell}(r/\sqrt{2}) \mathcal{R}_{n' \ell}(r/\sqrt{2}) \mathcal{R}_{\mathcal{N} \ell}(\sqrt{2} R) \mathcal{R}_{\mathcal{N}' \ell}(\sqrt{2} R),
\end{aligned}
\tag{2.2.9}
$$

where

$$2n_1+\ell_1+2n_2+\ell_2 = 2n+\ell+2\mathcal{N}+\mathcal{L},$$
$$2n_1'+\ell_1'+2n_2'+\ell_2' = 2n'+\ell+2\mathcal{N}'+\mathcal{L}, \tag{2.2.10}$$

and $\ell_1+\ell_2$, $\ell_1'+\ell_2'$ and $\ell+\mathcal{L}$ have the same parity.

With $\delta(\vec{r}-\vec{r}_{12})$, $\delta(r-r_{12})$ and $\delta(r-r_{12})\delta(R-R_{12})$ being spin-independent scalar observables, the factor $\delta_{SS'}\delta_{LL'}\delta_{M_L M_L'}$ arises naturally in the expressions of correlation functions.

2.2.3 Antisymmetrization

The above expressions are valid if particle 1 is in orbital $n_1\ell_1$ ($n_1'\ell_1'$) and particle 2 in orbital $n_2\ell_2$ ($n_2'\ell_2'$), that is, for non-antisymmetrized states in the bra and the ket. Since we deal with identical particles with $T=1$, states must be antisymmetrized. An normalized antisymmetrized state will be denoted by $|n_1\ell_1 n_2\ell_2;LS\rangle_{\rm nas}$ and has the form:

$$\begin{aligned}|n_1\ell_1 n_2\ell_2;LS\rangle_{\rm nas} &= \frac{|n_1\ell_1 n_2\ell_2;LS\rangle - (-)^{\ell_1+\ell_2+1/2+1/2-L-S}|n_2\ell_2 n_1\ell_1;LS\rangle}{\sqrt{2(1+\delta_{n_1n_2}\delta_{\ell_1\ell_2})}}\\ &= \frac{|n_1\ell_1 n_2\ell_2;LS\rangle + (-)^{\ell_1+\ell_2-L-S}|n_2\ell_2 n_1\ell_1;LS\rangle}{\sqrt{2(1+\delta_{n_1n_2}\delta_{\ell_1\ell_2})}},\end{aligned} \tag{2.2.11}$$

leading to the following expression for the matrix element of any scalar operator $\hat{O}_{12}$ between antisymmetrized states in the same LS configuration:

$$\begin{aligned}{}_{\rm nas}\langle n_1\ell_1 n_2\ell_2;LS|\hat{O}_{12}|n_1'\ell_1' n_2'\ell_2';LS\rangle_{\rm nas} &= \frac{1}{2\sqrt{(1+\delta_{n_1n_2}\delta_{\ell_1\ell_2})(1+\delta_{n_1'n_2'}\delta_{\ell_1'\ell_2'})}}\\ \times\ \Big(&\langle n_1\ell_1 n_2\ell_2;LS|\hat{O}_{12}|n_1'\ell_1' n_2'\ell_2';LS\rangle + \sigma\langle n_2\ell_2 n_1\ell_1;LS|\hat{O}_{12}|n_1'\ell_1' n_2'\ell_2';LS\rangle\\ &+\sigma'\langle n_1\ell_1 n_2\ell_2;LS|\hat{O}_{12}|n_2'\ell_2' n_1'\ell_1';LS\rangle + \sigma\sigma'\langle n_2\ell_2 n_1\ell_1;LS|\hat{O}_{12}|n_2'\ell_2' n_1'\ell_1';LS\rangle\Big),\end{aligned} \tag{2.2.12}$$

where $\sigma = (-)^{\ell_1+\ell_2-L-S}$ and $\sigma' = (-)^{\ell_1'+\ell_2'-L-S}$. Changing the coupling order, we get a direct term and an exchange term:

$$
\begin{aligned}
{}_{\text{nas}}\langle n_1\ell_1 n_2\ell_2; LS|\hat{O}_{12}|n_1'\ell_1' n_2'\ell_2'; LS\rangle_{\text{nas}} &= \frac{1}{\sqrt{(1+\delta_{n_1 n_2}\delta_{\ell_1\ell_2})(1+\delta_{n_1' n_2'}\delta_{\ell_1'\ell_2'})}} \\
\times \quad &\Big(\langle n_1\ell_1 n_2\ell_2; LS|\hat{O}_{12}|n_1'\ell_1' n_2'\ell_2'; LS\rangle + \sigma'\langle n_2\ell_2 n_1\ell_1; LS|\hat{O}_{12}|n_1'\ell_1' n_2'\ell_2'; LS\rangle\Big).
\end{aligned}
\tag{2.2.13}
$$

In the case of states of two particles in the same $n\ell$ orbital, the expression (2.2.13) can be simplified. Finally, three cases can be distinguished:

$$
\begin{aligned}
{}_{\text{nas}}\langle n_1\ell_1 n_2\ell_2; LS|\hat{O}_{12}|n_1'\ell_1' n_2'\ell_2'; LS\rangle_{\text{nas}} &= \langle n_1\ell_1 n_2\ell_2; LS|\hat{O}_{12}|n_1'\ell_1' n_2'\ell_2'; LS\rangle \\
&\quad +\sigma'\langle n_2\ell_2 n_1\ell_1; LS|\hat{O}_{12}|n_1'\ell_1' n_2'\ell_2'; LS\rangle, \\
{}_{\text{nas}}\langle n_1\ell_1 n_2\ell_2; LS|\hat{O}_{12}|n'\ell' n'\ell'; LS\rangle_{\text{nas}} &= \sqrt{2}\langle n_1\ell_1 n_2\ell_2; LS|\hat{O}_{12}|n'\ell' n'\ell'; LS\rangle, \\
{}_{\text{nas}}\langle n\ell n\ell; LS|\hat{O}_{12}|n'\ell' n'\ell'; LS\rangle_{\text{nas}} &= \langle n\ell n\ell; LS|\hat{O}_{12}|n'\ell' n'\ell'; LS\rangle,
\end{aligned}
\tag{2.2.14}
$$

where it is assumed that $(n_1\ell_1) \neq (n_2\ell_2)$ and $(n_1'\ell_1') \neq (n_2'\ell_2')$.

2.2.4 Correlation functions within a single orbital: $C_\alpha(r, R)$

With these preliminaries we can investigate the correlation functions of a pair of particles in different configurations. We start with a single orbital, and plot the correlation function $C_{(n\ell)^2;LS}(r,R) \equiv \langle (n\ell)^2; LS|\delta(r-r_{12})\delta(R-R_{12})|(n\ell)^2; LS\rangle$. It is worth mentioning that such a correlation function possesses a symmetry generated by the parity with respect to reflection about origin inherent in spherical harmonics. Let Π represent the parity operator that takes $\vec{r}$ to $-\vec{r}$:

$$
\Pi|\vec{r}\rangle = |-\vec{r}\rangle. \tag{2.2.15}
$$

It is hermitian

$$\Pi^\dagger = \Pi, \tag{2.2.16}$$

and has eigenvalues ± 1. The operator Π^2 is the identity operator

$$\Pi^2|\vec{r}\rangle = \Pi|-\vec{r}\rangle = |\vec{r}\rangle, \tag{2.2.17}$$

We differentiate parity operators for different particles by the subscript i, e.g. Π_1 is the parity operator for the first nucleon, and evaluate the matrix element $\langle (n\ell)^2; LS|\Pi_1 \delta(r - r_{12})\delta(R - R_{12})|(n\ell)^2; LS\rangle$.

$$\begin{aligned}
&\langle (n\ell)^2; LS|\Pi_1 \delta(r - r_{12})\delta(R - R_{12})|(n\ell)^2; LS\rangle \\
&= \langle (n\ell)^2; LS|\Big(\Pi_1 \delta(r - r_{12})\delta(R - R_{12})|(n\ell)^2; LS\rangle\Big) \\
&= \langle (n\ell)^2; LS|\left(\Pi_1 \delta(r - \left|\vec{r}_1 - \vec{r}_2\right|)\delta(R - \frac{\left|\vec{r}_1 + \vec{r}_2\right|}{2})|(n\ell)^2; LS\rangle\right) \\
&= \langle (n\ell)^2; LS|\delta(r - \left|-\vec{r}_1 - \vec{r}_2\right|)\delta(R - \frac{\left|-\vec{r}_1 + \vec{r}_2\right|}{2})\Pi_1|(n\ell)^2; LS\rangle \\
&= \langle (n\ell)^2; LS|\delta(r - 2R_{12})\delta(R - \frac{r_{12}}{2})\Pi_1|(n\ell)^2; LS\rangle \\
&= (-1)^\ell \langle (n\ell)^2; LS|\delta(\frac{r}{2} - R_{12})\delta(2R - r_{12})|(n\ell)^2; LS\rangle.
\end{aligned} \tag{2.2.18}$$

The last line follows from the fact that spherical harmonics have the parity of $(-1)^\ell$.

On the other hand, since Π is hermitian, we also have

$$\begin{aligned}
&\langle (n\ell)^2; LS|\Pi_1 \delta(r - r_{12})\delta(R - R_{12})|(n\ell)^2; LS\rangle \\
&= \Big(\langle (n\ell)^2; LS|\Pi_1\Big)\delta(r - r_{12})\delta(R - R_{12})|(n\ell)^2; LS\rangle \\
&= (-1)^\ell \langle (n\ell)^2; LS|\delta(r - r_{12})\delta(R - R_{12})|(n\ell)^2; LS\rangle.
\end{aligned} \tag{2.2.19}$$

Equating the last line of Eq. (2.2.18) with that of Eq. (2.2.19), we get

$$\begin{aligned}&\langle (n\ell)^2; LS|\delta(\frac{r}{2}-R_{12})\delta(2R-r_{12})|(n\ell)^2; LS\rangle \\ &\qquad = \langle (n\ell)^2; LS|\delta(r-r_{12})\delta(R-R_{12})|(n\ell)^2; LS\rangle, \end{aligned} \tag{2.2.20}$$

or

$$C_\alpha(r,R) = C_\alpha(2R,\frac{r}{2}), \tag{2.2.21}$$

a "reflection-like" symmetry about the plane defined by $r = 2R$ that will be frequently encountered throughout this section.

a. The s orbitals

Fig. 2.1 shows the correlation functions for different s orbitals. The fact that the total spin S has to be 0 signifies that the spatial wave function must be symmetric. For $|(ns)^2; 00\rangle$ with different radial quantum numbers n, $n+1$ maxima (peaks) are observed. The $n+1$ maxima are positioned on $n+1$ concentric circles radiating out from the center and all lie on the line $r = 2R$. In each figure, the farther the peaks are from the origin, the higher they are. The pattern of the recurring peaks can be easily understood as the effect of nodes inherent to radial wave functions, that is, a radial wave function characterized by the quantum number n has n nodes and hence $n+1$ maxima.

b. The $0p$ orbital

The three possible configurations for the $0p$ shell are $LS = 00, 11, 20$ whose correlation functions are shown in Fig. 2.2. Two maxima are observed for $|(0p)^2; 00\rangle$; one for $|(0p)^2; 11\rangle$, whereas an indistinct coexistence of two maxima can be perceived in the $|(0p)^2; 20\rangle$ plot.

A closer look at the expressions of correlation functions of the three possible

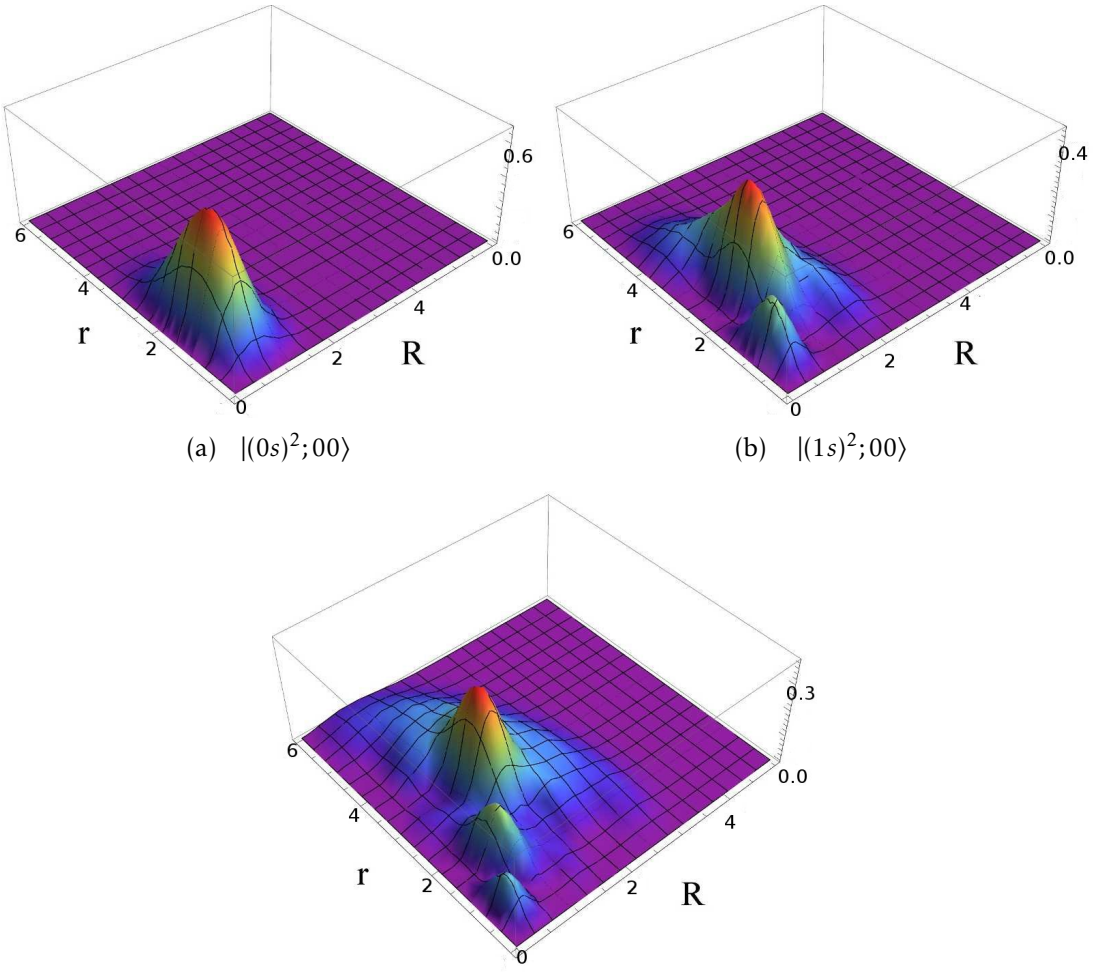

(a) $|(0s)^2;00\rangle$ (b) $|(1s)^2;00\rangle$

(c) $|(2s)^2;00\rangle$

Figure 2.1: The correlation function $C_\alpha(r,R)$ for different s-orbital two-particle configurations.

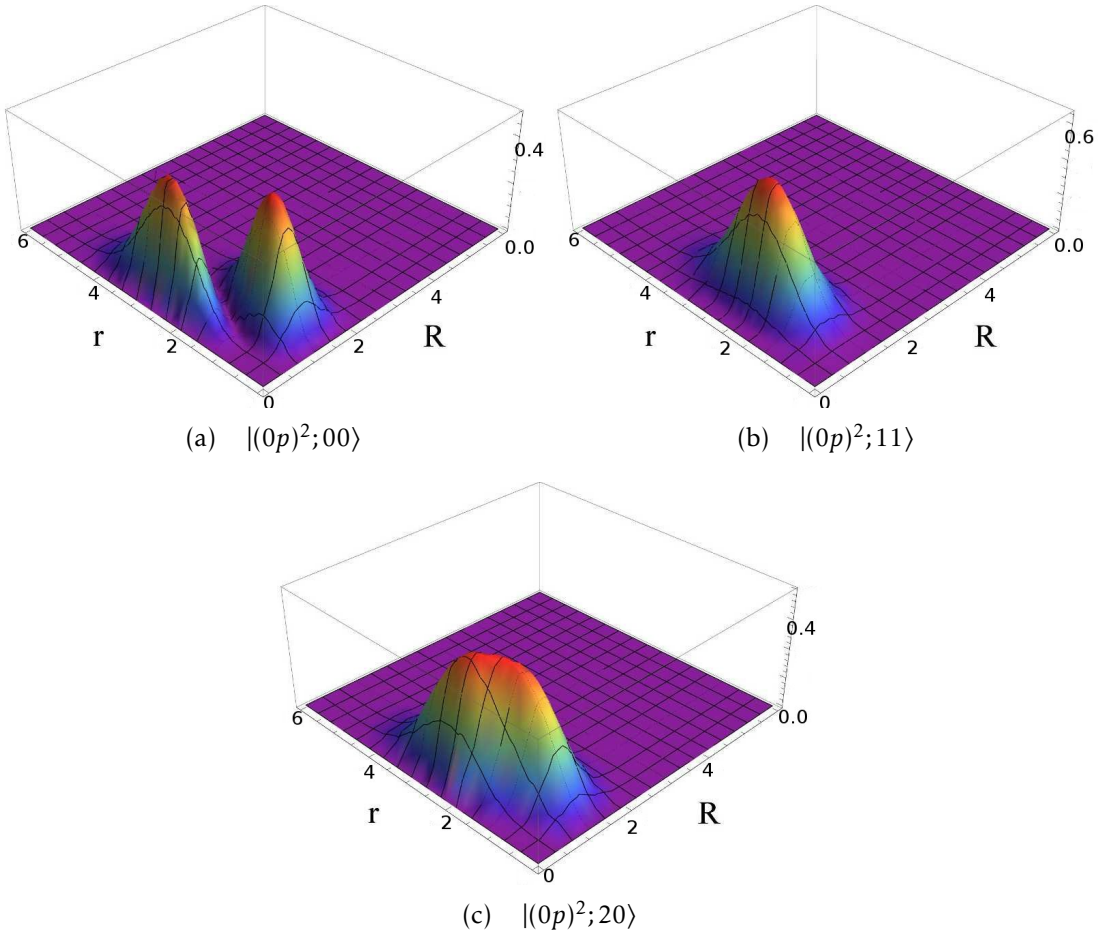

(a) $|(0p)^2;00\rangle$ (b) $|(0p)^2;11\rangle$

(c) $|(0p)^2;20\rangle$

Figure 2.2: The correlation function $C_\alpha(r,R)$ for different two-particle configurations in the $0p$ orbital.

states in the $0p$ orbital may shed some light on these results. If we substitute the dimensionless r and R for r/b and R/b respectively, the correlation functions for the three configurations become:

$$C_{(0p)^2;00}(r,R) = \frac{4}{3\pi}(e^{-\frac{r^2}{2}-2R^2}r^6R^2 - 8e^{-\frac{r^2}{2}-2R^2}r^4R^4 + 16e^{-\frac{r^2}{2}-2R^2}r^2R^6), \tag{2.2.22}$$

$$C_{(0p)^2;11}(r,R) = \frac{64}{9\pi}e^{-\frac{r^2}{2}-2R^2}r^4R^4, \tag{2.2.23}$$

$$C_{(0p)^2;20}(r,R) = \frac{8}{15\pi}(e^{-\frac{r^2}{2}-2R^2}r^6R^2 + 16e^{-\frac{r^2}{2}-2R^2}r^2R^6). \tag{2.2.24}$$

As expected from the relation in Eq. (2.2.21), the correlation function $C_{(0p)^2;00}(r,R)$ has two maxima at

$$(r,R) = \left(\sqrt{2(2-\sqrt{2})}, \sqrt{\frac{1}{2}(2+\sqrt{2})}\right) \qquad \text{and}$$
$$(r,R) = \left(\sqrt{2(2+\sqrt{2})}, \sqrt{\frac{1}{2}(2-\sqrt{2})}\right),$$

and $C_{(0p)^2;11}(r,R)$ has only one at (r,R)=$(2,1)$. As for $C_{(0p)^2;20}(r,R)$, it is a linear combination of $C_{(0p)^2;00}(r,R)$ and $C_{(0p)^2;11}(r,R)$:

$$C_{(0p)^2;20}(r,R) = \frac{2}{5}C_{(0p)^2;00}(r,R) + \frac{3}{5}C_{(0p)^2;11}(r,R), \tag{2.2.25}$$

which explains the vaguely perceivable two-maximum structure.

c. The $1p$ orbital

By analogy with the correlation functions of ns orbital particles, we expect to see, for the $1p$ orbital, that each plot in Fig. 2.2 is repeated in an approximate way on a circle farther away from the origin with higher peaks. This is confirmed by the plots in Fig. 2.3.

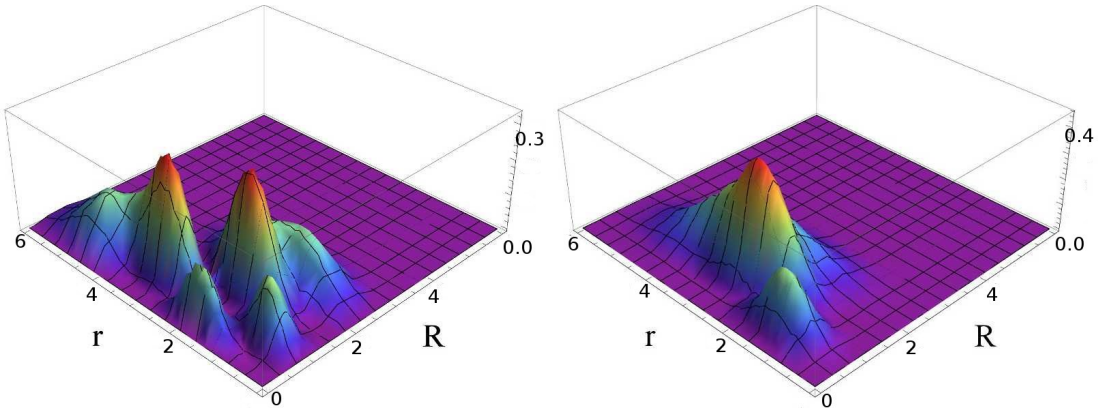

(a) $|(1p)^2;00\rangle$

(b) $|(1p)^2;11\rangle$

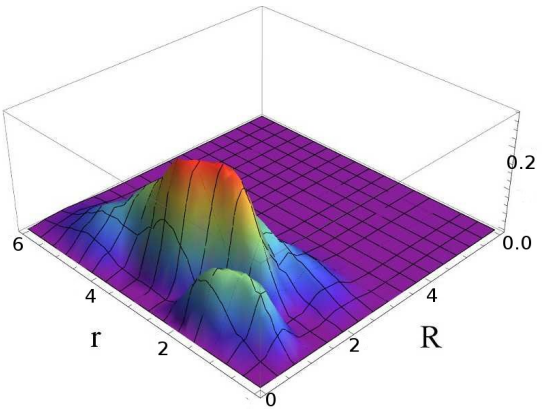

(c) $|(1p)^2;20\rangle$

Figure 2.3: The correlation function $C_\alpha(r,R)$ for different two-particle configurations in the $1p$ orbital.

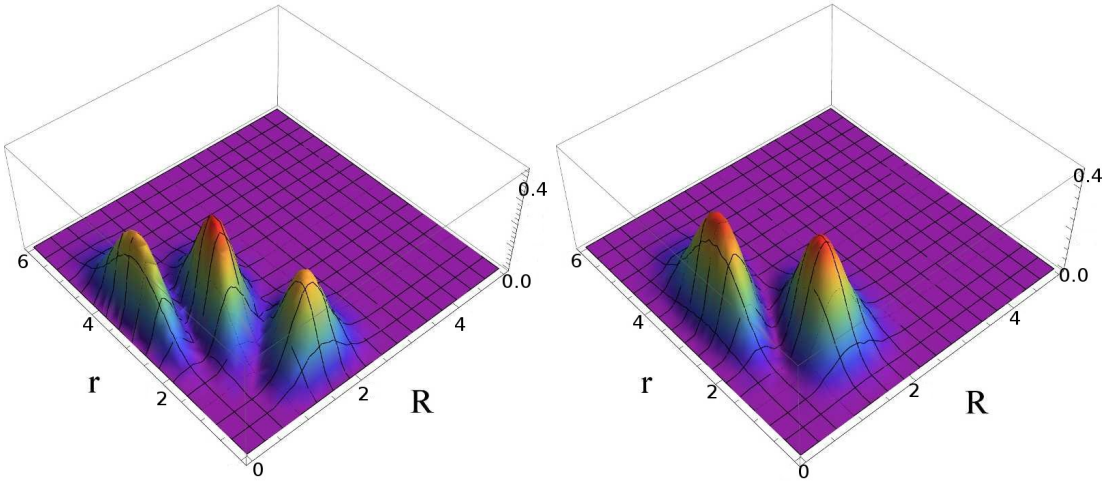

(a) $|(0d)^2;00\rangle$ (b) $|(0d)^2;11\rangle$

d. The $0d$ orbital

In addition to the pattern concerning the radial quantum number n, as one goes to higher orbitals, another pattern related to ℓ shows up. Examining the correlation functions for configurations in the $0d$ orbital in Fig. 2.4, we notice that as ℓ increases by 1 from p to d, for the $LS = 00$ state, we get one more maximum. Indeed, if we think back to what has been observed previously for s and p orbitals, when coupled to $LS = 00$, a pair of particles possesses one more maximum in the $0p$ orbital than in the $0s$ orbital. One is tempted to speculate that the number of peaks is related to ℓ and is equal to $\ell + 1$. A third pattern worth mentioning is that for the first few coupled configurations of a certain orbital, the number of maxima decreases by one as the total angular momentum L increases by one.

e. The $0f$ orbital

The patterns described above are confirmed as one examines other orbitals. For the $0f$ orbital, as shown in Fig. 2.5, the $LS = 00$, 11 and 20 configurations display four, three and two maxima respectively. For high total momenta the plots are less distinctly defined.

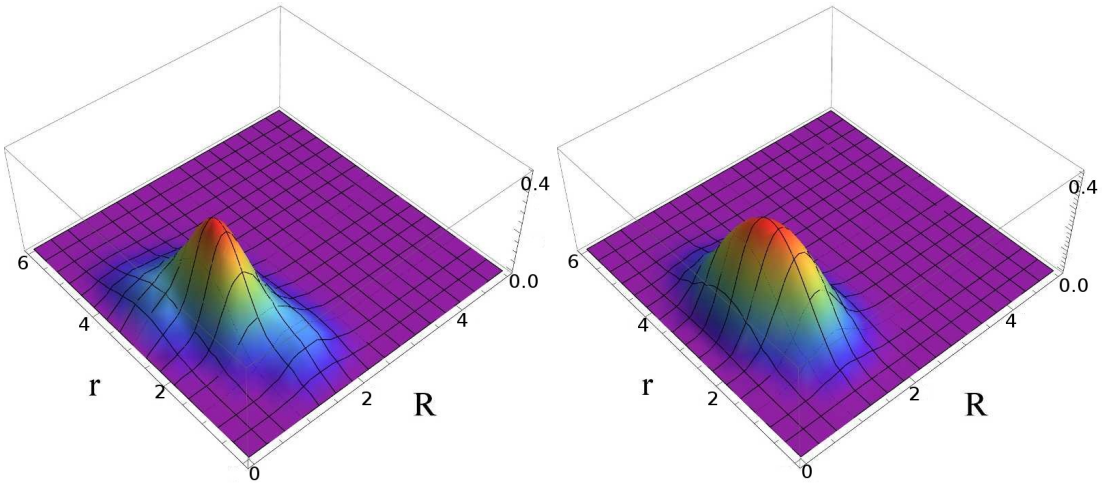

(c) $|(0d)^2;20\rangle$

(d) $|(0d)^2;31\rangle$

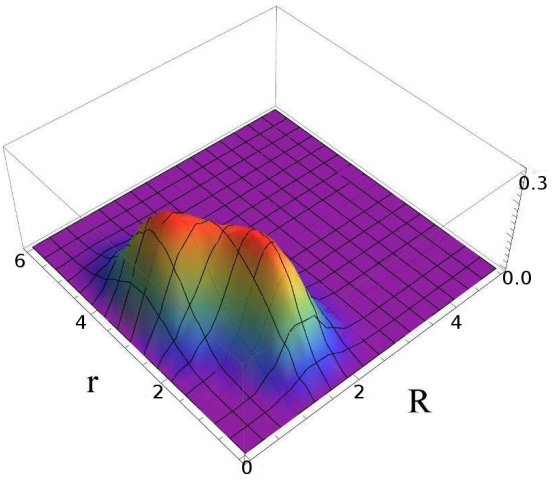

(e) $|(0d)^2;40\rangle$

Figure 2.4: The correlation function $C_\alpha(r,R)$ for different two-particle configurations in the $0d$ orbital.

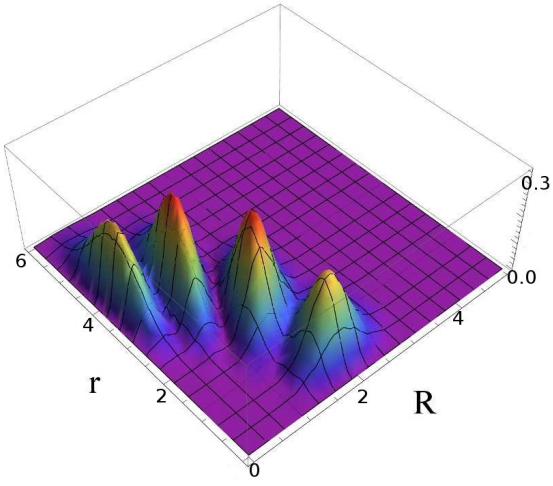

(a) $|(0f)^2;00\rangle$

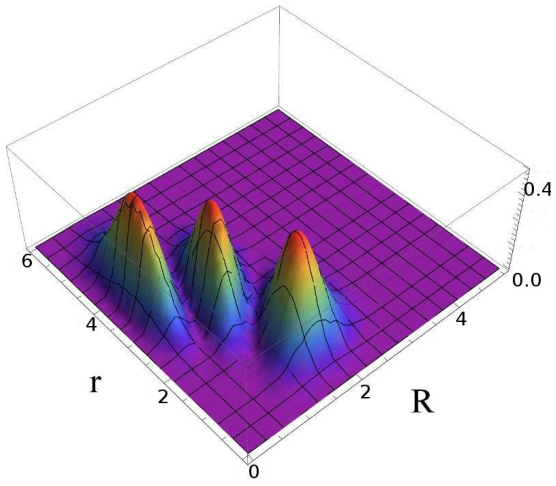

(b) $|(0f)^2;11\rangle$

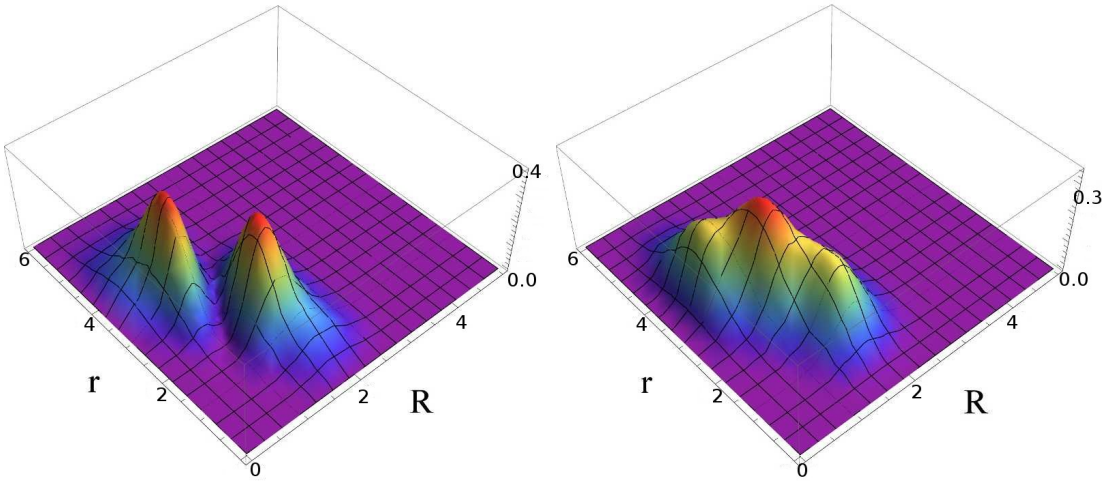

(c) $|(0f)^2;20\rangle$

(d) $|(0f)^2;31\rangle$

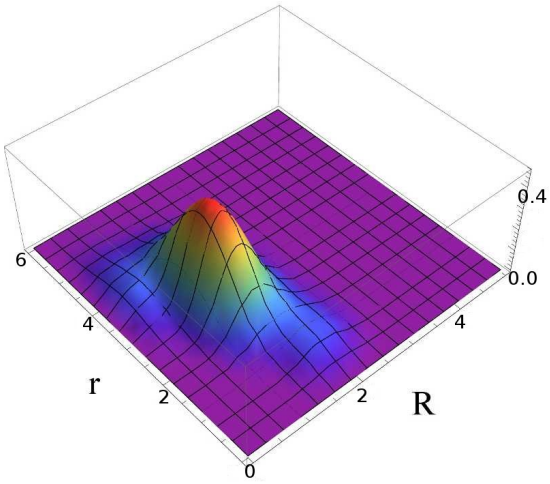

(e) $|(0f)^2;40\rangle$

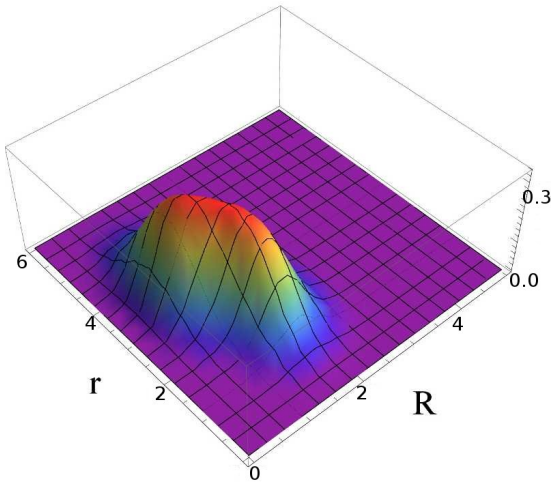

(f) $|(0f)^2;51\rangle$

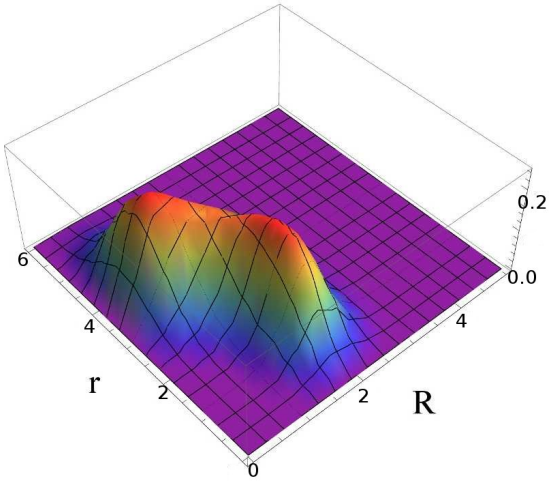

(g) $|(0f)^2;60\rangle$

Figure 2.5: The correlation function $C_\alpha(r,R)$ of different two-particle configurations in the $0f$ orbital.

f. Conclusions

To summarize, other than the "reflection-like" symmetry described by Eq. (2.2.21), the correlation function of two particles in the $n\ell$ orbital coupled to total angular momentum L exhibits a few patterns related to n, ℓ and L. Such a correlation function displays an $n+1$ circle structure in that, compared to the maxima observed for the configuration $|(0\ell)^2;LS\rangle$, $n+1$ times as many peaks positioned on $n+1$ concentric circles radiating out from the center exist for $|(n\ell)^2;LS\rangle$. This can be explained through the fact that the radial wave function $\mathcal{R}_{n\ell}(r)$ has n nodes and hence its square has $n+1$ maxima. On each circle, the number of maxima is related to ℓ and L. For $L=0$, there are $\ell+1$ maxima on each circle. As L increases by one, the number of maxima decreases by one for the first few L. For large values of L, the peak shapes become less defined. Catara *et al* [32], who studied two-particle correlations in the jj coupling scheme, made similar but less conclusive observations, and did not give any analytical explanation.

Section 2.2.6 will look into the ℓ and L related patterns from another point of view. We will find analytic explanations for the relations between the numbers of maxima on each circle and the quantum numbers ℓ and L.

2.2.5 Correlation functions between different orbitals: $C_{\alpha\alpha'}(r,R)$

This section has its interest in correlations between different orbitals: $C_{\alpha\alpha'}(r,R)$, where $|\alpha\rangle$ and $|\alpha'\rangle$ stand for different two-particle states $|(n\ell)^2;LS\rangle$ and $|(n'\ell')^2;LS\rangle$ respectively. As opposed to $C_\alpha(r,R)$, which has its physical interpretation as the probability distribution of the state $|\alpha\rangle$ versus r and R, $C_{\alpha\alpha'}(r,R)$ makes for better understanding of the interference of contributions from different orbitals. Such an understanding is useful when studying the correlation function, or the probability distribution of any state that is an admixture of $|(n\ell)^2;LS\rangle$ and $|(n'\ell')^2;LS\rangle$.

First of all, in order to examine the role of parity, some plots of correlation

functions $C_{\alpha\alpha'}(r,R)$ between a pair of orbitals of the same parity and a pair of orbitals of opposite parity are presented respectively in Fig. 2.6 and Fig. 2.7.

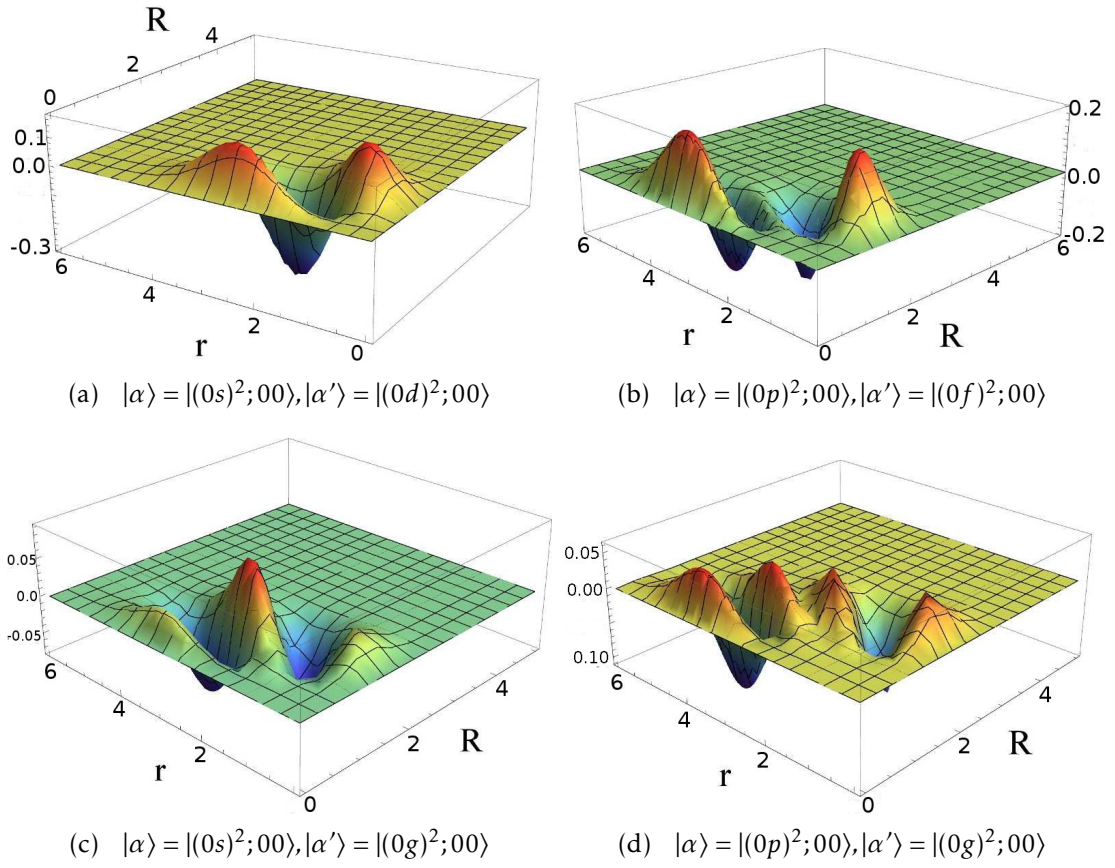

(a) $|\alpha\rangle = |(0s)^2;00\rangle, |\alpha'\rangle = |(0d)^2;00\rangle$

(b) $|\alpha\rangle = |(0p)^2;00\rangle, |\alpha'\rangle = |(0f)^2;00\rangle$

(c) $|\alpha\rangle = |(0s)^2;00\rangle, |\alpha'\rangle = |(0g)^2;00\rangle$

(d) $|\alpha\rangle = |(0p)^2;00\rangle, |\alpha'\rangle = |(0g)^2;00\rangle$

Figure 2.6: The off-diagonal correlation function $C_{\alpha\alpha'}(r,R)$ between orbitals of the same parity.

Following the argument leading to Eq. (2.2.21) in the previous section, it is straightforward to derive the relation satisfied by $C_{\alpha\alpha'}(r,R)$

$$(-1)^{\ell} C_{(n\ell)^2 LS,(n'\ell')^2 LS}(r,R) = (-1)^{\ell'} C_{(n\ell)^2 LS,(n'\ell')^2 LS}(2R,\frac{r}{2}). \tag{2.2.26}$$

Between a pair of orbitals of the same parity, $C_{\alpha\alpha'}(r,R)$ has a "reflection-like" symmetry as $C_{\alpha}(r,R)$ does, obeying the relation in Eq. (2.2.21), while between a pair of orbitals of opposite parity, the underlying relation becomes

$$C_{\alpha\alpha'}(r,R) = -C_{\alpha\alpha'}(2R,\frac{r}{2}), \tag{2.2.27}$$

giving rise to a "rotation-like" symmetry with respect to the line $r = 2R$.

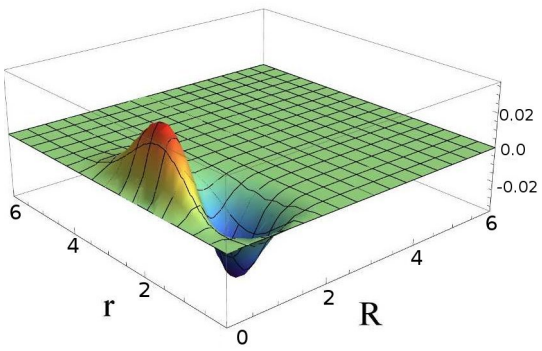

(a) $|\alpha\rangle = |(0s)^2;00\rangle, |\alpha'\rangle = |(0p)^2;00\rangle$

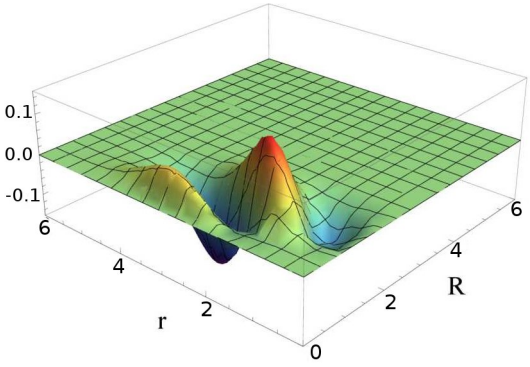

(b) $|\alpha\rangle = |(0s)^2;00\rangle, |\alpha'\rangle = |(0f)^2;00\rangle$

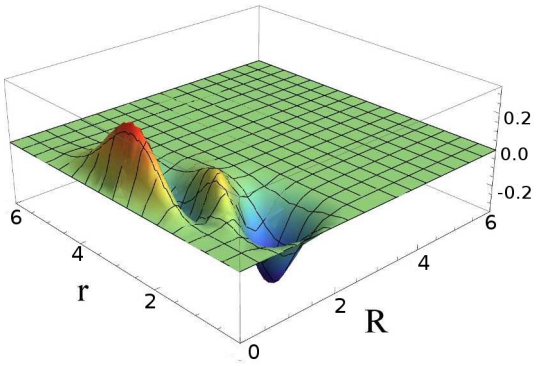

(c) $|\alpha\rangle = |(0p)^2;00\rangle, |\alpha'\rangle = |(0d)^2;00\rangle$

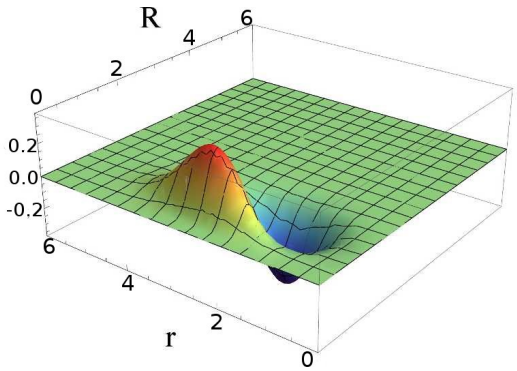

(d) $|\alpha\rangle = |(0p)^2;11\rangle, |\alpha'\rangle = |(0d)^2;11\rangle$

Figure 2.7: The off-diagonal correlation function $C_{\alpha\alpha'}(r,R)$ between orbitals of opposite parity.

The radial quantum number n also plays a role as indicated in Fig. 2.8. The radial wave functions with different values of n can contribute constructively or destructively in different regions due to their orthogonality.

2.2.6 The "angle" of angles

a. The angular correlation function

From another angle, spatial structures of two particles should be reflected by the angular separation between them. As a matter of fact, for a pair of particles in the same orbital that are coupled to 0^+, it follows from the spherical harmonic

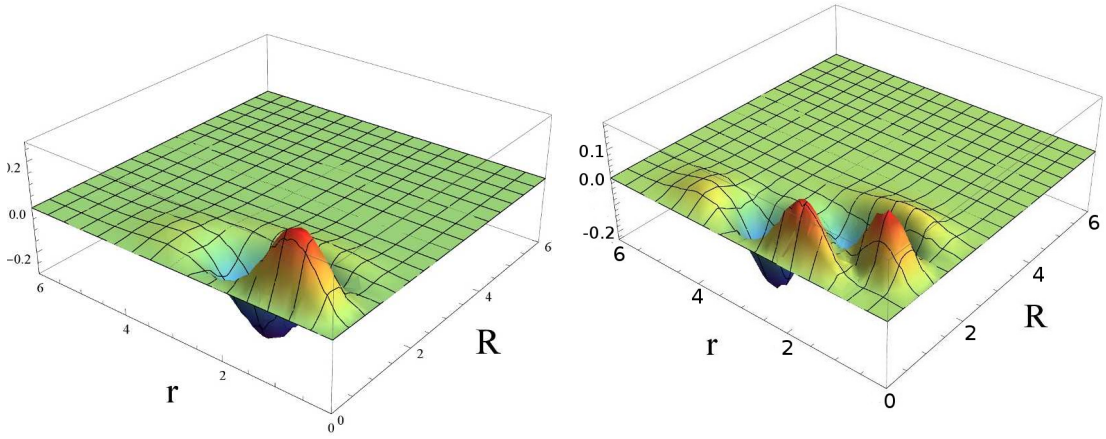

(a) $|\alpha\rangle = |(0s)^2;00\rangle, |\alpha'\rangle = |(1s)^2;00\rangle$ (b) $|\alpha\rangle = |(0p)^2;00\rangle, |\alpha'\rangle = |(1p)^2;00\rangle$

Figure 2.8: The off-diagonal correlation function $C_{\alpha\alpha'}(r,R)$ between orbitals of different n.

addition theorem

$$P_\ell(\cos\theta_{12}) = \frac{4\pi}{2\ell+1}\sum_{m=-\ell}^{\ell} \mathcal{Y}^*_{\ell m}(\theta_1,\phi_1)\mathcal{Y}_{\ell m}(\theta_2,\phi_2), \tag{2.2.28}$$

that its wave function can be expressed as

$$\begin{aligned}
&\langle \vec{r}_1, \vec{r}_2 | n_1\ell, n_2\ell; 0\rangle \\
&= \mathcal{R}_{n_1\ell}(r_1)\mathcal{R}_{n_2\ell}(r_2)\sum_{m=-\ell}^{\ell} \langle \ell m \ell - m | 00\rangle \mathcal{Y}_{\ell m}(\theta_1,\phi_1)\mathcal{Y}_{\ell -m}(\theta_2,\phi_2) \\
&= \mathcal{R}_{n_1\ell}(r_1)\mathcal{R}_{n_2\ell}(r_2)\sum_{m=-\ell}^{\ell} \frac{(-1)^{\ell-m}}{\sqrt{2\ell+1}}(-1)^m \mathcal{Y}_{\ell m}(\theta_1,\phi_1)\mathcal{Y}^*_{\ell m}(\theta_2,\phi_2) \\
&= \mathcal{R}_{n_1\ell}(r_1)\mathcal{R}_{n_2\ell}(r_2)(-1)^\ell \frac{\sqrt{2\ell+1}}{4\pi} P_\ell(\cos\theta_{12}),
\end{aligned} \tag{2.2.29}$$

where P_ℓ is the ℓth Legendre polynomial. The angular part of the wave function, therefore, is a function of the relative angle θ_{12} between the two particles.

This result brings us to wonder about the angular part of the probability density of a more general case: $|n_1\ell_1 n_2\ell_2; LS\rangle$ with any total angular momentum L. Without causing ambiguity, we denote the coordinates (r_i,θ_i,ϕ_i) of particle i by

(i) and write a two-particle wave function as

$$\begin{aligned}\langle \vec{r}_1, \vec{r}_2 | n_1 \ell_1 n_2 \ell_2; L M_L \rangle &\equiv [\phi_{n_1\ell_1}(1) \otimes \phi_{n_2\ell_2}(2)]^L_{M_L} \\ &= \mathcal{R}_{n_1\ell_1}(1)\mathcal{R}_{n_2\ell_2}(2) \sum_{m_1 m_2} \langle \ell_1 m_1 \ell_2 m_2 | L M_L \rangle \mathcal{Y}_{\ell_1 m_1}(1) \mathcal{Y}_{\ell_2 m_2}(2)\end{aligned} \tag{2.2.30}$$

To evaluate the angular probability density for an arbitrary total orbital angular momentum L, all the projections on z ($-L \leq M_L \leq L$) should be averaged as follows

$$\frac{1}{2L+1} \sum_{M_L} [\mathcal{Y}^*_{\ell_1}(1) \otimes \mathcal{Y}^*_{\ell_2}(2)]^L_{M_L} [\mathcal{Y}_{\ell_1}(1) \otimes \mathcal{Y}_{\ell_2}(2)]^L_{M_L}. \tag{2.2.31}$$

In the spirit of generality, we will first evaluate the expression

$$\frac{1}{2L+1} \sum_{M_L} [\mathcal{Y}^*_{\ell_1}(1) \otimes \mathcal{Y}^*_{\ell_2}(2)]^L_{M_L} [\mathcal{Y}_{\ell'_1}(1) \otimes \mathcal{Y}_{\ell'_2}(2)]^L_{M_L}, \tag{2.2.32}$$

of which expression (2.2.31) is a special case. The general expression (2.2.32) is analyzed in Appendix A and here we only cite the final result

$$\begin{aligned}&\frac{1}{2L+1} \sum_{M_L} [\mathcal{Y}^*_{\ell_1}(1) \otimes \mathcal{Y}^*_{\ell_2}(2)]^L_{M_L} [\mathcal{Y}_{\ell'_1}(1) \otimes \mathcal{Y}_{\ell'_2}(2)]^L_{M_L} \\ &= \frac{\hat{\ell}_1 \hat{\ell}_2 \hat{\ell}'_1 \hat{\ell}'_2}{(4\pi)^2} (-)^L \sum_{L_1} (-)^{L_1} \hat{L}_1^2 \begin{Bmatrix} \ell_2 & \ell'_2 & L_1 \\ \ell'_1 & \ell_1 & L \end{Bmatrix} \begin{pmatrix} \ell_1 & \ell'_1 & L_1 \\ 0 & 0 & 0 \end{pmatrix} \begin{pmatrix} \ell_2 & \ell'_2 & L_1 \\ 0 & 0 & 0 \end{pmatrix} P_{L_1}(\cos\theta_{12}).\end{aligned} \tag{2.2.33}$$

Expression (2.2.33) is a Legendre polynomial expansion having the cosine of the relative angle θ_{12} between the two particles as its argument; $\ell_1 + \ell'_1$ and $\ell_2 + \ell'_2$ have to be of the same parity, otherwise expression (2.2.33) vanishes. More specifically, if $\ell_1 + \ell'_1$ and $\ell_2 + \ell'_2$ are even, it is an expansion of even-degree Legendre polynomials, whereas if $\ell_1 + \ell'_1$ and $\ell_2 + \ell'_2$ are odd, it is an expansion of odd-degree Legendre polynomials.

Availing of the expression in (2.2.33) involving two two-particle states $|\ell_1\ell_2;LS\rangle$ and $|\ell_1'\ell_2';LS\rangle$, we can evaluate the angular probability density of two particles, in the same $n\ell$ orbital or in two orbitals characterized by the same ℓ, coupled to a total orbital angular momentum L. It takes the form of an expansion of even-degree Legendre polynomials,

$$\begin{aligned}&\frac{1}{2L+1}\sum_{M_L}[\mathcal{Y}_\ell^*(1)\otimes\mathcal{Y}_\ell^*(2)]^L_{M_L}[\mathcal{Y}_\ell(1)\otimes\mathcal{Y}_\ell(2)]^L_{M_L}\\&=\frac{(2\ell+1)^2}{(4\pi)^2}(-)^L\sum_{L_1}(2L_1+1)\begin{Bmatrix}\ell&\ell&L_1\\\ell&\ell&L\end{Bmatrix}\begin{pmatrix}\ell&\ell&L_1\\0&0&0\end{pmatrix}^2 P_{L_1}(\cos\theta_{12}).\end{aligned}\tag{2.2.34}$$

Without loss of generality, one of the particles can be assumed to be in the zenith direction. Consequently the angular separation θ_{12} is the polar angle of the other particle, the probability of finding which in the (differential) solid angle element $d\Omega=\sin\theta_{12}d\theta_{12}d\phi$ is

$$\frac{(2\ell+1)^2}{4\pi}(-)^L\sum_{L_1}(2L_1+1)\begin{Bmatrix}\ell&\ell&L_1\\\ell&\ell&L\end{Bmatrix}\begin{pmatrix}\ell&\ell&L_1\\0&0&0\end{pmatrix}^2 P_{L_1}(\cos\theta_{12})\sin\theta_{12}d\theta_{12}d\phi.\tag{2.2.35}$$

Integrating expression (2.2.35) over ϕ, we get the expression for the probability of finding the other particle within $d\theta_{12}$. We will refer to the corresponding probability density as the angular correlation function for two ℓ orbital particles coupled to L

$$\begin{aligned}&\mathcal{P}_{\ell L}(\theta_{12})\equiv\\&\qquad\frac{(2\ell+1)^2}{2}(-)^L\sum_{L_1}(2L_1+1)\begin{Bmatrix}\ell&\ell&L_1\\\ell&\ell&L\end{Bmatrix}\begin{pmatrix}\ell&\ell&L_1\\0&0&0\end{pmatrix}^2 P_{L_1}(\cos\theta_{12})\sin\theta_{12}.\end{aligned}\tag{2.2.36}$$

The angular correlation functions for the s, p, d and f orbitals are plotted in

Fig. 2.9 ∼ Fig. 2.12. They are to be compared with Fig. 2.1 ∼ Fig. 2.5. Both of them are illustrations of the spatial structure nucleon pairs, but from different perspectives.

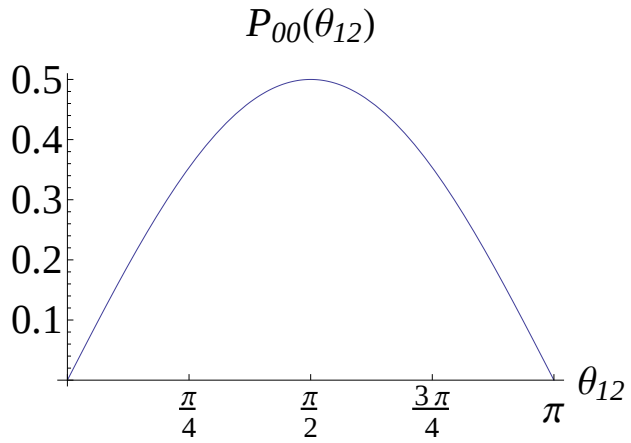

Figure 2.9: The angular correlation function $\mathcal{P}_{00}(\theta_{12})$ for configurations in the s orbitals.

The former (Fig. 2.9 ∼ Fig. 2.12) can be best described as the projected 2D images along the direction $r = 2R$ of the latter (Fig. 2.1 ∼ Fig. 2.5), which corroborates the observations made in the last section.

b. Understanding the patterns

We have seen in Sec. 2.2.4 that the number of circles and the number of peaks on one circle of a correlation function $C_\alpha(r,R)$ for two particles in a single orbital are directly connected with the radial quantum number n and the angular momentum ℓ characterizing the orbital respectively. The connection with n is explained by the properties of the radial wave function, while the connection concerning ℓ, as we will see, can be understood by analyzing the angular correlation function obtained in Eq. (2.2.36).

Between the Legendre polynomials and $3j$-symbols there exists the relation:

$$\frac{1}{2}\int_0^\pi P_{\ell_1}(\cos\theta)P_{\ell_2}(\cos\theta)P_{\ell_3}(\cos\theta)\sin\theta d\theta = \begin{pmatrix} \ell_1 & \ell_2 & \ell_3 \\ 0 & 0 & 0 \end{pmatrix}^2, \tag{2.2.37}$$

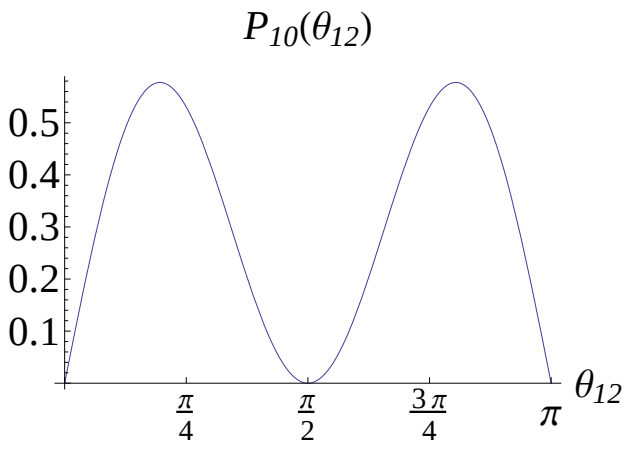

(a) $L = 0$

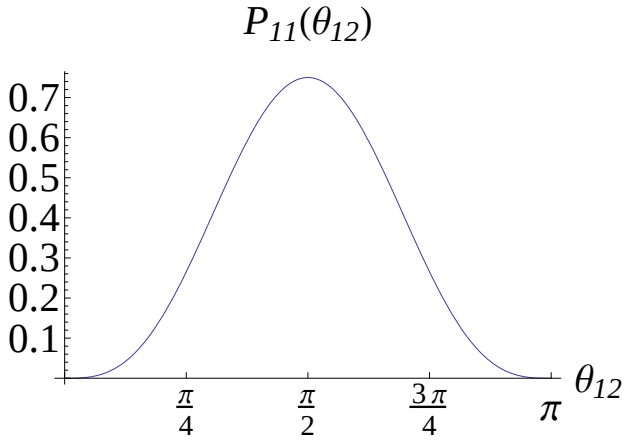

(b) $L = 1$

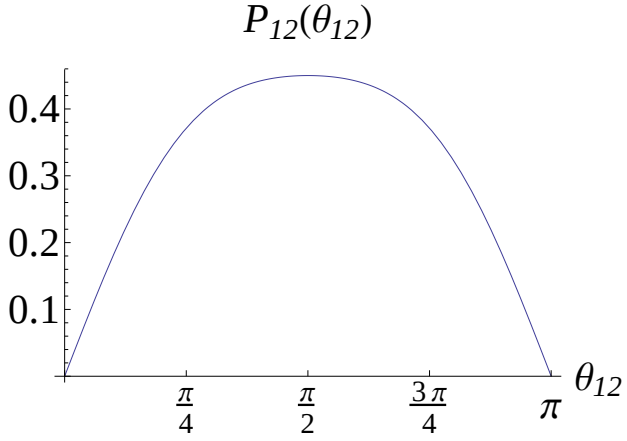

(c) $L = 2$

Figure 2.10: The angular correlation function $\mathcal{P}_{\ell L}(\theta_{12})$ for configurations in the p orbitals.

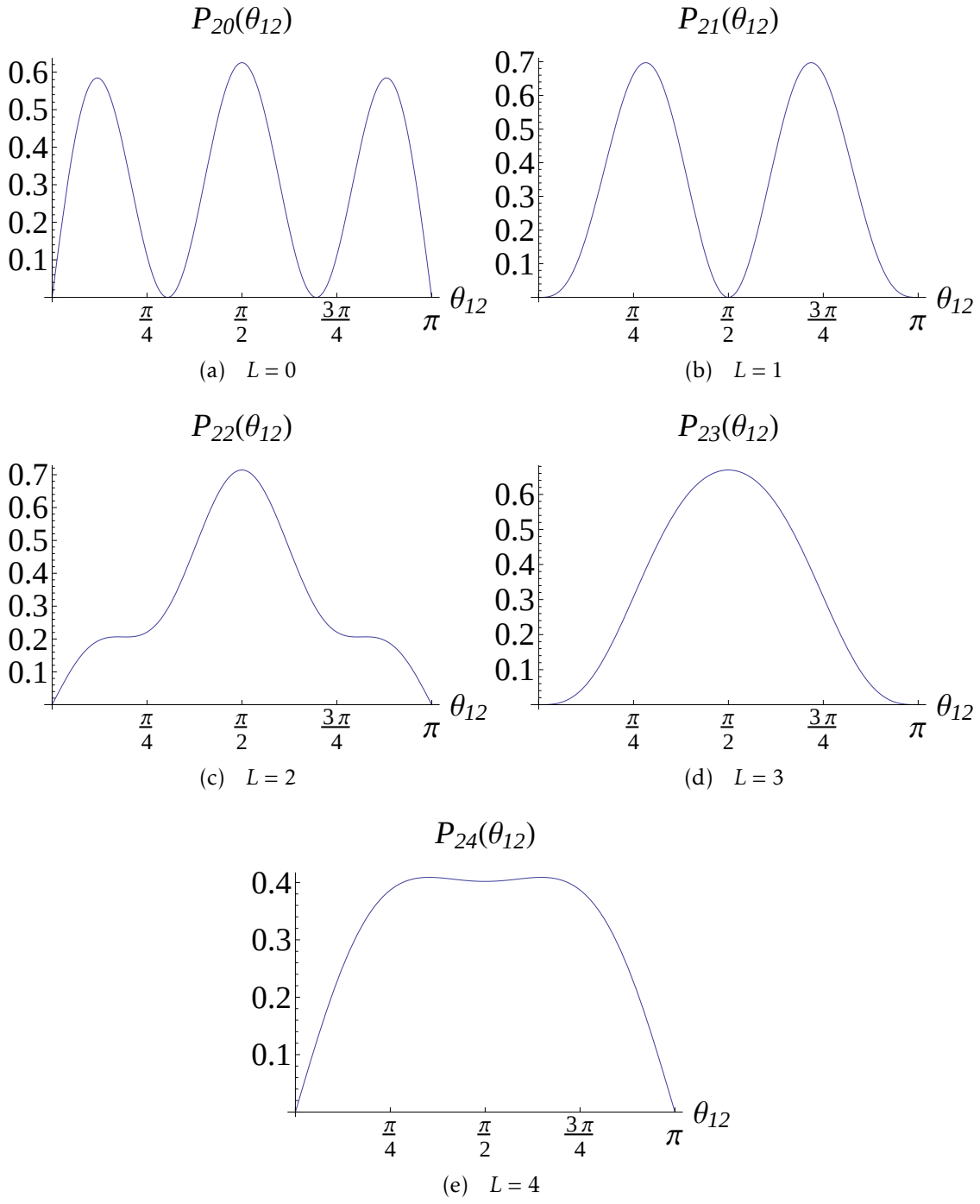

(a) $L = 0$ (b) $L = 1$

(c) $L = 2$ (d) $L = 3$

(e) $L = 4$

Figure 2.11: The angular correlation function $\mathcal{P}_{\ell L}(\theta_{12})$ for configurations in the d orbitals.

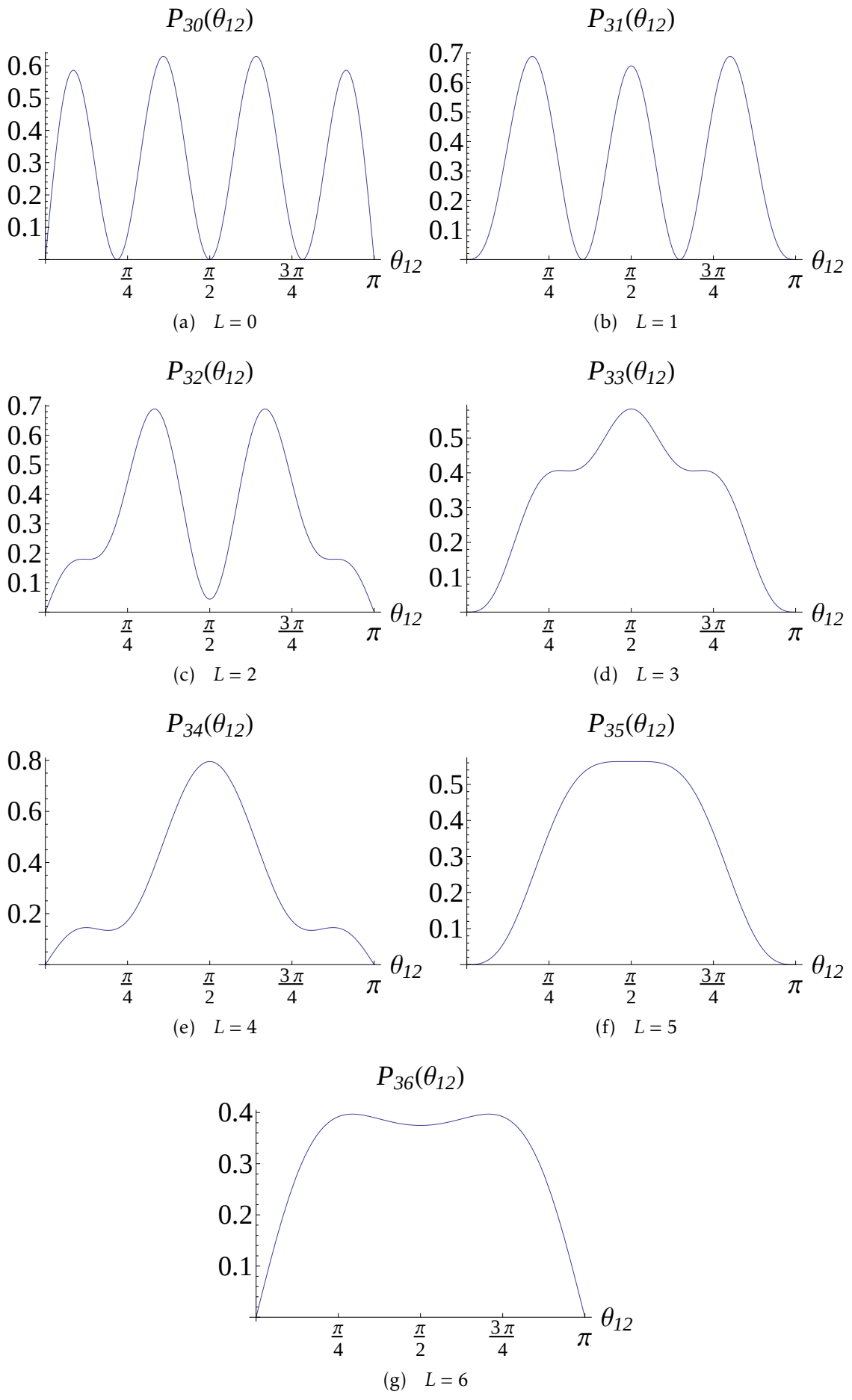

(a) $L = 0$ (b) $L = 1$ (c) $L = 2$ (d) $L = 3$ (e) $L = 4$ (f) $L = 5$ (g) $L = 6$

Figure 2.12: The angular correlation function $\mathcal{P}_{\ell L}(\theta_{12})$ for configurations in the f orbitals.

which, written in the bra-ket notation becomes

$$\frac{1}{2}\langle P_{\ell_1} P_{\ell_2} | P_{\ell_3}\rangle = \begin{pmatrix} \ell_1 & \ell_2 & \ell_3 \\ 0 & 0 & 0 \end{pmatrix}^2 . \tag{2.2.38}$$

Expression (2.2.36), then, can be reformulated in the bra-ket notation as follows:

$$\mathcal{P}_{\ell L}(\theta_{12}) \equiv \frac{(2\ell+1)^2}{2}(-)^L \sum_{L_1} \frac{2L_1+1}{2} \begin{Bmatrix} \ell & \ell & L_1 \\ \ell & \ell & L \end{Bmatrix} \langle P_\ell^2 | P_{L_1}\rangle\langle P_{L_1}|\cos\theta_{12}\rangle \sin\theta_{12}. \tag{2.2.39}$$

Since the Legendre polynomials are orthogonal yet unnormalized on the interval of orthogonality $[-1,1]$, the closure relation is written

$$\sum_n \frac{2n+1}{2} |P_n\rangle\langle P_n| = \hat{1}.$$

When L equals zero, we have

$$\begin{aligned} &\frac{(2\ell+1)^2}{2}(-)^L \sum_{L_1} \frac{2L_1+1}{2} \begin{Bmatrix} \ell & \ell & L_1 \\ \ell & \ell & L \end{Bmatrix} \langle P_\ell^2 | P_{L_1}\rangle\langle P_{L_1}| \\ &= \frac{2\ell+1}{2} \sum_{L_1} \frac{2L_1+1}{2} \langle P_\ell^2 | P_{L_1}\rangle\langle P_{L_1}| (-1)^{L_1} \\ &= \frac{2\ell+1}{2} P_\ell^2 \hat{1}. \end{aligned} \tag{2.2.40}$$

The Last line follows from the fact that for odd L_1, $\langle P_\ell^2 | P_{L_1}\rangle$ vanishes. As a result, the angular correlation function $\mathcal{P}_{\ell 0}(\cos\theta_{12})$ assumes a very simple form

$$\frac{2\ell+1}{2} P_\ell^2(\cos\theta_{12}) \sin\theta_{12}, \tag{2.2.41}$$

In this particular case of $L = 0$, the wave function in expression (2.2.29) can be equally used to directly obtain Eq. (2.2.41).

Eq. (2.2.41) is proportional to the square of the ℓth-degree Legendre polynomial. The degree ℓ of a Legendre polynomial $P_\ell(x)$ indicates that there are ℓ zeros on the x axis, and thus $P_\ell(x)$ changes sign ℓ times. Besides, $P_\ell(x)$ is either symmetric (for even ℓ) or antisymmetric (for odd ℓ), and has its maximal absolute values 1 on the boundaries $x = 1$ and $x = -1$. As a consequence, $P_\ell^2(x)$ has $\ell + 1$ maxima, two of which are on the boundaries, except for $P_0(x)$ that is a constant. The first five Legendre polynomials are drawn in Fig. 2.13(a), and their squares in Fig. 2.13(b).

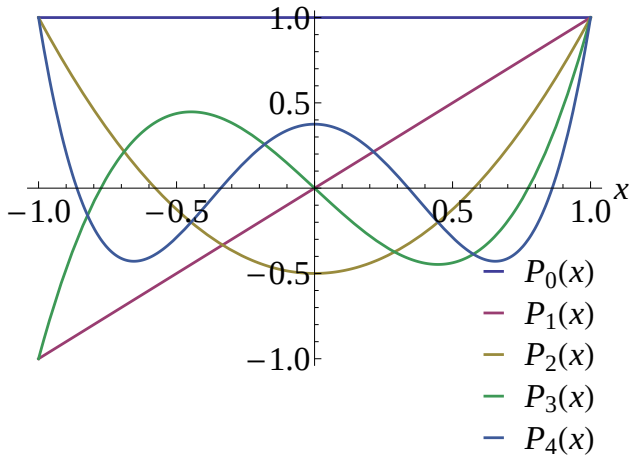

(a)

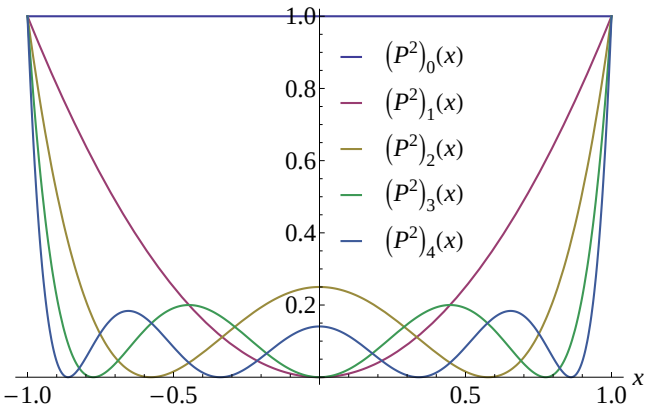

(b)

Figure 2.13: The first five Legendre polynomials and their squares.

Since $\cos\theta_{12}$ is a monotonically decreasing function on the interval $[0, \pi]$ and has the range $[1, -1]$, the aforementioned features of $P_\ell(x)$ and $P_\ell^2(x)$ are also true for $P_\ell(\cos\theta_{12})$ and $P_\ell^2(\cos\theta_{12})$ on the interval $[0, \pi]$. In expression (2.2.41),

$P_\ell^2(\cos\theta_{12})$ is multiplied with $\sin\theta_{12}$ introduced by the solid angle element. As far as the number of maxima is concerned, the $\ell+1$ maximum feature still holds except for the fact that each maximum on the boundary is pushed inwards a little bit, because on the boundaries the angular correlation function vanishes as does $\sin\theta_{12}$. The special case $P_0^2(x)$, when multiplied with $\sin\theta_{12}$, is simply $\sin\theta_{12}$, which has one maximum at $\theta_{12} = \pi/2$ and thus also fits the $\ell+1$ maximum rule. This is illustrated in Fig. 2.14. Thus we proved that the angular correlation function of two ℓ-orbital particles coupled to $L = 0$ is characterized by $\ell+1$ well-defined maxima (there is a zero between two adjacent maxima and on each boundary).

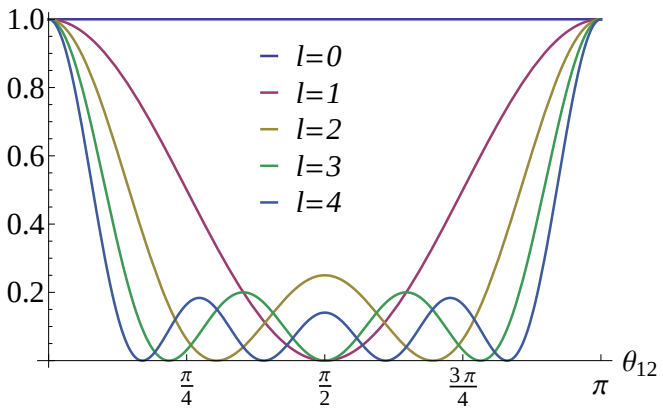

(a)

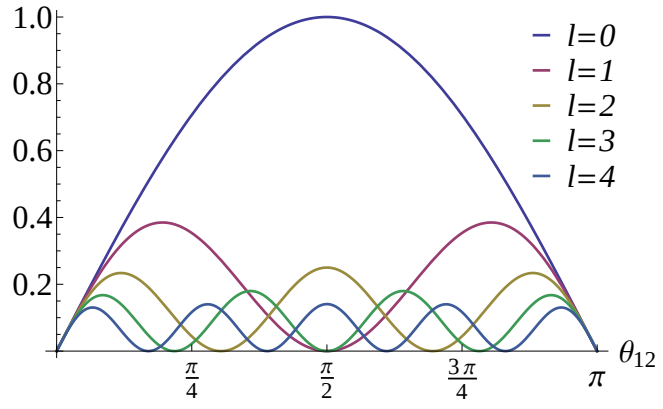

(b)

Figure 2.14: The functions $P_\ell^2(\cos\theta_{12})$ (a) and $P_\ell^2(\cos\theta_{12})\sin\theta_{12}$ (b) for a few angular momenta ℓ

For $L = 1$, we know from previous observations that one maximum is "miss-

ing" compared to the case $L = 0$. The evaluation of the angular correlation functions for $L = 1$ is a little trickier because the $6j$-symbol $\begin{Bmatrix} \ell & \ell & L_1 \\ \ell & \ell & L \end{Bmatrix}$, then, depends on L_1. The ℓ orbital angular correlation function (2.2.39) becomes

$$\mathcal{P}_{\ell 1}(\theta_{12}) = \frac{(2\ell+1)^2}{2}\sum_{L_1}\frac{2L_1+1}{2}\left(\frac{2\ell(\ell+1)-L_1(L_1+1)}{2\ell(\ell+1)(2\ell+1)}\right)\langle P_\ell^2|P_{L_1}\rangle\langle P_{L_1}|\cos\theta_{12}\rangle\sin\theta_{12}, \tag{2.2.42}$$

which can be separated into two sums:

$$\frac{2\ell+1}{2}\sum_{L_1}\frac{2L_1+1}{2}\langle P_\ell^2|P_{L_1}\rangle\langle P_{L_1}|\cos\theta_{12}\rangle\sin\theta_{12} - \frac{2\ell+1}{4\ell(\ell+1)}\sum_{L_1}\frac{2L_1+1}{2}(L_1(L_1+1))\langle P_\ell^2|P_{L_1}\rangle\langle P_{L_1}|\cos\theta_{12}\rangle\sin\theta_{12}. \tag{2.2.43}$$

The first summation equals $\mathcal{P}_{\ell 0}(\theta_{12})$ that has been solved above. The second summation, given that $L_1(L_1+1)$ is proportional to the eigenvalue of the square of the total angular momentum operator $\hat{\mathbf{L}}^2$ acting on an L_1th-rank spherical tensor, can be rewritten as

$$-\frac{2\ell+1}{4\ell(\ell+1)}\sum_{L_1}\frac{2L_1+1}{2}\langle P_\ell^2|\frac{\hat{\mathbf{L}}^2}{\hbar^2}|P_{L_1}\rangle\langle P_{L_1}|\cos\theta_{12}\rangle\sin\theta_{12} = -\frac{2\ell+1}{4\ell(\ell+1)}\langle P_\ell^2|\frac{\hat{\mathbf{L}}^2}{\hbar^2}|\cos\theta_{12}\rangle\sin\theta_{12}. \tag{2.2.44}$$

Once again, we used the closure relation for the Legendre polynomials.

Let's evaluate $\langle\cos\theta|\frac{\hat{\mathbf{L}}^2}{\hbar^2}|P_\ell^2\rangle \equiv \left(\langle P_\ell^2|\frac{\hat{\mathbf{L}}^2}{\hbar^2}|\cos\theta\rangle\right)^\dagger$ in the first place. The square of total angular momentum in space representation is

$$\hat{\mathbf{L}}^2 = -\hbar^2\left(\frac{1}{\sin\theta}\frac{\partial}{\partial\theta}\left(\sin\theta\frac{\partial}{\partial\theta}\right)+\frac{1}{\sin^2\theta}\frac{\partial^2}{\partial\phi^2}\right).$$

Then $\langle \cos\theta | \frac{\hat{\mathbf{L}}^2}{\hbar^2} | P_\ell^2 \rangle$ is equal to

$$
\begin{aligned}
&-\left(\frac{1}{\sin\theta}\frac{\partial}{\partial\theta}\left(\sin\theta\frac{\partial}{\partial\theta}\right)+\frac{1}{\sin^2\theta}\frac{\partial^2}{\partial\phi^2}\right)P_\ell^2(\cos\theta)\\
&=-\frac{1}{\sin\theta}\frac{\partial}{\partial\theta}\left(\sin\theta\frac{\partial}{\partial\theta}\right)P_\ell^2(\cos\theta)\\
&=4\cos\theta P_\ell(\cos\theta)P_\ell'(\cos\theta)-2\sin^2\theta P_\ell'^2(\cos\theta)-2\sin^2\theta P_\ell(\cos\theta)P_\ell''(\cos\theta).
\end{aligned}
\tag{2.2.45}
$$

The associated Legendre polynomials, of which the Legendre polynomials are a special case for $m = 0$, are solutions of the general Legendre equation

$$
(1-x^2)y''-2xy'+\left(\ell(\ell+1)-\frac{m^2}{1-x^2}\right)y=0. \tag{2.2.46}
$$

Therefore, the last line in (2.2.45) equals

$$
2\ell(\ell+1)P_\ell^2(\cos\theta)-2\sin^2\theta P_\ell'^2(\cos\theta). \tag{2.2.47}
$$

substituting the identity just obtained

$$
\langle \cos\theta | \frac{\hat{\mathbf{L}}^2}{\hbar^2} | P_\ell^2 \rangle = 2\ell(\ell+1)P_\ell^2(\cos\theta)-2\sin^2\theta P_\ell'^2(\cos\theta) \tag{2.2.48}
$$

into the expression (2.2.44) of the second summation, we get

$$
\begin{aligned}
&-\frac{2\ell+1}{4\ell(\ell+1)}\Big(2\ell(\ell+1)P_\ell^2(\cos\theta_{12})-2\sin^2\theta P_\ell'^2(\cos\theta_{12})\Big)\sin\theta_{12}\\
&=-\mathcal{P}_{\ell 0}(\theta_{12})+\frac{2\ell+1}{2\ell(\ell+1)}\sin^3\theta_{12}P_\ell'^2(\cos\theta_{12}).
\end{aligned}
\tag{2.2.49}
$$

Finally, expression (2.2.43) for $\mathcal{P}_{\ell 1}(\theta_{12})$ is equal to:

$$
\mathcal{P}_{\ell 1}(\theta_{12})=\frac{2\ell+1}{2\ell(\ell+1)}\sin^3\theta_{12}P_\ell'^2(\cos\theta_{12}). \tag{2.2.50}
$$

Following the same train of thought that has led us to the conclusion of $\ell+1$

maxima in $L = 0$ configurations previously, we readily see that P'_ℓ in the expression of $\mathcal{P}_{\ell 1}(\theta_{12})$ is of degree $\ell - 1$ due to the differentiation, one degree less than P_ℓ which is in the expression of $\mathcal{P}_{\ell 0}(\theta_{12})$; hence the ℓ maxima.

The single-ℓ angular correlation function for higher values of L can be derived similarly. However, as we said before that $\mathcal{P}_{\ell L}(\theta_{12})$ is a sum of even-degree Legendre polynomials up to the degree 2ℓ. There are $\ell+1$ of them. Consequently, for a certain orbital ℓ, its angular correlation functions are constructed from a basis of $\ell+1$ polynomials, less than the number $(2\ell+1)$ of total angular angular momenta to which the two particles can be coupled. This implies that all the $\mathcal{P}_{\ell L}(\theta_{12})$ are not independent, which explains in a way the less distinct maxima of $\mathcal{P}_{\ell L}(\theta_{12})$ shown earlier. For example, in section 2.2.4, we have seen in Eq. (2.2.25) that $\langle (0p)^2; 20 | C_\alpha(r,R) | (0p)^2; 20 \rangle$ is a combination of $\langle (0p)^2; 00 | C_\alpha(r,R) | (0p)^2; 00 \rangle$ and $\langle (0p)^2; 11 | C_\alpha(r,R) | (0p)^2; 11 \rangle$. The relation still holds if we replace each correlation function by their angular counterpart such that

$$\mathcal{P}_{12}(\theta_{12}) = \frac{2}{5}\mathcal{P}_{10}(\theta_{12}) + \frac{3}{5}\mathcal{P}_{11}(\theta_{12}). \tag{2.2.51}$$

c. Angular correlations between different angular momenta

We just studied the angular correlations for one pair of identical nucleons in the same orbital or in orbitals having the same ℓ. A more general angular correlation can be obtained similarly and is found to be:

$$\frac{\hat{\ell}_1\hat{\ell}_2\hat{\ell}'_1\hat{\ell}'_2}{2}(-)^L \sum_{L_1}(-)^{L_1}\hat{L}_1^2 \begin{Bmatrix} \ell_2 & \ell'_2 & L_1 \\ \ell'_1 & \ell_1 & L \end{Bmatrix} \begin{pmatrix} \ell_1 & \ell'_1 & L_1 \\ 0 & 0 & 0 \end{pmatrix} \begin{pmatrix} \ell_2 & \ell'_2 & L_1 \\ 0 & 0 & 0 \end{pmatrix} \times P_{L_1}(\cos\theta_{12}) \sin\theta_{12}. \tag{2.2.52}$$

For the purpose of comparison with the results presented in Fig. 2.6 and 2.7 in Sec. 2.2.5, several plots for angular correlation functions between two orbitals

with different angular momenta are given in Fig. 2.15, where $\mathcal{P}_{\ell\ell' L}(\theta_{12})$ equals

$$\frac{\hat{\ell}^2\hat{\ell}'^2}{2}(-)^L\sum_{L_1}(-)^{L_1}\hat{L}_1^2\begin{Bmatrix}\ell & \ell' & L_1\\ \ell' & \ell & L\end{Bmatrix}\begin{pmatrix}\ell & \ell' & L_1\\ 0 & 0 & 0\end{pmatrix}^2 P_{L_1}(\cos\theta_{12})\sin\theta_{12}. \qquad (2.2.53)$$

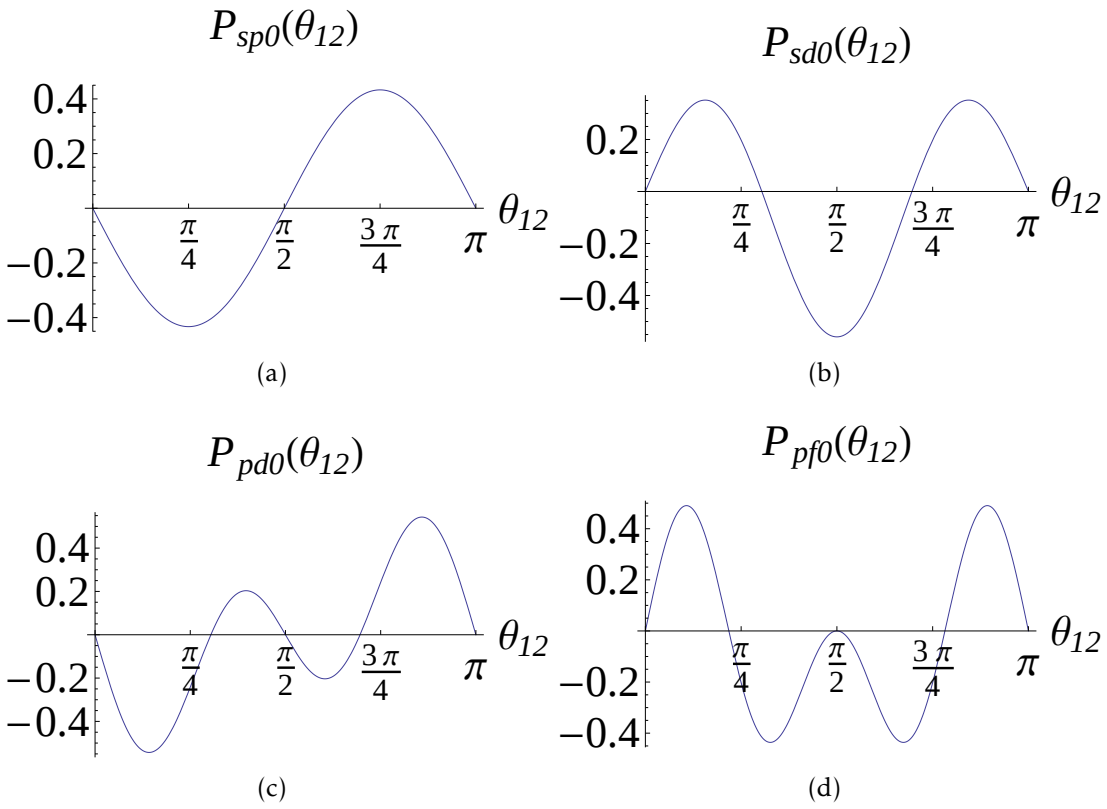

Figure 2.15: The angular correlation function $\mathcal{P}_{\ell\ell' L}(\theta_{12})$ between different angular momenta.

They are projected 2D images of the 3D plots of correlation function in Fig. 2.6 and 2.7. The reflection symmetry about the line $\theta_{12} = \frac{\pi}{2}$ between orbitals of the same parity and the rotational symmetry around the point $(\frac{\pi}{2}, 0)$ between orbitals of opposite parity are determined by the $3j$ symbol in the expression (2.2.53). If ℓ and ℓ' are both even or both odd, L_1 must be even, resulting in symmetric Legendre polynomials $P_{L_1}(x)$ and reflection symmetric $\mathcal{P}_{\ell\ell' L}(\theta_{12})$; otherwise only anti-symmetric Legendre polynomials contribute and the rotational symmetry ensues.

3

Two-particle correlations in ^{6}He with the δ interaction

3.1 Introduction

In the previous chapter, both spatial and angular correlation functions in the two-particle case were examined. In this chapter, the particular case of ^{6}He will be investigated. The harmonic oscillator potential will be used to describe the single particle motion, and the splittings induced by the spin-orbit interaction and the centrifugal term will be neglected [†] . The α particle being inert with the proton and neutron $0s_{1/2}$ shells filled up, only the two valence neutrons come into play. We consider the δ interaction, through which the two valence neutrons interact. Later we will draw our inspiration from the concept of the spurious component free cluster-orbital shell model (COSM) to eliminate the CM motion of the system.

[†] This will be discussed briefly in Sec. 3.3.

3.2 δ interaction

The δ interaction, a zero range interaction, is the extreme limit of short-range interactions. Defined as $-g\delta(\vec{r}_1 - \vec{r}_2)$, the δ interaction takes effect only when the two particles in question are in contact. In the definition, g is the positive strength of the interaction given in units of MeV·fm^3, and the minus sign serves to emphasize its attractive nature. Despite its seeming simplicity, the δ interaction reproduces fairly well many properties of nuclei.

Although spin variables do not appear in the definition of the δ interaction, the antisymmetrization introduces an implicit dependence on the total spin S. For a matrix element of the δ interaction to be non-zero, it is requisite that the spatial part of the wave function be symmetric, as any space antisymmetric state of the form $\phi_1(\vec{r}_1)\phi_2(\vec{r}_2) - \phi_2(\vec{r}_1)\phi_1(\vec{r}_2)$ vanishes whenever $\vec{r}_1 = \vec{r}_2$. Therefore, in order to obey the Pauli principle, the wave function concerning the other degrees of freedom must be antisymmetric. In other words, the sum of the total spin and the total isospin $S + T$ must be odd. Since we are dealing with two identical particles, T equals 1, which implies that S must be 0.

The matrix element of the δ interaction can be obtained using either the definition of the δ function in spherical coordinates or its multipole expansion. The δ function $\delta(\vec{r}_1 - \vec{r}_2)$ in spherical coordinates is

$$\delta(\vec{r}_1 - \vec{r}_2) = \frac{1}{r_1 r_2}\delta(r_1 - r_2)\delta(\cos\theta_1 - \cos\theta_2)\delta(\varphi_1 - \varphi_2),$$

whereby the following expression is obtained for the matrix element

$$\begin{aligned}
&\langle n_1\ell_1 n_2\ell_2; LM_L SM_S | - g\delta(\vec{r}_1 - \vec{r}_2) | n_1'\ell_1' n_2'\ell_2'; L'M_L' S'M_S' \rangle \\
&= -g\delta_{LL'}\delta_{M_L M_L'}\delta_{SS'}\delta_{M_S M_S'}\frac{\hat{\ell}_1\hat{\ell}_2\hat{\ell}_1'\hat{\ell}_2'}{4\pi}\begin{pmatrix} \ell_1 & \ell_2 & L \\ 0 & 0 & 0 \end{pmatrix}\begin{pmatrix} \ell_1' & \ell_2' & L \\ 0 & 0 & 0 \end{pmatrix} \\
&\times \int_0^{+\infty} \mathcal{R}_{n_1\ell_1}(r)\mathcal{R}_{n_2\ell_2}(r)\mathcal{R}_{n_1'\ell_1'}(r)\mathcal{R}_{n_2'\ell_2'}(r) r^2 dr. \qquad (3.2.1)
\end{aligned}$$

Alternatively, we use once again the multipole expansion

$$\delta(\vec{r}-\vec{r}_{12}) = \frac{\delta(r-r_{12})}{r r_{12}} \sum_{\lambda\mu} \mathcal{Y}^*_{\lambda\mu}(\theta,\varphi)\mathcal{Y}_{\lambda\mu}(\theta_{12},\varphi_{12}), \tag{3.2.2}$$

which has been introduced earlier in section 2.2 on the occasion of evaluating the correlation function $C_{\alpha\alpha'}(\vec{r})$. The matrix element obtained thereby in (2.2.3) of section 2.2 can be adopted for our current purpose if we simply take $\vec{r}_{12}$ and obtain

$$\begin{aligned}
&\langle n_1\ell_1 n_2\ell_2; LM_L SM_S | -g\delta(\vec{r}_1-\vec{r}_2) | n_1'\ell_1' n_2'\ell_2'; L'M_L'S'M_S'\rangle \\
&\quad = \quad -g\delta_{LL'}\delta_{M_L M_L'}\delta_{SS'}\delta_{M_S M_S'} \frac{1}{8\sqrt{2}\pi} \sum_{nn'\mathcal{N}\ell} a^{n_1\ell_1 n_2\ell_2}_{n\ell\mathcal{N}L,0}\; a^{n_1'\ell_1' n_2'\ell_2'}_{n'\ell\mathcal{N}L,0}\; \mathcal{R}_{n\ell}(0)\mathcal{R}_{n'\ell}(0) \\
&\quad = \quad -g\delta_{LL'}\delta_{M_L M_L'}\delta_{SS'}\delta_{M_S M_S'} \frac{1}{8\sqrt{2}\pi} \sum_{nn'\mathcal{N}} a^{n_1\ell_1 n_2\ell_2}_{n0\mathcal{N}L,L}\; a^{n_1'\ell_1' n_2'\ell_2'}_{n'0\mathcal{N}L,L}\; \mathcal{R}_{n0}(0)\mathcal{R}_{n'0}(0),
\end{aligned} \tag{3.2.3}$$

where the last step follows from the fact that only s-waves have non-vanishing values at the origin. From the conservation of oscillator quanta, we have the relations

$$\begin{aligned}
2n_1+\ell_1+2n_2+\ell_2 &= 2n+2\mathcal{N}+L, \quad \text{and} \\
2n_1'+\ell_1'+2n_2'+\ell_2' &= 2n'+2\mathcal{N}+L.
\end{aligned}$$

The matrix element (3.2.1) has a few interesting properties. To begin with, the δ interaction $\delta(\vec{r}_1-\vec{r}_2)$ is diagonal in the LS coupling scheme. Besides, $\ell_1+\ell_2+L$ and $\ell_1'+\ell_2'+L$ must be even, and accordingly $\ell_1+\ell_2$ and $\ell_1'+\ell_2'$ must be of the same parity, otherwise the $3j$ symbols would vanish and the quanta conservation relations would not hold. In the current context, our focus is on 0^+ states that necessitate equal ℓ_1 and ℓ_2 and equal ℓ_1' and ℓ_2', which results in even values of L, otherwise the matrix element (3.2.1) (or (3.2.3)) would vanish.

The diagonal matrix elements have the interpretation of energy shifts with

respect to the unperturbed energies of two-particle configurations. It is obvious from (3.2.1) that for a given ℓ, the *relative* energy splittings

$$\langle n_1\ell n_2\ell; LS| - g\delta(\vec{r}_1 - \vec{r}_2)|n_1\ell n_2\ell; LS\rangle$$
$$= -g\frac{(2\ell+1)^2}{4\pi}\begin{pmatrix}\ell & \ell & L\\ 0 & 0 & 0\end{pmatrix}^2 \int_0^{+\infty} \mathcal{R}^2_{n_1\ell}(r)\mathcal{R}^2_{n_2\ell}(r)r^2dr, \qquad (3.2.4)$$

depend uniquely on $\begin{pmatrix}\ell & \ell & L\\ 0 & 0 & 0\end{pmatrix}^2$ and are unaffected by the nature of the central potential, which only engenders an overall factor through the radial integral.

Although we are concerned with 0^+ configurations, it is worthwhile to digress from our main interest for a while to include higher angular momenta in our discussion.

In LS coupling, for a given ℓ, the energy splitting given in Eq. (3.2.4) is proportional to the quantity $\begin{pmatrix}\ell & \ell & L\\ 0 & 0 & 0\end{pmatrix}^2$, which is plotted for $\ell = 5$ in Fig. 3.1(a). A crucial result is that, for two identical particles in the same orbital, the energy of the $L^\pi = 0^+$ [†] state is lowered the most, followed by possible higher even total angular momenta: $L^\pi = 2^+, 4^+, 6^+ \cdots$. It is not, however, monotonic in the region of large values of L (towards the highest possible value of $L = 2\ell$). In terms of spacings between two consecutive levels, the one from 0^+ to 2^+ is the largest. The lowering of the 0^+ state is fundamental in accounting for why even-even nuclei have 0^+ ground states. The large gaps between 0^+ and 2^+ states are also in good agreement with experimental data.

It is not surprising that in the jj-coupling scheme, the energy splittings created by the δ interaction have quite similar properties to the LS coupling case, as illustrated in Fig. 3.1(b) for $j = 11/2$. The $J^\pi = 0^+$ state is lowered the most and the difference between 0^+ and 2^+ is big. Unlike the observation in LS coupling,

[†] When no confusion is likely to arise, in LS coupling, we denote a state of total orbital angular momentum L and total spin $S = 0$ by L^π, π as usual being the parity.

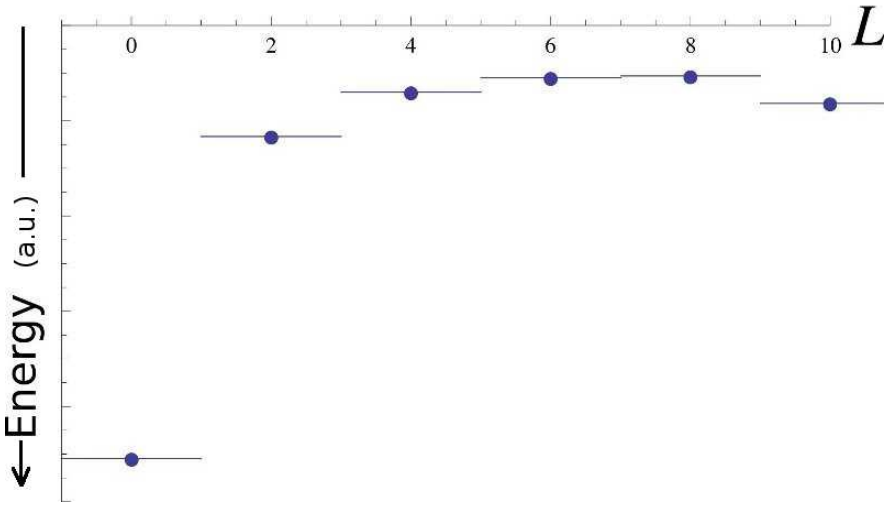

(a)

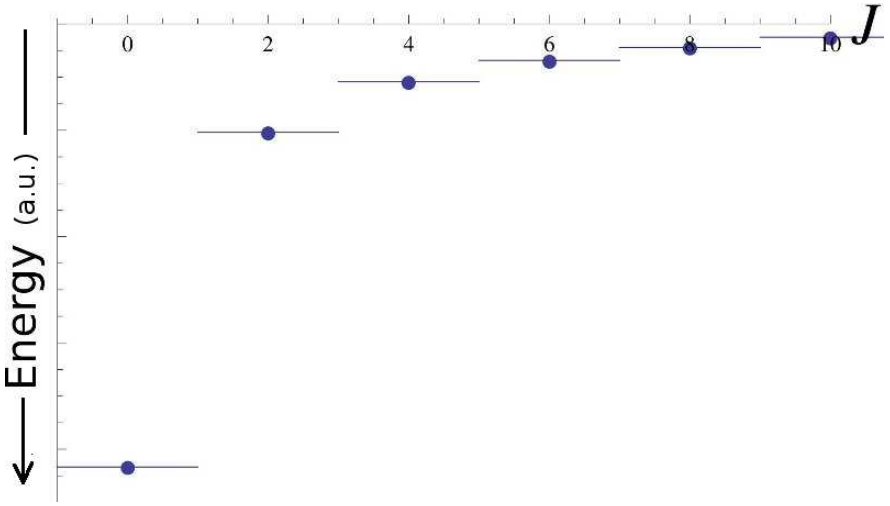

(b)

Figure 3.1: Splittings in LS and jj couplings (a) two particles in a orbital $\ell = 5$, (b) two particles in a orbital $j = \frac{11}{2}$.

the energy splitting in jj coupling is a monotonic function of J.

Now the last consequence to point out before finishing the discussion on the δ interaction: for an $L = 0$ state, the energy splitting is proportional to $2\ell + 1$, the degeneracy of the orbital ℓ.

3.3 Study of the $0p$ shell

Imagine supposedly the simplest description of ^{6}He in terms of an inert α-particle core with the neutron pair in the $0p$ orbital of a harmonic oscillator. In an approximation prompted by the choice of LS coupling, no splitting of single-particle levels due to spin-orbital effects will be considered. More on that below.

Obviously an interaction-free scenario where the two valence neutrons simply stay in any single-particle state would be dismissed as improbable, given that in a Borromean nucleus, any two-body subsystem is unbound. However, if a residual interaction is in action, the degeneracy of two-particle configurations is lifted. With the δ interaction in particular, the Hamiltonian of the form

$$\hat{H}_\delta = \frac{\vec{p}_1^{\,2}}{2m} + \frac{1}{2}m\omega^2\vec{r}_1^{\,2} + \frac{\vec{p}_2^{\,2}}{2m} + \frac{1}{2}m\omega^2\vec{r}_2^{\,2} - g\delta(\vec{r}_1 - \vec{r}_2) \tag{3.3.1}$$

is diagonal in LS coupling. Here $\vec{p}$ is the momentum, $\vec{r}$ is the position, m and ω are the mass and the angular frequency. The ground state 0^+ is lowered to a much greater extent than 2^+. The last possible configuration $LS = 11$ is left unaffected.

The nucleus ^{6}He has a $J^\pi = 0^+$ ground state, which can arise from $LS = 00$ or $LS = 11$. The argument above rules out the possibility that $LS = 11$ is a component of the ground state if the δ interaction is, indeed, the dominant interaction. Alternatively, the Cohen-Kurath effective interaction for the $0p$ shell [33] can be used to show that two nucleons in the $0p$ shell have 99% probability of being in the state $|(0p)^2;00\rangle$ and 1% probability of being in the state $|(0p)^2;11\rangle$.

The agreement between the two methods validates the choice of the LS coupling scheme. As for the spin-orbit splitting we have neglected so far, it would only lower slightly the total single particle energy of the $LS = 00$ states and would not alter the conclusions drawn below whatsoever.

When the neutron pair is confined to the $0p$ shell, the $C_\alpha(r,R)$ and $\mathcal{P}_{\ell L}(\theta_{12})$ for the three configurations $LS = 00, 11, 20$ in the $0p$ orbital are equivalent to the graphs in Fig. 2.2(a) and in Fig. 2.10(a) (For convenience, we set the oscillator length b to 1 fm for the moment, which only modifies the scale of the plots.). The cigar-like and the di-neutron configurations are manifested with equal probability in the ground state 0^+.

On a side note, Zhukov *et al.* [14], using the COSMA (cluster-orbital shell model approximation) model, have found a pure $(0p)^2$ configuration for ^{6}He that fits the r.m.s radius and the momentum distribution of realistic three-body calculations.

3.4 Study of many major harmonic oscillator shells

When confined to the $0p$ orbital, the two valence neutrons interacting through the δ interaction have the ground state $|(0p)^2; 00\rangle$. In this section, the restriction to the $0p$ orbital is removed. The effect of configuration mixing via the δ interaction on the two-particle correlation of the 0^+ ground state is examined. More explicitly, we study the properties of $C_\alpha(r,R)$ of the two-valence-neutron ground state as a function of $\xi \equiv gb^{-3}/\hbar\omega$, in the basis composed only of 0^+ states.

It is worth mentioning that since the spin-orbital interaction is neglected, the ground-state wave function and hence the two-particle correlation function, depend on a single parameter ξ, the ratio of the interaction strength g to the spacing between two consecutive harmonic-oscillator levels $\hbar\omega = \frac{\hbar^2}{mb^2}$, which indicates the competition between the harmonic oscillator potential and the δ interaction.

Our second interest concerns the effect of the valence space. We choose, a pri-

ori, a truncated valence space and examine the evolution of the spatial structure of the ground state by having ξ run from 0 to $+\infty$. Then more and more major shells will be allowed in the calculation to enlarge the valence space.

Major harmonic oscillator shells $N = 1, 2, 3$

We start with the valence space comprising major shells $N = 1$ ($0p$), $N = 2$ ($1s$, $0d$), and $N = 3$ ($1p$, $0f$).

The normalized ground-state (henceforth denoted by g. s.) correlation functions for ξ assuming increasing positive values are presented in Fig. 3.2.

As g increases, the δ interaction has different effects on the two maxima observed above in the ground state of two valence neutrons confined in the $0p$ shell. These effects stem from the interferences from other orbitals, either constructive or destructive. The di-neutron configuration stands firm while the cigar-like configuration subsides. The probability of the di-neutron configuration increases as ξ increases until ξ becomes very large ($\gg 100$ fm^3), when it drops a little bit from the maximum value of about 70%. This is due to the fact that higher orbitals in the valence space become more involved. As a result, we perceive small maxima originating from higher orbitals and arranged on concentric circles emerge at larger radii, a phenomenon resulting from the behavior of the correlation function $C_\alpha(r, R)$ that has been studied in section 2.2.4.

Contrastingly, the probability of the cigar configuration diminishes with increasing ξ until $\xi \gg 100$. Meanwhile, in both configurations the relative distances between the two particles also alter perceivably with increasing ξ. The two neutrons are drawn closer towards each other and the size of the neutron pair is reduced.

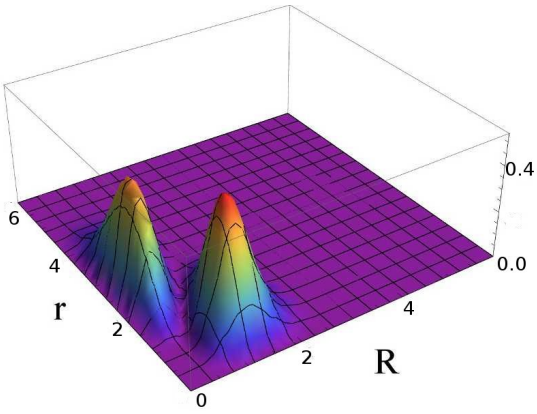

(a) $\xi = 1$

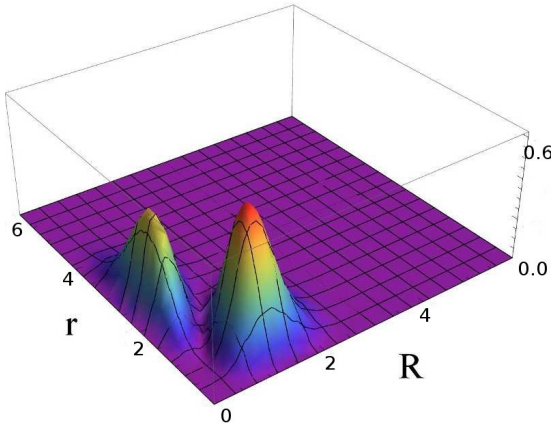

(b) $\xi = 5$

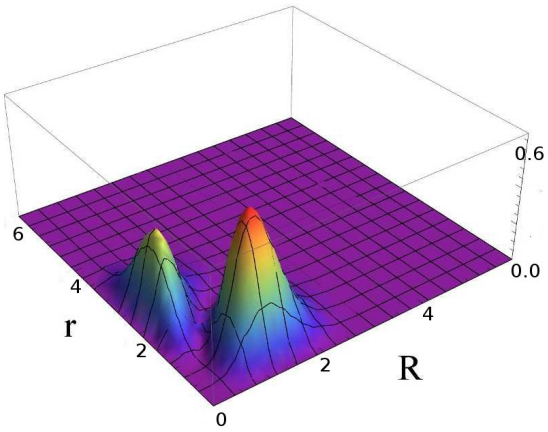

(c) $\xi = 10$

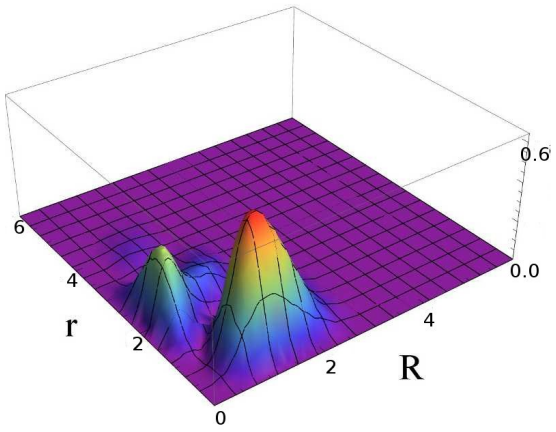

(d) $\xi = 30$

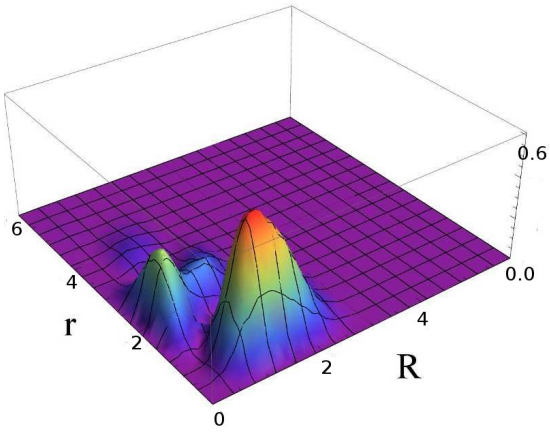

(e) $\xi = 50$

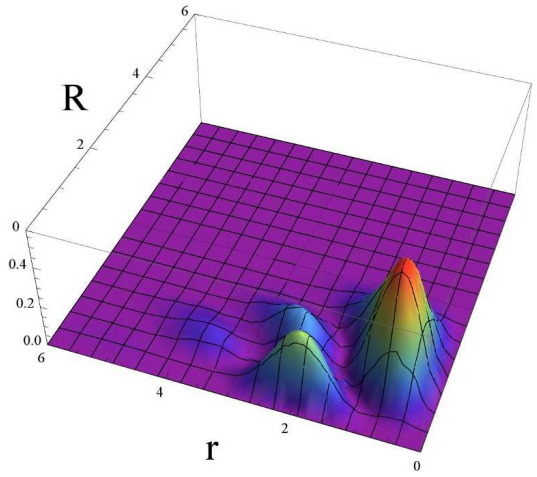

(f) $\xi = 100$

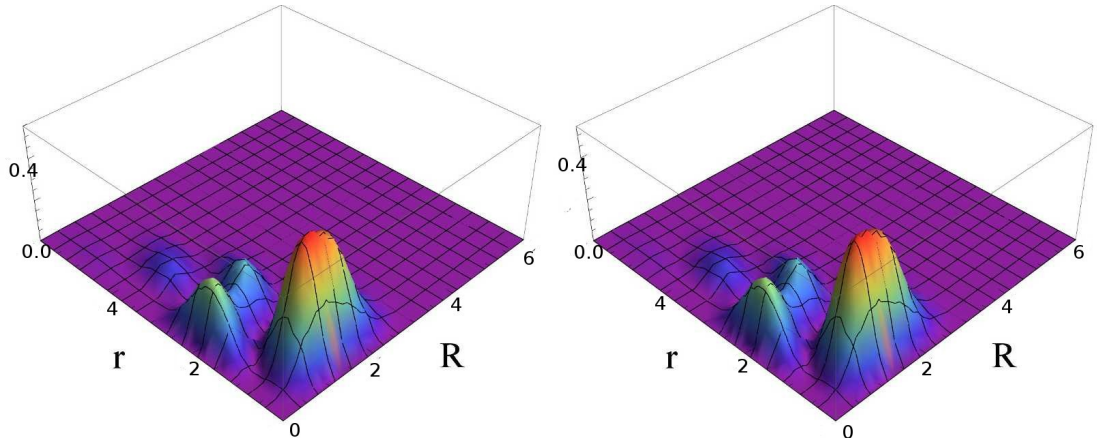

(g) $\xi = 1000$ (h) $\xi = 5000$

Figure 3.2: Evolution of the g. s. correlation function with increasing ξ in the valence space containing $N = 1, 2, 3$.

Major harmonic oscillator shells $N = 1, 2, 3, 4$

We now incorporate the $N = 4$ major shell, that is, the $2s$, $1d$ and $0g$ orbitals, and inspect the evolution of the g. s. correlation function in this valence space in Fig. 3.3. What has been observed above for the valence space up to $N = 3$ is still true.

As for the effect of the valence space dimension, the bigger the valence space is, the more sensitive the wave function and consequently the correlation function of the ground state are to the variation of ξ. For example, in the current valence space, a given value of ξ, say 5, brings about a stronger shrinkage (Fig. 3.3(a)) of the cigar configuration than it does previously (Fig. 3.2(b)). This is not a coincidence and has its physical interpretation to which we will return later in Sec. 3.5.3 while looking for realistic values of g.

Major harmonic oscillator shells $N = 1, 2, 3, 4, 5$

As we continue to expand the valence space, the evolution of the g.s. correlation function maintains the major properties observed above. For brevity, only graphs for some extreme values of ξ are presented in Fig. 3.4 for the valence

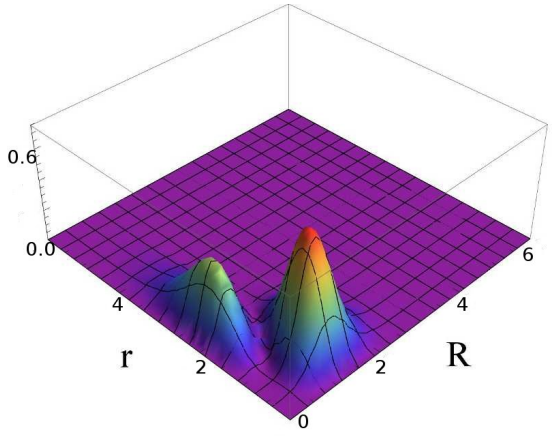

(a) $\xi = 5$

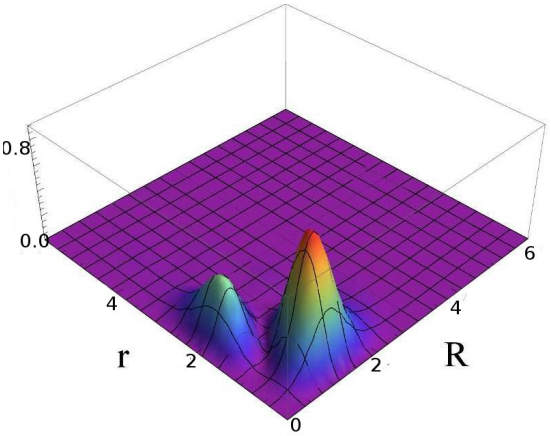

(b) $\xi = 10$

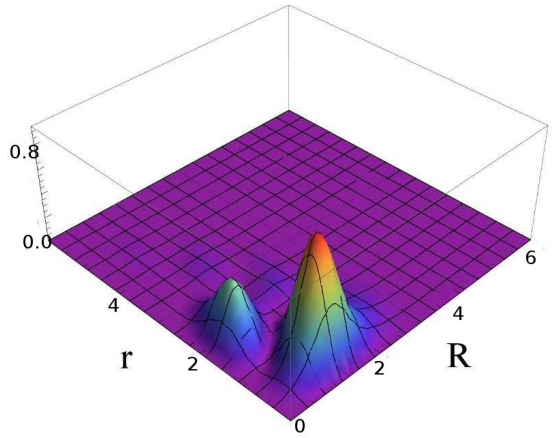

(c) $\xi = 20$

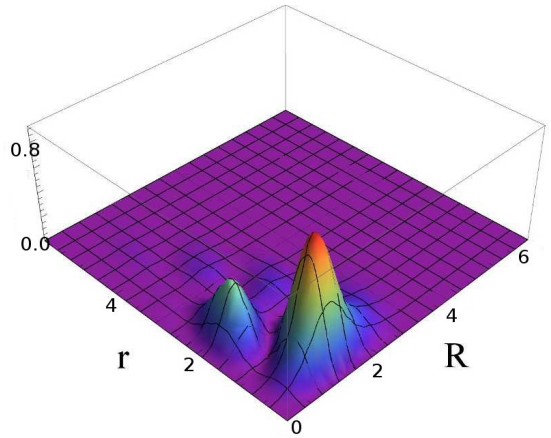

(d) $\xi = 30$

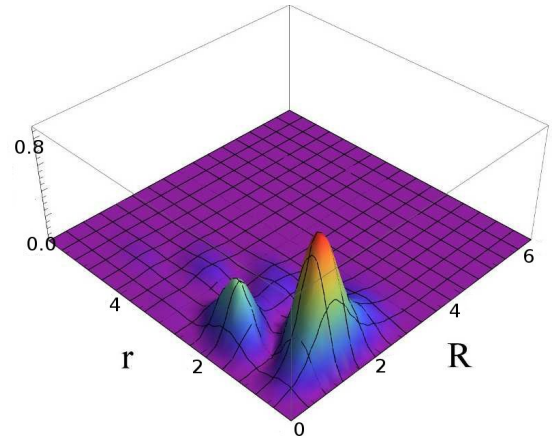

(e) $\xi = 50$

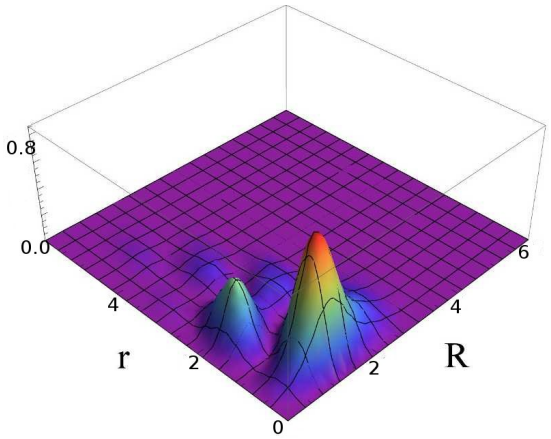

(f) $\xi = 100$

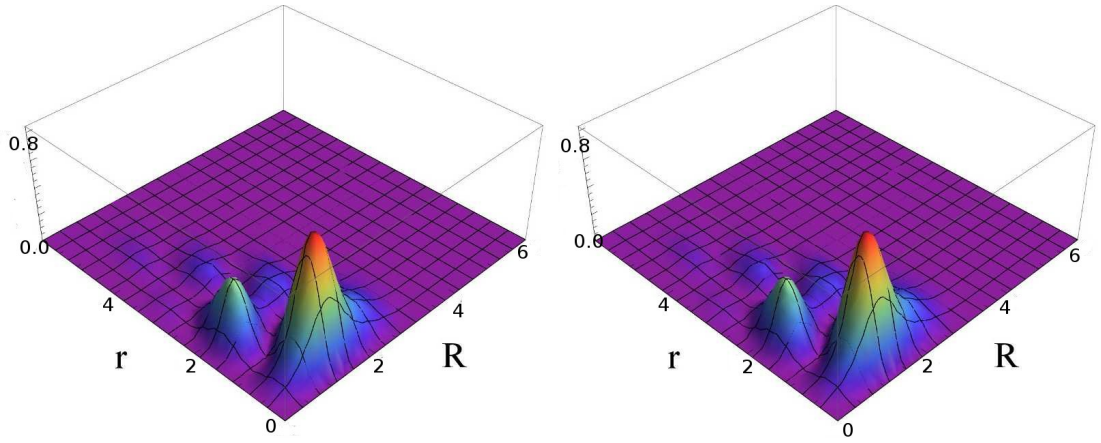

(g) $\xi = 200$ (h) $\xi = 500$

Figure 3.3: Evolution of the g.s. correlation function with increasing ξ in the valence space $N = 1, 2, 3, 4$.

space containing $N = 5$. We also notice that with expanding valence space, the di-neutron configuration grows more pronounced.

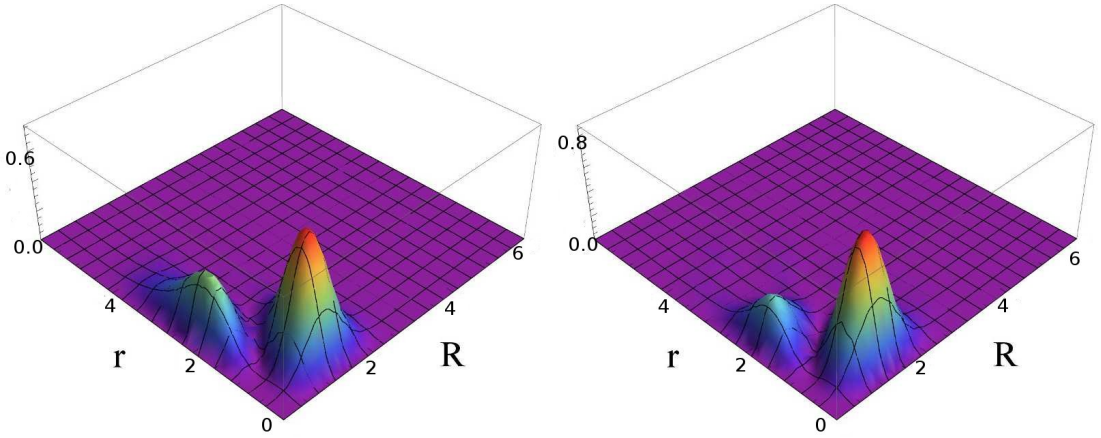

(a) $\xi = 5$ (b) $\xi = 10$

Major harmonic oscillator shells $N = 1, 2, 3, 4, 5, 6$

Fig. 3.5 shows the evolution of the g.s. correlation function in the valence space containing $N = 1, 2, 3, 4, 5, 6$. The results obtained so far provide us with the evidence indicating that the effect of the δ interaction behaves similarly in various many-shell valence spaces starting from the $0p$ shell.

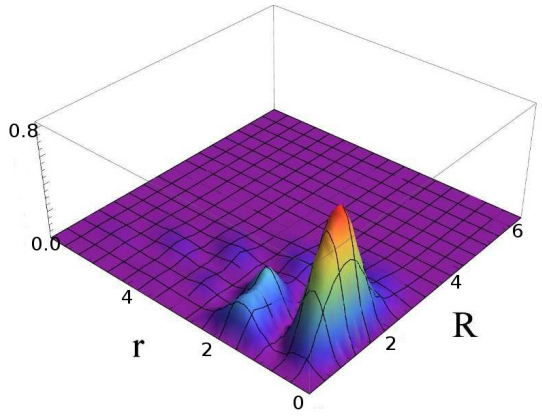

(c) $\xi = 100$

Figure 3.4: Evolution of the g.s. correlation function with increasing ξ in the valence space $N = 1, 2, 3, 4, 5$.

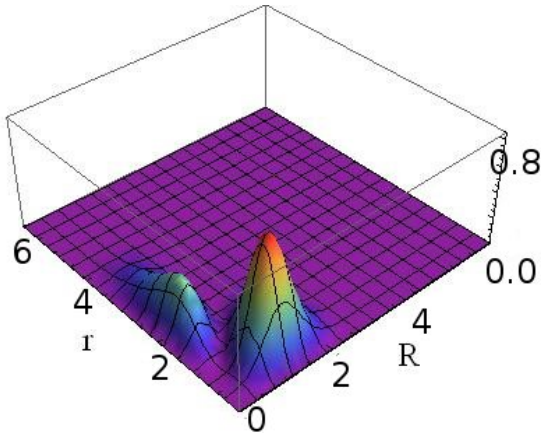

(a) $\xi = 5$

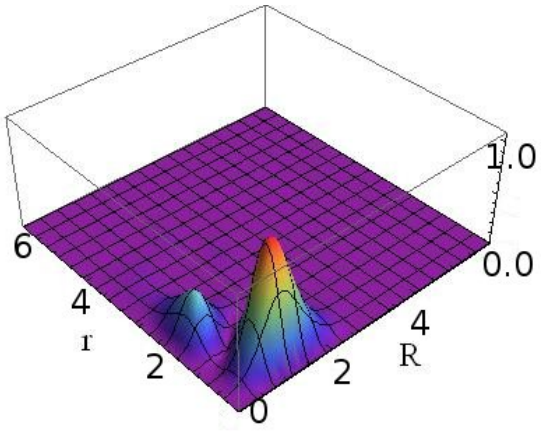

(b) $\xi = 10$

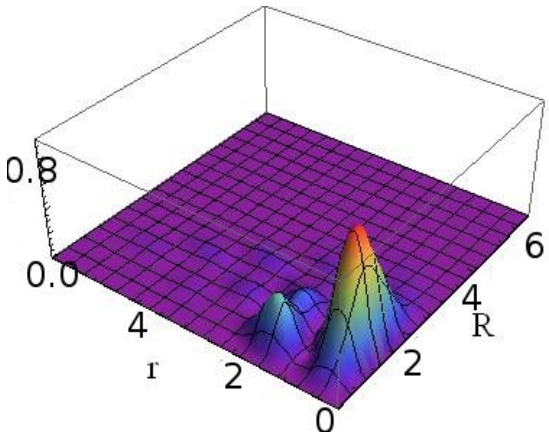

(c) $\xi = 100$

Figure 3.5: Evolution of the g.s. correlation function with increasing ξ in the valence space $N = 1, 2, 3, 4, 5, 6$.

3.5 Elimination of the center of mass motion

3.5.1 Spurious states

The assumption of a single-particle mean field essential to the shell model has a conceptual flaw that lies in the existence of a fixed origin of the single-particle potential. Such a fictitious origin is in violation of translational invariance that is a requisite for an internal nuclear Hamiltonian. In other words, a Hamiltonian H_0 with an origin fixed in space does not commute with the total momentum operator $\sum_{i=1}^{A} \vec{p}_i$, the generator of the translation group, and therefore contains a Hamiltonian for the center of mass that is not one for a free particle. What is termed a spurious state is a nuclear state whose CM wave function is not a plane wave.

In the study of the structure of an A-nucleon nucleus, only the relative movements of the A components are of interest, requiring $3(A-1)$ degrees of freedom in Euclidean space. The other 3 degrees of freedom belong to the CM and should be treated to remove the overall translation of the system.

In a harmonic oscillator potential, the CM Hamiltonian separates out nicely as shown in the following. For A nucleons in a harmonic oscillator potential, the Hamiltonian is

$$\hat{H}_0 = \frac{1}{2m}\sum_{i=1}^{A}\vec{p}_i^{\,2} + \frac{1}{2}m\omega^2\sum_{i=1}^{A}\vec{r}_i^{\,2}. \tag{3.5.1}$$

If we define the CM coordinate by

$$\vec{r} = \frac{1}{A}\sum_{i=1}^{A}\vec{r}_i, \tag{3.5.2}$$

and consequently the CM momentum by

$$\vec{p} = \sum_{i=1}^{A} \vec{p}_i, \tag{3.5.3}$$

H_0 can be divided into an intrinsic component of the relative coordinates and a CM component

$$\hat{H}_0 = \frac{1}{2m} \sum_{i=1}^{A} \vec{p}\,'^2_i + \frac{1}{2} m\omega^2 \sum_{i=1}^{A} \vec{r}\,'^2_i + \frac{1}{2mA} \vec{p}^{\,2} + \frac{1}{2} mA\omega^2 \vec{r}^{\,2}, \tag{3.5.4}$$

where $\vec{r}\,'_i$ are the relative coordinates and $\vec{p}\,'_i$ the relative momenta given by

$$\vec{r}\,'_i = \vec{r}_i - \vec{r}, \qquad \vec{p}\,'_i = \vec{p}_i - \frac{1}{A}\vec{p}. \tag{3.5.5}$$

Therefore, the CM Hamiltonian is also a harmonic oscillator with the mass Am.

3.5.2 Cluster-orbital shell model

A peculiarity of a halo nucleus is the formation of a more stable core with a few weakly bound nucleons penetrating into regions far from the core, resulting in a very different nuclear density from that of the core, both in dimension and in shape. In the case of ^{6}He, the matter r.m.s. radius of ^{4}He is 1.57 (4) fm [34] and that of ^{6}He is about 2.48 (3) fm [34], making the radius of the halo neutrons of the order of 4.01 fm. The ^{4}He core is strongly bound, while the valence neutrons are loosely bound to ^{4}He at 0.972(1) MeV [35] and do not have any bound excited state. This naturally makes one conjecture that few-body models in terms of an inert core plus the individual valence nucleons would be appropriate to describe halo nuclear systems. Furthermore, it has been argued, based on the total spins of halo neutrons determined by measurements, that in spite of the unusual extended neutron densities, the valence neutrons in many neutron-rich nuclei, such as ^{6}He $((0p_{3/2})^2)$, ^{8}He $((0p_{3/2})^4)$ and ^{11}Li $((0p_{3/2})^4(0p_{1/2})^2)$, to name a few, are still

very much likely to follow the orbital ordering that the shell model builds on.

Based on the arguments mentioned above, Suzuki *et al.* proposed the cluster-orbital shell model (COSM) [15, 36, 37] that unifies the shell model and the cluster model to account for different aspects of halo nuclei.

One great advantage of COSM is that it is free from spurious CM motion, which is achieved by introducing translationally invariant coordinates between the nucleons and the CM of the core. One set of coordinates used in COSM is defined as follows. If $\vec{r}_1, \vec{r}_2, \cdots, \vec{r}_n$ are the positions of the n valence nucleons and $\vec{r}_{n+1}, \vec{r}_{n+2}, \cdots, \vec{r}_{n+f}$ those of the f nucleons in the core, then the normalized CM coordinate of the core is

$$\vec{R}_c = \left(\frac{1}{f}\right)^{\frac{1}{2}} (\vec{r}_{n+1} + \vec{r}_{n+2} + \cdots + \vec{r}_{n+f}). \tag{3.5.6}$$

The valence nucleons coordinates $\vec{x}_i$ and the core nucleons coordinates $\vec{\rho}_i$ relative to the CM of the core become

$$\begin{aligned} \vec{x}_i &= \vec{r}_i - \left(\frac{1}{f}\right)^{\frac{1}{2}} \vec{R}_c, \qquad i = 1, 2, \ldots, n, \\ \vec{\rho}_i &= \vec{r}_{i+n} - \left(\frac{1}{f}\right)^{\frac{1}{2}} \vec{R}_c, \qquad i = 1, 2, \ldots, f, \end{aligned} \tag{3.5.7}$$

and the normalized total CM coordinate

$$\vec{R} = \left(\frac{1}{f+n}\right)^{\frac{1}{2}} (\vec{r}_1 + \vec{r}_2 + \cdots + \vec{r}_n) + \left(\frac{f}{f+n}\right)^{\frac{1}{2}} \vec{R}_c. \tag{3.5.8}$$

In the new system of coordinates, the total kinetic energy, after setting the CM momentum of the core to zero, is found to be

$$\hat{K} = \hat{K}_c + \sum_{i=1}^{n} \frac{1}{2\mu} \vec{p}_i^{\,2} + \sum_{j>i=1}^{n} \frac{1}{(f+1)\mu} \vec{p}_i \cdot \vec{p}_j. \tag{3.5.9}$$

In the expression (3.5.9), the first term $\hat{K}_c$ and and the second term $\sum_{i=1}^{n} \frac{1}{2\mu} \vec{p}_i^{\,2}$

are the internal kinetic energy of the core and that of the valence nucleons respectively, and as such are expressed in terms of $-i\hbar\vec{\nabla}_{\vec{\rho}_i}$ and $-i\hbar\vec{\nabla}_{\vec{x}_i}$, the momenta conjugate to the relative coordinates. The reduced mass $\mu = \frac{f}{f+1}m$ of the core plus one valence nucleon system arises when relative coordinates are used. The cross term in (3.5.9) is due to the non-orthogonality of the new coordinate system.

The total COSM Hamiltonian $\hat{H}$, the sum of the kinetic energy $\hat{K}$ and the nucleon-nucleon interactions $\hat{V}$:

$$\hat{V} = \hat{V}_c + \sum_{i=1}^{n}\sum_{j=n+1}^{n+f}\hat{v}_{ij} + \sum_{j>i=1}^{n}\hat{v}_{ij}, \tag{3.5.10}$$

is given by

$$\hat{H} = \hat{H}_c + \sum_{i=1}^{n}\hat{h}_i + \sum_{j>i=1}^{n}\left(\hat{v}_{ij} + \frac{1}{(f+1)\mu}\vec{p}_i\cdot\vec{p}_j\right), \tag{3.5.11}$$

with

$$\begin{aligned}\hat{h}_i &= \frac{1}{2\mu}\vec{p}_i^{\,2} + \sum_{j=n+1}^{n+f}\hat{v}_{ij},\\ \hat{H}_c &= \hat{K}_c + \hat{V}_c.\end{aligned} \tag{3.5.12}$$

Under the assumption that the core-valence nucleon interactions do not depend on the individual core nucleon coordinates $\vec{\rho}_i$, $\hat{h}_i$ can be replaced by a single-particle Hamiltonian $\hat{h}'_i$

$$\hat{h}'_i = \frac{1}{2\mu}\vec{p}_i^{\,2} + \hat{U}_i. \tag{3.5.13}$$

The total Hamiltonian of the valence neutrons, after the omission of $\hat{H}_c$, then takes the form

$$\hat{H} = \sum_{i=1}^{n}\left(\frac{1}{2\mu}\vec{p}_i^{\,2} + \hat{U}_i\right) + \sum_{j>i=1}^{n}\left(\hat{v}_{ij} + \frac{1}{(f+1)\mu}\vec{p}_i\cdot\vec{p}_j\right). \tag{3.5.14}$$

Despite the similarity between Eq. (3.5.13) and the usual shell-model Hamiltonian, the approximation of two-body interactions with a single-particle potential makes $\hat{U}_i$ generally a non-local potential [37].

3.5.3 Correlation function of ^{6}He after the elimination of the CM motion

Suzuki *et al.* have studied the helium isotopes in the strictly formulated cluster-orbital shell model (COSM) in Refs. [15, 37]. Our intention is not to replicate the results of earlier work, but to explore two-particle spatial correlations in a harmonic oscillator potential and to apply it to the testing ground ^{6}He, and the non-spurious COSM Hamiltonian provides a convenient means to exclude the undesired CM motion.

To eliminate the CM motion, Hamiltonian (3.3.1) should be modified to conform to Hamiltonian (3.5.14). With the δ force interaction, the modified Hamiltonian with $f = 4$ and $\mu = \frac{f}{f+1}m = \frac{4}{5}m$ reads

$$\begin{aligned}\hat{H}'_\delta &= \sum_{i=1}^{2}\left(\frac{1}{2\mu}\vec{p}_i^{\,2} + \frac{1}{2}\mu\omega^2\vec{x}_i^{\,2}\right) - g\delta(\vec{x}_1 - \vec{x}_2) + \frac{1}{(f+1)\mu}\vec{p}_1\cdot\vec{p}_2 \\ &= \sum_{i=1}^{2}\left(\frac{5}{8m}\vec{p}_i^{\,2} + \frac{2}{5}m\omega^2\vec{x}_i^{\,2}\right) - g\delta(\vec{x}_1 - \vec{x}_2) + \frac{1}{4m}\vec{p}_1\cdot\vec{p}_2, \end{aligned} \tag{3.5.15}$$

and has its potential origin properly defined as the CM of the α particle. Correlation functions in various valence spaces are to be re-evaluated with Hamiltonian (3.5.15). In addition, we will get an idea of the two-neutron separation energy S_{2n}.

Before going ahead to evaluate S_{2n}, due to the fact that a harmonic oscillator potential is always bound, we must first define phenomenologically the single-particle energy in the $0p$ shell, the lowest single-particle energy level available for the valence neutrons. This is equal to adding a constant potential term to

Hamiltonian (3.5.15). If we picture ^{5}He as an α particle plus one neutron in the $0p$ shell, as did Hafstad *et al.* in Ref. [38] and Friedrich in Ref. [39], both of whom obtained binding energies for ^{5}He in nice agreement with experimental data, the single-particle energy of the $0p$ shell relative to the α particle can be equated with the opposite of the neutron separation energy S_n of the single neutron in the unbound nucleus ^{5}He, which has been measured to be $-0.89(5)$ MeV [35].

The single-particle level spacing $\hbar\omega$ is related to the oscillator length b through

$$\hbar\omega = \frac{\hbar^2}{mb^2}. \tag{3.5.16}$$

The factor $\hbar^2/m$ has the value 41.43 MeV fm^2 for neutrons. With the COSM Hamiltonian, the reduced mass must be used. The oscillator length b is determined phenomenologically from the r.m.s. radius of the valence neutrons as follows. In the CM referential frame of the ^{6}He nucleus, the CM coordinates of the core $\vec{r}_c$ are

$$\vec{r}_c = -\frac{1}{6}(\vec{x}_1 + \vec{x}_2), \tag{3.5.17}$$

and those of the valence neutrons are

$$\vec{r}_{v1} = \frac{5}{6}\vec{x}_1 - \frac{1}{6}\vec{x}_2, \qquad \vec{r}_{v2} = \frac{5}{6}\vec{x}_2 - \frac{1}{6}\vec{x}_1. \tag{3.5.18}$$

where $\vec{x}_1$ and $\vec{x}_2$, together with $\vec{\rho}_i$ used below, are the coordinates relative to $\vec{r}_c$ defined above. Since the matter r.m.s. radius of ^{6}He, $R_m(^6\text{He})$, is measured in the CM referential frame of ^{6}He, we have

$$\begin{aligned} 6R_m^2(^6\text{He}) &= \sum_{i=1}^{2}\langle(\vec{r}_c + \vec{x}_i)^2\rangle + \sum_{i=1}^{4}\langle(\vec{r}_c + \vec{\rho}_i)^2\rangle \\ &= 6\langle\vec{r}_c^{\,2}\rangle + \sum_{i=1}^{2}\langle\vec{x}_i^{\,2}\rangle + \sum_{i=1}^{4}\langle\vec{\rho}_i^{\,2}\rangle + 2\sum_{i=1}^{2}\langle\vec{r}_c\cdot\vec{x}_i\rangle. \end{aligned} \tag{3.5.19}$$

If we take into account relation (3.5.17), Eq. (3.5.19) becomes

$$\begin{aligned} 6R_m^2(^6\mathrm{He}) &= \frac{1}{6}\langle(\vec{x}_1+\vec{x}_2)^2\rangle + \langle\vec{x}_1^2\rangle + \langle\vec{x}_2^2\rangle - \frac{1}{3}\langle(\vec{x}_1+\vec{x}_2)^2\rangle + \sum_{i=1}^{4}\langle\vec{\rho}_i^2\rangle \\ &= \frac{5}{6}\langle\vec{x}_1^2+\vec{x}_2^2\rangle - \frac{1}{3}\langle\vec{x}_1\vec{x}_2\rangle + 4R_m^2(^4\mathrm{He}) \\ &= \frac{5}{3}\langle\vec{x}_1^2\rangle - \frac{1}{3}\langle\vec{x}_1\cdot\vec{x}_2\rangle + 4R_m^2(^4\mathrm{He}). \end{aligned} \tag{3.5.20}$$

The expectation values $\langle\vec{x}_1^2\rangle$ and $\langle\vec{x}_1\cdot\vec{x}_2\rangle$ are directly related to b through the wave function. To get an idea of the order of magnitude of b, we consider the wave function of the neutrons both in the $0p$ shell coupled to the total orbital angular momentum $L=0$. In such a case, we have $\langle\vec{x}_1^2\rangle = (1+\frac{3}{2})b^2$ and $\langle\vec{x}_1\cdot\vec{x}_2\rangle$=0. Experimental estimates give 2.48 (3) fm for $R_m(^6\mathrm{He})$ and 1.57 (4) fm for $R_m(^4\mathrm{He})$, yielding 2.55 fm for b. It is with this value of b that we will re-examine the spatial correlation of ^{6}He.

The general properties that have been observed in Sec. 3.4 for the spatial correlation in ^{6}He obtained with Hamiltonian (3.3.1) are still valid despite the modification of the Hamiltonian, and hence will not be reiterated.

We have seen in Sec. 3.4 that the bigger the valence space is, the more sensitive $C_\alpha(r,R)$ is to the variation of g. However, we have yet to determine a realistic value of g, which we expect to diminish with expanding valence space. It is worthwhile to mention that the three-dimensional δ interaction only has physical meaning in a truncated space. It has been proved that for free neutrons, asymptotically, the magnitude of g varies inversely with the cutoff momentum in a momentum space [40]. Therefore, we must choose a truncation that suits our problem.

The δ interaction defined simply as $V_0\delta(\vec{r}_1-\vec{r}_2)$ with V_0 characterized in terms of the free neutron scattering length is often dismissed as overestimating the free interaction in the nuclear interior [41]. It is then often given a density dependence and called density dependent δ interaction (DDDI). The effective DDDI

can be translated into different forms. The most widely used effective DDDI is expressed as the free neutron δ interaction $V_0\delta(\vec{r}_1-\vec{r}_2)$ multiplied with a function of $(\vec{r}_1+\vec{r}_2)/2$ [40, 41] to simulate the effect of the density that is also supposed to be a function over $(\vec{r}_1+\vec{r}_2)/2$. The choice of parameters including the cutoff energy is done in such a way as to meet the experimental data, e.g., the separation energy, and to reproduce pairing gaps calculated with other forces. In another approach, Matsuo [42], by assuming a low-density uniform nuclear matter environment, studied the spatial structure of neutron Cooper pairs in relation to the total density by means of BCS calculations using a bare force and the effective Gogny interaction. He subsequently showed that a zero-rangle δ interaction of the form $\propto V_0(\rho_{tot})\delta(\vec{r}_1-\vec{r}_2)$ can also describe the spatial structure, provided that $V_0(\rho_{tot})$ and the cutoff energy is chosen specifically for each value of total density so that both the pairing gaps and the spatial structure are reasonably reproduced.

At first glance, it seems that there is no density dependence in our case. However, the interaction strength g plays the role of $V_0(\rho_{tot})$, even though ρ_{tot} will not be explicitly determined. Since the first excited state of ^{6}He is a 2^+ state found at 1.797(25) MeV [43], we will identify this value with the calculated 2^+-0^+ energy difference that is a function of g, and thus obtain a realistic value of g in each valence space, with which the spatial correlation will be examined and the ground-state energy evaluated.

We denote the value of g that reproduces the correct 2^+-0^+ energy difference by g_r (r for realistic), and plot in Fig. 3.6 the value of g_r in each valence space that has been tried from $N=2$ up to $N=19$. As expected, g_r goes down as the valence space expands.

With the values of g_r obtained above, the wave functions of the 0^+ ground state in various valence spaces are remarkably consistent with each other, with about 92% probability (probability amplitude of about 0.96) of being $|(0p)^2;00\rangle$, followed by about 4% probability (probability amplitude of about 0.2) of being $|(0d)^2;00\rangle$. The contributions from other basis vectors are extremely marginal. In

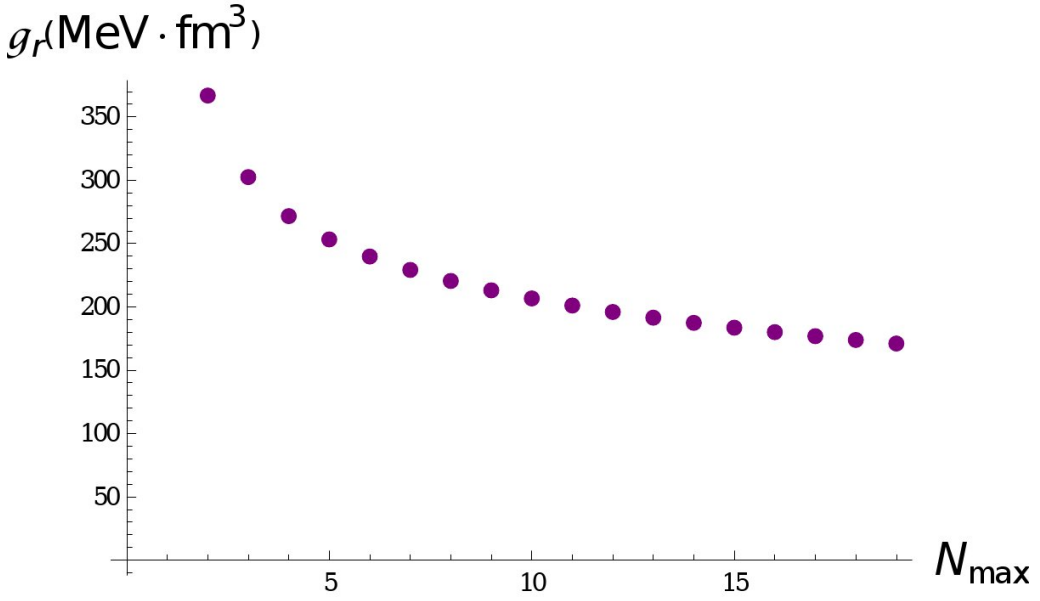

Figure 3.6: The value of g_r that generates the correct $2^+ - 0^+$ energy splitting vs. the number of orbits contained in the valence space.

consequence, the correlation function $C_\alpha(r,R)$ of the 0^+ ground state in a realistic case is determined by the two major components from $0p$ and $0d$ shells and practically does not depend on the size of the valence space as long as it contains the $N = 2$ major shell (to include the $0d$ shell). This is illustrated in Fig. 3.7. The probability of the di-neutron configuration reaches 60% with the first truncation and 61% with the second.

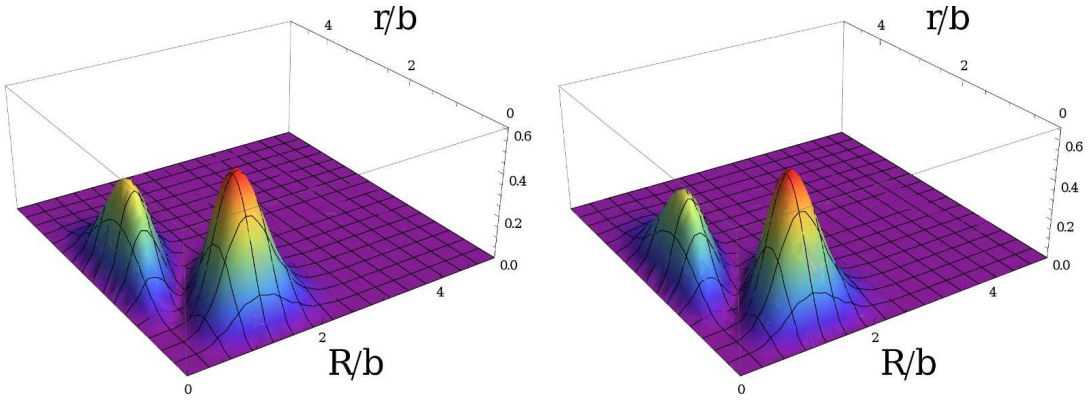

(a) $N_{max} = 3$, $g_r = 302$ MeV· fm^3 (b) $N_{max} = 4$, $g_r = 272$ MeV· fm^3

Figure 3.7: Realistic correlation function $C_\alpha(r,R)$ obtained with g_r in two different valence spaces.

Fig. 3.8 shows the ground-state energy in each valence space calculated with

g_r. The 0^+ ground-state energy, that is, the two neutron separation energy S_{2n} obtained thus decreases with the dimension of the valence space and would finally converge, should we continue to expand the valence space.

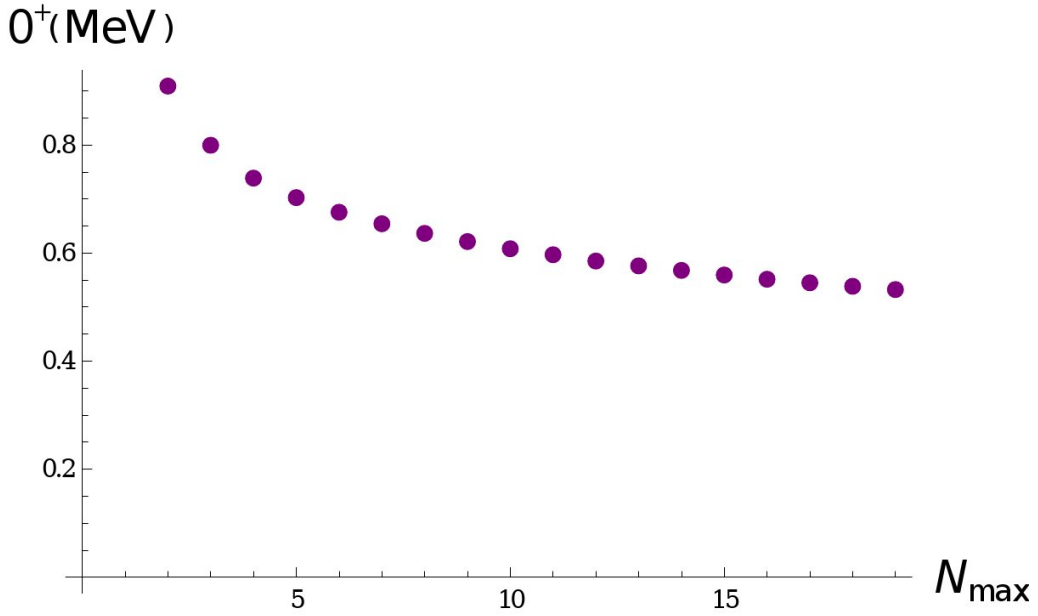

Figure 3.8: The energy of 0^+ vs. the number of orbits contained in the valence space.

The fact that the sought wave function is made up principally of $|(0p)^2;00\rangle$ with a much smaller contribution of $|(0d)^2;00\rangle$ and is influenced by the truncated valence space only negligibly as long as the cut-off on N has $N = 2$ included, agrees with the argument that halo nucleons can only exist in s and p waves [9] and gives us reason to believe that it is appropriate to truncate the valence space at $N = 2$ or at most $N = 3$. Once the valence space truncation is determined, so is S_{2n}. For $N = 2$, S_{2n} is 0.91 MeV and for $N = 3$, 0.81 MeV. They are in quite good agreement with the measured two-neutron separation energy 0.972(1) MeV for the ground state of ^{6}He.

3.6 Conclusions

In this chapter, we analyzed the two-particle spatial correlation of the halo neutron pair in ^{6}He. We first employed a simple harmonic oscillator potential to

describe the single-particle levels and the δ interaction as the residual interaction between the valence neutrons. The effects of the interaction as a function of $\xi \equiv gb^{-3}/\hbar\omega$, and the effects of truncated valence spaces were investigated. We showed that when the neutron pair is confined to the $0p$ shell, the two configurations show up with equal probability as a pure consequence of the geometry of the p shell in the LS coupling scheme. The cigar-like and the di-neutron configurations respond quite differently to the zero-range interaction. The former lessens in probability with increasing ξ until it becomes very large, whereas the latter is enhanced by the interaction. Commonly for both configurations, the neutron pair reduces in size.

Subsequently, a more realistic calculation was carried out based on the concept of COSM that is free from spurious center-of-mass motion. The origin of the harmonic oscillator potential is supposed to be the CM of the α particle, and the oscillator length is chosen phenomenologically. In different truncated valence spaces, the values of g_r that give the correct energy difference between the first excited state 2^+ and the ground state 0^+ are obtained and used to evaluate the wave function of the ground state and the two-neutron separation energy S_{2n} of ^{6}He. The ground-state wave function varies only insignificantly with the expansion of valence space and is mainly in the $0p$ orbit ($\approx 92\%$), the second biggest component being in the $0d$ orbital accounting for only 4% probability. The valence space is therefore truncated according to the wave function composition and S_{2n} is determined to be between -0.91 MeV and -0.81 MeV.

4

Two-particle correlations in ^{6}He with the pairing interaction

The δ interaction is a zero-range interaction defined in coordinate space. Its second quantized form is found with Eq. (4.0.1) that represents the one-to-one correspondence between a "normal" two-body operator $\hat{V}$ from first quantization and its second quantization representation.

$$\hat{V} = \frac{1}{4} \sum_{ijkl} {}_{\text{nas}}\langle ij|\hat{V}|kl\rangle_{\text{nas}} a_i^+ a_j^+ a_l a_k, \tag{4.0.1}$$

where ${}_{\text{nas}}\langle ij|\hat{V}|kl\rangle_{\text{nas}}$ are two-body matrix elements between normalized antisymmetrized wave functions, a_i^+ is the fermion creation operator of a particle in the state denoted by i and a_i the fermion annihilation operator of a particle in the state i. It is also possible to define interactions directly in second quantization. The pairing interaction that will be applied to the ^{6}He nucleus in this chapter is such an example that shows the tendency to correlate nucleons in zero-coupled pairs.

4.1 Pairing Interaction

The pairing interaction in a single orbital in the jj-coupling scheme [44] reads

$$\hat{V} = -G \sum_{m>0,m'>0} (-1)^{j+m}(-1)^{j+m'} a^+_{jm} a^+_{j-m} a_{j-m'} a_{jm'}. \tag{4.1.1}$$

It annihilates a pair of identical nucleons in the states (j,m') and $(j,-m')$ and scatters it into any other pair of states (j,m) and $(j,-m)$. The strength G, given in units of MeV, being constant for all values of m, the matrix elements of the pairing interaction in the two-particle subspace of nucleon pairs $(-1)^{j+m} a^+_{jm} a^+_{j-m}|0\rangle$ ($|0\rangle$ is a closed-shell state), is also constant:

$$\langle 0|(-1)^{j+m'} a_{j-m'} a_{jm'} |\hat{V}| (-1)^{j+m} a^+_{jm} a^+_{j-m}|0\rangle = -G,$$

which makes the scattering isotropic in "m" space.

Alternatively, by defining the pair creation operator

$$S^+_j = \frac{1}{\sqrt{\Omega_j}} \sum_{m>0} (-1)^{j+m} a^+_{jm} a^+_{j-m}, \tag{4.1.2}$$

that creates a nucleon pair in the $J^\pi = 0^+$ state, and its adjoint, the pair annihilation operator

$$S_j = \frac{1}{\sqrt{\Omega_j}} \sum_{m>0} (-1)^{j+m} a_{j-m} a_{jm}, \tag{4.1.3}$$

that annihilates a nucleon pair in the $J^\pi = 0^+$ state, the pairing interaction in Eq. (4.1.1) can be rewritten as

$$\hat{V} = -G\Omega_j S^+_j S_j. \tag{4.1.4}$$

Here $\Omega_j = j + \frac{1}{2}$ is the shell degeneracy or the maximum number of pairs in the

shell. The commutation relation between S_j^+ and S_j is

$$\left[S_j, S_j^+\right] = 1 - \frac{\hat{n}}{\Omega_j}, \tag{4.1.5}$$

where $\hat{n} = \sum_m a_{jm}^+ a_{jm}$ is the particle number operator. For small numbers of particles, $\left[S_j, S_j^+\right] \approx 1$, the reason why S_j and S_j^+ are often called quasi-boson operators. Some other useful relations are

$$\langle 0|(S_j)^n (S_j^+)^n|0\rangle = \frac{n!(\Omega_j - 1)!}{(\Omega_j)^{n-1}(\Omega_j - n)!}, \tag{4.1.6}$$

and

$$\left[S_j, (S_j^+)^n\right] = \frac{n}{\Omega_j}(\Omega_j - \hat{n} + n - 1)(S_j^+)^{n-1}. \tag{4.1.7}$$

Diagonalizing the matrix representation of $\hat{V}$ in the subspace of nucleon pairs $(-1)^{j+m} a_{jm}^+ a_{j-m}^+|0\rangle$

$$-G\begin{pmatrix} 1 & 1 & 1 & 1 & \cdot & \cdot \\ 1 & 1 & 1 & 1 & \cdot & \cdot \\ 1 & 1 & 1 & 1 & \cdot & \cdot \\ \cdot & \cdot & \cdot & \cdot & \cdot & \cdot \\ \cdot & \cdot & \cdot & \cdot & \cdot & \cdot \end{pmatrix}, \tag{4.1.8}$$

one gets the eigenstates and eigenvalues of the pairing interaction. The lowest eigenvalue is $-G\Omega_j$ and corresponds to the eigenstate $S_j^+|0\rangle$. All the other eigenstates ($J^\pi = 2^+, 4^+, \cdots, (2j-1)^+$) are degenerates at eigenvalue 0, indicating that they are not affected by such an interaction. This should be compared with the δ interaction, with which the 0^+ is lowered the most, and the other coupled states $J^\pi = 2^+, 4^+, \cdots, (2j-1)^+$, are also affected, albeit to a lesser extent. A schematic comparison between the two interactions is shown in Fig. 4.1. In Chapter 1, the link between pairing and attractive short-range interactions was explained by

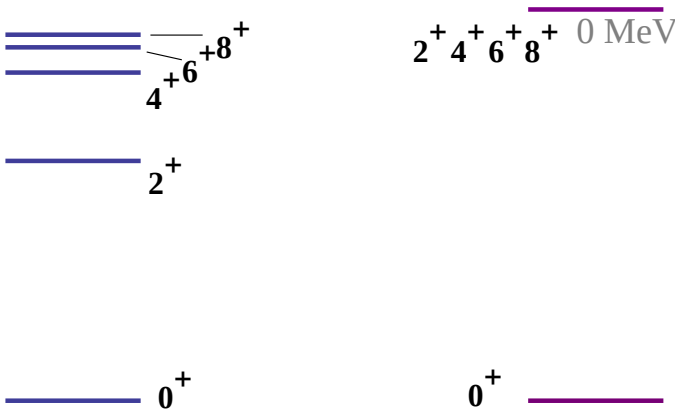

Figure 4.1: The energy levels of δ interaction (left, blue) and pairing interaction (right, purple).

way of multipole expansion. It is high multipole order components found to be important in short-range interactions that are responsible for pairing effect, e. g., the lowering of the 0^+ state and the succession of states with higher angular momenta much less affected than 0^+ in the level scheme. In this sense, the pairing interaction is an even "shorter" range interaction than the δ interaction, though strictly speaking, the pairing interaction is only defined in second quantization and thus has no counterpart in coordinate space.

The pairing interaction for a single shell in the jj coupling scheme can be extended to include more than one shell and to the LS-coupling scheme. We construct similarly a pair of nucleons with angular momentum ℓ and spin $s = 1/2$ coupled to $L = S = 0$ by defining the pair creation operator in the LS coupling

$$\begin{aligned} S^+_\ell &= \frac{1}{\sqrt{\Omega_\ell}} \sum_{m,m_s>0} (-1)^{\ell+m}(-1)^{s+m_s} a^+_{\ell m s m_s} a^+_{\ell -m s -m_s} \\ &= -\frac{1}{\sqrt{\Omega_\ell}} \sum_m (-1)^{\ell+m} a^+_{\ell m \frac{1}{2}} a^+_{\ell -m -\frac{1}{2}}, \end{aligned} \tag{4.1.9}$$

where m_s is the spin projection and $\Omega_\ell = 2\ell + 1$. In the last line of Eq. (4.1.9), the spin quantum number s is omitted since it is always 1/2 for nucleons. Its adjoint,

S_ℓ is accordingly

$$S_\ell = -\frac{1}{\sqrt{\Omega_\ell}} \sum_m (-1)^{\ell+m} a_{\ell -m -\frac{1}{2}} a_{\ell m \frac{1}{2}}. \tag{4.1.10}$$

The single-shell pairing interaction in LS coupling is therefore

$$\hat{V} = -G\Omega_\ell S_\ell^+ S_\ell, \tag{4.1.11}$$

which can be generalized to multiple shells

$$\hat{V} = -\sum_{n\ell,n'\ell'} G_{n\ell,n'\ell'} \sqrt{\Omega_\ell \Omega_{\ell'}} S_{n\ell}^+ S_{n'\ell'}. \tag{4.1.12}$$

The strength $G_{n\ell,n'\ell'}$ in the multi-shell pairing interaction (4.1.12) may be shell-dependent when it comes to scattering between different shells. Precaution must be taken with the sign of $G_{n\ell,n'\ell'}$. With the Biedenharn-Rose (BR) phase convention that uses spatial single-particle wave functions of the form

$$\phi_{n\ell m_\ell}(\vec{r}) = \mathcal{R}_{n\ell}(r) i^\ell \mathcal{Y}_{\ell m_\ell}(\theta, \varphi), \tag{4.1.13}$$

G_{ik} is invariably positive. The BR phase convention is quite often used in pairing theory. It has the advantage that by acting with the time-reversal operator on the wave function (4.1.13), a convenient phase factor is generated that is consistent with the phase factor required to transform the annihilation operator a_{jm} into a covariant tensor of rank j, $(-1)^{j+m} a_{jm}$ [45]. In this work, we use exclusively the Condon-Shortley (CS) convention defining single-particle wave functions without the phase factor i^ℓ. By inspecting the matrix elements of the zero-range attractive δ interaction between different orbitals, we see that

$$\begin{aligned} &\langle n\ell n\ell; 0|\delta(\vec{r}_1 - \vec{r}_2)|n'\ell' n'\ell'; 0\rangle = \\ &\quad (-1)^{\ell+\ell'} \frac{\sqrt{(2\ell+1)(2\ell'+1)}}{4\pi} \int_0^{+\infty} \mathcal{R}_{n\ell}^2(r) \mathcal{R}_{n'\ell'}^2(r) r^2 dr, \end{aligned} \tag{4.1.14}$$

which has the sign of $(-1)^{\ell+\ell'}$. Therefore, for the interaction in (4.1.12) to be short-range attractive, unlike G_{ik}, $G_{n\ell,n'\ell'}$ must also has the sign of $(-1)^{\ell+\ell'}$, a difference made by the phase $(i^{\ell})^2(i^{\ell'})^2$. To make this point explicit in the expression of the interaction, we reformulate (4.1.12) as

$$\hat{V} = -\sum_{n,\ell,n',\ell'} (-1)^{\ell+\ell'} G_{n\ell n'\ell'} \sqrt{\Omega_\ell \Omega_{\ell'}} S^+_{n\ell} S_{n'\ell'}, \tag{4.1.15}$$

so that $G_{n\ell n'\ell'}$ is invariably positive.

The matrix elements of the pairing interaction can be evaluated with relations (4.1.5), (4.1.6), and (4.1.7). For one pair of particles, we have, with the pairing interaction defined in (4.1.15)

$$\langle 0|S_{n'\ell'} \hat{V} S^+_{n\ell}|0\rangle = -(-1)^{\ell+\ell'} G_{n\ell n'\ell'} \Omega_\ell \Omega_{\ell'}. \tag{4.1.16}$$

4.2 Pairing Interaction in ^{6}He

In this section, we will study ^{6}He with basically the same approach as in Chapter 3 with the exception that instead of the δ interaction, a pairing interaction with constant $G_{n\ell n'\ell'} = G$ will be used. More specifically, the pairing Hamiltonian uncorrected for CM motion will first be used to examine correlation functions in a general sense, and then the CM will be corrected with the non-spurious COSM Hamiltonian (3.5.14) to allow for the evaluation of the two-neutron separation energy and the realistic values of G in several truncated spaces.

a. The pairing Hamiltonian uncorrected for CM motion

Since the pairing interaction is only defined in second quantization, the one-body part of the Hamiltonian should also be expressed in second quantization for con-

sistency. The pairing Hamiltonian uncorrected for CM motion is

$$\hat{H}_{pair} = \sum_{n\ell m m_s} \epsilon_{n\ell m m_s} a^+_{n\ell m m_s} a_{n\ell m m_s} - \sum_{n\ell n'\ell'} (-1)^{\ell+\ell'} G\sqrt{\Omega_\ell \Omega_{\ell'}} S^+_{n\ell} S_{n'\ell'}, \tag{4.2.1}$$

which, under the assumption that all the single-particle states in an orbital $n\ell$ are degenerate, can be also rewritten as

$$\hat{H}_{pair} = -\sum_{n\ell} \epsilon_{n\ell}\sqrt{2(2\ell+1)}[a^+_{n\ell\frac{1}{2}} \otimes \tilde{a}_{n\ell\frac{1}{2}}]^{00} - \sum_{n\ell n'\ell'} (-1)^{\ell+\ell'} G\sqrt{\Omega_\ell \Omega_{\ell'}} S^+_{n\ell} S_{n'\ell'}, \tag{4.2.2}$$

The operator $\tilde{a}_{\ell m\frac{1}{2}m_s}$, or $\tilde{a}_{jm}$ in jj coupling, is the hole creation operator defined in LS coupling or jj coupling respectively as follows,

$$\begin{aligned} \tilde{a}_{\ell m\frac{1}{2}m_s} &= (-1)^{\ell+m+\frac{1}{2}+m_s} a_{\ell -m\frac{1}{2}-m_s}, \\ \tilde{a}_{jm} &= (-1)^{j+m} a_{j-m}. \end{aligned} \tag{4.2.3}$$

The hole creation operator defined thus is a spherical tensor that can be coupled with other spherical tensors such as $a^+_{\ell m\frac{1}{2}m_s}$ or a^+_{jm} using Clebsch-Gordan coefficients. The coupled product, $[a^+_j \otimes \tilde{a}_{j'}]^J_M$ is expressed by

$$[a^+_j \otimes \tilde{a}_{j'}]^J_M = \sum_{mm'} \langle jmj'm'|JM\rangle a^+_{jm} \tilde{a}_{j'm'}. \tag{4.2.4}$$

It follows that the coupled product in the Hamiltonian (4.2.2) is

$$[a^+_{n\ell\frac{1}{2}} \otimes \tilde{a}_{n\ell\frac{1}{2}}]^{00} = -\frac{1}{\sqrt{2(2\ell+1)}} \hat{n}_{n\ell}, \tag{4.2.5}$$

with $\hat{n}_{n\ell}$ the number operator in the $n\ell$ orbital

$$\hat{n}_{n\ell} = \sum_{mm_s} a^+_{n\ell m m_s} a_{n\ell m m_s}. \tag{4.2.6}$$

As far as one pair of nucleons is concerned, the pairing Hamiltonian (4.2.2) only allows ground states of the form $\sum_{n\ell} \alpha_{n\ell} S^+_{n\ell}|0\rangle$ formed by a pair of nucleons

in the same orbital, as opposed to δ interaction, with which the ground state 0^+ is an admixture of zero-coupled states $|n\ell n'\ell;00\rangle$.

In the following, the correlation of the valence neutrons in the ground state of ^{6}He interacting via the pairing interaction in a HO potential will be investigated in terms of $\xi \equiv G/\hbar\omega$ and the size of valence space. We proceed in the same way as we did for the δ interaction in Sec.3.4. The correlation functions as a function of ξ in the valence spaces containing respectively the major shells $N = 1, 2, 3$ and $N = 1, 2, 3, 4$ are shown in Fig. 4.2 and 4.3.

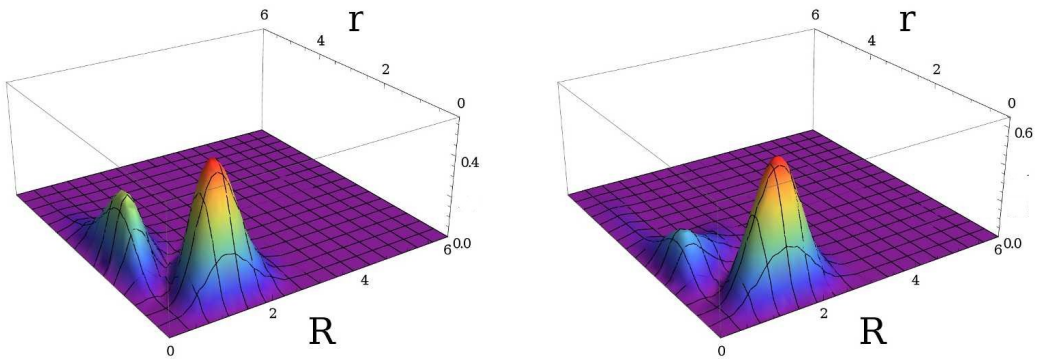

(a) $\xi = 0.1$ (b) $\xi = 0.2$

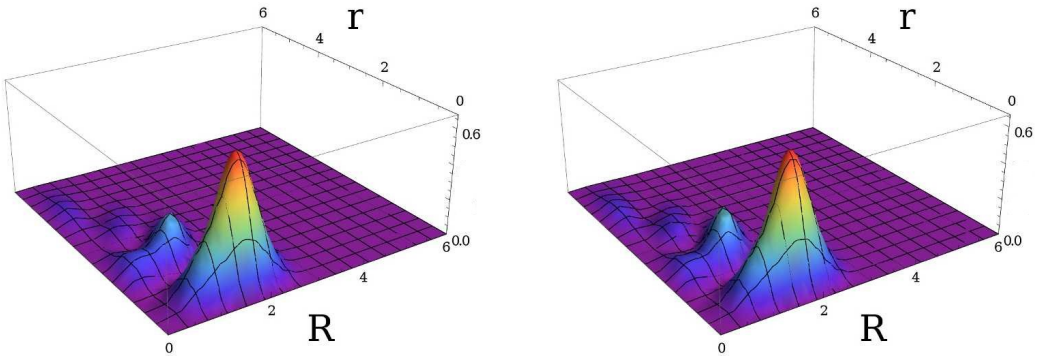

(c) $\xi = 1$ (d) $\xi = 100$

Figure 4.2: Evolution of the g.s. correlation function with increasing ξ in the valence space containing $N = 1, 2, 3$.

Inspecting Fig. 4.2 and 4.3, we see that the conclusion drawn in Sec.3.4 with the δ interaction concerning the evolution of the two major configurations under the influence of ξ and the valence space, etc still holds with pairing interaction.

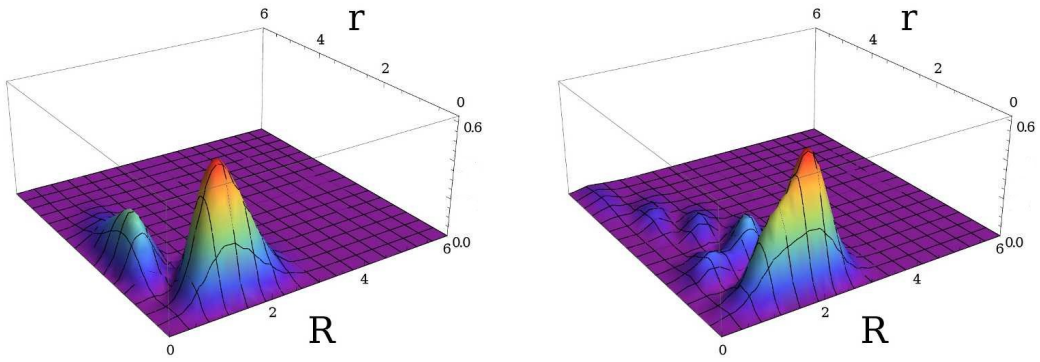

(a) $\xi = 0.1$ (b) $\xi = 100$

Figure 4.3: Evolution of the g.s. correlation function with increasing ξ in the valence space containing $N = 1, 2, 3, 4$.

With the pairing interaction, the effect of higher orbitals is more pronounced for large values of ξ. Another peculiarity is that when ξ tends to $+\infty$, the probability of the ground state being in a certain orbital is proportional to the degeneracy $\Omega = 2\ell + 1$ of that orbital. In other words, in the asymptotic ground-state wave function $\sum_{n\ell} \alpha_{n\ell} S^+_{n\ell}|0\rangle$, the coefficient $\alpha_{n\ell} \propto \sqrt{2\ell+1}$.

b. The pairing Hamiltonian corrected for CM motion

The next step is to correct the CM motion of the Hamiltonian (4.2.2) by adding the two-body cross term $\frac{1}{(f+1)\mu}\vec{p}_i \cdot \vec{p}_j$, which can be transformed into second quantized form with either Eq. (4.0.1), or its equivalent angular momentum coupled form for nucleons (4.2.7)

$$\hat{H} = -\frac{1}{4} \sum_{\substack{n_1\ell_1 n_2\ell_2 \\ n_3\ell_3 n_4\ell_4 LS}} \langle n_1\ell_1 \tfrac{1}{2} n_2\ell_2 \tfrac{1}{2}; LSM_LM_S|\hat{H}|n_3\ell_3 \tfrac{1}{2} n_4\ell_4 \tfrac{1}{2}; LSM_LM_S\rangle (1+\delta_{n_1\ell_1,n_2\ell_2})^{\frac{1}{2}}$$
$$(1+\delta_{n_3\ell_3,n_4\ell_4})^{\frac{1}{2}} \times (2L+1)^{\frac{1}{2}}(2S+1)^{\frac{1}{2}} \left[[a^+_{n_1\ell_1\frac{1}{2}} \otimes a^+_{n_2\ell_2\frac{1}{2}}]^{LS} \otimes [\tilde{a}_{n_3\ell_3\frac{1}{2}} \otimes \tilde{a}_{n_4\ell_4\frac{1}{2}}]^{LS} \right]^{00}. \tag{4.2.7}$$

Here, the four creation or annihilation operators are coupled into pairs using Clebsch-Gordan coefficients, and M_L and M_S are respectively the projection on z of the total orbital angular momentum L and that of the total spin S. Therefore,

in second quantization, the CM corrected Hamiltonian with pairing interaction is

$$\begin{aligned}\hat{H}_{pair} = &-\sum_{n\ell}\epsilon_{n\ell}\sqrt{2(2\ell+1)}[a^{+}_{\ell\frac{1}{2}}\otimes\tilde{a}_{\ell\frac{1}{2}}]^{00} - \sum_{n\ell n'\ell'}(-1)^{\ell+\ell'}G\sqrt{\Omega_{\ell}\Omega_{\ell'}}S^{+}_{n\ell}S_{n'\ell'}\\ &-\frac{1}{4}\sum_{\substack{n_1\ell_1 n_2\ell_2\\ n_3\ell_3 n_4\ell_4 LS}}\langle n_1\ell_1\frac{1}{2}n_2\ell_2\frac{1}{2};LSM_lM_S|\frac{1}{(f+1)\mu}\vec{p}_1\cdot\vec{p}_2|n_3\ell_3\frac{1}{2}n_4\ell_4\frac{1}{2};LSM_LM_S\rangle\\ &((1+\delta_{n_1\ell_1,n_2\ell_2})(1+\delta_{n_3\ell_3,n_4\ell_4}))^{\frac{1}{2}}\times(2L+1)^{\frac{1}{2}}(2S+1)^{\frac{1}{2}}\\ &\times\left[[a^{+}_{\ell_1\frac{1}{2}}\otimes a^{+}_{n_2\ell_2\frac{1}{2}}]^{LS}\otimes[\tilde{a}_{n_3\ell_3\frac{1}{2}}\otimes\tilde{a}_{n_4\ell_4\frac{1}{2}}]^{LS}\right]^{00}. \qquad (4.2.8)\end{aligned}$$

To evaluate the correlation function of ^{6}He with the pairing interaction, parameters such as the oscillator length b determined phenomenologically in Sec.3.5.3 are used. Realistic values of G, G_r, are still adjusted by the energy difference between 2^+ and 0^+ in various truncated valence spaces. The composition of wave function in various valence spaces is perfectly consistent with what has been found for δ interaction, that is, $\approx 92\%$ of $|(0p)^2;00\rangle$ and $\approx 4\%$ of $|(0d)^2;00\rangle$, with minor contributions from the other orbitals. The plots of the correlation functions (Fig. 4.4), as determined by the wave functions, are accordingly almost identical to Fig. 3.7. The probability of the di-neutron configuration is estimated to be $61\% \sim 62\%$.

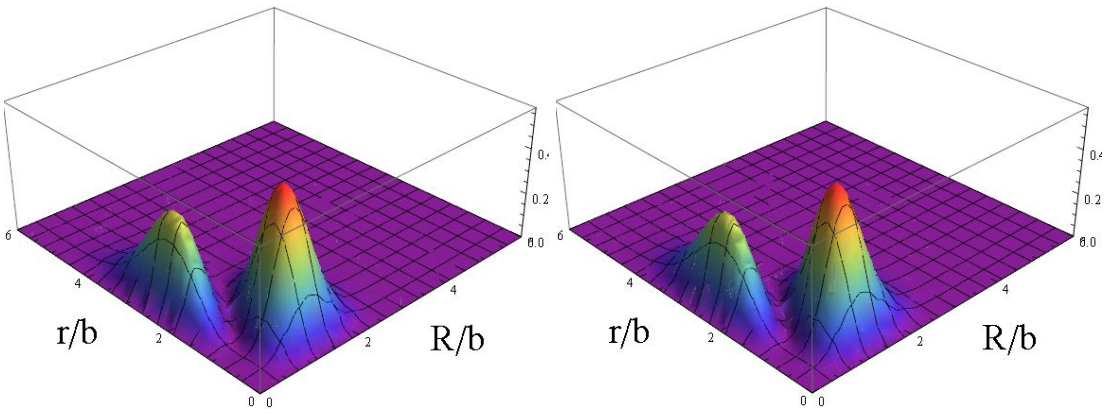

(a) $N_{max} = 3$, $G_r = 0.291$ MeV (b) $N_{max} = 4$, $G_r = 0.262$ MeV

Figure 4.4: The correlation functions $C_\alpha(r, R)$ in two different valence spaces obtained with G_r determined from the 2^+ excitation energy.

5

Angular correlations in ^{8}He

^{8}He is generally considered to have a $\alpha + 4n$ structure with the four valence neutrons in the $0p$ shell. From the point of view of shell model, in the ground state, the four neutrons should stay in the $0p_{\frac{3}{2}}$ shell. However, the four neutrons can also pair up in the state $(0p_{\frac{3}{2}})^2(0p_{\frac{1}{2}})^2$. Indeed, with ^{8}He bound by 3.1 MeV to ^{4}He, it is not hard to imagine that the double di-neutron structure plays a role. In this chapter we will try to shed some light on the geometry of the two 0^+ states of ^{8}He. The geometry of admixed states will also be discussed.

5.1 Configuration 0^+_1: $|(0p_{\frac{3}{2}})^4; 0\rangle$

We shall denote $|(0p_{\frac{3}{2}})^4; 0\rangle$, the 0^+ state in which the valence neutrons completely fill up the $0p_{\frac{3}{2}}$ shell by 0^+_1. In section 5.1.1 we shall obtain the expression for the angular part of its probability density and in section 5.1.2 the spatial configurations that possess the maximum angular probability density.

5.1.1 Angular probability density of 0_1^+

If single particle states are denoted by ϕ_{jm}, for example, $\phi_{\frac{3}{2}\frac{3}{2}} = |j = \frac{3}{2}, m = \frac{3}{2}\rangle$, the non-antisymmetric wave function is given by:

$$\phi_{\frac{3}{2}\frac{3}{2}}(1)\phi_{\frac{3}{2}\frac{1}{2}}(2)\phi_{\frac{3}{2}\frac{-1}{2}}(3)\phi_{\frac{3}{2}\frac{-1}{2}}(4). \tag{5.1.1}$$

As the core degrees of freedom are decoupled from those of the valence neutrons, only the wave function of the valence neutrons needs to be anti-symmetrized, which is done by taking the Slater determinant of wavefunction (5.1.1):

$$\frac{1}{\sqrt{4!}}\begin{vmatrix} \phi_{\frac{3}{2}\frac{3}{2}}(1) & \phi_{\frac{3}{2}\frac{1}{2}}(1) & \phi_{\frac{3}{2}\frac{-1}{2}}(1) & \phi_{\frac{3}{2}\frac{-3}{2}}(1) \\ \phi_{\frac{3}{2}\frac{3}{2}}(2) & \phi_{\frac{3}{2}\frac{1}{2}}(2) & \phi_{\frac{3}{2}\frac{-1}{2}}(2) & \phi_{\frac{3}{2}\frac{-3}{2}}(2) \\ \phi_{\frac{3}{2}\frac{3}{2}}(3) & \phi_{\frac{3}{2}\frac{1}{2}}(3) & \phi_{\frac{3}{2}\frac{-1}{2}}(3) & \phi_{\frac{3}{2}\frac{-3}{2}}(3) \\ \phi_{\frac{3}{2}\frac{3}{2}}(4) & \phi_{\frac{3}{2}\frac{1}{2}}(4) & \phi_{\frac{3}{2}\frac{-1}{2}}(4) & \phi_{\frac{3}{2}\frac{-3}{2}}(4) \end{vmatrix}. \tag{5.1.2}$$

The radial wave function of the $0p$ shell is:

$$\mathcal{R}(r) = \sqrt{\frac{8}{3\sqrt{\pi}b_0^3}}\left(\frac{r}{b_0}\right)\exp\left(-\frac{r^2}{2b_0^2}\right),$$

with b_0 the oscillator length. In the study of ^{8}He, we focus our interest on the angular aspect of its geometry; therefore the radial wave function is neglected in the following and subsequent discussions are valid for *any* p shell. After the omission of radial wave function, the single-particle wave functions in the $0p_{\frac{1}{2}}$ shell are

$$\begin{aligned}
\phi_{\frac{3}{2}\frac{3}{2}} &= \mathcal{Y}_{1,1}(\theta,\phi)\cdot\chi_{\frac{1}{2}}, \\
\phi_{\frac{3}{2}\frac{1}{2}} &= \sqrt{\frac{1}{3}}\mathcal{Y}_{1,1}(\theta,\phi)\cdot\chi_{\frac{-1}{2}} + \sqrt{\frac{2}{3}}\mathcal{Y}_{1,0}(\theta,\phi)\cdot\chi_{\frac{1}{2}}, \\
\phi_{\frac{3}{2}\frac{-1}{2}} &= \sqrt{\frac{1}{3}}\mathcal{Y}_{1,-1}(\theta,\phi)\cdot\chi_{\frac{1}{2}} + \sqrt{\frac{2}{3}}\mathcal{Y}_{1,0}(\theta,\phi)\cdot\chi_{\frac{-1}{2}},
\end{aligned}$$

$$\phi_{\frac{3}{2}\frac{-3}{2}} = \mathcal{Y}_{1,-1}(\theta,\phi)\cdot\chi_{\frac{-1}{2}}, \tag{5.1.3}$$

where $\mathcal{Y}_{l,m}$ are spherical harmonics:

$$\begin{aligned}
\mathcal{Y}_{1,1}(\theta,\phi) &= -\frac{1}{2}\sqrt{\frac{3}{2\pi}}\frac{(x+iy)}{r},\\
\mathcal{Y}_{1,0}(\theta,\phi) &= \frac{1}{2}\sqrt{\frac{3}{\pi}}\frac{z}{r},\\
\mathcal{Y}_{1,-1}(\theta,\phi) &= \frac{1}{2}\sqrt{\frac{3}{2\pi}}\frac{(x-iy)}{r},
\end{aligned}$$

and χ spinors defined as follows:

$$\chi_+ = \begin{pmatrix}1\\0\end{pmatrix}, \qquad \chi_- = \begin{pmatrix}0\\1\end{pmatrix}.$$

From now on, we use a shorthand notation leaving out the spin variable 1/2 and simplifying the projection quantum numbers $m_s = \pm 1/2$ to + and −.

Put the single particle wave functions in (5.1.3) back into the antisymmetric wave function (5.1.2) and we get the normalized antisymmetric wave function of the four neutrons coupled to 0^+ in the $0p_{\frac{3}{2}}$ shell written below. It is a linear combination of products of spatial wave functions of the four particles $\Phi_{0_1^+ m_1,m_2,m_3,m_4}(\vec{r}_1,\vec{r}_2,\vec{r}_3,\vec{r}_4)$ and tensor products of their spins $\chi_{m_1}(1)\chi_{m_2}(2)\chi_{m_3}(3)\chi_{m_4}(4)$. There are $2^4 - 2 = 14$ such tensor products since all four particles in the p shell cannot have the same spin projection, which excludes the tensor products $\chi_+(1)\chi_+(2)\chi_+(3)\chi_+(4)$ and $\chi_-(1)\chi_-(2)\chi_-(3)\chi_-(4)$. For brevity, the factor $\left(\frac{1}{2}\sqrt{\frac{3}{2\pi}}\right)^4 \frac{1}{r_1 r_2 r_3 r_4}\frac{1}{\sqrt{4!}}\frac{4}{3}$ is moved out of the sum. We obtain for the angular part of the wavefunction

$$\begin{aligned}
\Psi_{0_1^+}(\vec{r}_1,\vec{r}_2,\vec{r}_3,\vec{r}_4,\chi_1,\chi_2,\chi_3,\chi_4) &= \left(\frac{1}{2}\sqrt{\frac{3}{2\pi}}\right)^4 \frac{1}{r_1 r_2 r_3 r_4}\frac{1}{\sqrt{4!}}\frac{4}{3}\\
&\times \sum_{\substack{m_1,m_2\\ m_3,m_4}} \Phi_{0_1^+ m_1,m_2,m_3,m_4}(\vec{r}_1,\vec{r}_2,\vec{r}_3,\vec{r}_4)\cdot\chi_{m_1}(1)\chi_{m_2}(2)\chi_{m_3}(3)\chi_{m_4}(4),
\end{aligned} \tag{5.1.4}$$

with

$$\Phi_{0_1^+--++}(\vec{r}_1,\vec{r}_2,\vec{r}_3,\vec{r}_4) \tag{5.1.5}$$

$$\begin{aligned}
&= x_2x_4y_1y_3 - x_1x_4y_2y_3 - x_2x_3y_1y_4 + x_1x_3y_2y_4 + x_2x_4z_1z_3 + y_2y_4z_1z_3 \\
&- x_1x_4z_2z_3 - y_1y_4z_2z_3 - x_2x_3z_1z_4 - y_2y_3z_1z_4 + x_1x_3z_2z_4 + y_1y_3z_2z_4 \\
&+ i(-x_4y_2z_1z_3 + x_2y_4z_1z_3 + x_4y_1z_2z_3 - x_1y_4z_2z_3 + x_3y_2z_1z_4 - x_2y_3z_1z_4 \\
&- x_3y_1z_2z_4 + x_1y_3z_2z_4),
\end{aligned} \tag{5.1.6}$$

$$\Phi_{0_1^+++--}(\vec{r}_1,\vec{r}_2,\vec{r}_3,\vec{r}_4)$$

$$\begin{aligned}
&= x_2x_4y_1y_3 - x_1x_4y_2y_3 - x_2x_3y_1y_4 + x_1x_3y_2y_4 + x_2x_4z_1z_3 + y_2y_4z_1z_3 \\
&- x_1x_4z_2z_3 - y_1y_4z_2z_3 - x_2x_3z_1z_4 - y_2y_3z_1z_4 + x_1x_3z_2z_4 + y_1y_3z_2z_4 \\
&+ i(x_4y_2z_1z_3 - x_2y_4z_1z_3 - x_4y_1z_2z_3 + x_1y_4z_2z_3 - x_3y_2z_1z_4 + x_2y_3z_1z_4 \\
&+ x_3y_1z_2z_4 - x_1y_3z_2z_4),
\end{aligned} \tag{5.1.7}$$

$$\Phi_{0_1^+-+-+}(\vec{r}_1,\vec{r}_2,\vec{r}_3,\vec{r}_4)$$

$$\begin{aligned}
&= -x_3x_4y_1y_2 + x_1x_4y_2y_3 + x_2x_3y_1y_4 - x_1x_2y_3y_4 - x_3x_4z_1z_2 - y_3y_4z_1z_2 \\
&+ x_1x_4z_2z_3 + y_1y_4z_2z_3 + x_2x_3z_1z_4 + y_2y_3z_1z_4 - x_1x_2z_3z_4 - y_1y_2z_3z_4 \\
&+ i(x_4y_3z_1z_2 - x_3y_4z_1z_2 - x_4y_1z_2z_3 + x_1y_4z_2z_3 + x_3y_2z_1z_4 - x_2y_3z_1z_4 \\
&+ x_2y_1z_3z_4 - x_1y_2z_3z_4),
\end{aligned} \tag{5.1.8}$$

$$\Phi_{0_1^+-+-+}(\vec{r}_1,\vec{r}_2,\vec{r}_3,\vec{r}_4)$$

$$\begin{aligned}
&= -x_3x_4y_1y_2 + x_1x_4y_2y_3 + x_2x_3y_1y_4 - x_1x_2y_3y_4 - x_3x_4z_1z_2 - y_3y_4z_1z_2 \\
&+ x_1x_4z_2z_3 + y_1y_4z_2z_3 + x_2x_3z_1z_4 + y_2y_3z_1z_4 - x_1x_2z_3z_4 - y_1y_2z_3z_4 \\
&- i(x_4y_3z_1z_2 - x_3y_4z_1z_2 - x_4y_1z_2z_3 + x_1y_4z_2z_3 + x_3y_2z_1z_4 - x_2y_3z_1z_4 \\
&+ x_2y_1z_3z_4 - x_1y_2z_3z_4),
\end{aligned} \tag{5.1.9}$$

$$\Phi_{0_1^+-++-}(\vec{r}_1,\vec{r}_2,\vec{r}_3,\vec{r}_4)$$
$$= x_3x_4y_1y_2 - x_2x_4y_1y_3 - x_1x_3y_2y_4 + x_1x_2y_3y_4 + x_3x_4z_1z_2 + y_3y_4z_1z_2$$
$$- x_2x_4z_1z_3 - y_2y_4z_1z_3 - x_1x_3z_2z_4 - y_1y_3z_2z_4 + x_1x_2z_3z_4 + y_1y_2z_3z_4$$
$$+ i(x_4y_3z_1z_2 - x_3y_4z_1z_2 - x_4y_2z_1z_3 + x_2y_4z_1z_3 + x_3y_1z_2z_4 - x_1y_3z_2z_4$$
$$- x_2y_1z_3z_4 + x_1y_2z_3z_4), \tag{5.1.10}$$

$$\Phi_{0_1^+-+-+}(\vec{r}_1,\vec{r}_2,\vec{r}_3,\vec{r}_4)$$
$$= x_3x_4y_1y_2 - x_2x_4y_1y_3 - x_1x_3y_2y_4 + x_1x_2y_3y_4 + x_3x_4z_1z_2 + y_3y_4z_1z_2$$
$$- x_2x_4z_1z_3 - y_2y_4z_1z_3 - x_1x_3z_2z_4 - y_1y_3z_2z_4 + x_1x_2z_3z_4 + y_1y_2z_3z_4$$
$$- i(x_4y_3z_1z_2 - x_3y_4z_1z_2 - x_4y_2z_1z_3 + x_2y_4z_1z_3 + x_3y_1z_2z_4 - x_1y_3z_2z_4$$
$$- x_2y_1z_3z_4 + x_1y_2z_3z_4), \tag{5.1.11}$$

$$\Phi_{0_1^+---+}(\vec{r}_1,\vec{r}_2,\vec{r}_3,\vec{r}_4)$$
$$= -x_3y_2y_4z_1 + x_2y_3y_4z_1 + x_3y_1y_4z_2 - x_1y_3y_4z_2 - x_2y_1y_4z_3 + x_1y_2y_4z_3$$
$$+ i(x_3x_4y_2z_1 - x_2x_4y_3z_1 - x_3x_4y_1z_2 + x_1x_4y_3z_2 + x_2x_4y_1z_3 - x_1x_4y_2z_3), \tag{5.1.12}$$

$$\Phi_{0_1^++++-}(\vec{r}_1,\vec{r}_2,\vec{r}_3,\vec{r}_4)$$
$$= x_3y_2y_4z_1 - x_2y_3y_4z_1 - x_3y_1y_4z_2 + x_1y_3y_4z_2 + x_2y_1y_4z_3 - x_1y_2y_4z_3$$
$$+ i(x_3x_4y_2z_1 - x_2x_4y_3z_1 - x_3x_4y_1z_2 + x_1x_4y_3z_2 + x_2x_4y_1z_3 - x_1x_4y_2z_3), \tag{5.1.13}$$

$$\Phi_{0_1^+--+-}(\vec{r}_1,\vec{r}_2,\vec{r}_3,\vec{r}_4)$$
$$= x_4y_2y_3z_1 - x_2y_3y_4z_1 - x_4y_1y_3z_2 + x_1y_3y_4z_2 + x_2y_1y_3z_4 - x_1y_2y_3z_4$$
$$+ i(-x_3x_4y_2z_1 + x_2x_3y_4z_1 + x_3x_4y_1z_2 - x_1x_3y_4z_2 - x_2x_3y_1z_4 + x_1x_3y_2z_4), \tag{5.1.14}$$

$$\Phi_{0_1^+++-+}(\vec{r}_1,\vec{r}_2,\vec{r}_3,\vec{r}_4)$$
$$= -x_4y_2y_3z_1 + x_2y_3y_4z_1 + x_4y_1y_3z_2 - x_1y_3y_4z_2 - x_2y_1y_3z_4 + x_1y_2y_3z_4$$

$$+i(-x_3x_4y_2z_1+x_2x_3y_4z_1+x_3x_4y_1z_2-x_1x_3y_4z_2-x_2x_3y_1z_4+x_1x_3y_2z_4), \quad (5.1.15)$$

$$\begin{aligned}&\Phi_{0_1^+-+--}(\vec{r}_1,\vec{r}_2,\vec{r}_3,\vec{r}_4)\\&=-x_4y_2y_3z_1+x_3y_2y_4z_1+x_4y_1y_2z_3-x_1y_2y_4z_3-x_3y_1y_2z_4+x_1y_2y_3z_4\\&+i(x_2x_4y_3z_1-x_2x_3y_4z_1-x_2x_4y_1z_3+x_1x_2y_4z_3+x_2x_3y_1z_4-x_1x_2y_3z_4),\end{aligned} \quad (5.1.16)$$

$$\begin{aligned}&\Phi_{0_1^+-+++}(\vec{r}_1,\vec{r}_2,\vec{r}_3,\vec{r}_4)\\&=x_4y_2y_3z_1-x_3y_2y_4z_1-x_4y_1y_2z_3+x_1y_2y_4z_3+x_3y_1y_2z_4-x_1y_2y_3z_4\\&+i(x_2x_4y_3z_1-x_2x_3y_4z_1-x_2x_4y_1z_3+x_1x_2y_4z_3+x_2x_3y_1z_4-x_1x_2y_3z_4),\end{aligned} \quad (5.1.17)$$

$$\begin{aligned}&\Phi_{0_1^+-+--}(\vec{r}_1,\vec{r}_2,\vec{r}_3,\vec{r}_4)\\&=x_4y_1y_3z_2-x_3y_1y_4z_2-x_4y_1y_2z_3+x_2y_1y_4z_3+x_3y_1y_2z_4-x_2y_1y_3z_4\\&+i(-x_1x_4y_3z_2+x_1x_3y_4z_2+x_1x_4y_2z_3-x_1x_2y_4z_3-x_1x_3y_2z_4+x_1x_2y_3z_4),\end{aligned} \quad (5.1.18)$$

$$\begin{aligned}&\Phi_{0_1^+-+++}(\vec{r}_1,\vec{r}_2,\vec{r}_3,\vec{r}_4)\\&=-x_4y_1y_3z_2+x_3y_1y_4z_2+x_4y_1y_2z_3-x_2y_1y_4z_3-x_3y_1y_2z_4+x_2y_1y_3z_4\\&+i(-x_1x_4y_3z_2+x_1x_3y_4z_2+x_1x_4y_2z_3-x_1x_2y_4z_3-x_1x_3y_2z_4+x_1x_2y_3z_4).\end{aligned} \quad (5.1.19)$$

It can be observed that for a tensor product composed of two spins up and two spins down such as $\chi_-(1)\chi_-(2)\chi_+(3)\chi_+(4)$ (5.1.5), its spatial wave function $\Phi_{0_1^+--++}(\vec{r}_1,\vec{r}_2,\vec{r}_3,\vec{r}_4)$ and that of its opposite counterpart $\chi_+(1)\chi_+(2)\chi_-(3)\chi_-(4)$ (5.1.7) are complex conjugate to each other, while for a tensor product composed of only one spin different from the other three, such as $\chi_-(1)\chi_-(2)\chi_-(3)\chi_+(4)$ (5.1.12), its spatial wave function $\Phi_{0_1^+---+}(\vec{r}_1,\vec{r}_2,\vec{r}_3,\vec{r}_4)$ is the opposite of the complex conjugate of that of its opposite counterpart $\chi_+(1)\chi_+(2)\chi_+(3)\chi_-(4)$ (5.1.13).

We use the notation $\vec{r}_{ij}=(x_{ij},y_{ij},z_{ij})=\vec{r}_i\times\vec{r}_j=(y_iz_j-y_jz_i,z_ix_j-z_jx_i,x_iy_j-y_ix_j)$

and $\vec{r}_{ij,kl} = (x_{ij,kl}, y_{ij,kl}, z_{ij,kl}) = \vec{r}_{ij} \times \vec{r}_{kl}$, and calculate each term in sum (5.1.4):

$$
\begin{aligned}
&\Phi_{0_1^+--++}(\vec{r}_1, \vec{r}_2, \vec{r}_3, \vec{r}_4) \\
&= x_2x_4y_1y_3 - x_1x_4y_2y_3 - x_2x_3y_1y_4 + x_1x_3y_2y_4 + x_2x_4z_1z_3 + y_2y_4z_1z_3 \\
&- x_1x_4z_2z_3 - y_1y_4z_2z_3 - x_2x_3z_1z_4 - y_2y_3z_1z_4 + x_1x_3z_2z_4 + y_1y_3z_2z_4 \\
&+ i(-x_4y_2z_1z_3 + x_2y_4z_1z_3 + x_4y_1z_2z_3 - x_1y_4z_2z_3 + x_3y_2z_1z_4 - x_2y_3z_1z_4 \\
&- x_3y_1z_2z_4 + x_1y_3z_2z_4) \\
&= -x_4y_3(x_1y_2 - x_2y_1) + x_3y_4(x_1y_2 - x_2y_1) + x_4z_3(z_1x_2 - z_2x_1) - y_4z_3(y_1z_2 - y_2z_1) \\
&- x_3z_4(z_1x_2 - z_2x_1) + y_3z_4(y_1z_2 - y_2z_1)] + i[x_4z_3(y_1z_2 - y_2z_1) + y_4z_3(z_1x_2 - z_2x_1) \\
&- x_3z_4(y_1z_2 - y_2z_1) - y_3z_4(z_1x_2 - z_2x_1)] \\
&= (x_1y_2 - x_2y_1)(x_3y_4 - x_4y_3) + (z_1x_2 - z_2x_1)(z_3x_4 - z_4x_3) + (y_1z_2 - y_2z_1)(y_3z_4 - y_4z_3) \\
&+ i[(y_1z_2 - y_2z_1)(z_3x_4 - z_4x_3) - (z_1x_2 - z_2x_1)(y_3z_4 - y_4z_3)] \\
&= x_{12}x_{34} + y_{12}y_{34} + z_{12}z_{34} + i(x_{12}y_{34} - y_{12}x_{34}) \\
&= \vec{r}_{12} \cdot \vec{r}_{34} + i\ z_{12,34}, \qquad (5.1.20)
\end{aligned}
$$

$$
\Phi_{0_1^+++--}(\vec{r}_1, \vec{r}_2, \vec{r}_3, \vec{r}_4) = \vec{r}_{12} \cdot \vec{r}_{34} - i\ z_{12,34}, \qquad (5.1.21)
$$

$$
\begin{aligned}
&\Phi_{0_1^+-+-+}(\vec{r}_1, \vec{r}_2, \vec{r}_3, \vec{r}_4) \\
&= -x_3x_4y_1y_2 + x_1x_4y_2y_3 + x_2x_3y_1y_4 - x_1x_2y_3y_4 - x_3x_4z_1z_2 - y_3y_4z_1z_2 \\
&+ x_1x_4z_2z_3 + y_1y_4z_2z_3 + x_2x_3z_1z_4 + y_2y_3z_1z_4 - x_1x_2z_3z_4 - y_1y_2z_3z_4 \\
&+ i(x_4y_3z_1z_2 - x_3y_4z_1z_2 - x_4y_1z_2z_3 + x_1y_4z_2z_3 + x_3y_2z_1z_4 - x_2y_3z_1z_4 \\
&+ x_2y_1z_3z_4 - x_1y_2z_3z_4) \\
&= x_4y_2(x_1y_3 - x_3y_1) - x_2y_4(x_1y_3 - x_3y_1) - x_4z_2(z_1x_3 - z_3x_1) + y_4z_2(y_1z_3 - y_3z_1) \\
&+ x_2z_4(z_1x_3 - z_3x_1) - y_2z_4(y_1z_3 - y_3z_1) + i[-x_4z_2(y_1z_3 - y_3z_1) - y_4z_2(z_1x_3 - z_3x_1) \\
&+ y_2z_4(z_1x_3 - z_3x_1) + x_2z_4(y_1z_3 - y_3z_1)] \\
&= -(x_1y_3 - x_3y_1)(x_2y_4 - x_4y_2) - (z_1x_3 - z_3x_1)(z_2x_4 - z_4x_2) - (y_1z_3 - y_3z_1)(y_2z_4 - y_4z_2)]
\end{aligned}
$$

$$+ i[-(y_1z_3 - y_3z_1)(z_2x_4 - z_4x_2) + (z_1x_3 - z_3x_1)(y_2z_4 - y_4z_2)]$$
$$= -x_{13}x_{24} - y_{13}y_{24} - z_{13}z_{24} + i(y_{13}x_{24} - x_{13}y_{24})$$
$$= -\vec{r}_{13} \cdot \vec{r}_{24} - i\ z_{13,24}, \tag{5.1.22}$$

$$\Phi_{0_1^+ +-+-}(\vec{r}_1, \vec{r}_2, \vec{r}_3, \vec{r}_4) = -\vec{r}_{13} \cdot \vec{r}_{24} + i\ z_{13,24}, \tag{5.1.23}$$

$$\Phi_{0_1^+ -++-}(\vec{r}_1, \vec{r}_2, \vec{r}_3, \vec{r}_4)$$
$$= x_3x_4y_1y_2 - x_2x_4y_1y_3 - x_1x_3y_2y_4 + x_1x_2y_3y_4 + x_3x_4z_1z_2 + y_3y_4z_1z_2$$
$$- x_2x_4z_1z_3 - y_2y_4z_1z_3 - x_1x_3z_2z_4 - y_1y_3z_2z_4 + x_1x_2z_3z_4 + y_1y_2z_3z_4$$
$$+ i(x_4y_3z_1z_2 - x_3y_4z_1z_2 - x_4y_2z_1z_3 + x_2y_4z_1z_3 + x_3y_1z_2z_4 - x_1y_3z_2z_4$$
$$- x_2y_1z_3z_4 + x_1y_2z_3z_4)$$
$$= -x_4y_1(x_2y_3 - x_3y_2) + x_1y_4(x_2y_3 - x_3y_2) + x_4z_1(z_2x_3 - z_3x_2) - y_4z_1(y_2z_3 - y_3z_2)$$
$$- x_1z_4(z_2x_3 - z_3x_2) + y_1z_4(y_2z_3 - y_3z_2) + i[-x_4z_1(y_2z_3 - y_3z_2) - y_4z_1(z_2x_3 - z_3x_2)$$
$$+ y_1z_4(z_2x_3 - z_3x_2) + x_1z_4(y_2z_3 - y_3z_2)]$$
$$= (x_2y_3 - x_3y_2)(x_1y_4 - x_4z_1) + (z_2x_3 - z_3x_2)(z_1x_4 - z_4x_1) + (y_2z_3 - y_3z_2)(y_1z_4 - y_4z_1)$$
$$+ i[-(y_2z_3 - y_3z_2)(z_1x_4 - z_4x_1) + (z_2x_3 - z_3x_2)(y_1z_4 - y_4z_1)]$$
$$= z_{23}z_{14} + y_{23}y_{14} + x_{23}x_{14} + i(-x_{23}y_{14} + y_{23}x_{14})$$
$$= \vec{r}_{14} \cdot \vec{r}_{23} + i\ z_{14,23}, \tag{5.1.24}$$

$$\Phi_{0_1^+ +--+}(\vec{r}_1, \vec{r}_2, \vec{r}_3, \vec{r}_4) = \vec{r}_{14} \cdot \vec{r}_{23} - i\ z_{14,23}, \tag{5.1.25}$$

$$\Phi_{0_1^+ ---+}(\vec{r}_1, \vec{r}_2, \vec{r}_3, \vec{r}_4)$$
$$= -x_3y_2y_4z_1 + x_2y_3y_4z_1 + x_3y_1y_4z_2 - x_1y_3y_4z_2 - x_2y_1y_4z_3 + x_1y_2y_4z_3$$
$$+ i(x_3x_4y_2z_1 - x_2x_4y_3z_1 - x_3x_4y_1z_2 + x_1x_4y_3z_2 + x_2x_4y_1z_3 - x_1x_4y_2z_3)$$
$$= y_4z_1(x_2y_3 - x_3y_2) - y_4z_2(x_1y_3 - x_3y_1) + y_4z_3(x_1y_2 - x_2y_1)$$
$$+ i[-x_4z_1(x_2y_3 - x_3y_2) + x_4z_2(x_1y_3 - x_3y_1) - x_4z_3(x_1y_2 - x_2y_1)]$$

$$= (y_4 - i\ x_4)\begin{vmatrix} x_1 & x_2 & x_3 \\ y_1 & y_2 & y_3 \\ z_1 & z_2 & z_3 \end{vmatrix}, \tag{5.1.26}$$

$$\Phi_{0_1^+++-}(\vec{r}_1,\vec{r}_2,\vec{r}_3,\vec{r}_4) = -(y_4 + i\ x_4)\begin{vmatrix} x_1 & x_2 & x_3 \\ y_1 & y_2 & y_3 \\ z_1 & z_2 & z_3 \end{vmatrix}, \tag{5.1.27}$$

$$\begin{aligned}
&\Phi_{0_1^+--+-}(\vec{r}_1,\vec{r}_2,\vec{r}_3,\vec{r}_4) \\
&= x_4y_2y_3z_1 - x_2y_3y_4z_1 - x_4y_1y_3z_2 + x_1y_3y_4z_2 + x_2y_1y_3z_4 - x_1y_2y_3z_4 \\
&+ i(-x_3x_4y_2z_1 + x_2x_3y_4z_1 + x_3x_4y_1z_2 - x_1x_3y_4z_2 - x_2x_3y_1z_4 + x_1x_3y_2z_4) \\
&= -y_3z_1(x_2y_4 - x_4y_2) + y_3z_2(x_1y_4 - x_4y_1) - y_3z_4(x_1y_2 - x_2y_1) \\
&+ i[x_3z_1(x_2y_4 - x_4y_2) - x_3z_2(x_1y_4 - x_4y_1) + x_3z_4(x_1y_2 - x_2y_1)] \\
&= (-y_3 + i\ x_3)\begin{vmatrix} x_1 & x_2 & x_4 \\ y_1 & y_2 & y_4 \\ z_1 & z_2 & z_4 \end{vmatrix}
\end{aligned} \tag{5.1.28}$$

$$\Phi_{0_1^+++-+}(\vec{r}_1,\vec{r}_2,\vec{r}_3,\vec{r}_4) = (y_3 + i\ x_3)\begin{vmatrix} x_1 & x_2 & x_4 \\ y_1 & y_2 & y_4 \\ z_1 & z_2 & z_4 \end{vmatrix}, \tag{5.1.29}$$

$$\begin{aligned}
&\Phi_{0_1^+-+--}(\vec{r}_1,\vec{r}_2,\vec{r}_3,\vec{r}_4) \\
&= -x_4y_2y_3z_1 + x_3y_2y_4z_1 + x_4y_1y_2z_3 - x_1y_2y_4z_3 - x_3y_1y_2z_4 + x_1y_2y_3z_4 \\
&+ i(x_2x_4y_3z_1 - x_2x_3y_4z_1 - x_2x_4y_1z_3 + x_1x_2y_4z_3 + x_2x_3y_1z_4 - x_1x_2y_3z_4) \\
&= y_2z_1(x_3y_4 - x_4y_3) - y_2z_3(x_1y_4 - x_4y_1) + y_2z_4(x_1y_3 - x_3y_1) \\
&+ i[-x_2z_1(x_3y_4 - x_4y_3) + x_2z_3(x_1y_4 - x_4y_1) - x_2z_4(x_1y_3 - x_3y_1)]
\end{aligned}$$

$$= (y_2 - i\ x_2)\begin{vmatrix} x_1 & x_3 & x_4 \\ y_1 & y_3 & y_4 \\ z_1 & z_3 & z_4 \end{vmatrix} \tag{5.1.30}$$

$$\Phi_{0_1^+ +-++}(\vec{r}_1, \vec{r}_2, \vec{r}_3, \vec{r}_4) = -(y_2 + i\ x_2)\begin{vmatrix} x_1 & x_3 & x_4 \\ y_1 & y_3 & y_4 \\ z_1 & z_3 & z_4 \end{vmatrix}, \tag{5.1.31}$$

$$\begin{aligned}
&\Phi_{0_1^+ +---}(\vec{r}_1, \vec{r}_2, \vec{r}_3, \vec{r}_4) \\
&= x_4 y_1 y_3 z_2 - x_3 y_1 y_4 z_2 - x_4 y_1 y_2 z_3 + x_2 y_1 y_4 z_3 + x_3 y_1 y_2 z_4 - x_2 y_1 y_3 z_4 \\
&+ i(-x_1 x_4 y_3 z_2 + x_1 x_3 y_4 z_2 + x_1 x_4 y_2 z_3 - x_1 x_2 y_4 z_3 - x_1 x_3 y_2 z_4 + x_1 x_2 y_3 z_4) \\
&= -y_1 z_2 (x_3 y_4 - x_4 y_3) + y_i z_3 (x_2 y_4 - x_4 y_2) - y_1 z_4 (x_2 y_3 - x_3 y_2) \\
&+ i[x_1 z_2 (x_3 y_4 - x_4 y_3) - x_1 z_3 (x_2 y_4 - x_4 y_2) + x_1 z_4 (x_2 y_3 - x_3 y_2)] \\
&= (-y_1 + i\ x_1)\begin{vmatrix} x_2 & x_3 & x_4 \\ y_2 & y_3 & y_4 \\ z_2 & z_3 & z_4 \end{vmatrix},
\end{aligned} \tag{5.1.32}$$

$$\Phi_{0_1^+ -+++}(\vec{r}_1, \vec{r}_2, \vec{r}_3, \vec{r}_4) = (y_1 + i\ x_1)\begin{vmatrix} x_2 & x_3 & x_4 \\ y_2 & y_3 & y_4 \\ z_2 & z_3 & z_4 \end{vmatrix}. \tag{5.1.33}$$

Once the spatial wave functions $\Phi_{0_1^+ m_1, m_2, m_3, m_4}$ are simplified, $\Psi^*_{0_1^+}\Psi_{0_1^+}$, the probability density of the wave function (5.1.4), can be expressed as

$$\begin{aligned}
&\left[\left(\frac{1}{2}\sqrt{\frac{3}{2\pi}}\right)^4 \frac{1}{r_1 r_2 r_3 r_4}\frac{1}{\sqrt{4!}}\frac{4}{3}\right]^2 \sum_{\substack{m_1, m_2 \\ m_3, m_4}} \Phi^*_{0_1^+ m_1 m_2 m_3 m_4}(\vec{r}_1, \vec{r}_2, \vec{r}_3, \vec{r}_4)\Phi_{0_1^+ m_1 m_2 m_3 m_4}(\vec{r}_1, \vec{r}_2, \vec{r}_3, \vec{r}_4) \\
&= \frac{3}{2^{10}\pi^4}\frac{1}{r_1^2 r_2^2 r_3^2 r_4^2}\Big(\left\|\vec{r}_{12}\cdot\vec{r}_{34} + i\ z_{12,34}\right\|^2 + \left\|-\vec{r}_{13}\cdot\vec{r}_{24} - i\ z_{13,24}\right\|^2 + \left\|\vec{r}_{14}\cdot\vec{r}_{23} + i\ z_{14,23}\right\|^2
\end{aligned}$$

$$
\begin{aligned}
&+\|(y_4 - i\ x_4)\|^2 \begin{vmatrix} x_1 & x_2 & x_3 \\ y_1 & y_2 & y_3 \\ z_1 & z_2 & z_3 \end{vmatrix}^2 + \|(-y_3 + i\ x_3)\|^2 \begin{vmatrix} x_1 & x_2 & x_4 \\ y_1 & y_2 & y_4 \\ z_1 & z_2 & z_4 \end{vmatrix}^2 + \|(y_2 - i\ x_2)\|^2 \begin{vmatrix} x_1 & x_3 & x_4 \\ y_1 & y_3 & y_4 \\ z_1 & z_3 & z_4 \end{vmatrix}^2 \\
&+\|(-y_1 + i\ x_1)\|^2 \begin{vmatrix} x_2 & x_3 & x_4 \\ y_2 & y_3 & y_4 \\ z_2 & z_3 & z_4 \end{vmatrix}^2 \Bigg) \\
&= \frac{3}{2^{10}\pi^4} \frac{1}{r_1^2 r_2^2 r_3^2 r_4^2} \Bigg((\vec{r}_{12} \cdot \vec{r}_{34})^2 + (\vec{r}_{13} \cdot \vec{r}_{24})^2 + (\vec{r}_{14} \cdot \vec{r}_{23})^2 + z_{12,34}^2 + z_{13,24}^2 + z_{14,23}^2 \\
&+ (x_1^2 + y_1^2) \begin{vmatrix} x_2 & x_3 & x_4 \\ y_2 & y_3 & y_4 \\ z_2 & z_3 & z_4 \end{vmatrix}^2 + (x_2^2 + y_2^2) \begin{vmatrix} x_1 & x_3 & x_4 \\ y_1 & y_3 & y_4 \\ z_1 & z_3 & z_4 \end{vmatrix}^2 + (x_3^2 + y_3^2) \begin{vmatrix} x_1 & x_2 & x_4 \\ y_1 & y_2 & y_4 \\ z_1 & z_2 & z_4 \end{vmatrix}^2 \\
&+ (x_4^2 + y_4^2) \begin{vmatrix} x_1 & x_2 & x_3 \\ y_1 & y_2 & y_3 \\ z_1 & z_2 & z_3 \end{vmatrix}^2 \Bigg)
\end{aligned} \tag{5.1.34}
$$

The probability density in (5.1.34) can be simplified with the identities

$$
\begin{aligned}
&x_{12,34}^2 + x_{13,24}^2 + x_{14,23}^2 \\
&= x_1^2 \begin{vmatrix} x_2 & x_3 & x_4 \\ y_2 & y_3 & y_4 \\ z_2 & z_3 & z_4 \end{vmatrix}^2 + x_2^2 \begin{vmatrix} x_1 & x_3 & x_4 \\ y_1 & y_3 & y_4 \\ z_1 & z_3 & z_4 \end{vmatrix}^2 + x_3^2 \begin{vmatrix} x_1 & x_2 & x_4 \\ y_1 & y_2 & y_4 \\ z_1 & z_2 & z_4 \end{vmatrix}^2 + x_4^2 \begin{vmatrix} x_1 & x_2 & x_3 \\ y_1 & y_2 & y_3 \\ z_1 & z_2 & z_3 \end{vmatrix}^2
\end{aligned}
$$

and

$$
\begin{aligned}
&y_{12,34}^2 + y_{13,24}^2 + y_{14,23}^2 \\
&= y_1^2 \begin{vmatrix} x_2 & x_3 & x_4 \\ y_2 & y_3 & y_4 \\ z_2 & z_3 & z_4 \end{vmatrix}^2 + y_2^2 \begin{vmatrix} x_1 & x_3 & x_4 \\ y_1 & y_3 & y_4 \\ z_1 & z_3 & z_4 \end{vmatrix}^2 + y_3^2 \begin{vmatrix} x_1 & x_2 & x_4 \\ y_1 & y_2 & y_4 \\ z_1 & z_2 & z_4 \end{vmatrix}^2 + y_4^2 \begin{vmatrix} x_1 & x_2 & x_3 \\ y_1 & y_2 & y_3 \\ z_1 & z_2 & z_3 \end{vmatrix}^2
\end{aligned}
$$

that will be demonstrated below by using the vector cross product properties

$$(A\times B)\times(C\times D)=(A\cdot(B\times D))C-(A\cdot(B\times C))D, \tag{5.1.35}$$

and

$$A\cdot(B\times C)=\begin{vmatrix}A_x & B_x & C_x\\ A_y & B_y & C_y\\ A_z & B_z & C_z\end{vmatrix}. \tag{5.1.36}$$

By using the identity $(A\times B)\times(C\times D)=(A\cdot(B\times D))C-(A\cdot(B\times C))D$, we have:

$$\begin{aligned}
x_{12,34}&=(\vec{r}_1\cdot\vec{r}_{24})x_3-(\vec{r}_1\cdot\vec{r}_{23})x_4\\
x_{13,24}&=(\vec{r}_1\cdot\vec{r}_{34})x_2+(\vec{r}_1\cdot\vec{r}_{23})x_4\\
x_{14,23}&=-(\vec{r}_1\cdot\vec{r}_{34})x_2+(\vec{r}_1\cdot\vec{r}_{24})x_3\\
x_{34,12}&=(\vec{r}_2\cdot\vec{r}_{34})x_1-(\vec{r}_1\cdot\vec{r}_{34})x_2\\
x_{24,13}&=-(\vec{r}_2\cdot\vec{r}_{34})x_1-(\vec{r}_1\cdot\vec{r}_{24})x_3\\
x_{23,14}&=(\vec{r}_2\cdot\vec{r}_{34})x_1-(\vec{r}_1\cdot\vec{r}_{23})x_4
\end{aligned}$$

Consequently we find,

$$\begin{aligned}
&2(x_{12,34}^2+x_{13,24}^2+x_{14,23}^2)\\
&=x_{12,34}^2+x_{13,24}^2+x_{14,23}^2+x_{34,12}^2+x_{24,13}^2+x_{23,14}^2\\
&=\left[(\vec{r}_1\cdot\vec{r}_{24})x_3-(\vec{r}_1\cdot\vec{r}_{23})x_4\right]^2+\left[(\vec{r}_1\cdot\vec{r}_{34})x_2+(\vec{r}_1\cdot\vec{r}_{23})x_4\right]^2+\left[-(\vec{r}_1\cdot\vec{r}_{34})x_2+(\vec{r}_1\cdot\vec{r}_{24})x_3\right]^2+\left[(\vec{r}_2\cdot\vec{r}_{34})x_1-(\vec{r}_1\cdot\vec{r}_{34}\right.\\
&+\left[-(\vec{r}_2\cdot\vec{r}_{34})x_1-(\vec{r}_1\cdot\vec{r}_{24})x_3\right]^2+\left[(\vec{r}_2\cdot\vec{r}_{34})x_1-(\vec{r}_1\cdot\vec{r}_{23})x_4\right]^2\\
&=3(\vec{r}_1\cdot\vec{r}_{23})^2x_4^2+3(\vec{r}_1\cdot\vec{r}_{24})^2x_3^2+3(\vec{r}_1\cdot\vec{r}_{34})^2x_2^2+3(\vec{r}_2\cdot\vec{r}_{34})^2x_1^2-2x_3x_4(\vec{r}_1\cdot\vec{r}_{24})(\vec{r}_1\cdot\vec{r}_{23})+2x_2x_4(\vec{r}_1\cdot\vec{r}_{34})(\vec{r}_1\cdot\vec{r}_{23})\\
&-2x_2x_3(\vec{r}_1\cdot\vec{r}_{34})(\vec{r}_1\cdot\vec{r}_{24})-2x_1x_2(\vec{r}_2\cdot\vec{r}_{34})(\vec{r}_1\cdot\vec{r}_{34})\\
&+2x_1x_3(\vec{r}_2\cdot\vec{r}_{34})(\vec{r}_1\cdot\vec{r}_{24})-2x_1x_4(\vec{r}_2\cdot\vec{r}_{34})(\vec{r}_1\cdot\vec{r}_{23})\\
&=2(\vec{r}_1\cdot\vec{r}_{23})^2x_4^2+2(\vec{r}_1\cdot\vec{r}_{24})^2x_3^2+2(\vec{r}_1\cdot\vec{r}_{34})^2x_2^2+2(\vec{r}_2\cdot\vec{r}_{34})^2x_1^2
\end{aligned}$$

$$+\begin{vmatrix} x_1 & x_2 & x_3 & x_4 \\ y_1 & y_2 & y_3 & y_4 \\ z_1 & z_2 & z_3 & z_4 \\ x_1 & x_2 & x_3 & x_4 \end{vmatrix}^2$$

$$= 2\left((\vec{r}_1\cdot\vec{r}_{23})^2 x_4^2 + (\vec{r}_1\cdot\vec{r}_{24})^2 x_3^2 + (\vec{r}_1\cdot\vec{r}_{34})^2 x_2^2 + (\vec{r}_2\cdot\vec{r}_{34})^2 x_1^2\right). \tag{5.1.37}$$

Given the property that $A\cdot(B\times C) = \begin{vmatrix} A_x & B_x & C_x \\ A_y & B_y & C_y \\ A_z & B_z & C_z \end{vmatrix}$, Eq. (5.1.37) can be rewritten as:

$$\begin{aligned} & x_{12,34}^2 + x_{13,24}^2 + x_{14,23}^2 \\ &= x_1^2 \begin{vmatrix} x_2 & x_3 & x_4 \\ y_2 & y_3 & y_4 \\ z_2 & z_3 & z_4 \end{vmatrix}^2 + x_2^2 \begin{vmatrix} x_1 & x_3 & x_4 \\ y_1 & y_3 & y_4 \\ z_1 & z_3 & z_4 \end{vmatrix}^2 + x_3^2 \begin{vmatrix} x_1 & x_2 & x_4 \\ y_1 & y_2 & y_4 \\ z_1 & z_2 & z_4 \end{vmatrix}^2 + x_4^2 \begin{vmatrix} x_1 & x_2 & x_3 \\ y_1 & y_2 & y_3 \\ z_1 & z_2 & z_3 \end{vmatrix}^2 \end{aligned} \tag{5.1.38}$$

Similarly, we have

$$\begin{aligned} & y_{12,34}^2 + y_{13,24}^2 + y_{14,23}^2 \\ &= y_1^2 \begin{vmatrix} x_2 & x_3 & x_4 \\ y_2 & y_3 & y_4 \\ z_2 & z_3 & z_4 \end{vmatrix}^2 + y_2^2 \begin{vmatrix} x_1 & x_3 & x_4 \\ y_1 & y_3 & y_4 \\ z_1 & z_3 & z_4 \end{vmatrix}^2 + y_3^2 \begin{vmatrix} x_1 & x_2 & x_4 \\ y_1 & y_2 & y_4 \\ z_1 & z_2 & z_4 \end{vmatrix}^2 + y_4^2 \begin{vmatrix} x_1 & x_2 & x_3 \\ y_1 & y_2 & y_3 \\ z_1 & z_2 & z_3 \end{vmatrix}^2 \end{aligned} \tag{5.1.39}$$

Eq. (5.1.38) and (5.1.39) enable us to further simplify the probability density in (5.1.34).

$$\begin{aligned} & \Psi_{0_1^+}^* \Psi_{0_1^+} \\ &= \frac{3}{2^{10}\pi^4} \frac{1}{r_1^2 r_2^2 r_3^2 r_4^2} [(\vec{r}_{13}\cdot\vec{r}_{24})^2 + (\vec{r}_{14}\cdot\vec{r}_{23})^2 + (\vec{r}_{12}\cdot\vec{r}_{34})^2 + z_{12,34}^2 + z_{13,24}^2 + z_{14,23}^2 \\ &+ x_{12,34}^2 + x_{13,24}^2 + x_{14,23}^2 + y_{12,34}^2 + y_{13,24}^2 + y_{14,23}^2] \end{aligned}$$

$$= \frac{3}{2^{10}\pi^4}\frac{1}{r_1^2 r_2^2 r_3^2 r_4^2}[(\vec{r}_{13}\cdot\vec{r}_{24})^2 + (\vec{r}_{14}\cdot\vec{r}_{23})^2 + (\vec{r}_{12}\cdot\vec{r}_{34})^2 + \|\vec{r}_{12}\times\vec{r}_{34}\|^2 + \|\vec{r}_{13}\times\vec{r}_{24}\|^2$$
$$+ \|\vec{r}_{14}\times\vec{r}_{23}\|^2]$$
$$= \frac{3}{2^{10}\pi^4}\frac{1}{r_1^2 r_2^2 r_3^2 r_4^2}[(\vec{r}_{13}\cdot\vec{r}_{24})^2 + (\vec{r}_{14}\cdot\vec{r}_{23})^2 + (\vec{r}_{12}\cdot\vec{r}_{34})^2 + \|\vec{r}_{12}\times\vec{r}_{34}\|^2 + \|\vec{r}_{13}\times\vec{r}_{24}\|^2$$
$$+ \|\vec{r}_{14}\times\vec{r}_{23}\|^2]$$

Let θ_{ij} stand for the angle between $\vec{r}_i$ and $\vec{r}_j$ and $\theta_{ij,kl}$ the angle between $\vec{r}_{ij}$ and $\vec{r}_{kl}$. The dot product $\vec{r}_{ij}\cdot\vec{r}_{kl}$ and the cross product $\vec{r}_{ij}\times\vec{r}_{kl}$ are equal to $r_i r_j \sin\theta_{ij} r_k r_l \sin\theta_{kl}\cos\theta_{ij,kl}$ and $r_i r_j \sin\theta_{ij} r_k r_l \sin\theta_{kl}\sin\theta_{ij,kl}$ respectively. In consequence,

$$\begin{aligned}
&\Psi^*_{0_1^+}\Psi_{0_1^+} \\
&= \frac{3}{2^{10}\pi^4}\frac{1}{r_1^2 r_2^2 r_3^2 r_4^2}[(r_1 r_2\sin\theta_{12})^2(r_3 r_4\sin\theta_{34})^2\cos^2\theta_{12,34} \\
&+ (r_1 r_4\sin\theta_{14})^2(r_2 r_3\sin\theta_{23})^2\cos^2\theta_{14,23} + (r_1 r_3\sin\theta_{13})^2(r_2 r_4\sin\theta_{24})^2\cos^2\theta_{13,24} \\
&+ (r_1 r_2\sin\theta_{12})^2(r_3 r_4\sin\theta_{34})^2\sin^2\theta_{12,34} + (r_1 r_4\sin\theta_{14})^2(r_2 r_3\sin\theta_{23})^2\sin^2\theta_{14,23} \\
&+ (r_1 r_3\sin\theta_{13})^2(r_2 r_4\sin\theta_{24})^2\sin^2\theta_{13,24}] \\
&= \frac{3}{2^{10}\pi^4}(\sin^2\theta_{13}\sin^2\theta_{24} + \sin^2\theta_{14}\sin^2\theta_{23} + \sin^2\theta_{12}\sin^2\theta_{34})
\end{aligned} \tag{5.1.40}$$

We have just found the angular part of the probability density for the 0_1^+ state: $|\left(0p_{\frac{3}{2}}\right)^4;0\rangle$. It is a function of the six relative angles formed by the four vectors connecting the four neutrons and the α core, and is invariant under permutation of valence neutrons. Only five of the six relative angles are independent.

5.1.2 Geometry of 0_1^+ with the maximum probability density

In this section, we look for configurations at which the angular probability density of 0_1^+ has its absolute maximum.

For convenience, we define a factor $c = \frac{3}{2^{10}\pi^4}$ that will be used henceforth such

that the correlation function in terms of relative angles of the four particles takes a simpler form:

$$c(\sin^2\theta_{12}\sin^2\theta_{34}+\sin^2\theta_{13}\sin^2\theta_{24}+\sin^2\theta_{14}\sin^2\theta_{23}). \tag{5.1.41}$$

As has been said at the end of the last section, the six relative angles are not independent; one angle can be derived from the others. Besides, any five angles are correlated. As a result, it is practical to express function (5.1.41) in terms of the particles' azimuthal and polar angles in spherical coordinates. There are eight such angles, only five of which are independent because of rotation-invariance. Consequently, we can fix one of the particles, say, particle 4, in the zenith direction, i. e. $\theta_4 = 0$,, and another particle, say, particle 1, in the $\phi_1 = 0$ plane, so as to have five independent variables: $\theta_1, \theta_2, \theta_3, \phi_2, \phi_3$. Note that under such an assumption, we have $\theta_1 = \theta_{14}, \theta_2 = \theta_{24}, \theta_3 = \theta_{34}$. For convenience, we keep ϕ_1 for the moment and write:

$$\begin{aligned}
&f(\theta_1,\theta_2,\theta_3,\phi_1,\phi_2,\phi_3)\\
&= c(\sin^2\theta_{12}\sin^2\theta_{34}+\sin^2\theta_{13}\sin^2\theta_{24}+\sin^2\theta_{14}\sin^2\theta_{23})\\
&= c\Big\{\sin^2\theta_3\Big[1-(\cos\theta_1\cos\theta_2+\cos(\phi_1-\phi_2)\sin\theta_1\sin\theta_2)^2\Big]\\
&+\sin^2\theta_2\Big[1-(\cos\theta_1\cos\theta_3+\cos(\phi_1-\phi_3)\sin\theta_1\sin\theta_3)^2\Big]\\
&+\sin^2\theta_1\Big[1-(\cos\theta_2\cos\theta_3+\cos(\phi_2-\phi_3)\sin\theta_2\sin\theta_3)^2\Big]\Big\}.
\end{aligned} \tag{5.1.42}$$

The absolute maximum that we look for occurs at critical points where the first partial derivatives with respect to the 5 variables vanish. However, the search for the absolute maximum will be complicated by the fact that function (5.1.42) has a large number of local extrema and saddle points where the first partial derivatives also vanish.

The condition $\partial_{\theta_1} f = 0$ leads to:

$$
\begin{aligned}
&3 - \cos^2\theta_1 - \cos^2\theta_2 - \cos^2\theta_1\cos^2\theta_2 - \cos^2\theta_3 - \cos^2\theta_1\cos^2\theta_3 - \cos^2\theta_2\cos^2\theta_3 \\
&+ 3\cos^2\theta_1\cos^2\theta_2\cos^2\theta_3 - 2\cos(\phi_1-\phi_2)\cos\theta_1\cos\theta_2\sin\theta_1\sin\theta_2 \\
&+ 2\cos(\phi_1-\phi_2)\cos\theta_1\cos\theta_2\cos^2\theta_3\sin\theta_1\sin\theta_2 - \cos^2(\phi_1-\phi_2)\sin^2\theta_1\sin^2\theta_2 \\
&+ \cos^2(\phi_1-\phi_2)\cos^2\theta_3\sin^2\theta_1\sin^2\theta_2 - 2\cos(\phi_1-\phi_3)\cos\theta_1\cos\theta_3\sin\theta_1\sin\theta_3 \\
&+ 2\cos(\phi_1-\phi_3)\cos\theta_1\cos\theta_2^2\cos\theta_3\sin\theta_1\sin\theta_3 - 2\cos(\phi_2-\phi_3)\cos\theta_2\cos\theta_3\sin\theta_2\sin\theta_3 \\
&+ 2\cos(\phi_2-\phi_3)\cos^2\theta_1\cos\theta_2\cos\theta_3\sin\theta_2\sin\theta_3 - \cos^2(\phi_1-\phi_3)\sin^2\theta_1\sin^2\theta_3 \\
&+ \cos^2(\phi_1-\phi_3)\cos^2\theta_2\sin^2\theta_1\sin^2\theta_3 - \cos^2(\phi_2-\phi_3)\sin^2\theta_2\sin^2\theta_3 \\
&+ \cos^2(\phi_2-\phi_3)\cos^2\theta_1\sin^2\theta_2\sin^2\theta_3 \\
&= 0,
\end{aligned}
$$

which reduces to

$$
\begin{aligned}
&\cos^2\theta_{23}\sin^2\theta_1 + \cos^2\theta_{13}\sin^2\theta_2 + \cos^2\theta_{12}\sin^2\theta_3 \\
&- \cos\theta_{13}\frac{\cos\theta_3\sin^2\theta_2}{\cos\theta_1} - \cos\theta_{12}\frac{\cos\theta_2\sin^2\theta_3}{\cos\theta_1} - \sin^2\theta_1 = 0.
\end{aligned} \tag{5.1.43}
$$

Similarly, from $\partial_{\theta_2} f = 0$ we have

$$
\begin{aligned}
&\cos^2\theta_{23}\sin^2\theta_1 + \cos^2\theta_{13}\sin^2\theta_2 + \cos^2\theta_{12}\sin^2\theta_3 \\
&- \cos\theta_{23}\frac{\cos\theta_3\sin^2\theta_1}{\cos\theta_2} - \cos\theta_{12}\frac{\cos\theta_1\sin^2\theta_3}{\cos\theta_2} - \sin^2\theta_2 = 0,
\end{aligned} \tag{5.1.44}
$$

and from $\partial_{\theta_3} f = 0$

$$
\begin{aligned}
&\cos^2\theta_{23}\sin^2\theta_1 + \cos^2\theta_{13}\sin^2\theta_2 + \cos^2\theta_{12}\sin^2\theta_3 \\
&- \cos\theta_{23}\frac{\cos\theta_2\sin^2\theta_1}{\cos\theta_3} - \cos\theta_{13}\frac{\cos\theta_1\sin^2\theta_2}{\cos\theta_3} - \sin^2\theta_3 = 0.
\end{aligned} \tag{5.1.45}
$$

Note that Eqs. (5.1.44) and (5.1.45) can be obtained by permuting particle 1, 2 and particle 1, 3 in Eq. (5.1.43) respectively, which is obvious given that function

(5.1.41) is invariant under permutation of any two neutrons.

The condition $\partial_{\phi_1} f = 0$ leads to:

$$
\begin{aligned}
&2\cos\theta_1\cos\theta_2\sin(\phi_1-\phi_2)\sin\theta_1\sin\theta_2 - 2\cos\theta_1\cos\theta_2\cos^2\theta_3\sin(\phi_1-\phi_2)\sin\theta_1\sin\theta_2 \\
&+ 2\cos(\phi_1-\phi_2)\sin(\phi_1-\phi_2)\sin^2\theta_1\sin^2\theta_2 - 2\cos(\phi_1-\phi_2)\cos^2\theta_3\sin(\phi_1-\phi_2)\sin^2\theta_1\sin^2\theta_2 \\
&+ 2\cos\theta_1\cos\theta_3\sin(\phi_1-\phi_3)\sin\theta_1\sin\theta_3 - 2\cos\theta_1\cos^2\theta_2\cos\theta_3\sin(\phi_1-\phi_3)\sin\theta_1\sin\theta_3 \\
&+ 2\cos(\phi_1-\phi_3)\sin(\phi_1-\phi_3)\sin^2\theta_1\sin^2\theta_3 - 2\cos(\phi_1-\phi_3)\cos^2\theta_2\sin(\phi_1-\phi_3)\sin^2\theta_1\sin^2\theta_3 \\
&= 0,
\end{aligned}
$$

which reduces to

$$\sin\theta_1\sin\theta_2\sin\theta_3(\sin(\phi_1-\phi_3)\sin\theta_2\cos\theta_{13} + \sin(\phi_1-\phi_2)\sin\theta_3\cos\theta_{12}) = 0. \tag{5.1.46}$$

By permutation, we obtain the equations for the other two derivatives:

$$\sin\theta_1\sin\theta_2\sin\theta_3(\sin(\phi_2-\phi_3)\sin\theta_1\cos\theta_{23} - \sin(\phi_1-\phi_2)\sin\theta_3\cos\theta_{12}) = 0 \tag{5.1.47}$$

and

$$\sin\theta_1\sin\theta_2\sin\theta_3(\sin(\phi_2-\phi_3)\sin\theta_1\cos\theta_{23} + \sin(\phi_1-\phi_3)\sin\theta_2\cos\theta_{13}) = 0. \tag{5.1.48}$$

We note that Eqs. (5.1.46), (5.1.47) and (5.1.48) are not independent, to which one possible solution is $\sin\theta_1\sin\theta_2\sin\theta_3 = 0$. We can simplify Eqs. (5.1.46), (5.1.47) and (5.1.48) by removing the factor $\sin\theta_1\sin\theta_2\sin\theta_3$ without loss of generality because the resulting equations also allow the solution $\sin\theta_1\sin\theta_2\sin\theta_3 = 0$.

Let A stand for $\sin\theta_1\cos\theta_{23}$, B for $\sin\theta_2\cos\theta_{13}$ and C for $\sin\theta_3\cos\theta_{12}$. The

six equations transform to:

$$A^2 + B^2 + C^2 - B\frac{\cos\theta_3 \sin\theta_2}{\cos\theta_1} - C\frac{\cos\theta_2 \sin\theta_3}{\cos\theta_1} - \sin^2\theta_1 = 0, \tag{5.1.49}$$

$$A^2 + B^2 + C^2 - A\frac{\cos\theta_3 \sin\theta_1}{\cos\theta_2} - C\frac{\cos\theta_1 \sin\theta_3}{\cos\theta_2} - \sin^2\theta_2 = 0, \tag{5.1.50}$$

$$A^2 + B^2 + C^2 - B\frac{\cos\theta_1 \sin\theta_2}{\cos\theta_3} - A\frac{\cos\theta_2 \sin\theta_1}{\cos\theta_3} - \sin^2\theta_3 = 0, \tag{5.1.51}$$

$$B\sin(\phi_1 - \phi_3) = -C\sin(\phi_1 - \phi_2), \tag{5.1.52}$$

$$A\sin(\phi_2 - \phi_3) = C\sin(\phi_1 - \phi_2), \tag{5.1.53}$$

$$A\sin(\phi_2 - \phi_3) = -B\sin(\phi_1 - \phi_3). \tag{5.1.54}$$

To find the absolute maxima by solving the equation set (5.1.49)~(5.1.54) would be a tedious task because of all the local extrema and saddle points. By observing the equation set, one obvious possibility stands out

$$|A| = |B| = |C| \neq 0. \tag{5.1.55}$$

Here zero is ruled out because $|A| = |B| = |C| = 0$ leads to a trivial solution. The validity of the solution (5.1.55) as leading to the absolute maximum can be alternatively supported by a Monte-Carlo simulation that will be explained later on. In the following, we will look for the configurations with the maximum probability density satisfying Eq. (5.1.55).

If we set the extra degree of freedom ϕ_1 to 0, Eqs. (5.1.52), (5.1.53) as well as A, B, and C turn into:

$$\begin{aligned}&\sin\phi_3 \sin\theta_2(\cos\theta_1 \cos\theta_3 + \cos\phi_3 \sin\theta_1 \sin\theta_3)\\ &= -\sin\phi_2 \sin\theta_3(\cos\theta_1 \cos\theta_2 + \cos\phi_2 \sin\theta_1 \sin\theta_2),\end{aligned} \tag{5.1.56}$$

$$\begin{aligned}&\sin(\phi_2 - \phi_3)\sin\theta_1(\cos\theta_2 \cos\theta_3 + \cos(\phi_2 - \phi_3)\sin\theta_2 \sin\theta_3)\\ &= -\sin\phi_2 \sin\theta_3(\cos\theta_1 \cos\theta_2 + \cos\phi_2 \sin\theta_1 \sin\theta_2),\end{aligned} \tag{5.1.57}$$

$$A = \sin\theta_1(\cos\theta_2 \cos\theta_3 + \cos(\phi_2 - \phi_3)\sin\theta_2 \sin\theta_3), \tag{5.1.58}$$

$$B = \sin\theta_2(\cos\theta_1\cos\theta_3 + \cos\phi_3\sin\theta_1\sin\theta_3), \tag{5.1.59}$$

$$C = \sin\theta_3(\cos\theta_1\cos\theta_2 + \cos\phi_2\sin\theta_1\sin\theta_2). \tag{5.1.60}$$

Eq. (5.1.55) is equivalent to

$$\left|\sin(\phi_1-\phi_2)\right| = \left|\sin(\phi_1-\phi_3)\right| = \left|\sin(\phi_2-\phi_3)\right|. \tag{5.1.61}$$

We only consider the case $\sin(\phi_1-\phi_2) = \sin(\phi_1-\phi_3) = \sin(\phi_3-\phi_2)$, as the other cases such as $\sin(\phi_1-\phi_2) = \sin(\phi_1-\phi_3) = -\sin(\phi_3-\phi_2)$, etc, lead to the same results. Without loss of generality, we may suppose that $\phi_3 \geq \phi_2$. From $\phi_1 = 0$, we have

$$\sin\phi_2 = \sin\phi_3 = \sin(\phi_2-\phi_3) \qquad \phi_3 \geq \phi_2.$$

Several cases can be distinguished according to different values of ϕ_2:

$$\begin{cases} \phi_3 = \phi_2 & \text{if} \quad \phi_2 = 0 \\ \phi_3 = \phi_2 & \text{if} \quad \phi_2 = \pi \\ \phi_3 = \pi - \phi_2 & \text{if} \quad 0 \leq \phi_2 \leq \frac{\pi}{2} \\ \phi_3 = 3\pi - \phi_2 & \text{if} \quad \pi < \phi_2 \leq \frac{3\pi}{2}, \end{cases}$$

which leads to

$$\begin{cases} \phi_3 = \phi_2 = 0 \\ \phi_3 = \phi_2 = \pi \\ \sin(2\phi_2 - \pi) = \sin\phi_2 \\ \sin(2\phi_2 - 3\pi) = \sin\phi_2 \end{cases} \Rightarrow \begin{cases} \phi_3 = \phi_2 = 0 \\ \phi_3 = \phi_2 = \pi \\ \sin 2\phi_2 = -\sin\phi_2 \end{cases} \Rightarrow \begin{cases} \phi_3 = \phi_2 = 0 \\ \phi_3 = \phi_2 = \pi \\ \sin\phi_2 = 0 \\ \cos\phi_2 = -\frac{1}{2}. \end{cases}$$

Therefore, we find all the solutions to the condition $\sin(\phi_1-\phi_2) = \sin(\phi_1-\phi_3) =$

$\sin(\phi_3 - \phi_2)$:

$$\begin{cases} \phi_3 = \phi_2 = 0 \\ \phi_3 = \phi_2 = \pi \\ \phi_2 = 0, \phi_3 = \pi \\ \phi_2 = \frac{4\pi}{3}, \phi_3 = \frac{5\pi}{3}. \end{cases} \tag{5.1.62}$$

We shall see below that those solutions lead to configurations that fall into two categories that we shall name “great-circle (GC) configurations" (the first three solutions) and “tetrahedral configurations" (the last solution). In the 0_1^+ state, the former corresponds to local maxima while the latter corresponds to the absolute maxima.

i Great-circle configurations

When $\phi_1 = \phi_2 = \phi_3 = \phi_4 = 0$ (the first solution in (5.1.62)), the four particles are in a plane that passes through the center, i.e. they are on a great circle. As a result, expression (5.1.42) can be simplified to give:

$$f(\theta_1, \theta_2, \theta_3, 0, 0) = c\Big(\sin^2\theta_1 \sin^2(\theta_2 - \theta_3) + \sin^2\theta_2 \sin^2(\theta_1 - \theta_3) + \sin^2\theta_3 \sin^2(\theta_1 - \theta_2)\Big). \tag{5.1.63}$$

The partial derivatives with respect to θ_1, θ_2 and θ_3s are:

$$\begin{aligned} \partial_{\theta_1} f &= c\Big(\sin 2\theta_1 \sin^2(\theta_2 - \theta_3) + \sin^2\theta_2 \sin 2(\theta_1 - \theta_3) + \sin^2\theta_3 \sin 2(\theta_1 - \theta_2)\Big) = 0, \\ \partial_{\theta_2} f &= c\Big(\sin^2\theta_1 \sin 2(\theta_2 - \theta_3) + \sin 2\theta_2 \sin^2(\theta_1 - \theta_3) - \sin^2\theta_3 \sin 2(\theta_1 - \theta_2)\Big) = 0, \\ \partial_{\theta_3} f &= -c\Big(\sin^2\theta_1 \sin 2(\theta_2 - \theta_3) - \sin^2\theta_2 \sin 2(\theta_1 - \theta_3) + \sin 2\theta_3 \sin^2(\theta_1 - \theta_2)\Big) = 0. \end{aligned}$$

Adding up $\partial_{\theta_1} f$ and $\partial_{\theta_2} f$, $\partial_{\theta_1} f$ and $\partial_{\theta_3} f$, and $\partial_{\theta_2} f$ and $\partial_{\theta_3} f$ separately, we ob-

tain:

$$\begin{aligned}
&\sin 2\theta_1 \sin^2(\theta_2-\theta_3)+\sin^2\theta_2 \sin 2(\theta_1-\theta_3)+\sin^2\theta_1 \sin 2(\theta_2-\theta_3)+\sin 2\theta_2 \sin^2(\theta_1-\theta_3)\\
&=2\sin\theta_1 \sin(\theta_2-\theta_3)(\cos\theta_1 \sin(\theta_2-\theta_3)+\sin\theta_1 \cos(\theta_2-\theta_3))\\
&+2\sin\theta_2 \sin(\theta_1-\theta_3)(\cos\theta_2 \sin(\theta_1-\theta_3)+\sin\theta_2 \cos(\theta_1-\theta_3))\\
&=2\sin\theta_1 \sin(\theta_2-\theta_3)\sin(\theta_1+\theta_2-\theta_3)+2\sin\theta_2 \sin(\theta_1-\theta_3)\sin(\theta_1+\theta_2-\theta_3)\\
&=2(\sin\theta_1 \sin(\theta_2-\theta_3)+\sin\theta_2 \sin(\theta_1-\theta_3))\sin(\theta_1+\theta_2-\theta_3)\\
&=0,\\
&\sin 2\theta_1 \sin^2(\theta_2-\theta_3)+\sin^2\theta_3 \sin 2(\theta_1-\theta_2)-\sin^2\theta_1 \sin 2(\theta_2-\theta_3)+\sin 2\theta_3 \sin^2(\theta_1-\theta_2)\\
&=2\sin\theta_1 \sin(\theta_2-\theta_3)(\cos\theta_1 \sin(\theta_2-\theta_3)-\sin\theta_1 \cos(\theta_2-\theta_3))\\
&+2\sin\theta_3 \sin(\theta_1-\theta_2)(\cos\theta_3 \sin(\theta_1-\theta_2)+\sin\theta_3 \cos(\theta_1-\theta_2))\\
&=2\sin\theta_1 \sin(\theta_2-\theta_3)\sin(\theta_2-\theta_3-\theta_1)+2\sin\theta_3 \sin(\theta_1-\theta_2)\sin(\theta_1-\theta_2+\theta_3)\\
&=2(\sin\theta_1 \sin(\theta_2-\theta_3)-\sin\theta_3 \sin(\theta_1-\theta_2))\sin(\theta_2-\theta_3-\theta_1)\\
&=0,\\
&\sin 2\theta_2 \sin^2(\theta_1-\theta_3)-\sin^2\theta_3 \sin 2(\theta_1-\theta_2)-\sin^2\theta_2 \sin 2(\theta_1-\theta_3)+\sin 2\theta_3 \sin^2(\theta_1-\theta_2)\\
&=2\sin\theta_2 \sin(\theta_1-\theta_3)(\cos\theta_2 \sin(\theta_1-\theta_3)-\sin\theta_2 \cos(\theta_1-\theta_3))\\
&+2\sin\theta_3 \sin(\theta_1-\theta_2)(\cos\theta_3 \sin(\theta_1-\theta_2)-\sin\theta_3 \cos(\theta_1-\theta_2))\\
&=2\sin\theta_2 \sin(\theta_1-\theta_3)\sin(\theta_1-\theta_2-\theta_3)+2\sin\theta_3 \sin(\theta_1-\theta_2)\sin(\theta_1-\theta_2-\theta_3)\\
&=2(\sin\theta_2 \sin(\theta_1-\theta_3)+\sin\theta_3 \sin(\theta_1-\theta_2))\sin(\theta_1-\theta_2-\theta_3)\\
&=0.
\end{aligned}$$

Therefore, the requirement on the first partial derivatives reduces to:

$$(\sin\theta_1 \sin(\theta_2-\theta_3)+\sin\theta_2 \sin(\theta_1-\theta_3))\sin(\theta_1+\theta_2-\theta_3)=0, \tag{5.1.64}$$

$$(\sin\theta_1 \sin(\theta_2-\theta_3)-\sin\theta_3 \sin(\theta_1-\theta_2))\sin(\theta_2-\theta_3-\theta_1)=0, \tag{5.1.65}$$

$$(\sin\theta_2 \sin(\theta_1-\theta_3)+\sin\theta_3 \sin(\theta_1-\theta_2))\sin(\theta_1-\theta_2-\theta_3)=0. \tag{5.1.66}$$

We can choose that $\theta_1 \geq \theta_2 \geq \theta_3$. The solutions to Eqs. (5.1.64), (5.1.65) and (5.1.66) are:

1. $\theta_1 = \theta_2 = \theta_3$,
2. $\theta_2 = \theta_3 = 0$,
3. $\theta_2 = \pi, \theta_3 = 0$,
4. $\theta_1 = \pi, \theta_3 = 0$,
5. $\theta_1 = \theta_2 = \pi$,
6. $\theta_1 = \pi, \theta_2 = \theta_3 = \frac{1}{2}\pi$,
7. $\theta_1 = \theta_2 = \frac{1}{2}\pi, \theta_3 = 0$.

Except for the last two solutions ($\theta_1 = \pi, \theta_2 = \theta_3 = \frac{1}{2}\pi$; $\theta_1 = \theta_2 = \frac{1}{2}\pi, \theta_3 = 0$), all the other solutions yield zero for the probability density (5.1.63) and can be ruled out. Therefore, when $\phi_1 = \phi_2 = \phi_3 = \phi_4 = 0$, the probability density (5.1.63) reaches its maximum value $2c$ at the configuration $\theta_{14} = \theta_{24} = \frac{1}{2}\pi, \theta_{34} = 0$ (Fig. 5.1(a)) and $\theta_{14} = \pi, \theta_{24} = \theta_{34} = \frac{1}{2}\pi$ (Fig. 5.1(b)). Note that these figures, as well as the other geometric configurations in this chapter, are shown from such viewpoints as for them to be easy on the eye, rather than to have one particle in the zenith direction as is assumed in the calculation for convenience.

By inspecting function (5.1.42), we can see that it is inversion-invariant with respect to the origin. In other words, we can change the coordinates of any particle (θ, ϕ) to $(\pi - \theta, \pi + \phi)$ without changing the value of function (5.1.42). Thus, by inverting particle positions in configuration 5.1(a) or 5.1(b), a third configuration is found to be $\theta_1 = \pi, \phi_1 = 0; \theta_2 = \frac{1}{2}\pi, \phi_2 = \pi; \theta_3 = \frac{1}{2}\pi, \phi_3 = 0$ as shown in Fig. 5.1(c).

The configurations with the maximum probability density for the second and the third solution in (5.1.62) ($\phi_1 = \phi_2 = \phi_4 = 0, \phi_3 = \pi$ and $\phi_1 = \phi_4 = 0, \phi_2 = \phi_3 =$

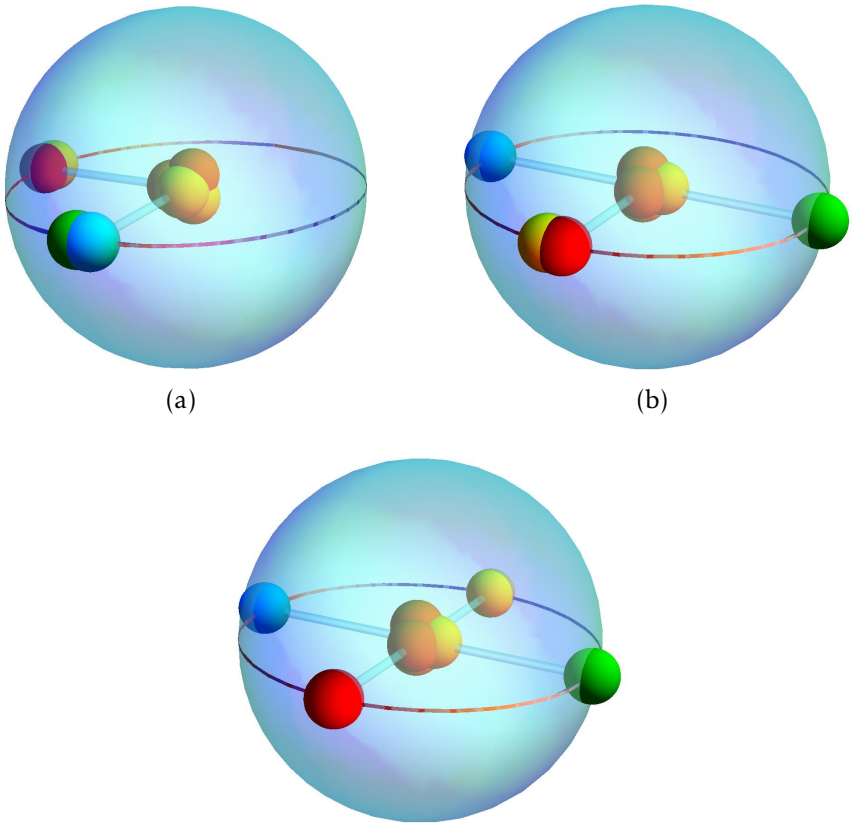

(a) (b)

(c)

Figure 5.1: Great-circle configurations of ^{8}He

π) can be obtained in the same manner and turn out to be equivalent to those that have just been found.

However, we have gotten a bit ahead of ourselves calling them “maximum" without verifying whether they are local maxima, local minima or saddle points. To do so, it is necessary to evaluate the Hessian matrix:

$$\begin{pmatrix} \partial^2_{\theta_1^2} f & \partial^2_{\theta_1\theta_2} f & \partial^2_{\theta_1\theta_3} f & \partial^2_{\theta_1\phi_2} f & \partial^2_{\theta_1\phi_3} f \\ \partial^2_{\theta_2\theta_1} f & \partial^2_{\theta_2^2} f & \partial^2_{\theta_2\theta_3} f & \partial^2_{\theta_2\phi_2} f & \partial^2_{\theta_2\phi_3} f \\ \partial^2_{\theta_3\theta_1} f & \partial^2_{\theta_3\theta_2} f & \partial^2_{\theta_3^2} f & \partial^2_{\theta_3\phi_2} f & \partial^2_{\theta_3\phi_3} f \\ \partial^2_{\phi_2\theta_1} f & \partial^2_{\phi_2\theta_2} f & \partial^2_{\phi_2\theta_3} f & \partial^2_{\phi_2^2} f & \partial^2_{\phi_2\phi_3} f \\ \partial^2_{\phi_3\theta_1} f & \partial^2_{\phi_3\theta_2} f & \partial^2_{\phi_3\theta_3} f & \partial^2_{\phi_3\phi_2} f & \partial^2_{\phi_3^2} f \end{pmatrix},$$

that is the square matrix of second partial derivatives of function (5.1.42) for each configuration in Fig. 5.1:

$$\begin{matrix} a \end{matrix} \quad \begin{matrix} b \end{matrix} \quad \begin{matrix} c \end{matrix}$$

$$\begin{pmatrix} -4 & 0 & 2 & 0 & 0 \\ 0 & -4 & 2 & 0 & 0 \\ 2 & 2 & -4 & 0 & 0 \\ 0 & 0 & 0 & 0 & 0 \\ 0 & 0 & 0 & 0 & 0 \end{pmatrix}, \begin{pmatrix} -4 & -2 & 2 & 0 & 0 \\ -2 & -4 & 0 & 0 & 0 \\ 2 & 0 & -4 & 0 & 0 \\ 0 & 0 & 0 & 0 & 0 \\ 0 & 0 & 0 & 0 & 0 \end{pmatrix}, \begin{pmatrix} -4 & -2 & 2 & 0 & 0 \\ -2 & -4 & 0 & 0 & 0 \\ 2 & 0 & -4 & 0 & 0 \\ 0 & 0 & 0 & 0 & 0 \\ 0 & 0 & 0 & 0 & 0 \end{pmatrix}. \quad (5.1.67)$$

A sufficient but not necessary condition for a function to have a local maximum at a point where all its first partial derivatives are zero is that the Hessian matrix is definite negative at that point. However the matrices for the great-circle configurations are all negative semi-definite, which is inconclusive. This is due to the fact that at those configurations the probability density has an improper maximum that will be explained below [46].

Definition. *A multivariate function $f(x_1, x_2, \cdots, x_n)$ is said to have at a definite position $(a_1, a_2, \cdots, a_n)$ a proper maximum (or a proper minimum) if n arbitrarily small*

positive quantities $\delta_\lambda(\lambda = 1, 2, \cdots, n)$ *can be found such that for all the points situated in the neighborhood*

$$|x_\lambda - a_\lambda| < \delta_\lambda \quad (\lambda = 1, 2, \cdots, n)$$

it is always true that

$$f(x_1, x_2, \cdots, x_n) - f(a_1, a_2, \cdots, a_n) < 0 \quad (or > 0)$$

The maximum or minimum is improper if the equality sign appears with the inequality sign, i.e

$$f(x_1, x_2, \cdots, x_n) - f(a_1, a_2, \cdots, a_n) \leq 0 \quad (or \geq 0)$$

takes the place of

$$f(x_1, x_2, \cdots, x_n) - f(a_1, a_2, \cdots, a_n) < 0 \quad (or > 0).$$

Indeed, if one of the θ, say, θ_1 equals 0 or π, function (5.1.42) reduces to $2c(1 - \cos^2\theta_2)(1 - \cos^2\theta_3)$ and is independent of ϕ_2 and ϕ_3. As a consequence, if the polar angles θ are chosen as they are in the three GC configurations found above, the probability density is independent of azimuthal angles, that is, the four particles can rotate around the z axis and retain the same probability density value $2c$. As an illustration of this particularity, two configurations having the same polar angles as GC configurations but randomly chosen ϕ_2 and ϕ_3 are shown in Fig. 5.2.

The second-derivative test (Hessian matrix) for local extremes and all types of saddle points is based on the quadratic approximation or the second-order Taylor expansion, because at stationary points we have, provided that the second-order

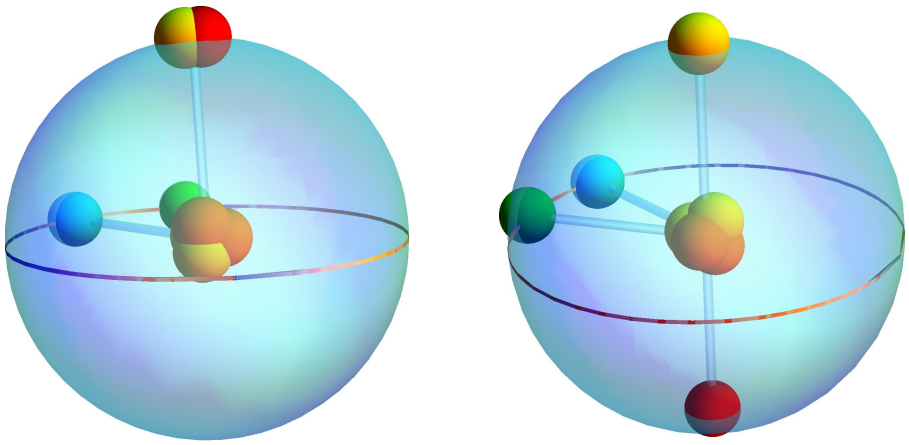

(a) (b)

Figure 5.2: Configurations with $\theta_1 = 0$ (a) or π (b) but random ϕ_2, ϕ_3

derivatives of the function $f(x_1, x_2, \cdots, x_n)$ do not all vanish:

$$\begin{aligned} & f(x_1 + h_1, x_2 + h_2, \cdots, x_n + h_n) - f(a_1, a_2, \cdots, a_n) \\ & = \frac{1}{2} \sum_{\lambda,\mu} \left\{ \left(\frac{\partial^2 f(x_1, x_2, \cdots, x_n)}{\partial x_\lambda \partial x_\mu} \right)_{a_1, \cdots, a_n} h_\lambda h_\mu \right\}. \end{aligned} \tag{5.1.68}$$

If for arbitrarily small values $h_1, h_2, \cdots, h_n$, the homogeneous quadratic form in expression (5.1.68) is always negative (or positive) at a stationary point $(a_1, a_2, \cdots, a_n)$, then $f(x_1, x_2, \cdots, x_n)$ has a maximum (or minimum) on that position.

As is stated above, the quadratic form in (5.1.68) is only negative semi-definite for the three configurations in Fig. 5.1, which requires further investigation before a conclusion can be drawn on their nature.

Note that in matrices (5.1.67) the sub-matrices comprised only of second derivatives with respect to θ_1, θ_2 and θ_3 are on the other hand negative definite. If we reformulate the quadratic form (5.1.68) by separating the second derivatives containing ϕ and those not, we have:

$$f(\theta_1 + h_{\theta_1}, \theta_2 + h_{\theta_2}, \theta_3 + h_{\theta_3}, \phi_2 + h_{\phi_2}, \phi_3 + h_{\phi_3}) - f(\theta_1, \theta_2, \theta_3, \phi_2, \phi_3)$$

$$= \frac{1}{2}\sum_{\theta_\lambda,\theta_\mu}\left\{\left(\frac{\partial^2 f(\theta_1,\theta_2,\theta_3,\phi_2,\phi_3)}{\partial\theta_\lambda\partial\theta_\mu}\right)_{\theta_1,\theta_2,\theta_3,\phi_2,\phi_3} h_{\theta_\lambda}h_{\theta_\mu}\right\}$$
$$+\frac{1}{2}\sum_{\phi_\lambda}\sum_{\alpha_\mu}\left\{\left(\frac{\partial^2 f(\theta_1,\theta_2,\theta_3,\phi_2,\phi_3)}{\partial\phi_\lambda\partial\alpha_\mu}\right)_{\theta_1,\theta_2,\theta_3,\phi_2,\phi_3} h_{\phi_\lambda}h_{\alpha_\mu}\right\}$$
$$\text{with}\quad \alpha\in\{\theta_1,\theta_2,\theta_3,\phi_2,\phi_3\}. \tag{5.1.69}$$

The only uncertain situation arises when $h_{\theta_1}, h_{\theta_2}$ and h_{θ_3} are all zero, in which case (5.1.69) vanishes. Nevertheless we have shown that when θ are chosen as they are in Fig. 5.1, $f(\theta_1,\theta_2,\theta_3,\phi_2,\phi_3)$ is a constant so that for those configurations we find that:

$$f(\theta_1+h_{\theta_1},\theta_2+h_{\theta_2},\theta_3+h_{\theta_3},\phi_2+h_{\phi_2},\phi_3+h_{\phi_3})-f(\theta_1,\theta_2,\theta_3,\phi_2,\phi_3)$$
$$\begin{cases}<0 & \delta_{h_{\theta_1},0}\delta_{h_{\theta_2},0}\delta_{h_{\theta_3},0}=0\\ =0 & \delta_{h_{\theta_1},0}\delta_{h_{\theta_2},0}\delta_{h_{\theta_3},0}=1\end{cases},$$

and no higher-order (higher than 2) Taylor expansion is needed to be sure of that. Therefore, the great-circle configurations in Fig. 5.1 are local maxima (improper) of expression (5.1.42). Such cannot be said of the configurations in Fig. 5.2 with randomly chosen angles ϕ because the submatrix of second partial derivatives with respect to θs may not be negative definite.

ii Tetrahedral configurations

When $\phi_2=\frac{4\pi}{3}$ and $\phi_3=\frac{5\pi}{3}$ (the fourth solution in (5.1.62)), according to Eqs. (5.1.52) $\sim$ (5.1.54), $A=B=-C$, so we have:

$$\begin{aligned}&A-B\\ &=\sin\theta_1\cos\theta_2\cos\theta_3-\sin\theta_2\cos\theta_1\cos\theta_3\\ &=\cos\theta_3\sin(\theta_1-\theta_2)\\ &=0\end{aligned}$$

that has the solutions

1. $\theta_2 = 0, \theta_1 = \pi$

2. $\theta_3 = \frac{\pi}{2}$

3. $\theta_1 = \theta_2$

The first possibility that $\theta_2 = 0, \theta_1 = \pi$ can be eliminated because it makes the probability density (5.1.42) vanish.

The second possibility $\theta_3 = \frac{\pi}{2}$ leads to $B + C = 0 = \cos\theta_1 \cos\theta_2$, and function (5.1.42) reduces to

$$\frac{9}{4}c - \frac{c}{4}(\cos^2\theta_1 + \cos^2\theta_2)$$

that has the maximum $\frac{9}{4}c$ when $\theta_1 = \theta_2 = \theta_3 = \frac{\pi}{2}$ where the Hessian matrix is indefinite. Therefore, we are left with the last possibility: $\theta_1 = \theta_2$.

When $\theta_1 = \theta_2$, we have

$$\begin{aligned} & B + C \\ & = 0 \\ & = \sin\theta_2 \cos\theta_1 \cos\theta_3 + \sin\theta_3 \cos\theta_1 \cos\theta_2 \\ & = \cos\theta_1 \sin(\theta_2 + \theta_3), \end{aligned}$$

whose solutions are:

1. $\theta_1 = \theta_2 = \frac{\pi}{2}$

2. $\theta_1 = \theta_2 = \pi - \theta_3$.

Again each solution will be checked. When $\theta_1 = \theta_2 = \frac{\pi}{2}$, we find again the solution $\theta_1 = \theta_2 = \theta_3 = \frac{\pi}{2}$ that has just been eliminated.

If $\theta_1 = \theta_2 = \pi - \theta_3$, the expression of B (5.1.59) and Eq. (5.1.49) become:

$$\begin{aligned} B &= \sin\theta_1(\frac{3}{2}\sin^2\theta_1 - 1) \\ 3B^2 &+ 2\sin\theta_1 B - \sin^2\theta_1 = 0 \end{aligned} \tag{5.1.70}$$

Equation set (5.1.70) can be easily solved

$$\begin{aligned} &3\sin^2\theta_1(\frac{3}{2}\sin^2\theta_1 - 1)^2 + 2\sin^2\theta_1(\frac{3}{2}\sin^2\theta_1 - 1) - \sin^2\theta_1 \\ &= \sin^2\theta_1\left[3(\frac{3}{2}\sin^2\theta_1 - 1)^2 + 2(\frac{3}{2}\sin^2\theta_1 - 1)) - 1\right] \\ &= \frac{9}{2}\sin^4\theta_1(\frac{3}{2}\sin^2\theta_1 - \frac{4}{3}) \\ &= 0 \qquad (0 < \theta < \pi) \end{aligned}$$

to give the solutions

1. $\sin\theta_1 = 0$
2. $\sin\theta_1 = \frac{2\sqrt{2}}{3}$

of which the first solution gives a probability density of 0 and so can be ruled out. The second solution $\sin\theta_1 = \frac{2\sqrt{2}}{3}$ yields two configurations:

$$\theta_1 = \theta_2 = 70.53°(0.39\pi), \theta_3 = 109.47°(0.61\pi), \phi_1 = 0, \phi_2 = 240°(\frac{4\pi}{3}), \phi_3 = 300°(\frac{5\pi}{3}),$$
$$\theta_1 = \theta_2 = 109.47°(0.61\pi), \theta_3 = 70.53°(0.39\pi), \phi_1 = 0, \phi_2 = 240°(\frac{4\pi}{3}), \phi_3 = 300°(\frac{5\pi}{3})$$

that correspond to Fig. 5.3(a) and 5.3(b). Applying inversion to particle positions in configuration 5.3(a) or 5.3(b), we obtain yet another one shown in Fig. 5.3(c) with $\theta_1 = \theta_2 = \theta_3 = 109.5°, \phi_1 = \pi, \phi_2 = \frac{\pi}{3}, \phi_3 = \frac{5\pi}{3}$. Their Hessian matrices are negative definite, which confirms that they are indeed maxima.

We note that in all three configurations, the relative angles θ_{ij} are either 109.47°, which is the tetrahedral angle in a regular tetrahedron, or 70.53°, the supplementary angle of the tetrahedral angle. As a matter of fact, as can be

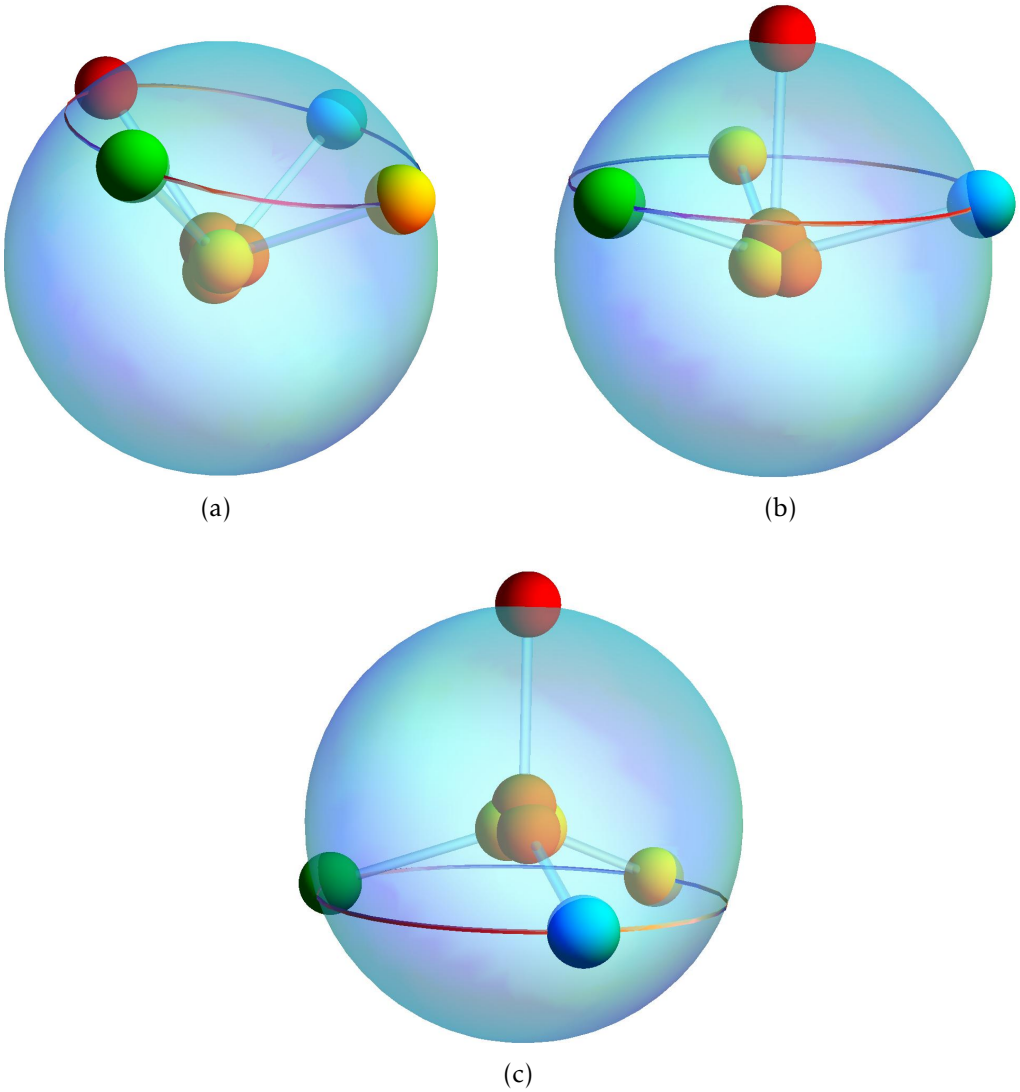

(a) (b)

(c)

Figure 5.3: Tetrahedral configurations of ^{8}He

clearly seen in Fig. 5.3(c), the four neutrons are at the vertices of a regular tetrahedron centered at the α core, and the other two configurations are its derivatives; hence the name "tetrahedral configurations". Also in all three configurations, $\sin\theta_{12} = \sin\theta_{34} = \sin\theta_{13} = \sin\theta_{24} = \sin\theta_{14} = \sin\theta_{23} = \frac{2\sqrt{2}}{3}$ and the probability density (5.1.42) equals $c(\sin^2\theta_{12}\sin^2\theta_{34} + \sin^2\theta_{13}\sin^2\theta_{24} + \sin^2\theta_{14}\sin^2\theta_{23}) = \frac{64}{27}c = 2.37c$, which is the absolute maximum. At the same time, we prove that the GC configurations (probability value $2c$) are local maxima as opposed to the absolute maxima represented by the tetrahedral configurations.

In parallel with the analytic work discussed above, a Monte-Carlo simulation aimed to look for the maximum probability density of 0_1^+ has also been done. Basically, a random input is generated for each of the five variables of function (5.1.42) on the basis of a uniform distribution. The probability density is evaluated for this set of random inputs. This procedure is repeated 10^5 times and only the set of inputs that yields the maximum value for function (5.1.42) is retained. Running this simulation as many times as required, one always finds one of the three tetrahedral configurations in Fig. 5.3, which corroborates the conclusion that the tetrahedral configurations are the absolute probability density maxima of the 0_1^+ state.

In this section, we obtained the function of the angular probability density of 0_1^+ and found the configurations for which the function has a maximum. We obtained two families of configurations with distinctive features: great-circle configurations and tetrahedral configurations. The GC configurations proved to be local maxima instead of absolute maxima represented by the tetrahedral configurations.

5.2 Configuration $|(0p_{\frac{3}{2}})^2;0\rangle|(0p_{\frac{1}{2}})^2;0\rangle$

We just studied the 0_1^+ state of ^{8}He. When the four neutrons are in the $0p$ shell, there exists another 0^+ state: $|(0p_{\frac{3}{2}})^2;0\rangle|(0p_{\frac{1}{2}})^2;0\rangle$ in which he neutrons are paired up two by two. This section will be organized in the same way as Sec. 5.1 is: first we will discuss the function of the angular probability density of 0_2^+ and then the maximum probability configurations.

5.2.1 Angular probability density of 0_2^+

The non-antisymmetric wavefunction of 0_2^+ is

$$\begin{aligned}
&\psi\left(j_1=\frac{3}{2}j_2=\frac{3}{2};0,0\right)\psi\left(j_3=\frac{1}{2}j_4=\frac{1}{2};0,0\right)\\
&=\left(\frac{1}{2}\psi_{\frac{3}{2}\frac{3}{2}}(1)\psi_{\frac{3}{2}\frac{-3}{2}}(2)-\frac{1}{2}\psi_{\frac{3}{2}\frac{1}{2}}(1)\psi_{\frac{3}{2}\frac{-1}{2}}(2)+\frac{1}{2}\psi_{\frac{3}{2}\frac{-1}{2}}(1)\psi_{\frac{3}{2}\frac{1}{2}}(2)-\frac{1}{2}\psi_{\frac{3}{2}\frac{-3}{2}}(1)\psi_{\frac{3}{2}\frac{3}{2}}(2)\right)\\
&\times\left(\frac{1}{\sqrt{2}}\psi_{\frac{1}{2}\frac{1}{2}}(3)\psi_{\frac{1}{2}\frac{-1}{2}}(4)-\frac{1}{\sqrt{2}}\psi_{\frac{1}{2}\frac{-1}{2}}(3)\psi_{\frac{1}{2}\frac{1}{2}}(4)\right)\\
&=\frac{1}{2\sqrt{2}}\left(\begin{vmatrix}\psi_{\frac{3}{2}\frac{3}{2}}(1) & \psi_{\frac{3}{2}\frac{-3}{2}}(1)\\ \psi_{\frac{3}{2}\frac{3}{2}}(2) & \psi_{\frac{3}{2}\frac{-3}{2}}(2)\end{vmatrix}-\begin{vmatrix}\psi_{\frac{3}{2}\frac{1}{2}}(1) & \psi_{\frac{3}{2}\frac{-1}{2}}(1)\\ \psi_{\frac{3}{2}\frac{1}{2}}(2) & \psi_{\frac{3}{2}\frac{-1}{2}}(2)\end{vmatrix}\right)\times\begin{vmatrix}\psi_{\frac{1}{2}\frac{1}{2}}(3) & \psi_{\frac{1}{2}\frac{-1}{2}}(3)\\ \psi_{\frac{1}{2}\frac{1}{2}}(4) & \psi_{\frac{1}{2}\frac{-1}{2}}(4)\end{vmatrix}.
\end{aligned}\tag{5.2.1}$$

In wavefunction (5.2.1), $\psi\left(j_1=\frac{3}{2}j_2=\frac{3}{2};0,0\right)$ and $\psi\left(j_3=\frac{1}{2}j_4=\frac{1}{2};0,0\right)$ are already antisymmetrized separately. Therefore, the antisymmetrization of wavefunction (5.2.1) yields:

$$\begin{aligned}
&\frac{1}{\sqrt{4!}\sqrt{2}}\left(\begin{vmatrix}\psi_{\frac{3}{2}\frac{3}{2}}(1) & \psi_{\frac{3}{2}\frac{-3}{2}}(1) & \psi_{\frac{1}{2}\frac{1}{2}}(1) & \psi_{\frac{1}{2}\frac{-1}{2}}(1)\\ \psi_{\frac{3}{2}\frac{3}{2}}(2) & \psi_{\frac{3}{2}\frac{-3}{2}}(2) & \psi_{\frac{1}{2}\frac{1}{2}}(2) & \psi_{\frac{1}{2}\frac{-1}{2}}(2)\\ \psi_{\frac{3}{2}\frac{3}{2}}(3) & \psi_{\frac{3}{2}\frac{-3}{2}}(3) & \psi_{\frac{1}{2}\frac{1}{2}}(3) & \psi_{\frac{1}{2}\frac{-1}{2}}(3)\\ \psi_{\frac{3}{2}\frac{3}{2}}(4) & \psi_{\frac{3}{2}\frac{-3}{2}}(4) & \psi_{\frac{1}{2}\frac{1}{2}}(4) & \psi_{\frac{1}{2}\frac{-1}{2}}(4)\end{vmatrix}-\begin{vmatrix}\psi_{\frac{3}{2}\frac{1}{2}}(1) & \psi_{\frac{3}{2}\frac{-1}{2}}(1) & \psi_{\frac{1}{2}\frac{1}{2}}(1) & \psi_{\frac{1}{2}\frac{-1}{2}}(1)\\ \psi_{\frac{3}{2}\frac{1}{2}}(2) & \psi_{\frac{3}{2}\frac{-1}{2}}(2) & \psi_{\frac{1}{2}\frac{1}{2}}(2) & \psi_{\frac{1}{2}\frac{-1}{2}}(2)\\ \psi_{\frac{3}{2}\frac{1}{2}}(3) & \psi_{\frac{3}{2}\frac{-1}{2}}(3) & \psi_{\frac{1}{2}\frac{1}{2}}(3) & \psi_{\frac{1}{2}\frac{-1}{2}}(3)\\ \psi_{\frac{3}{2}\frac{1}{2}}(4) & \psi_{\frac{3}{2}\frac{-1}{2}}(4) & \psi_{\frac{1}{2}\frac{1}{2}}(4) & \psi_{\frac{1}{2}\frac{-1}{2}}(4)\end{vmatrix}\right)\\
&=\frac{1}{\sqrt{4!}\sqrt{2}}\left(1-\hat{P}_{13}-\hat{P}_{14}-\hat{P}_{23}-\hat{P}_{24}+\hat{P}_{13}\hat{P}_{24}\right)
\end{aligned}$$

$$\left[\left(\begin{vmatrix}\psi_{\frac{3}{2}\frac{3}{2}}(1) & \psi_{\frac{3}{2}\frac{-3}{2}}(1)\\ \psi_{\frac{3}{2}\frac{3}{2}}(2) & \psi_{\frac{3}{2}\frac{-3}{2}}(2)\end{vmatrix} - \begin{vmatrix}\psi_{\frac{3}{2}\frac{1}{2}}(1) & \psi_{\frac{3}{2}\frac{-1}{2}}(1)\\ \psi_{\frac{3}{2}\frac{1}{2}}(2) & \psi_{\frac{3}{2}\frac{-1}{2}}(2)\end{vmatrix}\right) \times \begin{vmatrix}\psi_{\frac{1}{2}\frac{1}{2}}(3) & \psi_{\frac{1}{2}\frac{-1}{2}}(3)\\ \psi_{\frac{1}{2}\frac{1}{2}}(4) & \psi_{\frac{1}{2}\frac{-1}{2}}(4)\end{vmatrix}\right]. \tag{5.2.2}$$

As before, we leave out the radial wave function. In addition to the single-particle wave functions in the $0p_{\frac{3}{2}}$ shell that have been given in section 5.1, those in the $0p_{\frac{1}{2}}$ shell are also needed:

$$\begin{aligned}\psi_{\frac{1}{2}\frac{1}{2}} &= \sqrt{\frac{2}{3}}Y_{1,1}(\theta,\phi)\cdot\chi_{\frac{-1}{2}} - \sqrt{\frac{1}{3}}Y_{1,0}(\theta,\phi)\cdot\chi_{\frac{1}{2}},\\ \psi_{\frac{1}{2}\frac{-1}{2}} &= \sqrt{\frac{1}{3}}Y_{1,0}(\theta,\phi)\cdot\chi_{\frac{-1}{2}} - \sqrt{\frac{2}{3}}Y_{1,-1}(\theta,\phi)\cdot\chi_{\frac{1}{2}}.\end{aligned} \tag{5.2.3}$$

In what follows, we will proceed to obtain the 0_2^+ wavefunction and probability density in a rather similar fashion as in section 5.1 with 0_1^+. To avoid repetition, only the differences will be addressed.

The wave function is formulated similarly to (5.1.4):

$$\begin{aligned}&\Psi_{0_2^+}(\vec{r}_1,\vec{r}_2,\vec{r}_3,\vec{r}_4,\chi_1,\chi_2,\chi_3,\chi_4)\\ &= \left(\frac{1}{2}\sqrt{\frac{3}{2\pi}}\right)^4 \frac{1}{r_1r_2r_3r_4}\frac{1}{\sqrt{4!}\sqrt{2}}\frac{4}{3}\sum_{\substack{m_1,m_2\\ m_3,m_4}} \Phi_{0_2^+m_1m_2m_3m_4}(\vec{r}_1,\vec{r}_2,\vec{r}_3,\vec{r}_4)\cdot\chi_{m_1}(1)\chi_{m_2}(2)\chi_{m_3}(3)\chi_{m_4}(4).\end{aligned} \tag{5.2.4}$$

The expressions of $\Phi_{0_2^+m_1m_2m_3m_4}(\vec{r}_1,\vec{r}_2,\vec{r}_3,\vec{r}_4)\cdot\chi_{m_1}(1)\chi_{m_2}(2)\chi_{m_3}(3)\chi_{m_4}(4)$ are similar to those of $\Phi_{0_1^+m_1m_2m_3m_4}(\vec{r}_1,\vec{r}_2,\vec{r}_3,\vec{r}_4)\cdot\chi_{m_1}(1)\chi_{m_2}(2)\chi_{m_3}(3)\chi_{m_4}(4)$; some are even identical:

$$\begin{aligned}\Phi_{0_2^+--++}(\vec{r}_1,\vec{r}_2,\vec{r}_3,\vec{r}_4) &= -2\vec{r}_{12}\cdot\vec{r}_{34} + i\ z_{12,34},\\ \Phi_{0_2^++--}(\vec{r}_1,\vec{r}_2,\vec{r}_3,\vec{r}_4) &= -2\vec{r}_{12}\cdot\vec{r}_{34} - i\ z_{12,34},\\ \Phi_{0_2^+-+-+}(\vec{r}_1,\vec{r}_2,\vec{r}_3,\vec{r}_4) &= 2\vec{r}_{13}\cdot\vec{r}_{24} - i\ z_{13,24},\\ \Phi_{0_2^+-+-+}(\vec{r}_1,\vec{r}_2,\vec{r}_3,\vec{r}_4) &= 2\vec{r}_{13}\cdot\vec{r}_{24} + i\ z_{13,24},\\ \Phi_{0_2^+-++-}(\vec{r}_1,\vec{r}_2,\vec{r}_3,\vec{r}_4) &= -2\vec{r}_{14}\cdot\vec{r}_{23} + i\ z_{14,23},\end{aligned}$$

$$\Phi_{0_2^+-\!-\!-+}(\vec{r}_1,\vec{r}_2,\vec{r}_3,\vec{r}_4) = -2\vec{r}_{14}\cdot\vec{r}_{23} - i\ z_{14,23},$$

$$\Phi_{0_2^+-\!-\!-\!-+}(\vec{r}_1,\vec{r}_2,\vec{r}_3,\vec{r}_4) = (y_4 - i\ x_4)\begin{vmatrix} x_1 & x_2 & x_3 \\ y_1 & y_2 & y_3 \\ z_1 & z_2 & z_3 \end{vmatrix},$$

$$\Phi_{0_2^+-\!-\!-\!+-}(\vec{r}_1,\vec{r}_2,\vec{r}_3,\vec{r}_4) = -(y_4 + i\ x_4)\begin{vmatrix} x_1 & x_2 & x_3 \\ y_1 & y_2 & y_3 \\ z_1 & z_2 & z_3 \end{vmatrix},$$

$$\Phi_{0_2^+-\!-\!+-\!-}(\vec{r}_1,\vec{r}_2,\vec{r}_3,\vec{r}_4) = (-y_3 + i\ x_3)\begin{vmatrix} x_1 & x_2 & x_4 \\ y_1 & y_2 & y_4 \\ z_1 & z_2 & z_4 \end{vmatrix},$$

$$\Phi_{0_2^+-\!+\!-\!+}(\vec{r}_1,\vec{r}_2,\vec{r}_3,\vec{r}_4) = (y_3 + i\ x_3)\begin{vmatrix} x_1 & x_2 & x_4 \\ y_1 & y_2 & y_4 \\ z_1 & z_2 & z_4 \end{vmatrix},$$

$$\Phi_{0_2^+-\!+\!-\!-}(\vec{r}_1,\vec{r}_2,\vec{r}_3,\vec{r}_4) = (y_2 - i\ x_2)\begin{vmatrix} x_1 & x_3 & x_4 \\ y_1 & y_3 & y_4 \\ z_1 & z_3 & z_4 \end{vmatrix},$$

$$\Phi_{0_2^+-\!+\!-\!+}(\vec{r}_1,\vec{r}_2,\vec{r}_3,\vec{r}_4) = -(y_2 + i\ x_2)\begin{vmatrix} x_1 & x_3 & x_4 \\ y_1 & y_3 & y_4 \\ z_1 & z_3 & z_4 \end{vmatrix},$$

$$\Phi_{0_2^+-\!+\!+\!-}(\vec{r}_1,\vec{r}_2,\vec{r}_3,\vec{r}_4) = (-y_1 + i\ x_1)\begin{vmatrix} x_2 & x_3 & x_4 \\ y_2 & y_3 & y_4 \\ z_2 & z_3 & z_4 \end{vmatrix},$$

$$\Phi_{0_2^+-\!+\!+\!+}(\vec{r}_1,\vec{r}_2,\vec{r}_3,\vec{r}_4) = (y_1 + i\ x_1)\begin{vmatrix} x_2 & x_3 & x_4 \\ y_2 & y_3 & y_4 \\ z_2 & z_3 & z_4 \end{vmatrix},$$

$$\Phi_{0_2^+-\!+\!-\!-}(\vec{r}_1,\vec{r}_2,\vec{r}_3,\vec{r}_4) = (y_2 - i\ x_2)\begin{vmatrix} x_1 & x_3 & x_4 \\ y_1 & y_3 & y_4 \\ z_1 & z_3 & z_4 \end{vmatrix},$$

$$\Phi_{0_2^+ +-++}(\vec{r}_1,\vec{r}_2,\vec{r}_3,\vec{r}_4) = -(y_2 + i\ x_2)\begin{vmatrix} x_1 & x_3 & x_4 \\ y_1 & y_3 & y_4 \\ z_1 & z_3 & z_4 \end{vmatrix},$$

$$\Phi_{0_2^+ +---}(\vec{r}_1,\vec{r}_2,\vec{r}_3,\vec{r}_4) = (-y_1 + i\ x_1)\begin{vmatrix} x_2 & x_3 & x_4 \\ y_2 & y_3 & y_4 \\ z_2 & z_3 & z_4 \end{vmatrix},$$

$$\Phi_{0_2^+ -+++}(\vec{r}_1,\vec{r}_2,\vec{r}_3,\vec{r}_4) = (y_1 + i\ x_1)\begin{vmatrix} x_2 & x_3 & x_4 \\ y_2 & y_3 & y_4 \\ z_2 & z_3 & z_4 \end{vmatrix}.$$

The probability density of wave function (5.2.4), $\Psi^*_{0_2^+}\Psi_{0_2^+}$, is equal to

$$\left[\left(\frac{1}{2}\sqrt{\frac{3}{2\pi}}\right)^4 \frac{1}{r_1 r_2 r_3 r_4}\frac{1}{\sqrt{4!}\sqrt{2}}\frac{4}{3}\right]^2 \sum_{\substack{m_1,m_2\\ m_3,m_4}} \Phi^*_{0_2^+ m_1 m_2 m_3 m_4}(\vec{r}_1,\vec{r}_2,\vec{r}_3,\vec{r}_4)\Phi_{0_2^+ m_1 m_2 m_3 m_4}(\vec{r}_1,\vec{r}_2,\vec{r}_3,\vec{r}_4)$$

$$= \frac{3}{2^{12}\pi^4}\frac{1}{r_1^2 r_2^2 r_3^2 r_4^2}\Big(2\left\|-2\vec{r}_{12}\cdot\vec{r}_{34} + i\ z_{12,34}\right\|^2 + 2\left\|2\vec{r}_{13}\cdot\vec{r}_{24} - i\ z_{13,24}\right\|^2 + 2\left\|-2\vec{r}_{14}\cdot\vec{r}_{23} + i\ z_{14,23}\right\|^2$$

$$+ 2\|(y_4 - i\ x_4)\|^2\begin{vmatrix} x_1 & x_2 & x_3 \\ y_1 & y_2 & y_3 \\ z_1 & z_2 & z_3 \end{vmatrix}^2 + 2\|(-y_3 + i\ x_3)\|^2\begin{vmatrix} x_1 & x_2 & x_4 \\ y_1 & y_2 & y_4 \\ z_1 & z_2 & z_4 \end{vmatrix}^2 + 2\|(y_2 - i\ x_2)\|^2\begin{vmatrix} x_1 & x_3 & x_4 \\ y_1 & y_3 & y_4 \\ z_1 & z_3 & z_4 \end{vmatrix}^2$$

$$+ 2\|(-y_1 + i\ x_1)\|^2\begin{vmatrix} x_2 & x_3 & x_4 \\ y_2 & y_3 & y_4 \\ z_2 & z_3 & z_4 \end{vmatrix}^2\Big)$$

$$= \frac{3}{2^{12}\pi^4}\frac{1}{r_1^2 r_2^2 r_3^2 r_4^2}\Big(8(\vec{r}_{13}\cdot\vec{r}_{24})^2 + 8(\vec{r}_{14}\cdot\vec{r}_{23})^2 + 8(\vec{r}_{12}\cdot\vec{r}_{34})^2 + 2z_{12,34}^2 + 2z_{13,24}^2 + 2z_{14,23}^2$$

$$+ 2(x_1^2 + y_1^2)\begin{vmatrix} x_2 & x_3 & x_4 \\ y_2 & y_3 & y_4 \\ z_2 & z_3 & z_4 \end{vmatrix}^2 + 2(x_2^2 + y_2^2)\begin{vmatrix} x_1 & x_3 & x_4 \\ y_1 & y_3 & y_4 \\ z_1 & z_3 & z_4 \end{vmatrix}^2 + 2(x_3^2 + y_3^2)\begin{vmatrix} x_1 & x_2 & x_4 \\ y_1 & y_2 & y_4 \\ z_1 & z_2 & z_4 \end{vmatrix}^2$$

$$+2(x_4^2+y_4^2)\begin{vmatrix} x_1 & x_2 & x_3 \\ y_1 & y_2 & y_3 \\ z_1 & z_2 & z_3 \end{vmatrix}^2 \Bigg)$$

$$= \frac{3}{2^{11}\pi^4}\frac{1}{r_1^2 r_2^2 r_3^2 r_4^2}\Big(4(\vec{r}_{13}\cdot\vec{r}_{24})^2+4(\vec{r}_{14}\cdot\vec{r}_{23})^2+4(\vec{r}_{12}\cdot\vec{r}_{34})^2+z_{12,34}^2+z_{13,24}^2+z_{14,23}^2$$

$$+x_{12,34}^2+x_{13,24}^2+x_{14,23}^2+y_{12,34}^2+y_{13,24}^2+y_{14,23}^2\Big)$$

$$= \frac{3}{2^{11}\pi^4}\frac{1}{r_1^2 r_2^2 r_3^2 r_4^2}\Big(4(\vec{r}_{13}\cdot\vec{r}_{24})^2+4(\vec{r}_{14}\cdot\vec{r}_{23})^2+4(\vec{r}_{12}\cdot\vec{r}_{34})^2+\|\vec{r}_{12}\times\vec{r}_{34}\|^2+\|\vec{r}_{13}\times\vec{r}_{24}\|^2$$

$$+\|\vec{r}_{14}\times\vec{r}_{23}\|^2\Big)$$

$$= \frac{3}{2^{11}\pi^4}\Big(4\sin^2\theta_{13}\sin^2\theta_{24}\cos^2\theta_{13,24}+4\sin^2\theta_{14}\sin^2\theta_{23}\cos^2\theta_{14,23}$$

$$+4\sin^2\theta_{12}\sin^2\theta_{34}\cos^2\theta_{12,34}+\sin^2\theta_{13}\sin^2\theta_{24}\sin^2\theta_{13,24}+\sin^2\theta_{14}\sin^2\theta_{23}\sin^2\theta_{14,23}$$

$$+\sin^2\theta_{12}\sin^2\theta_{34}\sin^2\theta_{12,34}\Big)$$

$$= \frac{3}{2^{11}\pi^4}\Big(\sin^2\theta_{13}\sin^2\theta_{24}(1+3\cos^2\theta_{13,24})+\sin^2\theta_{14}\sin^2\theta_{23}(1+3\cos^2\theta_{14,23})$$

$$+\sin^2\theta_{12}\sin^2\theta_{34}(1+3\cos^2\theta_{12,34})\Big)$$

Thus we obtain the probability density of 0_2^+:

$$\frac{c}{2}\Big[\sin^2\theta_{13}\sin^2\theta_{24}(1+3\cos^2\theta_{13,24})+\sin^2\theta_{14}\sin^2\theta_{23}(1+3\cos^2\theta_{14,23})$$

$$+\sin^2\theta_{12}\sin^2\theta_{34}(1+3\cos^2\theta_{12,34})\Big] \quad (5.2.5)$$

5.2.2 Geometry of 0_2^+ with the maximum probability density

Looking for the maximum of function (5.2.5) in the same way as we did for function (5.1.41) in Sec. 5.1, we find again the two categories of configurations discussed in Sec. 5.1, the only difference being that it is the great-circle configurations that becomes favored as the absolute maxima with the value $4c$, while the

tetrahedral configurations are local maxima with the value $\frac{32}{27}c$.

5.3 Two-State Mixing

Interactions in the $0p$ shell as well as spin-orbit interactions mix the two 0^+ states of ^{8}He. In such a case the ground state is their linear combination:

$$\alpha \mid 0_1^+\rangle + \beta \mid 0_2^+\rangle = \alpha|(0p_{\frac{3}{2}})^4;0\rangle + \beta|(0p_{\frac{3}{2}})^2;0\rangle|(0p_{\frac{1}{2}})^2;0\rangle, \tag{5.3.1}$$

with $\alpha^2+\beta^2=1$. In this section, we will see how the probability density function as well as its maximum evolve with the mixing of the two states.

With functions (5.2.5) and (5.1.41) derived earlier, it is a simple matter to find that the probability density for an ad-mixed state f_{mix} is

$$\begin{aligned}
&\left(\alpha\Psi^*_{0_1^+}+\beta\Psi^*_{0_2^+}\right)\left(\alpha\Psi_{0_1^+}+\beta\Psi_{0_2^+}\right)\\
&\equiv f_{mix}(\theta_1,\theta_2,\theta_3,\phi_2,\phi_3)\\
&=\alpha^2\|\Psi_{0^+}\|^2+\beta^2\|\Psi_{0_2^+}\|^2+2\mathrm{Re}(\alpha\beta\Psi^*_{0^+}\Psi_{0_2^+})\\
&=\alpha^2 c\left(\sin^2\theta_{12}\sin^2\theta_{34}+\sin^2\theta_{13}\sin^2\theta_{24}+\sin^2\theta_{14}\sin^2\theta_{23}\right)\\
&+\beta^2\frac{c}{2}\Big[\sin^2\theta_{13}\sin^2\theta_{24}(1+3\cos^2\theta_{13,24})+\sin^2\theta_{14}\sin^2\theta_{23}(1+3\cos^2\theta_{14,23})\\
&+\sin^2\theta_{12}\sin^2\theta_{34}(1+3\cos^2\theta_{12,34})\Big]\\
&+2\alpha\beta\frac{c}{\sqrt{2}}\Big[\sin^2\theta_{13}\sin^2\theta_{24}(1-3\cos^2\theta_{13,24})+\sin^2\theta_{14}\sin^2\theta_{23}(1-3\cos^2\theta_{14,23})\\
&+\sin^2\theta_{12}\sin^2\theta_{34}(1-3\cos^2\theta_{12,34})\Big]\\
&=\sin^2\theta_{13}\sin^2\theta_{24}(\lambda+\mu\cos^2\theta_{13,24})+\sin^2\theta_{14}\sin^2\theta_{23}(\lambda+\mu\cos^2\theta_{14,23})\\
&+\sin^2\theta_{12}\sin^2\theta_{34}(\lambda+\mu\cos^2\theta_{12,34})
\end{aligned}\tag{5.3.2}$$

with $\lambda=\left(\alpha^2+\frac{1}{2}\beta^2+\sqrt{2}\alpha\beta\right)c,\quad \mu=\left(\frac{3}{2}\beta^2-3\sqrt{2}\alpha\beta\right)c.$

In function (5.3.2), “Re" stands for the real part. The properties of f_{mix} depend on the ratio of λ to μ, which represents the competition between

$$\sin^2\theta_{12}\sin^2\theta_{34}+\sin^2\theta_{13}\sin^2\theta_{24}+\sin^2\theta_{14}\sin^2\theta_{23}$$

that favors the tetrahedral configuration and

$$\sin^2\theta_{13}\sin^2\theta_{24}\cos^2\theta_{13,24}+\sin^2\theta_{14}\sin^2\theta_{23}\cos^2\theta_{14,23}+\sin^2\theta_{12}\sin^2\theta_{34}\cos^2\theta_{12,34}$$

that favors the great-circle configurations. Therefore it is convenient to write function (5.3.2) in terms of $\frac{\mu}{\lambda}$:

$$\begin{aligned}&\lambda\Big[\sin^2\theta_{13}\sin^2\theta_{24}(1+\frac{\mu}{\lambda}\cos^2\theta_{13,24})+\sin^2\theta_{14}\sin^2\theta_{23}(1+\frac{\mu}{\lambda}\cos^2\theta_{14,23})\\&+\sin^2\theta_{12}\sin^2\theta_{34}(1+\frac{\mu}{\lambda}\cos^2\theta_{12,34})\Big]\end{aligned}\tag{5.3.3}$$

when λ does not vanish; $\lambda=0$ will be discussed at the end of this section.

The ratio $\frac{\mu}{\lambda}$ ranges from -1 to $+\infty$, which can be easily seen as follows. We make the substitution $u=\frac{\beta}{\alpha}$,

$$\begin{aligned}\frac{\mu}{\lambda}&=\frac{\left(\frac{3}{2}\beta^2-3\sqrt{2}\alpha\beta\right)b}{\left(\alpha^2+\frac{1}{2}\beta^2+\sqrt{2}\alpha\beta\right)b}\\&=\frac{\frac{3}{2}u^2-3\sqrt{2}u}{1+\frac{1}{2}u^2+\sqrt{2}u}\\&=3-\frac{12\sqrt{2}(u+\sqrt{2})}{(u+\sqrt{2})^2}+\frac{18}{(u+\sqrt{2})^2}\\&=\frac{18}{(u+\sqrt{2})^2}-\frac{12\sqrt{2}}{u+\sqrt{2}}+3\\&=18\left(\frac{1}{u+\sqrt{2}}-\frac{\sqrt{2}}{3}\right)^2-1\end{aligned}\tag{5.3.4}$$

Since $\frac{1}{u+\sqrt{2}}$ can take all non-zero real numbers, $\frac{\mu}{\lambda}$ goes from -1 to $+\infty$. When $\frac{\mu}{\lambda}$ equals 0 or 3, we have the pure 0_1^+ or 0_2^+ state.

For admixtures of the two states, those critical points where the probability density peaks (locally or globally) that have been discussed for the pure 0_1^+ and 0_2^+ states in the last two sections also have vanishing first partial derivatives and thus are good candidates for maxima. Thus, it is tempting to examine the nature of the GC configurations and the tetrahedral configurations for admixtures of the two states.

5.3.1 Great-circle configurations

For great-circle configurations, f_{mix} equals $2(\lambda+\mu)$, or $2\lambda(1+\frac{\mu}{\lambda})$, linearly dependent on $\frac{\mu}{\lambda}$. Take the configuration $\theta_1=\pi$, $\theta_2=\theta_3=\frac{\pi}{2}$, $\phi_1=\phi_2=\phi_3=0$ [Fig. 5.1(b)] as an example. The Hessian matrix at this point takes the form of a block matrix:

$$\lambda\begin{pmatrix}\mathbf{A} & \mathbf{0}\\ \mathbf{0} & \mathbf{B}\end{pmatrix}=\lambda\begin{pmatrix}-4-4\frac{\mu}{\lambda} & 2+2\frac{\mu}{\lambda} & 2+2\frac{\mu}{\lambda} & 0 & 0\\ 2+2\frac{\mu}{\lambda} & -4-4\frac{\mu}{\lambda} & 0 & 0 & 0\\ 2+2\frac{\mu}{\lambda} & 0 & -4-4\frac{\mu}{\lambda} & 0 & 0\\ 0 & 0 & 0 & -4\frac{\mu}{\lambda} & 4\frac{\mu}{\lambda}\\ 0 & 0 & 0 & 4\frac{\mu}{\lambda} & -4\frac{\mu}{\lambda}\end{pmatrix}$$

Matrix **A** has eigenvalues $-4(1+\frac{\mu}{\lambda})$, $(2\sqrt{2}-4)(1+\frac{\mu}{\lambda})$, $(-2\sqrt{2}-4)(1+\frac{\mu}{\lambda})$ and is always negative-definite as $\frac{\mu}{\lambda}$ goes from -1 to infinity. Matrix **B** has eigenvalues 0, $-8\frac{\mu}{\lambda}$. The five eigenvalues are plotted in Fig. 5.4. For clarity, the factor λ is left out.

We have seen in section 5.1 that at $\frac{\mu}{\lambda}=0$, i.e. for the pure 0_1^+ state, the great-circle configurations are local maxima. To the left of the origin, the Hessian is indefinite; to the right of the origin, the Hessian is always negative semi-definite with one vanishing eigenvalue. However, the matrix **A** is negative-definite. Fol-

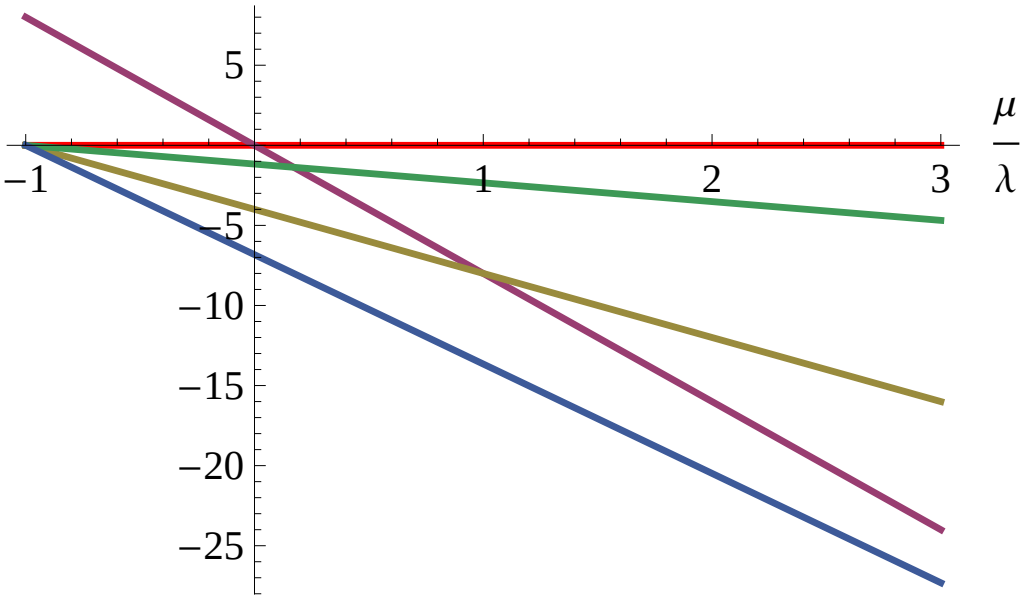

Figure 5.4: Eigenvalues of great-circle configurations

lowing the reasoning in Sec. 5.1, we have

$$
\begin{aligned}
&f_{mix}(\pi + h_{\theta_1}, \frac{\pi}{2} + h_{\theta_2}, \frac{\pi}{2} + h_{\theta_3}, h_{\phi_2}, h_{\phi_3}) - f_{mix}(\pi, \frac{\pi}{2}, \frac{\pi}{2}, 0, 0) \\
&= \frac{1}{2} \sum_{\theta_\lambda, \theta_\mu} \left\{ \left(\frac{\partial^2 f(\theta_1, \theta_2, \theta_3, \phi_2, \phi_3)}{\partial \theta_\lambda \partial \theta_\mu} \right)_{\pi, \frac{\pi}{2}, \frac{\pi}{2}, 0, 0} h_{\theta_\lambda} h_{\theta_\mu} \right\} \\
&+ \frac{1}{2} \sum_{\phi_\lambda} \sum_{\alpha_\mu} \left\{ \left(\frac{\partial^2 f(\theta_1, \theta_2, \theta_3, \phi_2, \phi_3)}{\partial \phi_\lambda \partial \alpha_\mu} \right)_{\pi, \frac{\pi}{2}, \frac{\pi}{2}, 0, 0} h_{\phi_\lambda} h_{\alpha_\mu} \right\} \quad \alpha \in \{\theta_1, \theta_2, \theta_3, \phi_2, \phi_3\}
\end{aligned}
\tag{5.3.5}
$$

Matrix **A** being negative-definite, the first term $\frac{1}{2} \sum_{\theta_\lambda, \theta_\mu} \left\{ \left(\frac{\partial^2 f(\theta_1, \theta_2, \theta_3, \phi_2, \phi_3)}{\partial \theta_\lambda \partial \theta_\mu} \right)_{\pi, \frac{\pi}{2}, \frac{\pi}{2}, 0, 0} h_{\theta_\lambda} h_{\theta_\mu} \right\}$ is always negative provided that h_{θ_1}, h_{θ_2} and h_{θ_3} do not all vanish. As for $\mathbf{B} = \begin{pmatrix} -4\frac{\mu}{\lambda} & 4\frac{\mu}{\lambda} \\ 4\frac{\mu}{\lambda} & -4\frac{\mu}{\lambda} \end{pmatrix}$, the second term:

$$
\frac{1}{2} \sum_{\phi_\lambda} \sum_{\alpha_\mu} \left\{ \left(\frac{\partial^2 f(\theta_1, \theta_2, \theta_3, \phi_2, \phi_3)}{\partial \phi_\lambda \partial \alpha_\mu} \right)_{\pi, \frac{\pi}{2}, \frac{\pi}{2}, 0, 0} h_{\phi_\lambda} h_{\alpha_\mu} \right\} = -2\frac{\mu}{\lambda} (h_{\phi_2} - h_{\phi_3})^2 \tag{5.3.6}
$$

is negative unless $h_{\phi_2} = h_{\phi_3}$, in which case it is equal to zero. As a result, unless h_{θ_1}, h_{θ_2} and h_{θ_3} all vanish and $h_{\phi_2} = h_{\phi_3}$, expression (5.3.5) is always negative. If h_{θ_1}, h_{θ_2} and h_{θ_3} do all vanish and $h_{\phi_2} = h_{\phi_3}$, expression (5.3.3) reduces to $\lambda(2+2\frac{\mu}{\lambda})$,

which is equal to $f_{mix}(\pi, \frac{\pi}{2}, \frac{\pi}{2}, 0, 0)$. This is obvious considering that configurations are rotation-invariant. If ϕ_2 and ϕ_3 in a great-circle configuration turn around axis z by the same amount, the configuration does not change. In conclusion,

$$f_{mix}(\pi + h_{\theta_1}, \frac{\pi}{2} + h_{\theta_2}, \frac{\pi}{2} + h_{\theta_3}, h_{\phi_2}, h_{\phi_3}) - f_{mix}(\pi, \frac{\pi}{2}, \frac{\pi}{2}, 0, 0)$$
$$\begin{cases} < 0 & \delta_{h_{\theta_1},0}\delta_{h_{\theta_2},0}\delta_{h_{\theta_3},0}\delta_{h_{\phi_2},h_{\phi_3}} = 0 \\ = 0 & \delta_{h_{\theta_1},0}\delta_{h_{\theta_2},0}\delta_{h_{\theta_3},0}\delta_{h_{\phi_2},h_{\phi_3}} = 1 \end{cases} \tag{5.3.7}$$

which proves that when $\frac{\mu}{\lambda} \geq 0$, $\theta_1 = \pi$, $\theta_2 = \theta_3 = \frac{\pi}{2}$, $\phi_1 = \phi_2 = \phi_3 = 0$ in Fig. 5.1(b) is a (local or absolute) improper maximum.

5.3.2 Tetrahedral configurations

For tetrahedral configurations, $f_{mix} = \frac{64}{27}\lambda$ and is independent of $\frac{\mu}{\lambda}$ since all the inter-cross-product angles ($\theta_{12,34}$, $\theta_{13,24}$, $\theta_{14,23}$) are either $\frac{\pi}{2}$ or $\frac{3\pi}{2}$.

As an example, let's take the configuration $\theta_1 = \theta_2 = \theta_3 = 70.5°$, $\phi_1 = 0$, $\phi_2 = 120°$, $\phi_3 = 240°$ [Fig. 5.3(b)]. It has the Hessian matrix

$$\begin{pmatrix} \frac{8}{9}(\frac{\mu}{\lambda} - 2) & -\frac{4}{9}(\frac{\mu}{\lambda} + \frac{2}{3}) & -\frac{4}{9}(\frac{\mu}{\lambda} + \frac{2}{3}) & \frac{8}{9}\sqrt{\frac{2}{3}}(\frac{\mu}{\lambda} - \frac{2}{3}) & -\frac{8}{9}\sqrt{\frac{2}{3}}(\frac{\mu}{\lambda} - \frac{2}{3}) \\ -\frac{4}{9}(\frac{\mu}{\lambda} + \frac{2}{3}) & \frac{8}{9}(\frac{\mu}{\lambda} - 2) & -\frac{4}{9}(\frac{\mu}{\lambda} + \frac{2}{3}) & 0 & \frac{8}{9}\sqrt{\frac{2}{3}}(\frac{\mu}{\lambda} - \frac{2}{3}) \\ -\frac{4}{9}(\frac{\mu}{\lambda} + \frac{2}{3}) & -\frac{4}{9}(\frac{\mu}{\lambda} + \frac{2}{3}) & \frac{8}{9}(\frac{\mu}{\lambda} - 2) & -\frac{8}{9}\sqrt{\frac{2}{3}}(\frac{\mu}{\lambda} - \frac{2}{3}) & 0 \\ \frac{8}{9}\sqrt{\frac{2}{3}}(\frac{\mu}{\lambda} - \frac{2}{3}) & 0 & -\frac{8}{9}\sqrt{\frac{2}{3}}(\frac{\mu}{\lambda} - \frac{2}{3}) & \frac{64}{81}(\frac{\mu}{\lambda} - 2) & -\frac{32}{81}(\frac{\mu}{\lambda} - 2) \\ -\frac{8}{9}\sqrt{\frac{2}{3}}(\frac{\mu}{\lambda} - \frac{2}{3}) & \frac{8}{9}\sqrt{\frac{2}{3}}(\frac{\mu}{\lambda} - \frac{2}{3}) & 0 & -\frac{32}{81}(\frac{\mu}{\lambda} - 2) & \frac{64}{81}(\frac{\mu}{\lambda} - 2) \end{pmatrix}$$

The evolution of the five eigenvalues

$$-\frac{64}{27}$$
$$\frac{2}{27}\left(-26 + 17\frac{\mu}{\lambda} - \sqrt{164 - 372\frac{\mu}{\lambda} + 289\frac{\mu}{\lambda}^2}\right)$$

$$\frac{2}{27}\left(-26+17\frac{\mu}{\lambda}+\sqrt{164-372\frac{\mu}{\lambda}+289\frac{\mu^2}{\lambda}}\right)$$
$$\frac{2}{81}\left(-46+35\frac{\mu}{\lambda}-\sqrt{580-1684\frac{\mu}{\lambda}+1225\frac{\mu^2}{\lambda}}\right)$$
$$\frac{2}{81}\left(-46+35\frac{\mu}{\lambda}+\sqrt{580-1684\frac{\mu}{\lambda}+1225\frac{\mu^2}{\lambda}}\right)$$

as a function of $\frac{\mu}{\lambda}$ is plotted in Fig. 5.5.

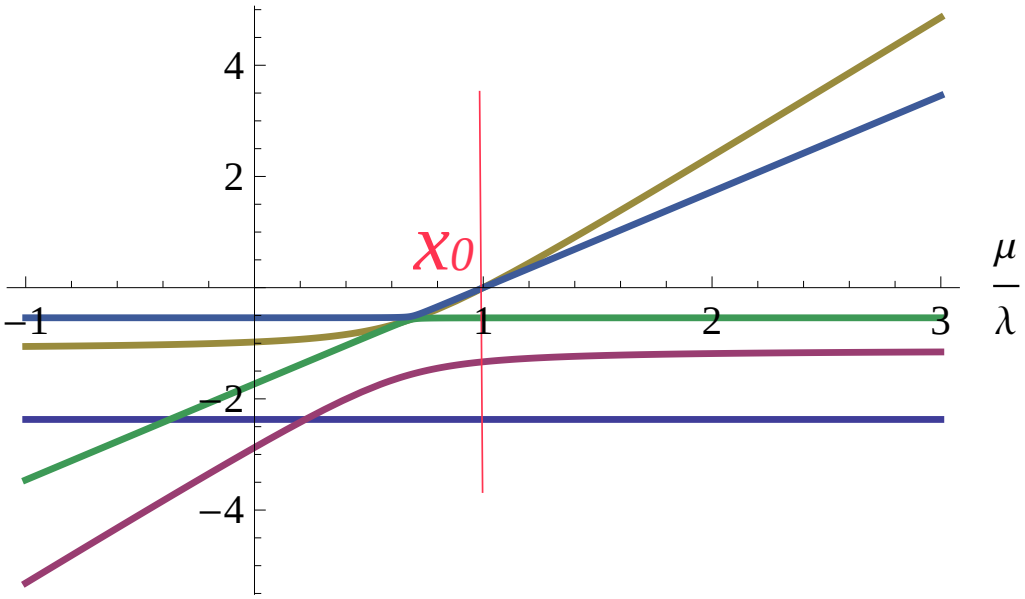

Figure 5.5: Eigenvalues of tetrahedral configurations

Two eigenvalues cross the x axis at $x_0 = 1$. To the left of x_0 all the eigenvalues are negative, i.e. the Hessian matrix is negative-definite and the tetrahedral configurations are maxima; to the right of x_0, some of the eigenvalues are positive and some are negative, i.e. the matrix is indefinite and the tetrahedral configurations are saddle points. Left unsolved is the tricky point x_0 itself.

At $x_0 = 1$, the Hessian matrix is negative semi-definite. The splitting lemma [47] provides a way of transforming a function in a neighborhood of a degenerate critical point to a canonical form through a series of changes of variables. The local properties at a degenerate critical point (or non-Morse critical point) then can be studied via the catastrophe germ that is left of the Taylor series expansion of the function at that point after the transformations.

First of all, we rewrite f_{mix} in terms of coordinates of particle 1, 2, 3 as we did previously

$$
\begin{aligned}
& f_{mix}(\theta_1,\theta_2,\theta_3,\phi_2,\phi_3) \\
& = \lambda\Big[(\sin^2\theta_{12}\sin^2\theta_{34}(1+\frac{\mu}{\lambda}\cos^2\theta_{12,34})+\sin^2\theta_{13}\sin^2\theta_{24}(1+\frac{\mu}{\lambda}\cos^2\theta_{12,34}) \\
& +\sin^2\theta_{14}\sin^2\theta_{23}(1+\frac{\mu}{\lambda}\cos^2\theta_{14,23})\Big] \\
& = \lambda\Big\{\sin^2\theta_3\Big[1-(\cos\theta_1\cos\theta_2+\cos(\phi_1-\phi_2)\sin\theta_1\sin\theta_2)^2\Big] \\
& +\frac{\mu}{\lambda}(\cos(\phi_1-\phi_3)\sin\theta_1\sin\theta_3\cos\theta_2-\cos(\phi_2-\phi_3)\sin\theta_2\sin\theta_3\cos\theta_1)^2 \\
& +\sin^2\theta_2\Big[1-(\cos\theta_1\cos\theta_3+\cos(\phi_1-\phi_3)\sin\theta_1\sin\theta_3)^2\Big] \\
& +\frac{\mu}{\lambda}(\cos(\phi_1-\phi_2)\sin\theta_1\sin\theta_2\cos\theta_3-\cos(\phi_2-\phi_3)\sin\theta_2\sin\theta_3\cos\theta_1)^2 \\
& +\sin^2\theta_1\Big[1-(\cos\theta_2\cos\theta_3+\cos(\phi_2-\phi_3)\sin\theta_2\sin\theta_3)^2\Big] \\
& +\frac{\mu}{\lambda}(\cos(\phi_1-\phi_3)\sin\theta_1\sin\theta_3\cos\theta_2-\cos(\phi_1-\phi_2)\sin\theta_1\sin\theta_3\cos\theta_2)^2\Big\}. \quad (5.3.8)
\end{aligned}
$$

It is convenient to take the point of interest to the origin of the coordinate system and rewrite f_{mix} as a function of θ_1', θ_2', θ_3', ϕ_2', ϕ_3' by replacing θ_1, θ_2, θ_3, ϕ_2, ϕ_3 with $\theta_1'+70.5°$, $\theta_2'+70.5°$, $\theta_3'+70.5°$, $\phi_2'+120°$, $\phi_3'+240°$. The fact that the Hessian matrix has a degenerate critical point means that one has to consider higher-degree terms in the Taylor expansion. In the first stage, we expand the function to the third degree and obtain

$$
\begin{aligned}
& 2.37037-0.395062\phi_2'^2+0.395062\phi_2'\phi_3'-0.395062\phi_3'^2+0.241925\phi_2'\theta_1'-0.241925\phi_3'\theta_1' \\
& -0.444444\theta_1'^2+0.241925\phi_3'\theta_2'-0.740741\theta_1'\theta_2'-0.444444\theta_2'^2-0.241925\phi_2'\theta_3' \\
& -0.740741\theta_1'\theta_3'-0.740741\theta_2'\theta_3'-0.444444\theta_3'^2-0.798311\phi_2'^2\phi_3'-0.798311\phi_2'\phi_3'^2 \\
& -1.32692\phi_2'^2\theta_1'+2.51416\phi_2'\phi_3'\theta_1'-1.32692\phi_3'^2\theta_1'-1.45407\phi_2'\theta_1'^2+1.45407\phi_3'\theta_1'^2 \\
& -0.139675\phi_2'^2\theta_2'+0.139675\phi_2'\phi_3'\theta_2'-1.32692\phi_3'^2\theta_2'+2.48047\phi_2'\theta_1'\theta_2'+1.30946\theta_1'^2\theta_2' \\
& -1.45407\phi_3'\theta_2'^2+1.30946\theta_1'\theta_2'^2-1.32692\phi_2'^2\theta_3'+0.139675\phi_2'\phi_3'\theta_3'-0.139675\phi_3'^2\theta_3' \\
& -2.48047\phi_3'\theta_1'\theta_3'+1.30946\theta_1'^2\theta_3'-2.48047\phi_2'\theta_2'\theta_3'+2.48047\phi_3'\theta_2'\theta_3'-0.733296\theta_1'\theta_2'\theta_3'
\end{aligned}
$$

$$+1.30946\theta_2'^2\theta_3' + 1.45407\phi_2'\theta_3'^2 + 1.30946\theta_1'\theta_3'^2 + 1.30946\theta_2'\theta_3'^2 + O(4), \qquad (5.3.9)$$

where $O(4)$ stands for terms of degrees higher than 3. Again, the factor λ is left out.

The next step is to find five independent linear combinations of the five variables and transform away all the second-degree cross terms. By using the five linearly independent eigenvectors, the Hessian matrix can be put in the form of:

$$H = P^{-1}\Lambda P, \qquad (5.3.10)$$

where Λ is the diagonal matrix whose diagonal elements are the eigenvalues of H and P is the invertible orthogonal matrix whose rows are normalized eigenvectors corresponding to the eigenvalues in Λ. For our critical point in question,

$$H = \begin{pmatrix} -\frac{8}{9} & -\frac{20}{27} & -\frac{20}{27} & \frac{8}{27}\sqrt{\frac{2}{3}} & -\frac{8}{27}\sqrt{\frac{2}{3}} \\ -\frac{20}{27} & -\frac{8}{9} & -\frac{20}{27} & 0 & \frac{8}{27}\sqrt{\frac{2}{3}} \\ -\frac{20}{27} & -\frac{20}{27} & -\frac{8}{9} & -\frac{8}{27}\sqrt{\frac{2}{3}} & 0 \\ \frac{8}{27}\sqrt{\frac{2}{3}} & 0 & -\frac{8}{27}\sqrt{\frac{2}{3}} & -\frac{64}{81} & \frac{32}{81} \\ -\frac{8}{27}\sqrt{\frac{2}{3}} & \frac{8}{27}\sqrt{\frac{2}{3}} & 0 & \frac{32}{81} & -\frac{64}{81} \end{pmatrix},$$

$$\Lambda = \begin{pmatrix} -\frac{64}{27} & 0 & 0 & 0 & 0 \\ 0 & -\frac{4}{3} & 0 & 0 & 0 \\ 0 & 0 & -\frac{44}{81} & 0 & 0 \\ 0 & 0 & 0 & 0 & 0 \\ 0 & 0 & 0 & 0 & 0 \end{pmatrix},$$

$$P = \begin{pmatrix} 0.57735 & 0.57735 & 0.57735 & 0 & 0 \\ 0.272166 & -0.136083 & -0.136083 & -0.666667 & 0.666667 \\ 0 & 0.369274 & -0.369274 & -0.603023 & -0.603023 \\ 0.648886 & 0 & -0.648886 & 0.39736 & 0. \\ 0.414174 & -0.715391 & 0.301217 & -0.184457 & -0.438086 \end{pmatrix}.$$

Through the linear transformation

$$\begin{pmatrix} x_1 \\ x_2 \\ x_3 \\ x_4 \\ x_5 \end{pmatrix} = P \cdot \begin{pmatrix} \theta_1' \\ \theta_2' \\ \theta_3' \\ \phi_2' \\ \phi_3' \end{pmatrix}, \tag{5.3.11}$$

the second-order terms in expansion (5.3.9) can be transformed to a diagonal form:

$$-\frac{32}{27}x_1^2 - \frac{2}{3}x_2^2 - \frac{22}{81}x_3^2. \tag{5.3.12}$$

where the factor for each term is one-half of the corresponding eigenvalue. As a result of the transformation, the sum in (5.3.9) becomes (after the constant term is dropped):

$$\begin{aligned} &-1.18519x_1^2 - 0.666667x_2^2 - 0.271605x_3^2 - 1.37091x_1^3 + 1.99252x_1x_2^2 + 0.31019x_2^3 \\ &+ 0.418787x_1x_3^2 - 0.58383x_2x_3^2 - 1.67429x_1x_2x_4 - 0.0585341x_2^2x_4 - 0.548293x_1x_3x_4 \\ &- 0.650155x_2x_3x_4 - 0.325971x_3^2x_4 + 0.203726x_1x_4^2 + 1.0279x_2x_4^2 + 0.0990851x_3x_4^2 \\ &- 1.06867x_1x_2x_5 - 0.0373614x_2^2x_5 + 0.85901x_1x_3x_5 + 1.0186x_2x_3x_5 - 0.208062x_3^2x_5 \\ &+ 0.0354642x_1x_4x_5 + 3.57869x_2x_4x_5 - 0.091992x_3x_4x_5 - 4.03897x_4^2x_5 + 0.187264x_1x_5^2 \\ &- 0.633353x_2x_5^2 - 0.0990851x_3x_5^2 - 0.703095x_4x_5^2 + 1.19673x_5^3 + O(4). \end{aligned} \tag{5.3.13}$$

Bear in mind that the ultimate goal is to put sum (5.3.9) in Morse canonical form [47]:

$$V = CG(l) + \sum_{j=l+1}^{n} \lambda_j y_j^2, \tag{5.3.14}$$

where n is the number of variables, l is the number of degenerate eigenvalues and the function $CG(l)$ is called catastrophe germ; therefore we have to get rid of all the third-degree terms that contain the "good" variables: x_1, x_2, x_3. To that end, we define an axis-preserving transformation:

$$x_r' = x_r + \Delta_r = x_r + \sum_{i \geq j=1}^{5} \alpha_r^{ij} x_i x_j + O(3) \qquad r = 1, 2, 3 \tag{5.3.15}$$

and then look for α_r^{ij} that transform away all the third-degree terms containing any good variable in Eq. (5.3.13). The coefficients α_r^{ij} are not uniquely determined. One particular choice can be made to yield the transformation:

$$\begin{aligned}
x_1' &= x_1 + 0.578353x_1^2 - 0.840595x_2^2 - 0.176676x_3^2 + 0.706341x_2x_4 + 0.231311x_3x_4 \\
&\quad - 0.0859469x_4^2 + 0.450845x_2x_5 - 0.362395x_3x_5 - 0.0149615x_4x_5 - 0.079002x_5^2 \\
x_2' &= x_2 - 0.232643x_2^2 + 0.437874x_3^2 + 0.0439007x_2x_4 + 0.487617x_3x_4 - 0.770927x_4^2 \\
&\quad + 0.0280211x_2x_5 - 0.763952x_3x_5 - 2.68402x_4x_5 + 0.475016x_5^2 \\
x_3' &= x_3 + 0.600083x_3x_4 - 0.182407x_4^2 + 0.383023x_3x_5 + 0.169349x_4x_5 + 0.182407x_5^2,
\end{aligned}$$

which turns expression (5.3.13) into:

$$\begin{aligned}
&- 1.18519x_1'^2 - 0.666667x_2'^2 - 0.271605x_3'^2 - 4.03897x_4^2x_5 - 0.703095x_4x_5^2 \\
&+ 1.19673x_5^3 + O(4).
\end{aligned} \tag{5.3.16}$$

We could go out to quartic terms in (5.3.13) and cubic terms in (5.3.15) to get rid of the quartic terms and rinse and repeat to do the higher-degree terms, but

the conclusion remains the same: the terms involving good variables can always be transformed to a diagonal quadratic form. As for the cubic terms concerning the "bad" variables x_4, x_5 in (5.3.16), it suffices to carry out a sequence of changes of variables in the same fashion. We ultimately obtain the form:

$$-1.18519x_1'^2 - 0.666667x_2'^2 - 0.271605x_3'^2 + (x_4'^2 x_5' - x_5'^3),$$

which satisfies the Morse canonical form.

The catastrophe term is cubic; thus we conclude that when $\frac{\mu}{\lambda} = 1$, the tetrahedral configurations are saddle points.

In short, when $\frac{\mu}{\lambda}$ is less than 1, the tetrahedral configurations are (local or absolute) maxima, but they are no longer for $\mu/\lambda \geq 1$.

When $\lambda = 0$, the tetrahedral configurations disappear ($\frac{64}{27}\lambda = 0$). The great-circle configurations, on the other hand, are absolute maxima with $f_{mix} = 2\mu c = 6c$.

5.3.3 Conclusions

Before ending the discussion in this section, let's say a few words about the connection between four-particle and two-particle geometries in p shells. We have seen that two identical particles in a p shell coupled to $LS = 00$ exhibit two spatial configurations: cigar-like and di-neutron. When a short-range attractive interaction is in effect, the di-neutron configuration becomes favored. For four particles, the $\lambda = 0$ case, and consequently the great-circle configurations correspond to $LS = 00$. The great-circle configuration in Fig. 5.1(a) can be seen as two di-neutron configurations, Fig. 5.1(b) a di-neutron and a cigar-like configuration and Fig. 5.1(c) two cigar-like configurations. When a short-range attractive interaction is in effect among the four particles, analogously one would guess that the configuration in Fig. 5.1(a) should be the predominant one among the six configurations discussed above. As a matter of fact, many studies have shown an

important contribution of the double di-neutron configuration to the ^{8}He ground state. [20, 21].

We summarize Sec. 5.3 with Fig. 5.6 in which the angular probability densities weighted by $1/\lambda$ of the two classes of configurations are plotted. The green lines give the correspondence between the parameter $\frac{\mu}{\lambda}$ and the configurations with the maximum probability density. Between $\frac{\mu}{\lambda} = -1$ and $\frac{\mu}{\lambda} = \frac{5}{27}$, the tetrahedral configurations are absolute maxima. The transition occurs at $\frac{\mu}{\lambda} = \frac{5}{27}$, at which point the role of the maximum configuration changes hands as the angular probability density of the great-circle configurations is equal to that of the tetrahedral configurations. When $\frac{\mu}{\lambda}$ goes from 0 to $\frac{5}{27}$, the great-circle configurations are local maxima, and when it goes from $\frac{5}{27}$ to 1 (not including 1), the tetrahedral configurations are local maxima.

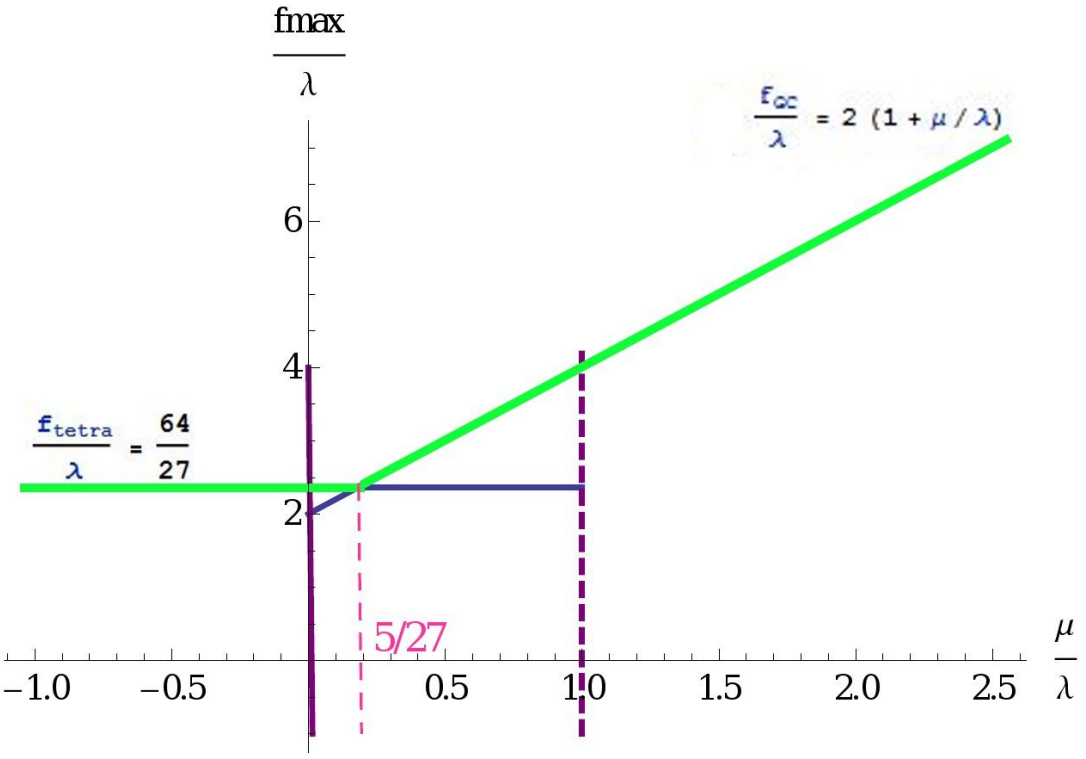

Figure 5.6: The maximum configurations for an admixed state, and the natures of the two classes of configurations as a function of $\frac{\mu}{\lambda}$.

6

Conclusions and perspectives

To sum up this work, we studied the geometry of two identical nucleons in the LS coupling scheme in a general sense with an emphasis on zero-coupled states, and those of four identical nucleons in the p shells.

We proved analytically that two-particle systems characterized by a valence nucleon pair outside a stable core have some fascinating geometric properties linked to the radial and angular momentum quantum numbers n and ℓ, as well as the total angular momentum L. In the particular case of ^{6}He which we studied in great detail, the two neutrons may correlate in two geometric configurations: the di-neutron configuration (with a small relative distance between the two neutrons), and the cigar-like configuration (with a large relative distance) (see also Figs. 1.1 and 1.2). We showed that when the neutron pair is confined to the $0p$ shell, the two configurations show up with equal probability as a pure consequence of the geometry of the p shell in the LS coupling scheme. In addition, if the nucleon pair, while keeping paired up, is free to scatter into higher orbitals, the presence of an attractive short-range interaction tends to hamper the appearance of the cigar-like configuration and enhance the di-neutron configuration. For ^{6}He, reasonable two neutron separation energies were also obtained.

Meanwhile, the predictions that we have made for two-particle systems in the other orbitals await experimental exploration, through, say knockout reactions that probe the shape of the nuclear surface and surface nucleons in a nucleus.

We also studied four-particle correlations. Here, we concentrated on ^{8}He and calculated the angular probability densities of both the 0^+_1 state ($(0p_{3/2})^4$) and the 0^+_2 state ($(0p_{3/2})^2(0p_{1/2})^2$), as well as their mixing. The angular correlation function in terms of relative angle in two-particle cases was generalized to that in four-particle cases through six relative angles. One class of three equi-probable configurations was found for each 0^+ state. The two classes of configurations were named great-circle and tetrahedral configurations according to their geometries. The great-circle configurations can be identified with the di-neutron and cigar-like configurations in ^{6}He, and represent the realistic spatial configurations of ^{8}He. A phase diagram for the geometry of admixed four-particle 0^+ states in p shells is established. The transition point where the role of the absolute maximum switches from one class to the other class of configurations for an admixed state was found.

There is still much work to do in the future. For ^{8}He, it would be interesting to look into the evolution of its spatial structure when scattering into higher orbitals is allowed. We also would like to get a holistic picture of the geometry of four-particle systems, and make predictions for the geometry of an arbitrary shell as we do for two-particle systems. More specifically, the ^{18}C nucleus with four neutrons in the $0d_{5/2}$ shell is worth studying. Furthermore, the geometry of correlated different types of nucleons (and hence the role of isospin) are to be explored.

A

Derivation of the angular correlation function

In this appendix, we evaluate the general expression

$$\frac{1}{2L+1}\sum_{M_L}[\mathcal{Y}^*_{\ell_1}(1)\otimes\mathcal{Y}^*_{\ell_2}(2)]^L_{M_L}[\mathcal{Y}_{\ell'_1}(1)\otimes\mathcal{Y}_{\ell'_2}]^L_{M_L}. \tag{A.1}$$

$$\begin{aligned}
&\frac{1}{2L+1}\sum_{M_L}[\mathcal{Y}^*_{\ell_1}(1)\otimes\mathcal{Y}^*_{\ell_2}(2)]^L_{M_L}[\mathcal{Y}_{\ell'_1}(1)\otimes\mathcal{Y}_{\ell'_2}]^L_{M_L}\\
&=\frac{1}{2L+1}\sum_{M_L}\sum_{m_1m_2}\langle\ell_1m_1\ell_2m_2|LM_L\rangle\mathcal{Y}^*{}_{\ell_1m_1}(1)\mathcal{Y}^*{}_{\ell_2m_2}(2)\\
&\times\sum_{m'_1m'_2}\langle\ell'_1m'_1\ell'_2m'_2|LM_L\rangle\mathcal{Y}_{\ell'_1m'_1}(1)\mathcal{Y}_{\ell'_2m'_2}(2)\\
&=\frac{1}{2L+1}\sum_{M_L}\sum_{\substack{m_1m_2\\m'_1m'_2}}(-1)^{m_1+m_2}\langle\ell_1m_1\ell_2m_2|LM_L\rangle\langle\ell'_1m'_1\ell'_2m'_2|LM_L\rangle\\
&\times\mathcal{Y}_{\ell_1-m_1}(1)\mathcal{Y}_{\ell_2-m_2}(2)\mathcal{Y}_{\ell'_1m'_1}(1)\mathcal{Y}_{\ell'_2m'_2}(2).
\end{aligned} \tag{A.2}$$

For spherical harmonics $\mathcal{Y}_{\ell m}(\vec{r})$, one has the relation

$$\mathcal{Y}_{\ell_1 m_1}(\vec{r})\mathcal{Y}_{\ell_2 m_2}(\vec{r}) = \sum_{\ell m} \frac{\hat{\ell}_1\hat{\ell}_2\hat{\ell}}{4\pi} \begin{pmatrix} \ell_1 & \ell_2 & \ell \\ m_1 & m_2 & m \end{pmatrix} \mathcal{Y}^*_{\ell m}(\vec{r}) \begin{pmatrix} \ell_1 & \ell_2 & \ell \\ 0 & 0 & 0 \end{pmatrix}. \tag{A.3}$$

Expression (A.2), then, can be expanded to give:

$$\begin{aligned} &\frac{1}{2L+1} \sum_{M_L} \sum_{\substack{m_1 m_2 \\ m_1' m_2'}} (-1)^{m_1+m_2} \langle \ell_1 m_1 \ell_2 m_2 | L M_L \rangle \langle \ell_1' m_1' \ell_2' m_2' | L M_L \rangle \\ &\times \sum_{L_1 m} \frac{\hat{\ell}_1\hat{\ell}_2\hat{L}_1}{4\pi} \begin{pmatrix} \ell_1 & \ell_1' & L_1 \\ -m_1 & m_1' & m \end{pmatrix} \mathcal{Y}^*_{L_1 m}(1) \begin{pmatrix} \ell_1 & \ell_1' & L_1 \\ 0 & 0 & 0 \end{pmatrix} \\ &\times \sum_{L_2 m'} \frac{\hat{\ell}_1'\hat{\ell}_2'\hat{L}_2}{4\pi} \begin{pmatrix} \ell_2 & \ell_2' & L_2 \\ -m_2 & m_2' & m' \end{pmatrix} \mathcal{Y}^*_{L_2 m'}(2) \begin{pmatrix} \ell_2 & \ell_2' & L_2 \\ 0 & 0 & 0 \end{pmatrix}, \end{aligned}$$

which, given the relation between $3j$-symbols and Clebsch-Gordan coefficients, leads to

$$\begin{aligned} &\frac{\hat{\ell}_1\hat{\ell}_2\hat{\ell}_1'\hat{\ell}_2'}{4\pi} \sum_{M_L} \sum_{\substack{m_1 m_2 \\ m_1' m_2'}} (-1)^{m_1+m_2} (-1)^{M_L+M_L} \begin{pmatrix} \ell_1 & \ell_2 & L \\ m_1 & m_2 & -M_L \end{pmatrix} \begin{pmatrix} \ell_1' & \ell_2' & L \\ m_1' & m_2' & -M_L \end{pmatrix} \\ &\times (-1)^{\ell_1-\ell_2+\ell_1'-\ell_2'} \sum_{\substack{L_1 m \\ L_2 m'}} \hat{L}_1\hat{L}_2 \begin{pmatrix} \ell_1 & \ell_1' & L_1 \\ -m_1 & m_1' & m \end{pmatrix} \begin{pmatrix} \ell_1 & \ell_1' & L_1 \\ 0 & 0 & 0 \end{pmatrix} \mathcal{Y}^*_{L_1 m}(1) \\ &\times \begin{pmatrix} \ell_2 & \ell_2' & L_2 \\ -m_2 & m_2' & m' \end{pmatrix} \begin{pmatrix} \ell_2 & \ell_2' & L_2 \\ 0 & 0 & 0 \end{pmatrix} \mathcal{Y}^*_{L_2 m'}(2) \\ &= \frac{\hat{\ell}_1\hat{\ell}_2\hat{\ell}_1'\hat{\ell}_2'}{4\pi} \sum_{M_L} \sum_{\substack{m_1 m_2 \\ m_1' m_2'}} \sum_{\substack{L_1 m \\ L_2 m'}} (-1)^{m_1+m_2} (-1)^{m+m'} (-1)^{L_1+L_2} \hat{L}_1\hat{L}_2 \mathcal{Y}_{L_1 -m}(1) \mathcal{Y}_{L_2 -m'}(2) \\ &\times \begin{pmatrix} \ell_1 & \ell_2 & L \\ m_1 & m_2 & -M_L \end{pmatrix} \begin{pmatrix} \ell_1' & \ell_2' & L \\ m_1' & m_2' & -M_L \end{pmatrix} \begin{pmatrix} \ell_1 & \ell_1' & L_1 \\ -m_1 & m_1' & m \end{pmatrix} \begin{pmatrix} \ell_2 & \ell_2' & L_2 \\ -m_2 & m_2' & m' \end{pmatrix} \\ &\times \begin{pmatrix} \ell_1 & \ell_1' & L_1 \\ 0 & 0 & 0 \end{pmatrix} \begin{pmatrix} \ell_2 & \ell_2' & L_2 \\ 0 & 0 & 0 \end{pmatrix} \end{aligned}$$

$$= \frac{\hat{\ell}_1\hat{\ell}_2\hat{\ell}'_1\hat{\ell}'_2}{4\pi}\sum_{M_L}\sum_{\substack{m_1 m_2\\ m'_1 m'_2}}\sum_{L_1 L_2 m'}(-1)^{m_1+m_2}(-1)^{L_1+L_2}\hat{L}_1\hat{L}_2\mathcal{Y}_{L_1-m}(1)\mathcal{Y}_{L_2-m'}(2)$$
$$\times\begin{pmatrix}\ell_1 & \ell_2 & L\\ m_1 & m_2 & -M_L\end{pmatrix}\begin{pmatrix}\ell'_1 & \ell'_2 & L\\ m'_1 & m'_2 & -M_L\end{pmatrix}\begin{pmatrix}\ell_1 & \ell'_1 & L_1\\ -m_1 & m'_1 & m\end{pmatrix}\begin{pmatrix}\ell_2 & \ell'_2 & L_2\\ -m_2 & m'_2 & -m\end{pmatrix}$$
$$\times\begin{pmatrix}\ell_1 & \ell'_1 & L_1\\ 0 & 0 & 0\end{pmatrix}\begin{pmatrix}\ell_2 & \ell'_2 & L_2\\ 0 & 0 & 0\end{pmatrix} \tag{A.4}$$

where we have used the notation $\hat{j} = \sqrt{2j+1}$. In the expression above, $m + m' = m_1 - m'_1 + m_2 - m'_2 = M_L - M_L = 0$, and therefore $(-1)^{m+m'} = 1$ and $m = -m'$. Also, $\ell_1 + \ell'_1 + L_1$ and $\ell_2 + \ell'_2 + L_2$ have to be even, otherwise the $3j$ symbol $\begin{pmatrix}\ell_1 & \ell'_1 & L_1\\ 0 & 0 & 0\end{pmatrix}$ and $\begin{pmatrix}\ell_2 & \ell'_2 & L_2\\ 0 & 0 & 0\end{pmatrix}$ would vanish.

Expression (A.4) can be simplified with the following relation between $3j$-symbols and $6j$-symbols:

$$\begin{pmatrix}J_1 & J_2 & J_3\\ M_1 & M_2 & M_3\end{pmatrix}\begin{Bmatrix}J_1 & J_2 & J_3\\ J_4 & J_5 & J_6\end{Bmatrix} = \sum_{M_4 M_5 M_6}(-1)^{J_4+J_5+J_6+M_4+M_5+M_6}$$
$$\times\begin{pmatrix}J_1 & J_5 & J_6\\ M_1 & M_5 & -M_6\end{pmatrix}\begin{pmatrix}J_4 & J_2 & J_6\\ -M_4 & M_2 & M_6\end{pmatrix}\begin{pmatrix}J_4 & J_5 & J_3\\ M_4 & -M_5 & M_3\end{pmatrix}. \tag{A.5}$$

If we change the coupling order in the $3j$-symbols in expression (A.4) using symmetry properties of $3j$-symbols, we obtain a more convenient form of (A.4) that corresponds to relation (A.5):

$$\frac{\hat{\ell}_1\hat{\ell}_2\hat{\ell}'_1\hat{\ell}'_2}{4\pi}\sum_{M_L}\sum_{\substack{m_1 m_2\\ m'_1 m'_2}}\sum_{L_1 L_2 m}(-1)^{m_1+m_2}\hat{L}_1\hat{L}_2\mathcal{Y}_{L_1-m}(1)\mathcal{Y}_{L_2 m}(2)$$
$$\times\begin{pmatrix}\ell_2 & \ell_1 & L\\ m_2 & m_1 & -M_L\end{pmatrix}\begin{pmatrix}\ell'_1 & \ell'_2 & L\\ -m'_1 & -m'_2 & M_L\end{pmatrix}\begin{pmatrix}\ell'_1 & \ell_1 & L_1\\ m'_1 & -m_1 & m\end{pmatrix}\begin{pmatrix}\ell_2 & \ell'_2 & L_2\\ -m_2 & m'_2 & -m\end{pmatrix}$$

$$\times \begin{pmatrix} \ell_1 & \ell_1' & L_1 \\ 0 & 0 & 0 \end{pmatrix} \begin{pmatrix} \ell_2 & \ell_2' & L_2 \\ 0 & 0 & 0 \end{pmatrix}. \tag{A.6}$$

Now we can identify J_1, M_1, J_2, M_2, J_3, M_3, J_4, M_4, J_5, M_5, J_6 and M_6 with ℓ_2, m_2, ℓ_2', $-m_2'$, L_1, m, ℓ_1', m_1', ℓ_1, m_1, L, and M_L respectively and apply relation (A.5) to get:

$$\begin{aligned}
&\sum_{m_1 m_1' M_L} (-1)^{m_1+m_2} \begin{pmatrix} \ell_2 & \ell_1 & L \\ m_2 & m_1 & -M_L \end{pmatrix} \begin{pmatrix} \ell_1' & \ell_2' & L \\ -m_1' & -m_2' & M_L \end{pmatrix} \begin{pmatrix} \ell_1' & \ell_1 & L_1 \\ m_1' & -m_1 & m \end{pmatrix} \\
&= (-1)^{m+L+L_1} \sum_{m_1 m_1' M_L} (-1)^{\ell_1+\ell_1'+L+m_1+m_1'+M_L} \\
&\times \begin{pmatrix} \ell_2 & \ell_1 & L \\ m_2 & m_1 & -M_L \end{pmatrix} \begin{pmatrix} \ell_1' & \ell_2' & L \\ -m_1' & -m_2' & M_L \end{pmatrix} \begin{pmatrix} \ell_1' & \ell_1 & L_1 \\ m_1' & -m_1 & m \end{pmatrix} \\
&= (-1)^{m+L+L1} \begin{pmatrix} \ell_2 & \ell_2' & L_1 \\ m_2 & -m_2' & m \end{pmatrix} \begin{Bmatrix} \ell_2 & \ell_2' & L_1 \\ \ell_1' & \ell_1 & L \end{Bmatrix}.
\end{aligned} \tag{A.7}$$

Expression (A.6), then, can be further simplified:

$$\begin{aligned}
&\frac{\hat{\ell}_1 \hat{\ell}_2 \hat{\ell}_1' \hat{\ell}_2'}{4\pi} \sum_{m_2 m_2'} \sum_{L_1 L_2 m} (-1)^{m+L+L_1} \hat{L}_1 \hat{L}_2 \mathcal{Y}_{L_1 -m}(1) \mathcal{Y}_{L_2 m}(2) \\
&\times \begin{pmatrix} \ell_2 & \ell_2' & L_1 \\ m_2 & -m_2' & m \end{pmatrix} \begin{Bmatrix} \ell_2 & \ell_2' & L_1 \\ \ell_1' & \ell_1 & L \end{Bmatrix} \begin{pmatrix} \ell_2 & \ell_2' & L_2 \\ -m_2 & m_2' & -m \end{pmatrix} \begin{pmatrix} \ell_1 & \ell_1' & L_1 \\ 0 & 0 & 0 \end{pmatrix} \begin{pmatrix} \ell_2 & \ell_2' & L_2 \\ 0 & 0 & 0 \end{pmatrix} \\
&= \frac{\hat{\ell}_1 \hat{\ell}_2 \hat{\ell}_1' \hat{\ell}_2'}{4\pi} \sum_{m_2 m_2'} \sum_{L_1 L_2 m} (-1)^{m+L+L_1} \hat{L}_1 \hat{L}_2 \mathcal{Y}_{L_1 -m}(1) \mathcal{Y}_{L_2 m}(2) \\
&\times \begin{pmatrix} \ell_2 & \ell_2' & L_1 \\ m_2 & -m_2' & m \end{pmatrix} \begin{Bmatrix} \ell_2 & \ell_2' & L_1 \\ \ell_1' & \ell_1 & L \end{Bmatrix} \begin{pmatrix} \ell_2 & \ell_2' & L_2 \\ m_2 & -m_2' & m \end{pmatrix} \begin{pmatrix} \ell_1 & \ell_1' & L_1 \\ 0 & 0 & 0 \end{pmatrix} \begin{pmatrix} \ell_2 & \ell_2' & L_2 \\ 0 & 0 & 0 \end{pmatrix} \\
&= \frac{\hat{\ell}_1 \hat{\ell}_2 \hat{\ell}_1' \hat{\ell}_2'}{4\pi} \sum_{L_1 L_2 m} (-1)^{m+L+L_1} \hat{L}_1 \hat{L}_2 \frac{1}{2L_1+1} \delta_{L_1 L_2} \mathcal{Y}_{L_1 -m}(1) \mathcal{Y}_{L_2 m}(2) \\
&\times \begin{Bmatrix} \ell_2 & \ell_2' & L_1 \\ \ell_1' & \ell_1 & L \end{Bmatrix} \begin{pmatrix} \ell_1 & \ell_1' & L_1 \\ 0 & 0 & 0 \end{pmatrix} \begin{pmatrix} \ell_2 & \ell_2' & L_2 \\ 0 & 0 & 0 \end{pmatrix}
\end{aligned}$$

$$= \frac{\hat{\ell}_1\hat{\ell}_2\hat{\ell}'_1\hat{\ell}'_2}{4\pi}\sum_{L_1 m}(-1)^{m+L+L_1}\begin{Bmatrix}\ell_2 & \ell'_2 & L_1\\ \ell'_1 & \ell_1 & L\end{Bmatrix}\begin{pmatrix}\ell_1 & \ell'_1 & L_1\\ 0 & 0 & 0\end{pmatrix}\begin{pmatrix}\ell_2 & \ell'_2 & L_1\\ 0 & 0 & 0\end{pmatrix}\mathcal{Y}_{L_1-m}(1)\mathcal{Y}_{L_1 m}(2) \tag{A.8}$$

The last three lines of expression (A.8) follow from the orthogonality relations of $3j$-symbols.

Once again, we apply the spherical harmonic addition theorem (2.2.28) to the result in (A.8) and obtain

$$\begin{aligned}&\frac{1}{2L+1}\sum_{M_L}[\mathcal{Y}^*_{\ell_1}(1)\otimes\mathcal{Y}^*_{\ell_2}(2)]^L_{M_L}[\mathcal{Y}_{\ell'_1}(1)\otimes\mathcal{Y}_{\ell'_2}(2)]^L_{M_L}\\ &= \frac{\hat{\ell}_1\hat{\ell}_2\hat{\ell}'_1\hat{\ell}'_2}{(4\pi)^2}(-1)^L\sum_{L_1}(-1)^{L_1}\hat{L}_1^2\begin{Bmatrix}\ell_2 & \ell'_2 & L_1\\ \ell'_1 & \ell_1 & L\end{Bmatrix}\begin{pmatrix}\ell_1 & \ell'_1 & L_1\\ 0 & 0 & 0\end{pmatrix}\begin{pmatrix}\ell_2 & \ell'_2 & L_1\\ 0 & 0 & 0\end{pmatrix}P_{L_1}(\cos\theta_{12}).\end{aligned} \tag{A.9}$$

Introduction

Cette thèse est motivée par notre volonté de comprendre et de décrire la géométrie de différents noyaux, en particulier l'^{6}He et l'^{8}He, pour les raisons qui seront décrites ci-dessous.

Systèmes à deux particules

Les systèmes à deux particules se réfèrent à des noyaux avec deux nucléons de valence identiques. Ils sont bien illustrés par l'^{6}He, qui est généralement dépeint comme un ^{4}He particulièrement stable (particule α) ayant la couche proton $0s_{1/2}$ et la couche neutron $0s_{1/2}$ pleines, accompagné de deux neutrons de valence. Aussi simple que cela puisse paraître, l'^{6}He a été au coeur d'un long débat quant à savoir si les neutrons de valence se représentent comme une configuration di-neutron (Fig. 1.1) , ou une configuration cigare. (Fig. 1.2) (voir Sec. 1.1.3). L'^{6}He possède des caractéristiques intéressantes, parmi lesquels sont l'appariement, le phénomène de halo, les noyaux borroméens, etc.

L'appariement

Les nucléons identiques ont tendance à s'apparier. L'appariement explique pourquoi tous les noyaux pair-pair ont des états fondamentaux $J^\pi = 0^+$, et que

les noyaux pair-impair ont le moment cinétique total du dernier nucléon impair [†]. Une autre preuve directe est la différence de masse entre les noyaux pairs et impairs, soulignant le fait que pour le même type de nucléons, les protons ou les neutrons, le gain en énergie de liaison est plus important lorsqu'un noyau doublement pair est formé que lorsque ses voisins isotoniques ou isotopiques de masses impaires sont formés. Ceci est illustré dans la Fig. 1.3 par l'échelonnement des énergies de séparation du neutron $S(n)$ (Fig. 1.3(a)) de certains isotopes du ruthénium près du $^{100}_{44}$ Ru, et des énergies de séparation du proton $S(p)$ (Fig. 1.3(b)) de certains isotones du $^{100}_{44}$ Ru.

Dans ce contexte ci, le fait que ^{6}He ait un état fondamental 0^+, alors que l'^{5}He, l'isotope de l'^{6}He avec un neutron en moins, ne soit pas lié et ait le moment cinétique total $3/2^-$, ne peut s'expliquer que par un phénomène d'appariement important.

Les noyaux à halo et les noyaux borroméens

La notion de halo est présente dans de diverses disciplines scientifiques. Il s'agit d'une composante anormalement diluée et étendue autour d'un noyau plus solide et massif. En physique nucléaire, la loi de puissance 1/3

$$R = r_0 A^{1/3}, \tag{A.10}$$

où $r_0 = 1.25$ fm et A est le nombre de masse, qui est approximativement vérifiée pour les rayons des noyaux stables, est dérogée par les noyaux sur les lignes d'instabilité. L'^{6}He, le ^{11}Li, le ^{11}Be, le ^{19}C et le ^{17}Ne, entre autres, présentent tous des distributions de la matière nucléaire très étendues. Le ^{11}Li, pour sa part, a le même rayon de la matière que celui du ^{208}Pb qui est beaucoup plus lourd [4].

[†] Strictement parlant, les noyaux avec plus d'un nucléon de valence peut avoir un moment cinétique total autre que celui du dernier nucléon impair dans l'état fondamental en raison des interactions résiduelles. Par exemple, bien que le $^{45}_{22}$Ti et le $^{47}_{22}$Ti aient tous les deux le dernier neutron impair dans la couche $0f_{7/2}$, le premier a un état fondamental $7/2^-$ tandis que le second, un état fondamental $5/2^-$ en raison de la corrélation quadripolaire.

En outre, dans tous ces noyaux, la distribution de la matière étendue est générée par les quelques nucléons de valence qui, en étant faiblement liés au coeur plus stable, pénètrent dans les régions interdites par la physique classique. Le nom du halo a été ainsi inventé.

Une classe intrigante de noyaux halo est les noyaux borroméens nommés d'après les anneaux de Borromée (Fig. 1.6) figurant sur le blason de la famille italienne des Borromée depuis le XIXe siècle. Les trois anneaux sont imbriqués de telle manière qu'il n'existe pas de sous-système à deux corps lié ; si l'un d'eux est cassé, les deux autres s'effondrent. Par analogie, les noyaux borroméens sont des noyaux à halo à trois corps, où aucun des sous-systèmes à deux corps est lié, et pourtant dans leur ensemble, les trois constituants conduisent à un état lié. Si on retire un neutron de valence de l'^{6}He (ou du ^{11}Li), l'isotope résultant, le ^{5}He (ou le ^{10}Li) est non-lié. Par ailleurs, le sous-système de di-neutron est également non-lié. Par conséquent, l'^{6}He et le ^{11}Li sont deux noyaux borroméens.

Notre intention est d'abord de montrer que, dans l'^{6}He, les deux configurations di-neutron et cigare, apparaissent comme une pure conséquence géométrique d'une paire de nucléons identiques dans la couche p couplés à zéro en couplage LS, et de fournir des prédictions théoriques pour les géométries d'une paire de particules identiques dans une couche arbitraire. Puis, l'^{6}He étant un laboratoire idéal pour étudier la corrélation de deux particules, il sera étudié dans un second temps afin de comprendre les particularités des noyaux borroméens (Chapitre 3 et 4).

Systèmes à quatre particules

Afin de poursuivre l'étude de la géométrie des particules plus loin, l'^{8}He, un prototype des systèmes à quatre particules corrélées sera étudié. La nature des quatre neutrons de valence dans l'^{8}He n'est pas encore très claire. Certains croient que comme son isotope l'^{6}He, l'^{8}He est aussi un noyau halo avec quatre

neutrons appartenant au halo et un coeur de particule α en raison de sa distribution diluée des neutrons. D'autres soulignent que la distribution des neutrons est mieux comprise comme une peau de neutron épaisse [16]. Dans l'état fondamental de l'^{8}He, les quatre neutrons sont normalement considérés comme formant une sous-couche complète $0p_{3/2}$ [17], alors que des études récentes [18, 19, 20, 21] suggèrent une présence non négligeable de la structure double di-neutron $(0p_{3/2})^2(0p_{1/2})^2$.

Quant aux configurations géométriques de l'^{8}He, nous avons l'intention d'étendre les résultats obtenus pour les systèmes à deux particules à un état 0^+ général de quatre particules identiques corrélées dans les couche p, et de trouver le lien avec le cas de deux particules, i.e. l'^{6}He (Chapitre 5).

Présentation du programme scientifique

Chapitre 1 Introduction

Chapitre 2 Corrélations à deux particules

2.1 Description de l'approche

2.1.1 Le choix du couplage *LS*

2.1.2 Fonctions de corrélation à deux particules

2.2 Deux particules identiques en couplage *LS*

2.2.1 Transformation Talmi-Moshinsky

2.2.2 Eléments de matrice des fonctions de corrélation

2.2.3 Antisymmétrisation

2.2.4 Fonctions de corrélation dans une seule couche

2.2.5 Fonctions de corrélation entre différentes couches

2.2.6 En termes d'angles

Chapitre 3 Corrélations dans l'^{6}He avec l'interaction δ

3.1 Introduction

Conclusions et perspectives

En résumé, nous avons étudié la géométrie de deux nucléons identiques en couplage LS dans un sens général avec un accent sur les états 0^+, ainsi que la géométrie de quatre nucléons identiques dans les couche p.

Nous avons prouvé analytiquement que les systèmes à deux particules caractérisés par une paire de nucléons de valence en dehors d'un noyau stable ont des propriétés géométriques fascinantes liées au nombre quantique radial n, au moment angulaire ℓ, ainsi qu'au moment angulaire total L. Dans le cas particulier de l'^{6}He que nous avons étudié en détail, les deux neutrons peuvent être corrélés dans deux configurations géométriques : la configuration di-neutron et la configuration cigare. Nous avons montré que, si la paire de neutrons est confinée dans la couche $0p$, les deux configurations se présentent avec la même probabilité comme une pure conséquence de la géométrie de la couche p. En outre, si la paire de neutrons, tout en restant appariée, est autorisée à se diffuser dans des couche supérieures, la présence d'une interaction attractive à courte portée tend à entraver l'apparition de la configuration cigare et à faire croître la configuration di-neutron. Pour l'^{6}He, des énergies de séparation des deux neutrons raisonnables ont également été obtenues. En même temps, les prédictions faites pour les systèmes à deux particules dans les autres couches attendent des explorations expérimentales, par, par exemple les réactions de knockout qui sondent la forme de la surface nucléaire et les nucléons de surface dans un noyau.

Nous avons également étudié des corrélations de quatre particules. Nous nous sommes concentrés sur l'^{8}He et avons calculé dans ce cas les densités de probabilité angulaire pour l'état 0_1^+ ($(0p_{3/2})^4$) et pour l'état 0_2^+ ($(0p_{3/2})^2(0p_{1/2})^2$), ainsi que pour leur combinaison linéaire. La fonction de corrélation angulaire en termes d'un angle relatif dans le cas de deux particules a été généralisée aux cas de quatre particules en termes de six angles relatifs. Une classe de trois configurations équiprobables a été trouvée pour chaque état 0^+. Les deux classes de configurations ont été nommées les configurations grand-cercle et les configurations tétraédriques d'après leurs géométries. Les configurations grand-cercle peuvent être identifiées avec la configuration di-neutron et la configuration cigare de l'^{6}He, et représentent les configurations spatiales réalistes de l'^{8}He. Un diagramme de phase pour la géométrie de quatre particules dans les couche p a été établi. Le point de transition où le rôle du maximum global passe d'une classe de configurations à l'autre pour un état mixé a été trouvé.

Il y a encore beaucoup de travail à faire à l'avenir. Pour ^{8}He, il serait intéressant d'examiner l'évolution de sa structure spatiale si la diffusion dans les couches supérieures est autorisée. Nous aimerions également obtenir une image globale de la géométrie des systèmes à quatre particules, et faire des prédictions pour la géométrie d'une couche arbitraire comme nous le faisons pour les systèmes à deux particules. Plus précisément, le ^{18}C avec quatre neutrons dans la couche $0d_{5/2}$ est un noyau intéressant à étudier. Par ailleurs, la géométrie des. différents types de nucléons (et donc le rôle de l'isospin) doivent être explorées.

Bibliography

[1] I. Talmi, *Simple Models of Complex Nuclei. The Shell Model and Interacting Boson Model* (Harwood, Chur, 1993).

[2] K.L.G. Heyde, Int. J. Mod. Phys. A4 2063 (1989).

[3] R. F. Casten, *Nuclear structure from a simple perspective* (Oxford, New York, 2000).

[4] I. Tanihata et al., Phys. Rev. Lett. 55, 2676 (1985).

[5] B. Jonson, Phys. Rep. 389, 1 (2004).

[6] T. Kobayashi et al., Phys. Rev. Lett. 60, 2599 (1988).

[7] T. Kobayashi et al., Phys. Lett. B 232, 51 (1989).

[8] K. Riisager, D. V. Fedorov, and A. S. Jensen, Europhys. Lett. 49, 547 (2000).

[9] A.S. Jensen, K. Riisager, D.V. Fedorov, and E. Garrido, Rev. Mod. Phys. 76 (2004).

[10] A. Chatterjee et al., Phys. Rev. Lett. 101, 032701 (2008).

[11] D. T. Khoa and W. Von Oertzen, Phys. Lett. B 595, 193 (2004).

[12] M. Assié et al., Eur. Phys. J. A 42, 441 (2009)

[13] E. Sauvan et al., Phys. Rev. Lett. 87, 042501 (2001).

[14] M.V. Zhukov, B.V. Danilin, D.V. Fedorov, J.M. Bang, I.J. Thompson, and J.S. Vaagen, Physics. Reports. 231, 151 (1993).

[15] Y. Suzuki, Nucl. Phys. A 528, 395 (1991).

[16] M. Takechi et al. AIP Conference Proceedings, 891, 187 (2007)

[17] M. V. Zhukov, A. A. Korsheninnikov, and M. H. Smedberg Phys. Rev. C 50, 1 (1994).

[18] L. V. Chulkov et al., Nucl. Phys. A 759, 43 (2005).

[19] N. Keeley et al., Phys. Lett. B 646, 222 (2007).

[20] K. Hagino et al., Phys. Rev. C 77, 054317 (2008).

[21] N. Itagaki, M. Ito, K. Arai, S. Aoyama, and Tz. Kokalova, Phys. Rev. C 78, 17306 (2008).

[22] M.G. Mayer, Phys. Rev. 75, 1969 (1949).

[23] J.H.D. Jensen, H. Suess, and O. Haxel, Die Naturwissenschaften 36, 155 (1949).

[24] B.A. Brown and W.A. Richter, Phys. Rev. C 74, 034315 (2006).

[25] M. Honma, T. Otsuka, B.A. Brown, and T. Mizusaki, Phys. Rev. C 69, 034335 (2004).

[26] D.H. Wilkinson, Annu. Rev. Nucl. Part. Sci. 45, 1 (1995).

[27] I. Talmi, Helv. Phys. Acta 25, 185 (1952)

[28] M. Moshinsky, Nucl. Phys. 13, 104 (1959)

[29] M. Moshinsky and Yu.F. Smirnov, *The Harmonic Oscillator in Modern Physics.* (Harwood. Academic Publishers, Amsterdam, 1996).

[30] A. Barber and B.S. Cooper, Nucl. Data Tables 10, 49 (1971).

[31] T.A. Brody and M. Moshinsky, *Tables of Transformation Brackets* (Monografias delo Instituto de Fisica, Mexico, 1960).

[32] F. Catara and A. Insolia, Phys. Rev. C 29, 3 (1984).

[33] S. Cohen and D. Kurath, Nucl. Phys. 73, 1 (1965).

[34] A. Ozawa et al., Nucl. Phys. A 693, 32 (2001).

[35] G. Audi et al., Nucl. Phys. A 729, 337 (2003).

[36] Y. Suzuki and K. Ikeda, Phys. Rev. C 38, 1 (1988).

[37] Y. Suzuki and J.J. Wang, Phys. Rev. C 41, 2 (1990).

[38] L.R. Hafstad and E. Teller, Phys. Rev. 54, 9 (1938).

[39] H. Friedrich, Phys. Lett. B 146, 3 (1984).

[40] H. Esbensen, G.F. Bertsch, and K. Hencken, Phys. Rev. C 56, 3054 (1997).

[41] G. F. Bertsch and H. Esbensen, Ann. Phys. (N.Y.) 209, 372 (1991).

[42] M. Matsuo, Phys. Rev. C 73, 044309 (2006)

[43] D.R. Tilley et al., Nucl. Phys. A 708, 3 (2002).

[44] K.L.G. Heyde, *The Nuclear Shell Model* (Springer-Verlag, Berlin, 1990).

[45] D.J. Rowe and J.L. Wood *Fundamentals of Nuclear Models* (World Scientific, 2010).

[46] Harris Hancock, *Theory of Maxima and Minima* (Ginn and Company, 1917).

[47] Robert Gilmore, *Catastrophe Theory for Scientists and Engineers* (Wiley-Interscience, 1981).

Résumé:
Dans un système nucléaire, chaque nucléon est soumis aux forces nucléaires exercées par les autres. L'état fondamental témoigne de la nature des interactions. La fonction d'onde d'un noyau est une mesure de la probabilité d'une géométrie particulière. De ce fait, elle montre une image illustrative des structures géométriques à l'intérieur du noyau. La connaissance des géométries de la matière nucléaire dans des états quantiques spécifiques aide à comprendre la structure et les interactions nucléaires, fournit une validation théorique et permet une prédiction des résultats expérimentaux. Cette thèse porte sur les géométries des systèmes à deux et à quatre particules identiques, en particulier celles résultant du caractère attractif et à courte portée d'interactions nucléaires. Pour les systèmes à deux particules couplées à un moment angulaire arbitraire, on trouve des configurations spatiales et angulaires distinctes liées aux nombres quantiques, ce qui est expliqué analytiquement. L'application au ^{6}He, un noyau halo Borroméen, avec d'abord l'interaction δ et ensuite l'interaction d'appariement montre la coexistence de la configuration di-neutron et de la cigare, avec une prédominance de la première sur la dernière. Quant aux systèmes à quatre particules, ^{8}He est étudié comme prototype. L'expression de la densité de probabilité angulaire est déduite analytiquement pour un état 0^+ général. Les configurations avec la densité de probabilité angulaire maximale entrent dans deux catégories de géométries avec des symétries spécifiques, ce qui peut être considéré comme la généralisation des géométries d'un système à deux particules à celles d'un système à quatre particules.

Spatial particle correlations in ^{6}He and ^{8}He

Abstract:
In a nuclear system, each nucleon is subject to nuclear forces exerted by the others, and the structure of states provides evidence of the nature of the interactions. On the other hand, the nuclear wave function is a measure of the probability of a particular geometry. As such, it provides an illustrative picture of the geometric structures inside the nucleus. Knowledge of the geometries of nuclear matter in specific quantum states helps understand nuclear structure and interactions, provides theoretical validation and allows prediction of experimental results. This thesis has its focus on the geometries of two and four identical particle systems, in particular, those resulting from the short-range attractive nature of nuclear interactions. For two-particle systems coupled to an arbitrary angular momentum, distinct spatial and angular configurations are found regularly related to the quantum numbers, which is explained analytically. Application to the Borromean halo nucleus ^{6}He with first the δ interaction and then the pairing interaction shows the coexistence of the di-neutron and the cigar-like configurations, with a predominance of the former over the latter. As for four-particle systems, ^{8}He is studied as a prototype. The expression of the angular probability density is derived analytically for a general 0^+ state. Configurations in terms of relative angles where the angular probability density peaks fall into two categories of geometries with specific symmetries, which can be considered as the generalization of the geometries of a two-particle system to those of a four-particle system.

Mots clés: Physique nucléaire; Mécanique quantique; Structure nucléaire; Problème à plusieurs corps

Discipline: Constituants élémentaires et physique théorique

Grand Accélérateur National d'Ions Lourds
Bd Henri Becquerel- BP 55027 - 14076 CAEN Cedex 05